

MITNE-237

NUCLEAR ENGINEERING
READING ROOM - M.I.T.

**An Assessment of Internal
Blankets for Gas-Cooled
Fast Reactors**

by

D. B. Lancaster and
M. J. Driscoll

October 1980

RECEIVED
RESEARCH CENTER
MIT

Massachusetts Institute of Technology
Department of Nuclear Engineering
Cambridge, Massachusetts

AN ASSESSMENT OF INTERNAL BLANKETS FOR GAS-COOLED FAST REACTORS

by

D. Lancaster

and

M.J. Driscoll

October 1980

MITNE-237

Sponsored by General Atomic Company



Room 14-0551
77 Massachusetts Avenue
Cambridge, MA 02139
Ph: 617.253.2800
Email: docs@mit.edu
<http://libraries.mit.edu/docs>

DISCLAIMER

MISSING PAGE(S)

Pages 192 & 195 are missing.

ABSTRACT

An assessment of the use of internal blanket assemblies in GCFRs has been performed. This required the self-consistent optimization of a homogeneous design (a conventional core without internal blankets) and a heterogeneous design with internal blankets. The optimization was followed by a detailed comparative analysis of representative versions of the two types of cores.

The procedure started with the establishment of a set of parameters characterizing a representative commercial-sized GCFR. Using constraints on the peak clad temperature (750°C) and the peak linear heat generation rate (15 KW/ft), a thermal-hydraulic analysis was performed to yield acceptable fuel assembly designs for fuel pin diameters varying between 6 and 12 mm (corresponding to fuel volume fractions of 0.236 to 0.487). Neutronic analysis of these assemblies in a homogeneous core arrangement allowed comparison of their doubling time, energy growth potential and fuel cycle costs. The 8 mm pin diameter (0.357 fuel volume fraction) was selected as the optimum. The reasons for the doubling time dependence on pin diameter (or fuel volume fraction) were explored and explained in a generalized framework applicable to all FBR designs.

The heterogeneous core optimization was performed by successively adding internal blanket assemblies to cores made up from the acceptable fuel assembly designs. Since the fuel volume fraction of the internal blanket assemblies was as high as practicable (0.5), this procedure allowed a steady progression to higher core-averaged effective fuel volume fractions. It was found that for small driver fuel pin diameters the addition of internal blankets reduced the doubling time; whereas, for large fuel pin diameters the addition of internal blankets increased the doubling time. It was also found that for all fuel volume fractions the optimized homogeneous core had a shorter doubling time than the heterogeneous cores. Thus the optimum number of internal blanket assemblies was, in fact, zero. To continue the analysis, a heterogeneous core with 132 internal blanket assemblies, and 348 fuel assemblies, having a 7 mm fuel pin diameter, was selected as a reference design, since its core-averaged fuel volume fraction was the same as that of the optimum homogeneous core. Various blanket arrangements were studied and found to have very little impact on doubling time.

Detailed analysis of the heterogeneous and homogeneous cores revealed that the former had: 1) a 5% longer doubling time, 2) a 10% larger fissile inventory, 3) a 15% decrease in the core mixed-mean ΔT , 4) a 14% reduction in the fast fluence, 5) a 24% increase in the peak burn-up, 6) a 41% decrease in the power-density-weighted Doppler co-efficient, 7) a 15% increase in the fuel cycle cost, and 8) a 25% higher capital-cost-adjusted fuel cycle cost (\$60 million higher capital costs attributed to system changes required to accommodate the heterogeneous core). Overall, in view of these findings the homogeneous design is strongly preferred for the GCFR.

ACKNOWLEDGEMENTS

The work described in this report has been performed primarily by the principal author, D. Lancaster, who has submitted substantially the same report in partial fulfillment of the requirements for the Ph.D. degree at MIT.

The funding for the present work was supplied by the General Atomic Company. Some of the work for this report was performed at their facility in San Diego. The authors wish to acknowledge the helpfulness and friendliness of all the persons contacted working on the GCFR project.

The authors wish to thank Ms. Annette Holman for her help, patience, and cheerfulness in the typing of the final manuscript.

TABLE OF CONTENTS

ABSTRACT	2
ACKNOWLEDGEMENTS	4
LIST OF FIGURES	9
LIST OF TABLES	13
CHAPTER 1. INTRODUCTION	17
1.1 Foreword	17
1.2 Background	19
1.3 Initial Investigations of Heterogeneous Cores	23
1.4 Doubling Time	28
1.5 Review of Recent Developments	31
1.6 Outline of Present Work	32
CHAPTER 2. NEUTRONIC DATA BASE AND COMPUTER CODES	37
2.1 Introduction	37
2.2 Cross Section Data Base and Treatment	38
2.2.1 LIB-IV	39
2.2.2 SPHINX Treatment	43
2.2.2.1 Resonance Self-Shielding	44
2.2.2.2 The Group Collapse	48
2.2.3 Fission Product Cross Sections	56
2.2.4 Summary Remarks on the Adequacy of the Cross Section Treatment	59
2.3 Description of the Computer Codes Used	63
2.3.1 CALIØP	63
2.3.2 2DB	67
2.3.3 PERT-V	68
2.4 Summary	69
CHAPTER 3. HOMOGENEOUS CORE ANALYSIS	74
3.1 Introduction	74
3.2 Parameters Independent of the Homogeneous Design Comparison	75

TABLE OF CONTENTS (contd.)

3.2.1	Basic GCFR Design Selection	76
3.2.2	Constrained Assembly Design	77
3.2.3	Blanket Assembly Design	83
3.3	Optimum Core Design Selection	85
3.3.1	Neutronics Methods for the Optimization	86
3.3.2	Doubling Time Optimization	90
3.3.3	Energy Growth Potential Optimization	107
3.3.4	Fuel Cycle Cost Optimization	111
3.3.5	Power Generation Cost Optimization	117
3.3.6	Homogeneous Core Optimization; Summary	118
3.4	Fuel Management and Burnup Analysis	122
3.4.1	Fuel Loading and Shuffling Scheme	123
3.4.2	Analytical Techniques Used to Arrive at the Equilibrium Cycle	126
3.5	Analysis of the Optimized Homogeneous Core Equilibrium Cycle	130
3.5.1	Mass Flows and Doubling Time	130
3.5.2	Power, Burnup, Flux, and Fluence Distributions	135
3.5.3	β_{eff} and Delayed Neutron Parameters	145
3.5.4	Control Rod Analysis	147
3.5.4.1	Control Rod Requirements	147
3.5.4.2	Doppler Coefficients and Temperature Defects	150
3.5.4.3	Control Rod Worths	154
3.5.4.4	Summary of the Control Rod Analysis	157
3.5.5	Material Worths	157
3.5.6	Summary of the Homogeneous Core Analysis	165
3.6	Summary	165
CHAPTER 4.	HETEROGENEOUS CORE ANALYSIS	167
4.1	Introduction	167
4.2	Heterogeneous Core Optimization	169
4.2.1	Determination of the Driver Pin Diameter and the Number of Internal Blanket Assemblies	169
4.2.1.1	Technique for Determining the Optimum Effective Fuel Volume Fractions	171

TABLE OF CONTENTS (contd.)

4.2.1.2	Optimum Effective Fuel Volume Fraction: Results and Discussion	184
4.2.1.3	Summary of the Determina- tion of the Driver Fuel Pin Diameter and the Num- ber of Internal Blanket Assemblies	194
4.2.2	Investigation of the Effect of the Heterogeneous Core Arrangement	195
4.2.3	Summary of the Selection of an Optimum Heterogeneous Core	205
4.3	Fuel Management and Burnup Analysis	206
4.3.1	Fuel Loading and Shuffling Scheme	206
4.3.2	Analytical Techniques Used to Arrive at the Equilibrium Cycle	212
4.4	Analysis of the Optimized Heterogeneous Core Equilibrium Cycle	214
4.4.1	Mass Flows and Doubling Time	214
4.4.2	Power Analysis Distributions	223
4.4.3	Flux, Fluence, and Burnup Analysis	235
4.4.4	β_{eff} and Delayed Neutron Parameters	244
4.4.5	Control Rod Analysis	244
4.4.5.1	Control Rod Requirements	246
4.4.5.2	Doppler Coefficients and Temperature Defects	246
4.4.5.3	Control Rod Worths	252
4.4.6	Material Worths	254
4.4.7	Summary of the Equilibrium Hetero- geneous Core Analysis	257
4.5	Summary	259
CHAPTER 5.	ECONOMIC ANALYSIS	260
5.1	Introduction	260
5.2	Fuel Cycle Costs	261
5.2.1	Fuel Cycle Cost Model	261
5.2.2	Fuel Cycle Costs for the Heterogeneous and Homogeneous Designs Using Nominal Cost Assumptions	264
5.2.3	Sensitivity to Plutonium Value	269
5.2.4	Sensitivity to Fabrication Costs	271
5.2.5	Sensitivity to Reprocessing Costs	275
5.2.6	Sensitivity to the Time Value of Money	275
5.2.7	Fuel Cycle Cost Summary	277

TABLE OF CONTENTS (contd.)

5.3	Capital Cost Differences	279
5.4	Summary	280
CHAPTER 6.	SUMMARY, CONCLUSIONS, AND RECOMMENDATIONS	282
6.1	Introduction and Background	282
6.2	Overview of Procedure	283
6.3	Salient Observations	288
6.3.1	Doubling Time Dependence on Fuel Volume Fraction	289
6.3.2	Method for Heterogeneous Core Optimization	292
6.3.3	Qualitative Explanation for Doubling Time Differences	294
6.4	Conclusions	297
6.4.1	Real Heterogeneous Effects	297
6.4.2	Recommendations for the GCFR	301
6.4.3	Comments Relevant to the LMFBR	302
6.5	Recommendations for Future Work	303
APPENDIX A.	Changes to 2DB	306
A.1	30° Symmetry Changes	307
A.2	Search-Burn Capability and Added Edits	312
A.3	Temporary Changes for Shuffling	318
A.4	Summary	320
APPENDIX B.	Changes in PERT-V	321
B.1	Buckling and Current Edit	321
B.2	Zone-wise Reactivity Edit	329
B.3	Changes in MAIN and INP	330
B.4	Summary	335
REFERENCES		338

LIST OF FIGURES

<u>Fig. No.</u>		
1.1	Reactor Core Arrangements in the Four 1000 MWe Design Studies of 1964	20
1.2	The Parfait Blanket Concept	22
1.3	Comparison of CRBR Core Configurations	27
2.1	One-Dimensional Radial Model of a GCFR Used for SPHINX Group-Condensation	51
2.2	Calculational Path Employed in the Present Work	73
3.1	Basic GCFR Upflow Core Configuration	79
3.2	Homogeneous Core Layout	87
3.3	R-Z Model Used for the Homogeneous Core Analyses	88
3.4	Doubling Time as a Function of Fuel Pin Diameter	95
3.5	Doubling Time as a Function of Fuel Volume Fraction	96
3.6	Fissile Inventory as a Function of Fuel Volume Fraction	98
3.7	Net Fissile Gain as a Function of Fuel Volume Fraction	99
3.8	Breeding Ratio as a Function of Fuel Volume Fraction	100
3.9	Doubling Time as a Function of Fuel Volume Fraction Under Various Constraints	103
3.10	Power Potential Index as a Function of Fuel Pin Diameter at Various Years After GCFR Introduction	110
3.11	Fuel Cycle Cost as a Function of Fuel Pin Diameter	114
3.12	Fuel Cycle Costs Adjusted for Capital Cost Differences as a Function of Fuel Pin Diameter	120

LIST OF FIGURES (contd.)

Fig. No.

3.13	Fuel Loading Pattern for the Reference Homogeneous Core	124
3.14	The Ratios of the Local Power Density to the Active Core Height Averaged Power Density as a Function of the Vertical Distance from the Core Midplane	138
3.15	The Ratio of the Local Power Density to the Active Core Height Averaged Power Density for Each of the Radial Blanket Rows	139
3.16	Peak Kw/ft at BOEC for the Reference Homogeneous Core	140
3.17	Peak Kw/ft at EOEC for the Reference Homogeneous Core	141
3.18	BOEC Peak Flux for the Reference Homogeneous Core	143
3.19	EOEC Peak Flux for the Reference Homogeneous Core	144
3.20	Homogenous Core Neutron Energy Spectrum	146
3.21	Doppler Coefficient at the Core Midplane for the Reference Homogeneous Core	152
3.22	Axial Traverse of the Doppler Coefficient for the Reference Homogeneous Core	153
3.23	Adjoint Spectrum for the Homogeneous Core	160
3.24	Axial Traverse of the HT-9 Reactivity Worth for the Reference Homogeneous Core	162
3.25	Fuel Worth as a Function of Radial Position for the Reference Homogeneous Core	163
3.26	Fuel Reactivity Worth as a Function of Axial Position for the Reference Homogeneous Core	164
4.1	Heterogeneous Core I with 18 Internal Blanket Assemblies and 378 Fuel Assemblies	172
4.2	Heterogeneous Core II with 36 Internal Blanket Assemblies and 372 Fuel Assemblies	173

LIST OF FIGURES (contd.)

<u>Fig. No.</u>		
4.3	Heterogeneous Core III with 54 Internal Blanket Assemblies and 366 Fuel Assemblies	174
4.4	Heterogeneous Core IV with 96 Internal Blanket Assemblies and 354 Fuel Assemblies	175
4.5	Heterogeneous Core V with 132 Internal Blanket Assemblies and 348 Fuel Assemblies	176
4.6	Heterogeneous Core VI with 204 Internal Blanket Assemblies and 342 Fuel Assemblies	177
4.7	R-Z Model for Heterogeneous Core I	178
4.8	R-Z Model for Heterogeneous Core II	179
4.9	R-Z Model for Heterogeneous Core III	180
4.10	R-Z Model for Heterogeneous Core IV	181
4.11	R-Z Model for Heterogeneous Core V	182
4.12	R-Z Model for Heterogeneous Core VI	183
4.13	Doubling Time as a Function of the Effective Fuel Volume Fraction for Various Homogeneous and Heterogeneous Designs	189
4.14	Fissile Inventory as a Function of Effective Fuel Volume Fraction	193
4.15	Heterogeneous Core Arrangement VA	196
4.16	Heterogeneous Core Arrangement VB	197
4.17	Heterogeneous Core Arrangement VC	198
4.18	Heterogeneous Core Arrangement VD	199
4.19	Heterogeneous Core Arrangement VE	200
4.20	Heterogeneous Core Arrangement VF	201
4.21	Fuel Loading Pattern for the Reference Heterogeneous Core	209
4.22	Normalized Axial Power Shape for the Driver Assemblies of the Reference Heterogeneous Core	225

LIST OF FIGURES (contd.)

<u>Fig. No.</u>		
4.23	Normalized Axial Power Shapes for the Burned and Fresh Internal Blankets for the Reference Heterogeneous Core	227
4.24	Peak Kw/ft for Assemblies at BOEC for the Reference Heterogeneous Core	228
4.25	Peak Kw/ft for Assemblies at EOEC for the Reference Heterogeneous Core	229
4.26	Peak Flux for BOEC for the Reference Heterogeneous Core	236
4.27	Peak Flux for EOEC for the Reference Heterogeneous Core	237
4.28	Neutron Energy Spectrum in the Driver Fuel Regions of the Reference Heterogeneous Core	239
4.29	Neutron Energy Spectrum in an Internal Blanket Assembly of the Reference Heterogeneous Core	240
5.1	Sensitivity of Fuel Cycle Costs to the Value of Plutonium	270
5.2	Sensitivity of the Fuel Cycle Cost to the Driver Fuel Fabrication Cost	272
5.3	Sensitivity of the Fuel Cycle Cost to the Blanket Fabrication Cost	274
5.4	Sensitivity of the Fuel Cycle Cost to the Reprocessing Cost	276
5.5	Sensitivity of the Fuel Cycle Cost to the Discount Rate	278
6.1	Flow Chart for the Comparison of Heterogeneous and Homogeneous Cores	285
6.2	Doubling Time as a Function of Fuel Volume Fraction under Various Constraints	290
6.3	Doubling Time as a Function of the Effective Fuel Volume Fraction for Various Homogeneous and Heterogeneous Designs	295
A.1	A 30° Symmetry Mesh Map	308

LIST OF TABLES

<u>Table No.</u>		
1.1	A Representative Comparison of Parfait Blanket and Conventional LMFBR's	24
1.2	A Comparison of Homogeneous and Heterogeneous CRBR Cores	26
1.3	Summary of Homogeneous Versus Heterogeneous Core Comparisons	33
2.1	Neutron Energy Group Boundaries for Ten Group Design Level Cross Section Sets	49
2.2	Collapsing Spectrum Employed as a Function of Assembly Type	52
2.3	Errors Introduced by Group Condensation	55
2.4	Energy Boundaries for the Japanese Fission Products and for LIB-IV Cross Sections	57
2.5	Comparison of Intra-Laboratory Integral Parameter Results	61
2.6	Neutron Spectrum Comparison from CSEWG Problem 1: ZPR-6-7 Infinite Homogeneous Medium Flux	62
2.7	Reactor Design Areas Supported by Critical Experiments for CRBR	71
2.8	ZPPR Criticality Predicted by CRBRP Design Methods	71
2.9	ZPPR Reaction Rate Summary	72
2.10	ZPPR Control Rod Worth Calculation-To-Experiment Ratios	72
3.1	Key Characteristics of the GCFR Used in the Present Work	78
3.2	Compatible Fuel Assembly Designs for Various Fuel Pin Diameters	82
3.3	Control and Shield Compositions	89
3.4	Results of the Analysis of Homogeneous Cores Using Acceptable Thermal-Hydraulic Assembly Designs	94

LIST OF TABLES (contd.)

<u>Table No.</u>		
3.5	Analysis of Homogenous Cores Without Thermal-Hydraulic Constraints	102
3.6	Analysis of Homogeneous Cores Without Thermal-Hydraulic Constraints and Critical Only at the Beginning-of-Cycle	105
3.7	Fuel Cycle Costs for Various Homogeneous Core Designs	113
3.8	Results of Analysis Using A Constant Burnup Assumption	116
3.9	Power Generation Cost Optimization	119
3.10	Homogeneous Core Optimization Summary	121
3.11	Eigenvalues at the Start and End of the First Six Cycles for Fixed Assembly Feed Compositions	127
3.12	Mass Flows for the Homogeneous Core	131
3.13	Homogeneous Core Doubling Time	134
3.14	β_{eff} and Delayed Neutron Parameters for the Reference Homogeneous Core	148
3.15	Homogeneous Doppler Coefficients	151
3.16	Temperature Defect and Control Requirements for the Reference Homogeneous Core	155
3.17	Control Rod Worths and Requirements for the Reference Homogeneous Core	156
3.18	Material Worths for the Reference Homogeneous Core	158
4.1	Key Results of Heterogeneous Core Analysis	185
4.2	Comparison of Cores with the Same Effective Fuel Volume Fraction but Different Numbers of Internal Blanket Assemblies	190
4.3	Performance of Heterogeneous Core Arrangements Having the Same Driver Fuel Pin Diameter and Number of Internal Blanket Assemblies	203

LIST OF TABLES (contd.)

<u>Table No.</u>		
4.4	Heterogeneous Core Feed Enrichments and End of Cycle k_{eff} for the First Six Cycles	211
4.5	Mass Flows for the Heterogeneous Core	215
4.6	Comparison of Parameters Determining the Doubling Time of the Reference Equilibrium Homogeneous and Heterogeneous Cores	218
4.7	Detailed Neutron Balance for BOEC Reference Heterogeneous and Homogeneous Designs	220
4.8	β_{eff} and Delayed Neutron Parameters for the Reference Heterogeneous Core	245
4.9	Heterogeneous Core Doppler Coefficients	247
4.10	Temperature Defect and Control Requirements for the Reference Heterogeneous Core	249
4.11	Time Constants for the Heterogeneous and Homogeneous Fuel and Blanket Pins	250
4.12	Control Rod Worths and Requirements for the Reference Heterogeneous Core	253
4.13	Material Worths for the Reference Heterogeneous Core	255
5.1	Fuel Cycle Costs for the Reference Homogeneous Core	265
5.2	Fuel Cycle Costs for the Reference Heterogeneous Core	267
6.1	Some Important Characteristics of the GCFR Adopted as "Given Conditions" for the Present Work	286
6.2	Summary Comparison of the Reference Homogeneous and Heterogeneous Cores	299
A.1	The INNER2 Subroutine for 30° Symmetry	310

LIST OF TABLES (contd.)

Table No.

A.2	Changes in INP for Improved Storage	314
A.3	The SHUF Subroutine Allowing Shuffling of Number Densities Between Cross Section Sets	319
B.1	The SLOPE Subroutine Modified to Provide a Zone-wise Flux, Current, and Axial Buckling Edit	323
B.2	Sample Output of the Zone-wise Reactivity Worth Calculation	328
B.3	Sample Output From the Edit of Zone-wise Fluxes, Currents, and Axial Bucklings	331
B.4	The CALZ Subroutine to Calculate Zone-wise Reactivity Worths	332
B.5	The MAIN Subroutine Modified for the PERT-V Improvements	334
B.6	Changes to the Subroutine INP	336

CHAPTER 1

INTRODUCTION

1.1 Foreword

Over the past several years the use of internal blankets (in so-called heterogeneous core designs) has attracted considerable attention among liquid metal cooled fast breeder reactor (LMFBR) designers. However, except for an examination of its alternative fuel cycle potential by ORNL as part of the NASAP/INFCE programs (W1), little has been done to assess the utility of heterogeneous designs for the gas-cooled fast reactor (GCFR). Thus the objective of the present work, undertaken under contract to the General Atomic Company, is to evaluate whether a heterogeneous core is advantageous for a GCFR.

The term "heterogeneous" in the present context refers to the use of depleted uranium assemblies inside the fissile fueled core zones. Due to the low power density of these assemblies they can be constructed of larger diameter fuel pins and with a higher fuel volume fraction than the fissile fueled assemblies. The internal blanket assemblies are very similar to radial blanket assemblies, but since the internal blankets run at a higher power density than the radial blankets the pin diameters of the internal blankets in this work have been made slightly smaller (127 pins per internal

blanket assembly versus 91 pins per radial blanket assembly and 271 pins per fissile fueled assembly).

It is now generally accepted that the primary incentive for the introduction of heterogeneity into LMFBR designs is the resulting decrease in sodium void worths. Clearly this is not a valid motivation in the case of the GCFR. At the outset of the present study a number of alternative improvements conferred by the use of internal blankets were postulated for the GCFR: better breeding, reduction of fluence, less reactivity swing per cycle, and the like. All of these hypotheses will be explored, but the main focus of this work will be to find the design which will yield the lowest power generation cost. Design and safety implications will be evaluated, but in general they will not intervene as limiting criteria. Since the LMFBR and the GCFR are similar in a number of ways this work will also have implications regarding the value of changing an LMFBR to a heterogeneous core design when the total cost rather than the sodium void worth is the figure of merit. Thus, although this work centers on GCFRs, comments on the applicability to LMFBRs will be included wherever appropriate.

This work concentrates on the uranium/plutonium fuel cycle, since it permits by far the best neutronic and economic performance. The use of thorium internal blankets has been investigated by White and Burns (W1), who found no advantages of note over the conventional uranium/plutonium

fuel cycle, but instead found the normal degradation in core neutronic performance associated with substituting thorium for uranium in a fast reactor. Further investigation would require incentives not now in evidence. Hence the thorium fuel cycle has been left for further work.

1.2 Background

For all practical purposes breeder reactors provide access to an inexhaustible energy supply, with all of the desirable implications that this capability conveys. This considerable incentive to develop breeders was recognized in the mid-1940's by Enrico Fermi and his associates (F1). Since that time there has been continuous work to conceptualize and implement improvements in breeder designs. The first breeder was an LMFBR, EBR-I; it went critical in August 1951. It was also the first nuclear power plant of any type to produce electricity, a goal achieved on December 20, 1951. EBR-II and the Fermi Fast Breeder Reactor followed over the next two decades. It is interesting to note that the early design of EBR-II had seven internal blanket assemblies for power flattening (B1) which, however, were removed from design plans by 1958.

In the early 1960's plans were being made for large commercial LMFBR's. By this time it was known that coherent large-volume sodium voiding could cause a large reactivity insertion. Thus all four design concepts developed for the AEC by 1964 had "spoiled" geometries (T1). Figure 1.1 shows

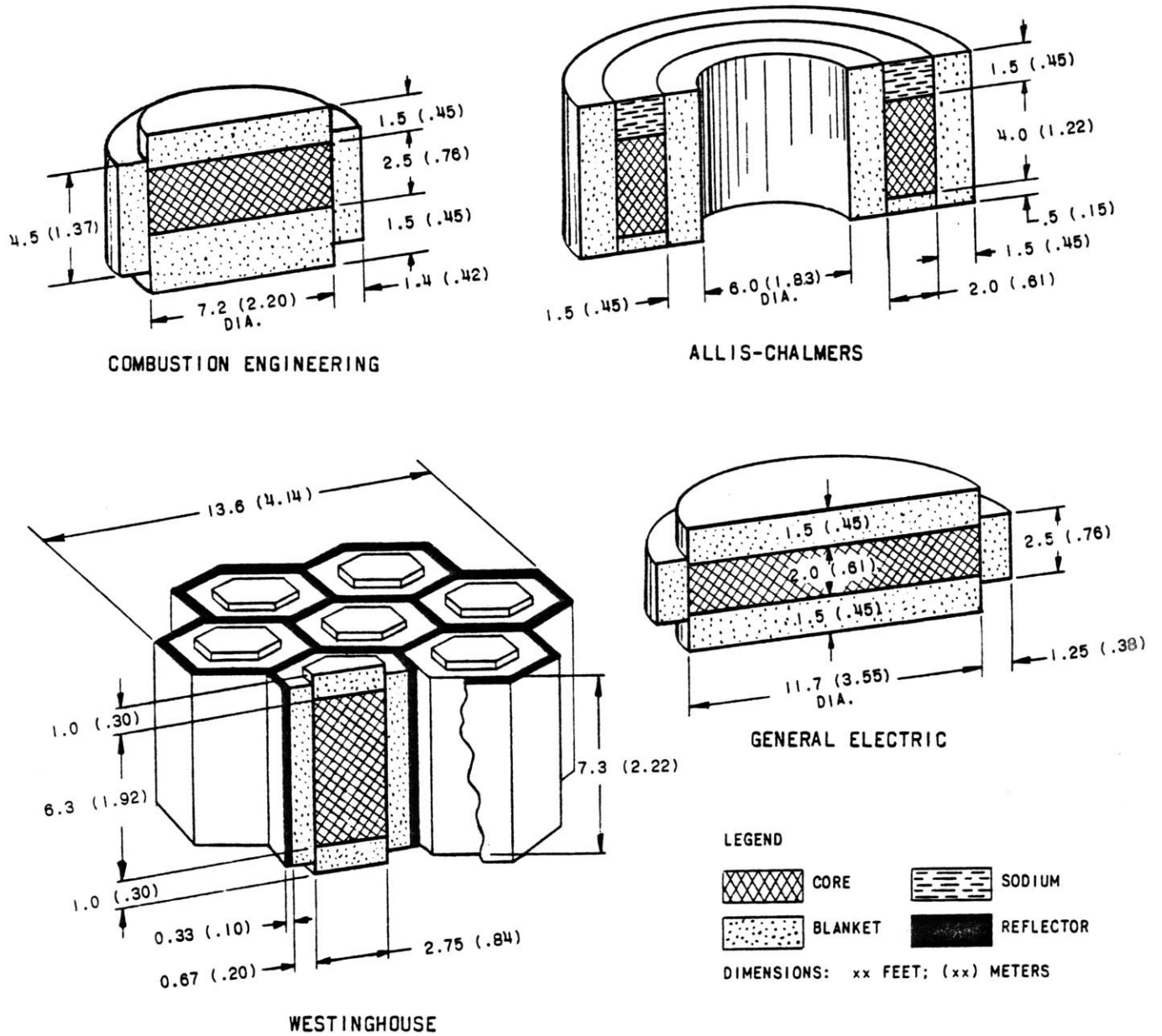


Fig. 1.1 REACTOR CORE ARRANGEMENTS IN THE FOUR 1000 MWe DESIGN STUDIES OF 1964 (T1)

the four designs envisioned at that time. Two of these designs had what today would be called internal blankets. The core with the best predicted economic performance was the carbide core evaluated by Combustion Engineering, which did not employ internal blankets. It should be pointed out, however, that the dominant design constraint on all these cores was sodium voiding, with the economics playing a distinctly secondary role. It was during this same period (from 1961 on) that GCFRs were being first developed. Since there was no sodium void problem with a GCFR no "spoiled" geometries were investigated (helium loss through depressurization is accompanied by a comparatively small reactivity addition). Gradually through the sixties the "spoiled" geometry design lost favor to the simpler cylindrical "homogeneous" designs, since it was concluded that coherent large-scale sodium voiding required "a major accident of an incredible nature" (H1). However, even as late as 1969 Westinghouse was still proposing a modular core, although pointing out its economic disadvantages (T2).

From 1970 to 1975 it was generally agreed that the preferred design of a fast reactor, whether GCFRs or LMFBRs, would be to incorporate a cylindrical homogeneous core. One exception to this mainstream effort is reflected in work by Ducat, who evaluated the "parfait blanket" concept for fast breeder reactors (D1). In this approach depleted uranium was placed in the center of each fuel assembly, as shown in Fig. 1.2. Many of the advantages and disadvantages put forth

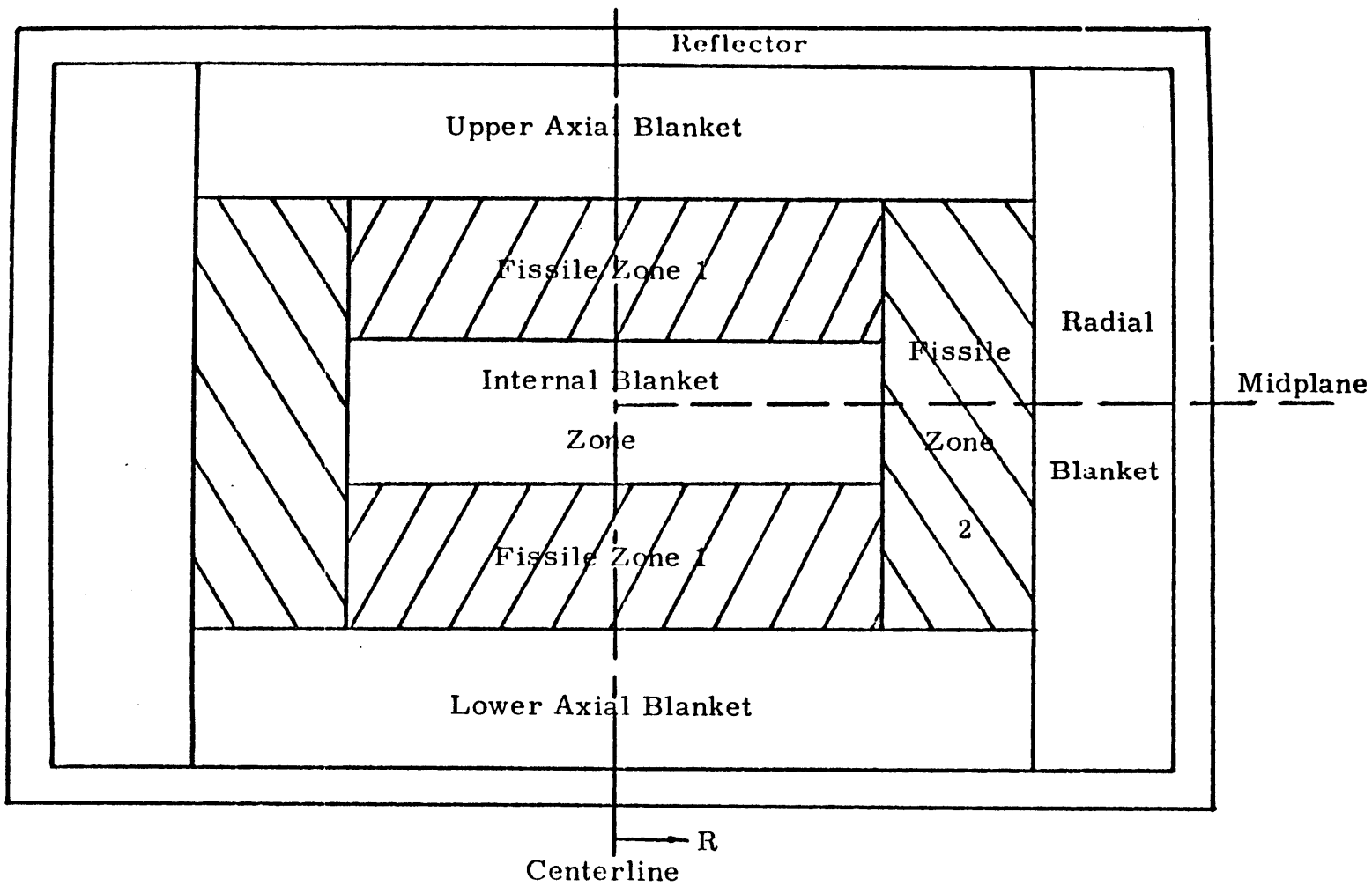


FIG. 1.2 The Parfait Blanket Concept (D1)

by Ducat for the parfait concept, as summarized in Table 1.1, are also associated with the heterogeneous core concept.

At this point some nomenclature should be clarified. In this work the term "heterogeneous" is used to refer to any core containing full length radial-blanket-like assemblies of depleted uranium in the active core region. Because of many common features between this and the "parfait" cores described by Ducat the term "parfait" has been widely used by many working in this area to describe any core with internal blankets, be they full length assemblies of depleted uranium or axial sections of depleted uranium in a fuel assembly. In this work the term "parfait" will be left for the Ducat type core only. Another potential point of confusion is with the term "internal blanket." Clearly the parfait cores have segments that could be referred to as internal blankets, but in this work the term is reserved for full length radial-blanket-like assemblies of depleted uranium.

1.3 Initial Investigations of Heterogeneous Cores

Most of the controversy over the true nature of heterogeneous core performance starts with the paper presented by Mougnot at the European Nuclear Conference in April, 1975 (M1). In this paper it is claimed that the heterogenous core shortens the doubling time (from 22 to 11 years for the example used), decreases the reactivity swing over a cycle, lowers the fast fluence, and decreases the sodium void worth.

Table 1.1

A Representative Comparison of Parfait Blanket and
Conventional LMFBRs (D1)

Advantages

Increased breeding ratio (2%)
Decreased doubling time (10%)
Decreased peak fast flux (25.5%)
Decreased wrapper tube elongation (29%)
Decreased wrapper tube dilation (37.5%)
Decreased burnup reactivity swing (25%)
Fewer control rods in core
More fuel assemblies in core
Reduced losses of neutrons to control poisons
Decreased peak power density (5%)
Decreased peak fuel burnup (7.6%)
Decreased fuel swelling
Increased overpower operating margin
Flatter radial flux and power profiles in the inner core zone
Decreased thermal bowing
Decreased fluence-induced bowing
More favorable sodium void characteristics
Potential for higher core fuel volume fraction

Disadvantages

Increased core fissile inventory (3.9%)
Reduced power Doppler coefficient (8%)
Higher peak clad temperature (17°F)

The paper was reviewed in some detail by Chang (C1) at Argonne National Laboratory (ANL), who identified a number of inconsistencies. First, the peak linear heat generation rates were not the same in the heterogeneous and homogeneous cores compared. Second, the external blankets of the heterogeneous core were much thicker. Third, the homogeneous core was at an off-optimum fuel volume fraction. Chang concluded that the doubling time cannot be improved by utilizing the heterogeneous concept. Although Chang shows that most of the doubling time advantage claimed by Mougnot is not due to heterogeneity, a fully convincing demonstration that heterogeneity cannot yield any advantage has not yet been presented.

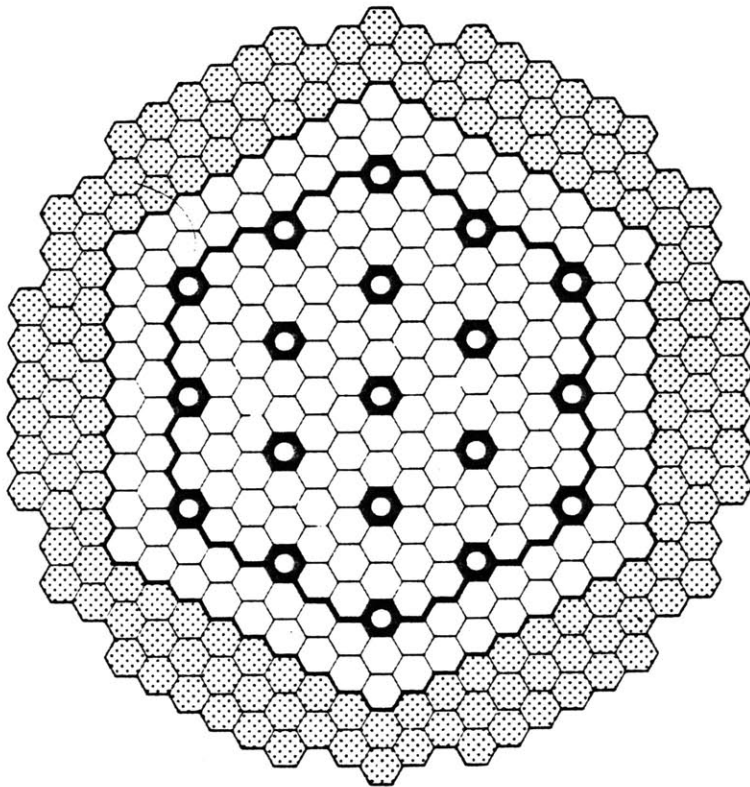
In spite of the dispute over the reality of doubling time improvement, the heterogeneous concept was enlisted to improve the performance of the Clinch River Breeder Reactor (CRBR). As demonstrated in Table 1.2 the CRBR shows great improvement with the use of internal blankets. Figure 1.3 shows the reference and an early heterogeneous design of the CRBR. The heterogeneous design, called the Alternate Fuel Management Scheme (AFMS), was reviewed by Chang, et al. (C2). They concluded that the doubling time improvement in the CRBR was due to the increase in the volume-averaged fuel volume fraction rather than the heterogeneity per se. Once again Chang concludes that comparably-optimized heterogeneous cores will always have slightly longer doubling times. In arriving at this conclusion homogeneous and heterogeneous cores




Table 1.2

A Comparison of Homogeneous and Heterogeneous CRBR Cores
(C2, C3, L4)

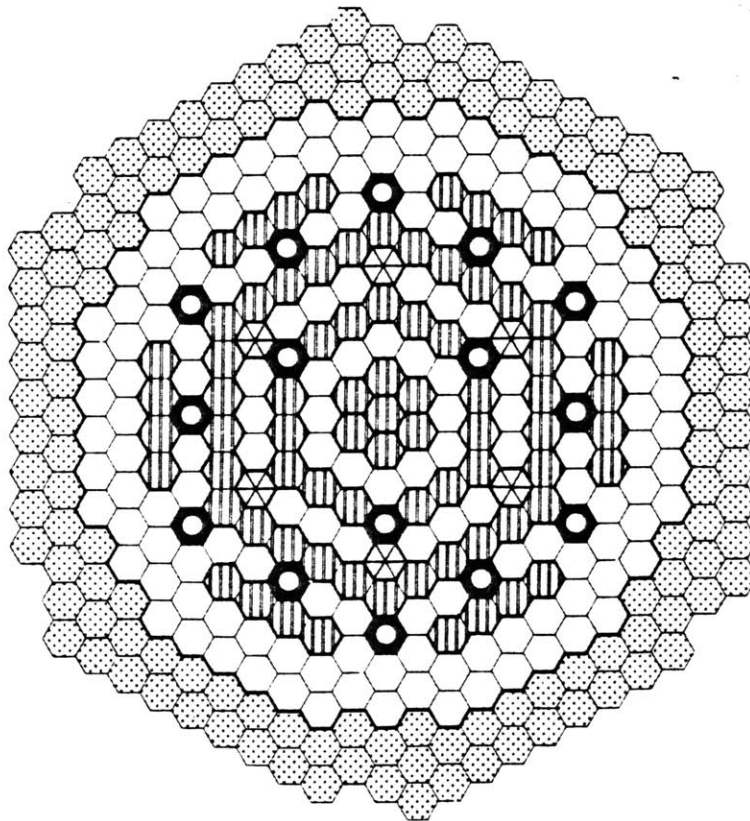
	<u>Homogeneous</u>	<u>Heterogeneous</u>
Breeding Ratio	1.08	1.21
Fissile Inventory (Kg)	1273	1582
Doubling Time (yr)	95.	36.
Maximum Sodium Void Worth (\$)		
BOC	\$3.90	\$1.88
EOC	\$4.00	\$3.90
Fast Fluence (n/cm ²)	$\sim 2.0 \times 10^{23}$	1.4×10^{23}
Doppler Coefficient (BOC, - T dK/dT . 10 ⁴)		
Fuel	55.9	23.2
Total	67.3	72.4

HOMOGENEOUS CRBR



	Fuel Assemblies	198
	Radial Blanket Assemblies	150
	Control Assemblies	19

HETEROGENEOUS CRBR








	Fuel Assemblies	156
	Internal Blanket Assemblies	76
	Fuel/ Blanket Assemblies	6
	Radial Blanket Assemblies	132
	Control Assemblies	15

Fig. 1.3 Comparison of CRBR Core Configurations (C3)

were compared in a number of ways. However, the number of realistic homogeneous and heterogeneous designs examined (two heterogeneous and three homogeneous) was too small to give confidence that further optimization of each core may not lead to different conclusions. Nevertheless, Chang et al., did focus attention on the major reason for the improved performance of the heterogeneous CRBR, namely that the homogeneous CRBR employed an off-optimum pin diameter. This is not surprising, since the pin diameter of the CRBR was constrained to be the same as that in the Fast Flux Test Facility (FFTF), since most of the data on mixed oxide fuel performance was at this pin diameter.

With the debate on heterogeneous cores well started, numerous papers were subsequently written comparing heterogeneous to homogeneous LMFBRs. Since the present work will cover much the same ground, but for the GCFR, a retrospective review of some of the earlier papers is in order. The parameter of merit used in most studies of this genre has been doubling time. Thus, in order to prepare for the review of these earlier papers a discussion of doubling time follows.

1.4 Doubling Time

Doubling time, the time required to double the fissile material committed to a reactor, is an indicator of the growth and economic potential of a given reactor design. Energy planners concerned about the adequacy of future nuclear fuel

supplies often use doubling time as their figure of merit. Energy economists likewise frequently use doubling time, since it is a good measure of the return on investment. Doubling time can be written as:

$$\text{Doubling Time} = \frac{\text{Fissile Inventory}}{\text{Annual Fissile Return}} \quad (1.1)$$

Since the fissile investment is the largest monetary investment in the fuel cycle, the reciprocal of the doubling time is a good estimate of the rate of return on the investment.

Doubling time alone is not enough to calculate the actual fuel cycle costs or even the true energy potential in any year but it is commonly used as a figure of merit since it can be determined directly from the core physics analysis with very few added assumptions. A more complete discussion of figures of merit will follow in Section 3.3 of Chapter Three.

The doubling time is often expressed in terms of various other familiar parameters to aid in understanding its optimization. One such representation uses the breeding ratio (BR), the fissile capture-to-fission ratio (α), the total core thermal power (P), the ratio of fertile fission-to-fissile-fission (δ), and the fissile inventory (FI). The breeding ratio measures the production of fissile material per absorption in fissile material. (BR-1), then, is the net gain of fissile material per absorption. Multiplying this by $(1+\alpha)/(1+\delta)$, the ratio of fissile absorption to total fissions, yields the

production of fissile material per fission. The power (P) is related to the mass fissioned per unit time, and can therefore be used to convert the production of fissile material per fission to a rate of production of fissile material. Using these factors and the fissile inventory which is to be doubled the following equation can be written for the doubling time:

$$DT = (2.6 \text{ MW}\cdot\text{yr/Kg}) \frac{FI (1+\delta)}{(BR-1)(1+\alpha)P} \quad (1.2)$$

where

DT is the doubling time in years

FI is the kilograms of fissile material tied up by the reactor (in and out of core)

BR is the breeding ratio

α is the fissile capture to fission ratio

δ is the ratio of fertile to fissile fissions

and P is the thermal power in MW.

This simple equation can be further elaborated upon, as was done by Aldrich (A3), but for this discussion this elementary version is all that is needed. The detailed doubling time definition for the present work is presented in Subsection 3.3.2 of Chapter 3.

From this equation it is clear that the doubling time can be made shorter by decreasing the fissile inventory or by increasing the breeding ratio or power. The fissile inventory can be decreased by shortening the cycle length (requiring

thereby less excess reactivity) by decreasing the core leakage, by decreasing the non-fissile absorption, or by increasing the fission cross section (by changing the neutron spectrum). The breeding ratio can be increased by decreasing reactor leakage, decreasing parasitic absorption, hardening the spectrum, or increasing the fertile capture cross section. The peak thermal power of a reactor design is generally as high as materials limits permit. In order to increase the thermal power the average conditions should be brought closer to the peak conditions, i.e.: improve the power flattening.

Unfortunately some of these objectives conflict with others: for example, decreasing fissile inventory by decreasing non-fissile absorption is in direct conflict with increasing the breeding ratio by increasing the fertile capture cross section. The present work will concentrate only on those effects on doubling time brought about by heterogeneity. We will strive to compare equally optimized homogeneous and heterogeneous designs: comparable optimization with respect to fuel volume fraction, fuel management, power flattening, and thermal hydraulic design is a foremost objective.

1.5 Review of Recent Developments

Shortly after the initial papers already discussed, the majority of the LMFBR community agreed that heterogeneous cores were desirable primarily because they decreased the sodium void worth and thereby were expected to have less-energetic accidents. The argument as to whether or not they could also

improve economics was not pursued with any intensity since the sodium void worth became the preferred figure of merit. Papers have appeared upon occasion which compared heterogeneous to homogeneous cores, but no major effort to resolve the differences among the various design communities has been made. Since the GCFR design does not depend on sodium (or even helium) void worth the question of whether it would benefit from a heterogeneous core was left unresolved. Table 1.3 compiles most of the more prominent comparisons made to date. A number of the publications are short, making resolution of the differences difficult. Whenever possible, comments are included in the table to help identify obvious inconsistencies in the comparisons.

1.6 Outline of the Present Work

The underlying objective of the present work is to provide a sufficient basis for deciding whether or not a GCFR should have a heterogeneous core design. In view of the reservations with respect to the adequacy of the comparisons just outlined, this analysis contains an optimization study of both the homogeneous and heterogeneous cores. Because system economics is to be preferred as the controlling figure of merit, the study not only includes comparisons of fuel cycle costs, but also differential capital costs that would accompany either option. Finally, this study necessarily involves numerous assumptions, so that the uncertainty in the final results due to these assumptions is also addressed.

Table 1.3

Summary of Homogeneous Versus Heterogeneous Core Comparisons

Date	Lab	Doubling Time (yrs)		Reference	Comments
		Homogeneous	Heterogeneous		
4/75	CEA/CEN-Cadarache	22	11	M1	Fuel volume fraction and thermal-hydraulics not equally optimized. (KW/ft not constant and the homogeneous core pin diameter too small.)
late '75	WARD	95	36	Later published as C3	Fuel volume fraction not equally optimized (homogeneous core pin diameter too small)
4/19	ANL	21.6	23.0	C2	Not equally optimized fuel management. (The homogeneous core had a shorter cycle.) In general, however, this work was a good comparative study.
10/5/76	EPRI	16.9	18.2	S1	Modular core, no optimization
2/8/77	ANL	16.9	20.7	B2	Heterogeneous core is off the optimum fuel volume fraction since internal blankets are added to an optimized homogeneous core.
6/77	WARD	19.5	16.	P1	PLBR design
6/13/77	CEA	24	16.	S2	Fuel volume fraction not equally optimized.
6/13/77	AI	19	19	V1	PLBR design.

Table 1.3 (continued)

Date	Lab	Doubling Time (yrs)		Reference	Comments
		Homogeneous	Heterogeneous		
6/13/77	GE- Sunny- vale	13	14	B3	
7/5/77	ANL	20.7	22.7	T3	
10/77	HEDL	11.6	19.0	C4	
11/5/77	ANL	68.6	30.1	B4	Constrained to off optimum pin diameter for the homogeneous core.
12/77	SNR 2 Project	T	0.5T	M2	
12/77	UK AEA	24	39	T4	
12/77	CEA	29.5	12.8	E1	Off optimum fuel pin diameter in the homogeneous core.
4/78	ANL	16.5	18.8	B5	
4/78	GE- Sunnyvale	22.2	16.7	L1	Constrained to an off optimum homogeneous fuel pin diameter.
4/20/78	ANL	13.7	17.2	O1	
6/78	AI	12.1	14.2	V2	Carbide fuel.
12/78	ORNL	12.7	10.2	A1	
5/79	UK- Risley	38.0	28	B6	Constrained to an off optimum homogeneous fuel pin diameter.
6/79	ORNL	12.6	11.4	W1	Unoptimized GCFR: performed mainly as a scoping study of alternate fuels.

In the chapter just concluded the background necessary to define and understand the central problem posed has been established, and the previous applicable work has been presented. In Chapter Two the physics data base is discussed along with the computer codes used in the analysis. The cross section treatment is discussed and the assumptions and limitations are pointed out. Although no new computer codes of any note were written for this work, modifications were made to existing codes and these modifications are introduced in the second chapter and discussed in detail in the appendices.

The third chapter is devoted to the analysis and optimization of the homogeneous core. It starts with a short review of GCFR plant parameters considered independent of the heterogeneous versus homogeneous core design decision, and contains a justification as to why some of these parameters were selected. After that the optimum fuel pin diameter is selected and the reasons for the existence of an optimum are explained. With the pin diameter selected, the detailed analysis of the core is presented, along with a discussion of the methods used. The analysis includes fuel cycle mass flows; power, flux and fluence distributions; Doppler coefficients, control rod requirements and worths; and fuel, clad, and helium worths.

Chapter Four covers the selection and analysis of the heterogeneous core. The optimization of a heterogeneous core is discussed and the results of this optimization is presented. Again, as in Chapter Three, follow-on analyses provide all the relevant details needed for fuel cycle analysis and safety assessment.

The cost analysis is performed in Chapter Five. Using data from Chapters Three and Four the fuel cycle costs are calculated, and associated capital cost differences are presented. After all the costs have been analyzed the cost differential between the heterogeneous and homogeneous cores is evaluated. The sensitivity of the cost differential to all the main economic data and cost assumptions is then calculated.

The last chapter, Chapter Six, summarizes the findings of the present work. It compares the costs, energy growth potential, safety, and proliferation concerns associated with the heterogeneous and homogeneous cores. The implications of the work for the homogeneous versus heterogeneous decision are presented, and recommendations for future work are made.

CHAPTER 2

NEUTRONIC DATA BASE AND COMPUTER CODES

2.1 Introduction

This work depends heavily on large computer code calculations. In order to have confidence in such analyses the algorithms used in the codes and the data base supplied to the codes must be documented and validated. As in most engineering problems many assumptions must be made to allow solution of the problem within reasonable time and cost constraints. This chapter reviews the assumptions used in the cross section treatment and introduces the computer codes used in this work. The assumptions and approximations required in subsequent analyses are discussed as the need occurs in the later chapters.

The chapter begins with a discussion of LIB-IV, the cross section library used in this study. This is the state-of-the-art library currently used by a number of fast reactor contractors, including Westinghouse. After the underlying assumptions used in the production of LIB-IV are pointed out, an explanation of the local cross section treatment is presented. SPHINX, a code recently released by Westinghouse, is used for this task (D2). The LIB-IV library as presently constituted does not have adequate fission product cross sections for fast breeder reactor studies of the

type of interest here, hence a discussion of this topic follows the section on SPHINX. This completes the description of the cross section treatment, which is concluded by a comparison with various other treatments.

Following the cross section exposition is a brief abstract of each major computer code used in the remainder of this work. The codes are CALIØP, 2DB, and PERT-V. CALIØP is an optimization code used by the General Atomic Company. Since there is as yet no published documentation on CALIØP it is described in more detail than the other codes. 2DB, a two dimensional diffusion theory burnup code, and PERT-V, a perturbation theory code, are well documented and are therefore only briefly described in this chapter. However, modifications were made to both of these codes; hence the changes are specifically noted. The coding for the changes is relegated to the appendices.

This chapter is concluded with a summary of the benchmarking of these methods against critical assembly data. Although the benchmarking was done by other laboratories, it adds considerable confidence to the validity of the techniques used in this work.

2.2 Cross Section Data Base and Treatment

All of the cross sections used for this work come from the Evaluated Nuclear Data Files, ENDF/B-IV (G2). They came to MIT in two forms: 1) LIB-IV and 2) a Japanese Nuclear Data Committee report on fission products. The LIB-IV cross

sections are treated with SPHINX, and then combined with the Japanese fission products to form the cross section sets used in the present work.

2.2.1 LIB-IV

LIB-IV is a well documented and tested library of multigroup constants for reactor design (K1). It is nationally available, and is in the form of Committee for Computer Code Coordination (CCCC) interface files (C5). It contains 49 fast energy groups and one thermal group, and therefore is mainly for use in fast reactor design. The library is in the form of ISØTXS, BRKØXS, and DLAYXS files which are all described in the CCCC reference (C5). There are data for 101 isotopes and, when the ENDF/B data permitted, the P_0 , P_1 , P_2 , and P_3 Legendre components are included.

The library used in the present work was generated from the ENDF/B-IV data using the MINX program (W2). MINX takes the pointwise data and resonance parameters of ENDF/B-IV and applies an assumed flux shape to yield group constants. The flux shape assumed is:

$$\phi(E, T, \sigma_0) = \frac{C(E)}{\sigma_0 + \sigma_t(E, T)} \quad (2.1)$$

where

- ϕ is the neutron flux,
- E is the energy of the neutrons,
- T is the temperature of the isotope of interest,

σ_o is the background cross section contributed by other nuclides in the mixture,
 σ_t is the total cross section for the isotope under consideration,

and

$C(E)$ is the smoothly varying function chosen to describe the overall flux shape.

Using this flux shape the cross sections are collapsed from a continuous energy form to a group constant form using the following equation:

$$\sigma_x(T, \sigma_o) = \frac{\int_g \sigma_x(E, T) \phi(E, T, \sigma_o) dE}{\int_g \phi(E, T, \sigma_o) dE} \quad (2.2)$$

where the x subscript refers to an arbitrary reaction of type x, and the g subscript refers to the energy group.

This technique should be recognized as the Bondarenko self-shielding method (B7), where composition-independent cross sections are generated as a function of σ_o , the background cross section. The LIB-IV ISOTXS file contains the infinitely dilute cross sections, which correspond to $\sigma_o = \infty$. The LIB-IV BRKØXS file contains the self-shielding factors ("F-factors") for a set of temperature and σ_o values which span the entire range of designer interest. The F factors are defined as the ratio of a cross section to its infinitely dilute value:

$$F_{xg}(T, \sigma_o) \equiv \sigma_{xg}(T, \sigma_o) / \sigma_{xg}(o, \infty) \quad (2.3)$$

These F factors and the infinitely dilute cross sections are used by SPHINX to generate composition dependent cross sections as described in the next section.

If the cross sections are known as a function of energy,¹ the major approximation used to generate LIB-IV is contained in the assumed slowly varying flux shape, C(E). The slowly varying flux shape, C(E), used for LIB-IV was a fission spectrum down to 820.8 KeV; from there down to 0.1 eV a 1/E weighting was used, and for the lowest energies a Maxwellian with a temperature of 0.025 eV was used. Using these shapes, the equation for the flux (Eq. 2.1) is never rigorously correct; however, some familiar equations arise. At high energies the flux shape assumption takes the form:

$$\phi(E) = \frac{\bar{\chi}(E)}{\Sigma_t(E)} \quad (2.4)$$

where $\bar{\chi}(E)$ is the fission spectrum.

This formulation is valid, strictly speaking, if the down-scattering source of neutrons into dE about E is small compared to the fission source. Since this approximation is used only above 820.8 KeV, this treatment represents a reasonable simplification. For the rest of the energies important to a GCFR the flux shape assumption can be reduced to:

¹Determining the correct cross section shape as a function of energy is non-trivial, especially in the unresolved resonance region. For the MINX approach see reference (W2).

$$\phi(E) = \frac{1}{E \Sigma_t(E)} \quad (2.5)$$

This flux shape would be correct for a hydrogenous system with negligible absorption. It is also approximately the correct shape for a mixture of heavy nuclides exhibiting weak absorption (assuming $\xi(E)$ is almost energy independent over any energy group). Unfortunately, since absorption is implicit in problems of present interest, this flux shape is imprecise; fortunately the resulting error is small for several reasons. First, this flux is used to collapse only to the fine group structure. Since there are fifty fine groups, the shape discrepancy over the narrow energy bands involved is small. Second, if the cross sections themselves do not change significantly as a function of energy, the shape of the flux used for intra-group weighting has no effect. Many of the important cross sections do not vary substantially in the energy band bracketed by a fine group. Finally, although the slowly varying flux shape may not be correct, the flux shape at a resonance is controlled by the $1/\Sigma_t(E)$ factor, which is a good approximation if the loss in neutron energy in a scattering collision is large compared to the resonance width. In other words, Eq. 2.5 should be recognized as the narrow resonance approximation, which is a reasonable approximation for fast reactors.

Another assumption in the Bondarenko method is that the flux shape is smooth except for the dips caused by the

resonances of the particular isotope under consideration. This is clearly not the case since resonances of Pu-239 and U-238 do overlap. This problem is hard to quantify, and as greater cross section accuracy is attained may force adoption of an improved method. Most of the overlapping resonances occur in the lower energy groups which are not important to a GCFR with respect to its economic performance. However, most of the contribution to the Doppler-broadening reactivity occurs at these neutron energies.

Unfortunately, due to the cost of running problems in 50 energy groups, more approximations must be made to reduce the data to composition-dependent 10 energy group cross sections. In order to do this the code SPHINX was used.

2.2.2 SPHINX Treatment

The SPHINX code is the mate to MINX in the CCCC plan for cross section treatment (D2). The code has two major sections. The first section generates the composition-dependent fine group cross section library by finding the correct F factors and then applying them. The second section uses a one dimensional diffusion calculation to deduce the fifty group flux by region. That flux is then used to collapse the cross sections to any specified broad group structure.

For this work the number of SPHINX treatments was limited to two analyses as part of the overall compromise involved in allocating resources to the various subtasks. From these

two runs, however, 162 individual collapsed cross section sets were obtained. To describe these cross sections and the approximations involved, the collapsing process and the resonance self-shielding will be discussed separately.

2.2.2.1 Resonance Self-Shielding

Nine different composition-temperature sets were used for the resonance self shielding. They were:

- 1) Inner Core, which has approximately a 12% fissile plutonium enrichment. The fuel was assumed to be at 1300°K. The clad and helium were assumed to be at 800°K. (Approximate hot full power temperatures.)
- 2) Inner Core again, but with 600°K and 500°K assumed for the fuel and structure/helium temperatures respectively. (Approximate shutdown temperatures)
- 3) Outer Core, which has approximately an 18% fissile plutonium enrichment. Temperatures were assumed to be the same as the hot full power temperatures assumed for the inner core.
- 4) Outer Core at the shutdown temperatures.
- 5) Radial Blanket of depleted uranium (no plutonium). The same hot full power temperatures were assumed.
- 6) Radial Blanket at shutdown temperatures.
- 7) Axial Blanket of depleted uranium (no plutonium). The same hot full power temperatures were assumed.
- 8) Axial Blanket at shutdown temperatures, and
- 9) The Shield, taken to be at 600°K.

The number densities for these mixes were obtained from the General Atomic submittal to the Nonproliferation Alternative Systems Assessment Program (NASAP) (G-1), and do not correspond directly to any of the mixes used later in this work.

The actual treatment of these mixes is straightforward. Since the mixes are assumed homogeneous, σ_o is found by adding up the macro total cross sections of all the isotopes other than the one being considered and dividing it by the number density of the isotope under consideration. In mathematical terms:

$$\sigma_o^j = \frac{1}{N^j} \sum_{\substack{i \\ i \neq j}} N^i \sigma_t^i \quad (2.6)$$

where

i and j are superscripts identifying the isotopes involved,

N is the number density (nuclei per barn cm),

σ_t^i is the total microscopic cross section for isotope i (barns),

and σ_o^j is the background cross section for isotope j .

Since σ_t changes as the self shielding is imposed, the procedure requires iteration. For this work five iterations were performed. The iteration proceeds as follows. First the σ_o for an isotope in the mixture is calculated. Second, using this σ_o and the temperature an interpolation among the σ_o

values and temperatures in the Bondarenko file (BRKØXS) is performed to find a particular F factor. (LIB-IV contains six different σ_0 s and three temperatures). Once the F factor is determined the infinitely dilute cross section is multiplied by the F factor, and the resulting cross section replaces the old value. Separate F factors are computed for the capture cross section, fission cross section, and elastic scattering cross section. The calculations are performed for every isotope in the mixture before starting the next iteration. Finally, this iteration is performed for each energy group.

A number of fairly important assumptions were made in the resonance treatment. The first major assumption was that five sets of compositions were sufficient. This assumption is important, since in the five sets selected there is no low-enrichment plutonium set corresponding to the case at the end of life in an internal blanket. All of the plutonium isotopes are assumed to be infinitely dilute in the blanket mixes. This omission is satisfactory since the spectrum averaged one-group σ_f for Pu-239 only decreases 1% if the full self shielding of a core mix is used. The second major assumption was that the core cross sections, which were based on a design that had a fuel volume fraction of 28.5%, would be valid for all of the various designs investigated. In order to evaluate this concern, the spectrum averaged one group capture cross section for U-238 in the axial blanket (0.285 fuel volume fraction) was compared to the one group capture cross section

for U-238 in the radial blanket (0.5 fuel volume fraction). Both were collapsed over the same spectrum. The difference was 2.3%, with the axial blanket cross section the lower of the two, as expected. Since the fuel volume fractions investigated in this work varied from 0.24 to 0.48, which is close to the range examined, and since the variation observed is tolerable, this simplification was also judged acceptable.

Another assumption is the characterization of these five mixes as homogeneous and infinite. No pin description and associated Dancoff factor was used since the actual geometry and pin sizes were not yet known and also since the assumption of homogeneity is a reasonably good one for fast reactors. The homogeneous approximation was investigated by ANL for the second Large Core Code Evaluation Working Group benchmark. They found that it decreased k_{eff} by 0.2 to 0.3% in an LMFBR; a lesser impact would be expected in the harder spectrum of the GCFR. The committee concluded that "heterogeneity effects are not sufficient to impact on scoping studies" (K3). The effect is small due to the fact that the mean free path of resonance energy neutrons is about 15 mm, which is approximately twice the pin diameter.

The infinite medium assumption has been shown by Saidi (S3) to be sound by both experiment and analysis. He showed that interfacial effects in fast breeder reactor media are important only in the first three or so centimeters on either side of the interface. In the present work the

performance assessments will be based on the average behavior of zones one or more assemblies in radial extent, and much longer in axial extent.

Finally, assumptions as to the average temperatures had to be made. It was assumed that the fuel pellets were at 1300°K and all other materials were at 800°K for all the analyses except the Doppler calculations. This clearly does not allow for the fact that blanket assemblies are over-cooled at the start of life. The resulting error, however, is quite small, since the one group capture cross section for U-238 varies only 3.9% between 1300°K and 600°K, which is much larger than the expected variation in the mean fuel or blanket assembly temperatures over a burnup cycle.

2.2.2.2 The Group Collapse

Once the fifty group resonance self shielded cross sections are known, it is desirable to reduce the data to fewer energy groups. This is done in SPHINX by use of a one dimensional diffusion calculation of the reactor under consideration. Regionwise fluxes from this calculation are used to collapse the cross sections. Although the collapsing of the cross sections is straightforward, some key decisions must be made. First, the correct broad group structure must be selected so as to minimize future computational effort without loss of significant detail. For this work the group structure used for design work by General Atomic was selected. Table 2.1 shows the energy boundaries. Second,

Table 2.1
Neutron Energy Group Boundaries
for Ten Group Design Level Cross Section Sets

Group	Upper Energy Boundary	Groups Condensed from 50 Group Set
1	15.0 MeV	3
2	3.6788 MeV	2
3	1.3534 MeV	2
4	497.87 KeV	4
5	183.16 KeV	4
6	67.379 KeV	4
7	24.788 KeV	4
8	9.1188 KeV	4
9	3.3546 KeV	8
10	0.454 KeV	15
Lowest Energy	0.00001 eV	

the number of collapsed sets and the spectra used for each collapse must be selected. Clearly the two choices are related since using very few energy groups would require the use of more cross section sets. The General Atomic group structure used here has a generous ten energy groups, so that relatively few cross section sets are required.

All the collapsing spectra used in this work came from a one-dimensional radial traverse through the center of a homogeneous GCFR. Figure 2.1 shows the model used for this purpose in SPHINX (this same model was run twice: once at the nominal temperatures and once at the lower temperatures to obtain the cross sections for Doppler calculations). Table 2.2 lists the various types of assemblies which were employed in the present investigation and the spectrum over which their cross sections were collapsed.

With the reduction of data must come some added error in the analysis (unless all the cores analyzed are identical to the model used for the collapse). Of particular concern is the use of the first row radial blanket flux to collapse the cross sections for the internal blanket assemblies. In order to investigate this concern the fifty group flux at the first mesh point (of the five used for the collapse) in the first row of the radial blanket was used to collapse σ_c of U-238 and σ_f at Pu-239 to one group. These were then compared to the collapsed one group cross sections that would be obtained if the average flux over all five mesh points in the first row

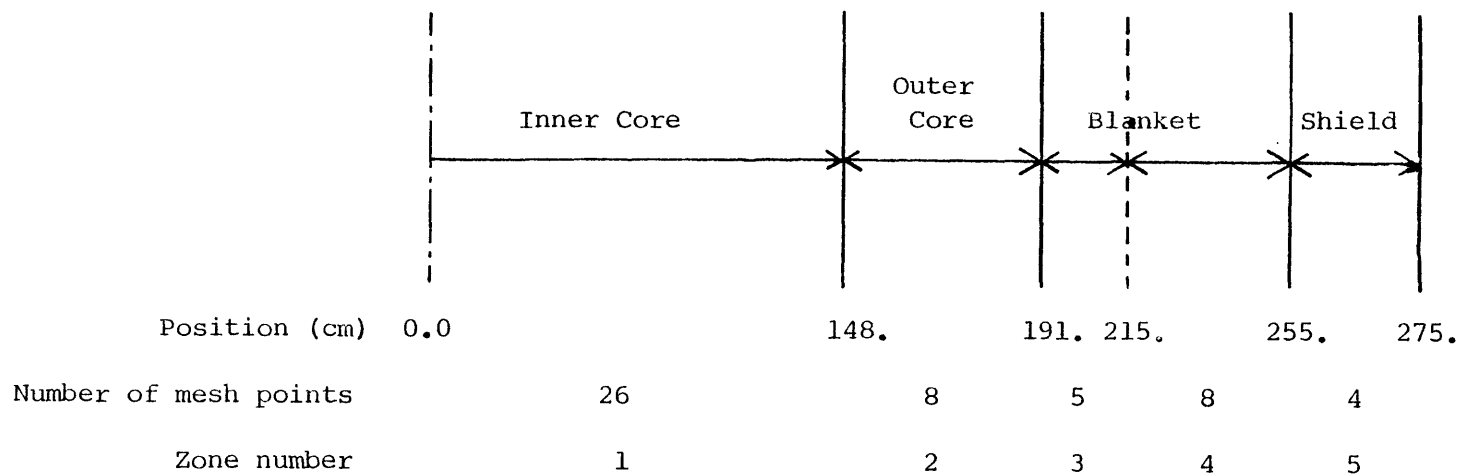


Fig. 2.1 ONE-DIMENSIONAL RADIAL MODEL OF A GCFR USED FOR SPHINX GROUP-CONDENSATION

Table 2.2
Collapsing Spectrum Employed as a Function of
Assembly Type

Type of Assembly	Collapsing Spectrum	Zone Number (in Fig. 2.1)
Homogeneous Core Zone 1	Inner Core	1
Homogeneous Core Zone 2	Inner Core	1
Homogeneous Core Zone 3	Inner Core	1
Control Assemblies	Outer Core	2
Heterogeneous Core Zone 1	Outer Core	2
Heterogeneous Core Zone 2	Outer Core	2
1st Row Radial Blanket	1st Row Radial Blanket	3
Internal Blanket	1st Row Radial Blanket	3
2nd and 3rd Row Radial Blanket	2nd & 3rd Row Radial Blanket	4
Radial Shield	Radial Shield	5
Axial Shield	Radial Shield	5
Axial Blanket	1st Row Radial Blanket	3

of the radial blanket was used instead. The difference was found to be less than 0.2% for the U-238 capture and 0.3% for the Pu-239 fission cross sections. Therefore, it is believed that the harder spectrum seen by an internal blanket should be handled well by this set. Of lesser concern are potential problems due to the fact that some core designs will have a higher or lower enrichment than the core used for the group collapse. To assess the magnitude of this problem one group cross sections collapsed from the fifty group flux in the inner core were compared to the one group cross sections derived from collapsing the outer core ten group cross sections in the same flux. This time the microscopic capture cross section for U-238 changed by only 0.12% and the microscopic fission cross section for Pu-239 changed even less: 0.06%. From this it is concluded that the error introduced by varying enrichment in the design calculations is negligible.

The error due to the group collapsing was kept small by keeping more "fast" groups (where most of the flux and neutron reactions occur in a GCFR) and condensing mainly the lower energy groups. Table 2.1 shows how many of the original fifty groups are contained in each of the collapsed ten groups. For this reason, whenever the spectrum is hard, as in the core and internal blankets, the error due to the group collapse is quite small. The largest error is actually at the blanket/reflector interface. Here the spectrum averaged over the second and third rows of radial blanket is not soft enough, and

an error of as much as 41% for σ_f for Pu-239 occurs. This, however, is not of concern since this is a very low power (and low neutronic worth) position. Further, if enough plutonium could be built up there to make this a higher power position the spectrum would no longer be as soft and the error would be less.

The final concern is now easy to address. Only beginning-of-cycle-one (BOC1) (i.e.: clean core) cross sections are used for this work. One may then wonder if this is adequate for later on in the cycle. As the cycle proceeds all the spectra get harder due to the fission product poisoning in the core and the buildup of plutonium in the blankets. It is clear that the error is small since the ten group set has a large number of fast groups, and the relative importance of the epithermal groups will diminish. The core/blanket interface error previously cited is probably a good indicator of the error expected in the blankets later on in the cycle. The enrichment sensitivity analysis also suggests that the error in the core assemblies will be small.

To summarize the investigation into the errors due to group collapsing, Table 2.3 is presented. As a rule of thumb roughly a 1% decrease in σ_f for Pu-239 would yield 0.5% decrease in k_{eff} and a 1% decrease in σ_c for U-238 would yield a 0.5% increase in k_{eff} . These rules of thumb are only applicable if they refer to the core averaged values. Clearly, since decreasing the cross sections of Pu-239 and U-238 produce opposing effects on k_{eff} many errors (such as

Table 2.3

Errors Introduced by Group Condensation

One Group Cross Section Comparisons

<u>Case Examined</u>	<u>U-238 σ_c</u>			<u>Pu-239 σ_f</u>		
	<u>Used</u>	<u>Actual</u>	<u>% Error</u>	<u>Used</u>	<u>Actual</u>	<u>% Error</u>
<u>Blanket Assemblies</u>						
Core/Blanket Interface	0.277	0.277	<0.2%	1.785	1.780	0.3%
Blanket/Reflector Interface	0.66	0.68	3.0%	5.04	7.13	41.0%
<u>Core Assemblies</u>						
Core/Blanket Interfaces	0.250	0.251	0.4%	1.725	1.729	0.2%
Use of the Outer Core σ Set for the Inner Core	0.249	0.249*	<0.2%	1.719	1.720*	<0.1%

*All other values in this column show an actual error. This value shows the error if the inner core spectrum was miscalculated and was as hard as the outer core spectrum. Such an error is not expected.

an error in the neutron energy spectrum)are self-compensatory.

2.2.3 Fission Product Cross Sections

Although there are fission product cross sections in LIB-IV they are not suitable for fast reactor analysis. The fission products in LIB-IV are from a 1966 evaluation made for thermal reactors (W3). No downscattering matrix is included with the LIB-IV fission products. Because of this, another set of lumped fission product cross sections was employed. The Japanese Nuclear Data Committee recently evaluated and reported a 70 energy group set of lumped fission products for fast reactor analysis (K2). Their compilation was re-worked for present purposes.

Since the Japanese set has a seventy group structure, as shown in Table 2.4, which does not match the fifty group structure of LIB-IV, also shown in Table 2.4, a program was written to convert the Japanese set into the fifty group structure of LIB-IV. To do this the flux shape was assumed to be the same as used by the Japanese in developing their seventy group constants: i.e., a fission spectrum down to 1 MeV, followed by a 1/E spectrum. Once the data was in a fifty group format the fission product cross sections were further collapsed to ten groups using the fifty group regionwise fluxes calculated by SPHINX, as already described for the LIB-IV nuclides.

In order to keep the number of fission product cross section sets used to a minimum, some assumptions were made. First, it was decided that the Pu-239 fission products would

Table 2.4

Energy Boundaries for the Japanese
Fission Products and for LIB-IV Cross Sections

<u>Japanese Group Structure</u>				<u>LIB-IV Group Structure</u>	
<u>Group number</u>	<u>Upper energy (eV)</u>	<u>Group number</u>	<u>Upper energy (eV)</u>	<u>Group number</u>	<u>Upper energy (eV)</u>
1	1.05 +7	36	1.66 +3	01	1.5000E+07
2	8.30 +6	37	1.29 +3	02	1.0000E+07
3	6.50 +6	38	1.00 +3	03	6.0653E+06
4	5.10 +6	39	7.73 +2	04	3.6788E+06
5	4.00 +6	40	5.98 +2	05	2.2313E+06
6	3.10 +6	41	4.65 +2	06	1.3534E+06
7	2.50 +6	42	3.60 +2	07	8.2085E+05
8	1.90 +6	43	2.78 +2	08	4.9787E+05
9	1.40 +6	44	2.15 +2	09	3.6774E+05
10	1.10 +6	45	1.66 +2	10	3.0197E+05
11	8.00 +5	46	1.29 +2	11	2.3518E+05
12	6.30 +5	47	1.00 +2	12	1.8316E+05
13	5.00 +5	48	7.73 +1	13	1.4264E+05
14	4.00 +5	49	5.98 +1	14	1.1109E+05
15	3.10 +5	50	4.65 +1	15	9.6517E+04
16	2.50 +5	51	3.60 +1	16	6.7379E+04
17	2.00 +5	52	2.78 +1	17	5.2475E+04
18	1.50 +5	53	2.15 +1	18	4.0868E+04
19	1.20 +5	54	1.66 +1	19	3.1828E+04
20	1.00 +5	55	1.29 +1	20	2.4788E+04
21	7.73 +4	56	1.00 +1	21	1.9305E+04
22	5.98 +4	57	7.73	22	1.5034E+04
23	4.65 +4	58	5.98	23	1.1709E+04
24	3.60 +4	59	4.65	24	9.1188E+03
25	2.78 +4	60	3.60	25	7.1017E+03
26	2.15 +4	61	2.78	26	5.5308E+03
27	1.66 +4	62	2.15	27	4.3074E+03
28	1.29 +4	63	1.66	28	3.3546E+03
29	1.00 +4	64	1.29	29	2.6126E+03
30	7.73 +3	65	1.00	30	2.0347E+03
31	5.98 +3	66	7.73 -1	31	1.5846E+03
32	4.65 +3	67	5.98 -1	32	1.2341E+03
33	3.60 +3	68	4.65 -1	33	9.6112E+02
34	2.78 +3	69	3.60 -1	34	7.4852E+02
35	2.15 +3	70	2.78 -1	35	5.8295E+02
				36	4.5400E+02
				37	3.5358E+02
				38	2.7536E+02
				39	1.6702E+02
				40	1.0130E+02
				41	6.1442E+01

Lowest energy 0.215

Table 2.4 (Cont'd.)

Energy Boundaries for the Japanese
Fission Products and for LIB-IV Cross Sections

LIB-IV Group Structure

<u>Group Number</u>	<u>Upper energy (eV)</u>
42	3.7267E+01
43	2.2603E+01
44	1.3710E+01
45	8.3153E+00
46	5.0435E+00
47	3.0590E+00
48	1.8554E+00
49	1.1254E+00
50	6.8256E-01

Lowest energy 1.0E-5

be used for all fissions. The U-238 lumped fission product cross section (σ_a) differs by less than 5% from that for the Pu-239 fission products when collapsed to one group (K2). This difference is quite small when one considers the large discrepancy among different parent cross section sets for fission products from the same fissile nuclide. Hence, using only the Pu-239 fission product cross section is quite satisfactory. Second, although the fission product cross sections vary with time, only one time-independent set was used. After the first 60 days the variation in their effective one group cross section is less than 10% (K2). For that reason the fission product cross sections for a core burned for 360 days by the Japanese were selected with confidence. A 1.5 year burnup (or 384 full power days if a capacity factor of 70% is used) is the average burnup of a three batch annual-reload core. The 360-day-burn results reported by the Japanese were the closest available to the 384-day-burn cross sections needed here.

2.2.4 Summary Remarks on the Adequacy of the Cross Section Treatment

Thus far in the discussion of the cross section treatment the only comparisons made have been among alternative approaches, but with the same initial cross section file and the same computer codes. Since the cross section library, LIB-IV and the computer code, SPHINX, are widely used, a comparison of the techniques used here to those in other organizations is

available (H2). Furthermore, critical experiments have been examined using the same techniques used in this work. With this data an absolute indication of error is possible. Since the critical experiment analyses require the use of other codes in addition to the cross section processing codes they will be discussed in the last section of this chapter.

To compare results from various laboratories, ERDA/DØE formed a number of working committees. One of these working committees had the task of evaluating cross section processing codes. The committee decided to analyze the ZPR-6 Assembly 7 benchmark critical. This critical assembly is a simple single core zone representation of a plutonium fueled homogeneous LMFBR (T8). Table 2.5 shows the results submitted by the participants. Note that the technique used by WARD and ORNL is the technique used in the present work. The VIM analysis in Table 2.5 is a Monte Carlo analysis based on the ENDF data, and therefore is relatively free of any processing error. As can be seen from the table, k_{∞} is over-predicted when compared to the Monte Carlo calculation by roughly 0.5%. Table 2.6 is included to illustrate the group-wise error with the MINX/SPHINX technique. Again the WARD values represent the technique used in this work. As can be seen, much larger errors occur at the lower energies. This is acceptable for the present work due to the small number of neutrons at these low energies in a GCFR.

It is not possible to investigate all errors that may have

Table 2.5

Comparison of Intra-Laboratory Integral Parameter Results (H2)

$B^2 = 0$	ANL		LASL		GA	ORNL *	ARD *	BNL	CE
	VIM	MC ² -2	MINX/1DX	ETOX/1DX	GCC-5	MINX/SPHINX	MINX/SPINX	MINX/1DX	MINX/TDOWN
	(7/30/75)	(3/31/77)	(1/13/76)	(10/23/75)	(12/4/75)	(4/15/77)	(10/23/75)	(10/23/75)	(12/13/76)
k_{∞}	1.2100 ± .0011	1.2096	1.2144	1.2162	1.2132	1.2150	1.2146	1.2167	1.2150
f^{28}/f^{49}	.01951 ± .00013	.01941	.01976	-	.01950	0.01956	.01951	-	.02022
c^{28}/f^{49}	.1666 ± .0002	.1666	.1656	-	.1641	0.1644	.1632	-	.1660
f^{25}/f^{49}	1.128 ± .001	1.128	1.128	-	1.119	1.129	1.124	-	1.126
$B = 7.3 \times 10^{-4}$	P_1	B_1							
k	1.0028	1.0040	-	-	1.0174	-	-	-	1.0060
f^{28}/f^{49}	.02259	.02258	-	-	.02244	-	-	-	.02348
c^{28}/f^{49}	.1585	.1585	-	-	.1573	-	-	-	.1581
f^{25}/f^{49}	1.095	1.095	-	-	1.091	-	-	-	1.093

*These two laboratories used the same procedures as in the present work.

Table 2.6

Neutron Spectrum Comparison from CSEWG Problem 1:

ZPR-6-7 Infinite Homogeneous Medium Flux (Normalized to 1.0) (H2)

GROUP	ENERGY	VIM	HC**2-2/VIM	LASL/VIM	GE/VIM	ARD/VIM *
1	1.0000E+07	2.1852E-03 (2.700%)	1.044	1.122	1.139	1.018
2	6.0653E+06	9.5430E-03 (1.440%)	0.990	1.026	0.951	1.024
3	3.6788E+06	2.4712E-02 (1.170%)	0.991	0.960	1.036	0.964
4	2.2313E+06	3.6507E-02 (0.832%)	0.998	0.997	1.020	0.974
5	1.3534E+06	4.6067E-02 (0.869%)	1.008	1.024	0.724	1.118
6	8.2085E+05	8.6710E-02 (0.575%)	0.997	1.000	1.286	1.009
7	4.9787E+05	8.2494E-02 (0.424%)	1.002	0.951	0.944	0.980
8	3.0197E+05	1.0368E-01 (0.374%)	0.998	1.015	0.993	1.034
9	1.8316E+05	1.1237E-01 (0.288%)	0.999	0.990	0.922	0.992
10	1.1109E+05	1.0219E-01 (0.268%)	0.997	1.010	1.063	1.005
11	6.7300E+04	8.7938E-02 (0.279%)	0.998	1.012	0.903	0.996
12	4.0868E+04	7.0499E-02 (0.280%)	1.007	0.982	1.146	0.969
13	2.4788E+04	7.3097E-02 (0.294%)	0.996	1.026	0.931	1.006
14	1.5034E+04	5.5023E-02 (0.312%)	0.999	0.982	0.926	0.958
15	9.1108E+03	3.1203E-02 (0.297%)	1.002	1.030	1.035	0.999
16	5.5308E+03	1.9727E-02 (0.323%)	1.005	0.988	0.953	0.958
17	3.3546E+03	7.1516E-03 (0.357%)	1.004	0.981	1.328	0.950
18	2.0347E+03	2.1214E-02 (0.283%)	1.006	1.013	0.982	0.976
19	1.2341E+03	1.4138E-02 (0.394%)	1.009	1.007	0.995	0.968
20	7.4852E+02	7.9696E-03 (0.540%)	1.010	1.010	0.963	0.968
21	4.5400E+02	3.3893E-03 (0.718%)	1.019	1.027	0.966	0.987
22	2.7536E+02	1.5157E-03 (0.848%)	1.023	1.110	0.957	1.064
23	1.6702E+02	5.3939E-04 (1.240%)	1.019	1.086	0.775	1.062
24	1.0130E+02	1.1817E-04 (2.180%)	1.062	1.228	1.301	1.209
25	6.1442E+01	1.5105E-05 (6.220%)	1.178	2.146	2.128	2.131
26	3.7267E+01	3.1115E-06 (12.600%)	1.016	4.463	5.531	4.531
27	2.2603E+01	7.1989E-07 (28.000%)	0.666	3.482	4.483	2.906

*The same technique as that used in the present work.

been introduced by approximations in the cross section treatment. Specific concerns have been addressed, and all the errors identified seem tolerably small. An overall check is provided by the Monte Carlo code, and here too it appears that the errors are reasonable. The ultimate check is the comparison to experiment, but then there are many more errors involved than those which come solely from the cross section treatment. Hence, this comparison is deferred until the entire code package is discussed.

2.3 Description of the Computer Codes Used

Three major computer codes were used in the remainder of the present work. Small editing programs were also used, but they will be described when the need occurs. The three major codes are:

- 1) CALIØP : a scoping code for core optimization,
- 2) 2DB : a two-dimensional diffusion theory code with burnup capability, and
- 3) PERT-V : an editing code for the calculation of material worths using perturbation theory.

A description of these codes follows.

2.3.1 CALIØP

CALIØP is a multichannel design code for GCFRs (T5). Its major application is in quick design iterations. The code runs in under thirty seconds CPU time on a Univac 1108. In that time it sizes the fuel pin, lattice pitch and core length, finds the enrichments by zone, calculates the breeding ratio

and doubling time for the equilibrium core, and, finally, costs the fuel cycle. CALIØP has been a constantly evolving code which started with a single channel thermal-hydraulic code called GAZELLE (F2) combined with a one-group two-dimensional diffusion theory subroutine, VFRAC (D4). As time progressed more and more complexity has been added to CALIØP, and still more complexity is being added at the present time. For that reason CALIØP does not have published documentation and is not being widely distributed.

CALIØP is a complicated coupled neutronic/thermal-hydraulic code with many optional ways of progressing through a calculation. For this work only three different types of CALIØP problems were run. They were:

- 1) For a fixed geometry, to calculate the effect of small perturbations, i.e.: changing the number of grid spacers, lowering the inlet temperature, or increasing the theoretical density of the fuel,
- 2) To find the pitch, core length, mixed mean outlet temperature, and pumping power when the peak KW/ft and the maximum clad temperature are given,
- 3) For a given pumping power, mixed mean outlet temperature, and maximum clad temperature, to calculate the core length, pitch, and peak KW/ft.

CALIØPs neutronic calculations are done using one energy group. For a fast reactor such as a GCFR this causes errors due to the significant consequences of spectral changes. To account for some of the spectral change effects, the one group uranium and plutonium cross sections are made enrichment

dependent. It is possible to input successive one group cross sections into CALIØP so that, as reactor designs change, the one group cross section error can be held to a minimum. Due to the combined effect of this, and other less important approximations, the error in doubling time has been as large as 30% when CALIØP results are compared to higher-order calculations. Most of the time the error is less than 10%. This error should not be viewed as statistical, but as a bias which is heavily dependent on how far a given case is from one which has been renormalized against a higher-order calculation.

The thermal-hydraulic calculations in CALIØP are fairly straightforward, since the calculations include no subchannel mixing and are only for the steady state. The reactor is assumed to be divided into a number of concentric rings of fuel. Each ring is treated as a single pin with helium flowing around it. The radial blanket analysis is done separately. For a fixed geometry problem the mass flow rate is varied to match the maximum permissible clad temperature, and the outlet temperature and the pumping power are determined as a result. A fixed geometry problem could also be run where the outlet temperature is given; then the mass flow rate and pumping power are known, so that the maximum clad temperature is the key output.

Calculations of non-fixed geometries are somewhat more difficult. For these cases the channel power, pressure drop and the maximum clad temperatures are always known. The

calculations always assume ideal orificing (i.e.: the ΔT across each channel is the same), so only the peak power channel need be calculated. When designing the core to its materials' limits, the peak KW/ft is also known. From this the core length is determined, since the power of the channel and the pins per channel are known. A pitch is assumed and the mass flow rate to yield the given pressure drop is determined. With this the maximum clad temperature is determined. If the maximum clad temperature is not the input value the pitch is varied until a match is obtained.

Since GCFRs require large, high power circulators, restrictions on their sizes are sometimes necessary [M3]. This requires implementation of the third type of problem in CALIØP. This time the pressure drop and mass flow rate (which determine the circulator power) are known. Since the power per channel is known, the ΔT is also known. For a given pitch the length of core to give the pre-selected ΔP can be calculated. This allows the maximum clad temperature to be calculated and compared to the input value. If they are not the same the pitch is varied as before until agreement is obtained.

With the neutronics and thermal-hydraulics established the calculation of fuel cycle costs is an easy additional step. A code is being developed at this time by General Atomic that uses CALIØP and adds cost estimates for changes in the plant apparatus necessary to accommodate the design changes. This code is called SOFAST.

CALIØP is used in the present work for the thermal hydraulic design of assemblies and to determine which pin diameter yields the optimum performance for the homogeneous core. All other results generated by CALIØP were considered too crude for the present work.

2.3.2 2DB

2DB is a multigroup two dimensional diffusion theory code with burnup capability. It can solve problems with R-Z, X-Y, R- θ , and triangular (hexagonal) geometries. It solves for k_{eff} or performs criticality searches on buckling, time absorption, reactor composition or reactor dimensions. Both the forward and the adjoint solutions can be obtained. Further, 2DB can compute flux distributions from an arbitrary fixed source. The burnup equations allow for any number of isotopes and any burnup chain. The code is widely distributed, heavily used, and well documented (L2).

Although 2DB is a flexible tool, a number of labs such as BNL, CE, WARD, and GA, have found it desirable to change the code slightly. Such code changes are generally proprietary, so that each lab has done its changes independently. For this work it was decided to change 2DB in a fashion similar to some of these prior changes; however, this work is not proprietary so that a complete listing of the changes from the nationally-available 2DB version is included in Appendix A. None of the changes were particularly difficult but are very helpful to the user. The changes were:

- 1) 30° symmetry for triangular problems was added. Before this change the only symmetry possible was 90° symmetry; 60° or 120° symmetry is still not coded, since it was of no use to the present work, but the additional effort is trivial.
- 2) For composition searches an array of search parameters was added to the input requirements. This change in the input method for search calculations allows for easier input, and further allows for search calculations to be directly followed by burnup calculations.
- 3) A total inventory edit was added. The sum of the total kilograms of each isotope in the reactor is given. Before this change only a zone-wise edit existed. This allows for quicker mass flow calculations and simplifies doubling time calculations.

These changes are discussed in greater detail along with the actual coding in Appendix A.

2.3.3 PERT-V

PERT-V is a two-dimensional perturbation theory code. It calculates reactivity coefficient traverses, the effective delayed neutron fraction, the neutron generation time, and activity traverses using the flux and adjoint from 2DB. As with 2DB, PERT-V is widely distributed, heavily used, and well documented [H3].

Just as with 2DB, PERT-V has been modified by many of its users. For this work PERT-V was modified in a similar manner. The modifications made were:

- 1) A leakage and buckling edit by zone was added. This edit gives added insight to reactor design and makes possible zonewise buckling for hexagonal 2DB calculations.
- 2) A zone-wise calculation of reactivities was added. The present nationally available version of PERT-V contains only reactivity traverse calculations.
- 3) A differencing approach to obtain the cross section perturbation was applied. This allows one to calculate the worth of substituting a new macro cross section for an original macro in the reactor model.

These modifications are discussed in greater detail in Appendix B along with the actual coding of the changes.

2.4 Summary

In this chapter the neutronic data base and its treatment have been presented. This was followed by a brief abstract of the large computer codes used and the modifications made to these codes. The implicit and explicit assumptions in the cross section treatment, and estimates of the magnitude of the errors resulting from these assumptions have been presented. A more detailed overall error analysis was deferred because many more assumptions will be made in the chapters which follow.

The procedures used for analysis in this work follow most closely the codes and procedures used by Westinghouse Advanced Reactor Division (WARD) for the CRBR. No separate criticals analysis was done for the present work; we instead relied on the criticals verification of the WARD CRBR analysis.

A review of this verification was recently published (D3) and Tables 2.7 to 2.10 are included, which were taken directly from that paper. A criticals analysis was also performed by General Atomic (GA) on GCFR mockups with correspondingly good results (H5). The GA results add considerable confidence, but their cross section treatment was different than that used in the present work. Further, the GCFR criticals were all homogeneous cores.

In conclusion, the methods used for analysis in this work rely heavily on the techniques used at WARD and/or GA, both of which have been well-benchmarked. Furthermore, the present work is to be a consistently executed comparative study, so that even some consistent bias would be tolerable.

The overall computation path used in this work is shown in Fig. 2.2.

Table 2.7

Reactor Design Areas Supported by Critical Experiments
for CRBR (D3)

<u>POWER REACTOR DESIGN PARAMETER</u>	<u>CRITICAL EXPERIMENT DATA SOURCE</u>
1) Fuel Enrichment, k_{eff}	Critical Fuel Loading, Doppler and Core Expansion Worth, Core Conversion Ratio
2) Power Distribution	Isotopic Fission and Capture Rate Distributions, Gamma Heating, Blanket Spiking Studies
3) Control Rod Margin	Control Rod Subcritical Reactivity Worth
4) Reactivity Coefficient	
Doppler	Small Heated-Sample U^{238} Doppler Worth
Sodium Void	Large Zone-Voiding Reactivity Worth
Core Restraint (expansion)	Small-Sample Worth Distributions, Sector Expansion Worth
CDA-related	Sodium Void Worth, Fuel and Steel Slumping Worth
5) Miscellaneous Performance Characteristics	
Breeding Ratio	C^{238}/F^{239}
Temperature Defect, Power Coefficient	Doppler Worth, Core Expansion Worth
Ex-Core Detector Capability	Control Rod Worth Measurements with Ex-Core Detectors
Fast Flux/Fluence	Neutron Energy Spectrum, Spectral Indices

Table 2.8

ZPPR Criticality Predicted by CRBRP Design Methods (D3)

<u>HOMOGENEOUS: ZPPR-4</u>			<u>HETEROGENEOUS: ZPPR-7</u>				
	<u>Measured k_{eff}</u>	<u>Calculated k_{eff}</u>	<u>C/E</u>		<u>Measured k_{eff}</u>	<u>Calculated k_{eff}</u>	<u>C/E</u>
ZPPR-4/1	1.00080	0.99740	0.9966	ZPPR-7A	1.00028	0.99019	0.9899
ZPPR-4/2	1.00065	0.99899	0.9983	ZPPR-7B	1.00064	0.98924	0.9886
ZPPR-4/3	1.00088	0.99885	0.9981	ZPPR-7C	1.00002	0.99089	0.9909
ZPPR-4/4	1.00083	0.99674	0.9959	ZPPR-7D	1.00001	0.99347	0.9935
		mean C/E = 0.9972		ZPPR-7F	1.00058	0.98873	0.9882
		$1\sigma = \pm 0.12\% \Delta k$		ZPPR-7G	1.00053	0.98858	0.9881
						mean C/E = 0.9899	
						$1\sigma = \pm 0.21\% \Delta k$	

Table 2.9

ZPPR* Reaction Rate Summary (D3)

	REGION	NUMBER OF DATA POINTS	NORMALIZATION	MEAN C/E	RMS DEVIATION
ZPPR-4, Pu ²³⁹ (n,f)	core	245	1.000	0.997	+1.93%
ZPPR-7, Pu ²³⁹ (n,f)	core	106	1.000	1.000	+1.76
ZPPR-7, Pu ²³⁹ (n,f)	inner blankets	66	1.000	1.012	+1.29
ZPPR-4, U ²³⁵ (n,f)	core	234	1.022	0.989	+2.10
ZPPR-7, U ²³⁵ (n,f)	core	173	1.040	1.000	+1.56
ZPPR-7, U ²³⁵ (n,f)	inner blankets	93	1.040	1.001	+1.70
ZPPR-4, U ²³⁸ (n,f)	core	289	0.938	0.997	+5.50
ZPPR-7, U ²³⁸ (n,f)	core	148	0.832	1.002	+4.08
ZPPR-7, U ²³⁸ (n,f)	inner blankets	92	0.832	1.131	+4.93
ZPPR-4, U ²³⁸ (n,γ)	core	291	1.057	1.001	+1.90
ZPPR-7, U ²³⁸ (n,γ)	core	148	1.097	1.002	+2.56
ZPPR-7, U ²³⁸ (n,γ)	inner blankets	92	1.097	0.994	+1.75
ZPPR-4 Gamma Heating	core	32	unnormalized		+10%*
ZPPR-7 Gamma Heating	core and inner blankets	18	unnormalized		+10%*

*ZPPR-4 phases 1-4, ZPPR-7 phase A-E

*uncertainty estimated from scatter in preliminary data. No statistical significance implied.

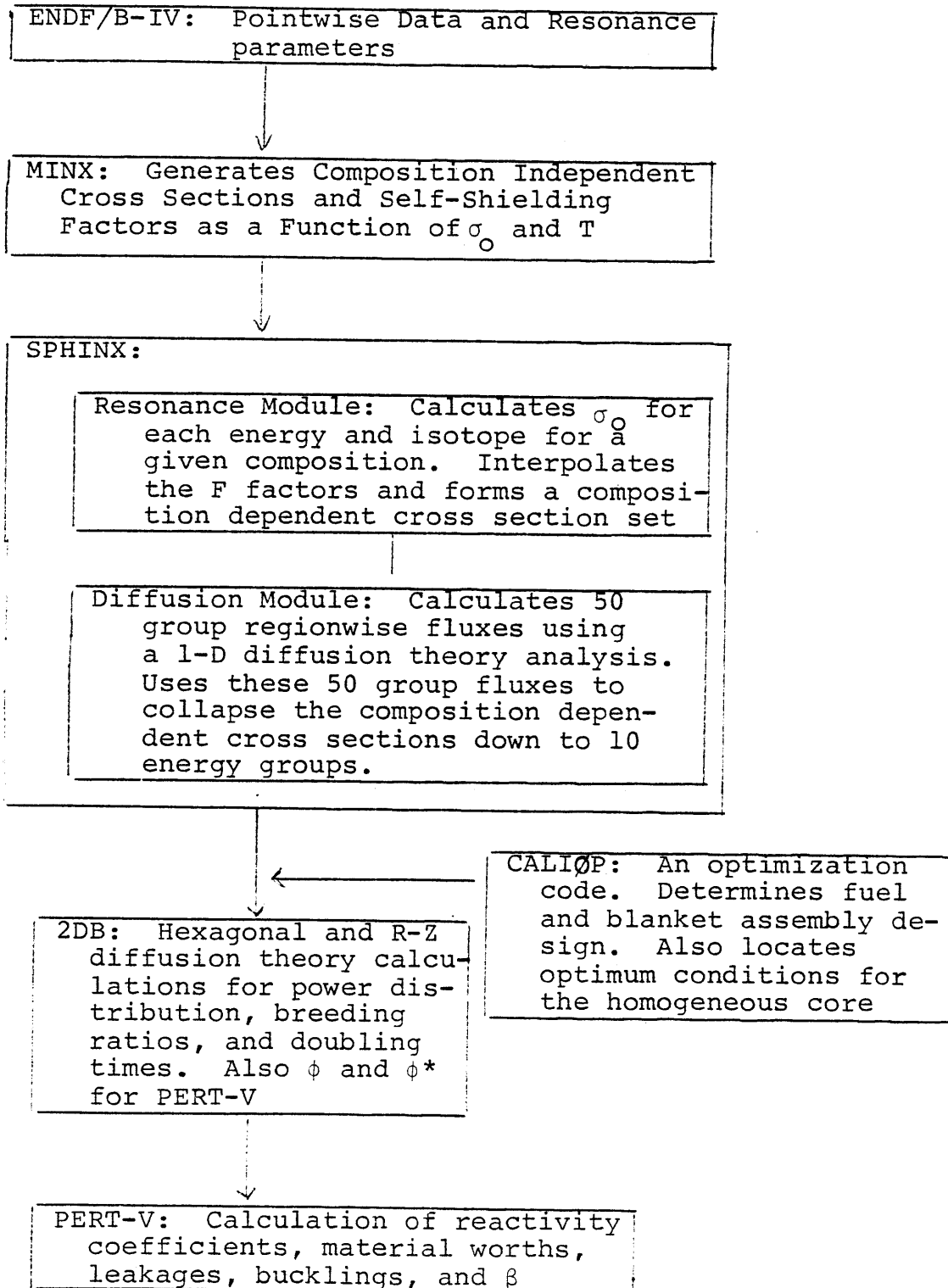
Table 2.10

ZPPR Control Rod Worth Calculation-to-Experiment Ratios (D3)

ZPPR-4, Phases 1-4 (Homogeneous)		ZPPR-7 (Heterogeneous)	
	C/E	Beginning-of-Life, Phase B C/E	End-of-Life, Phase C C/E
central rod	0.973		
row 4	0.977	row 4 0.916 (0.965)*	0.906 (0.973)
row 7 flat (or C+R7F)	0.981	row 7 flat 0.899 (0.987)	0.940
row 7 corner (or C+R7C)	0.995	row 7 corner 0.990 (1.074)	0.905 (0.987)

*values in () from 4-mesh-per-drawer diffusion calculations.

Figure 2.2
Computational Path Employed in the Present Work



CHAPTER 3

HOMOGENEOUS CORE ANALYSIS

3.1 Introduction

For a meaningful comparison of heterogeneous and homogeneous core designs, both should be equally well optimized. In this chapter the optimization and detailed analysis of the homogeneous core design are presented. The ground rules and constraints established in this chapter are used for both the homogeneous and the heterogeneous designs. Also, since many of the analytic techniques are the same for both core designs this chapter contains most of the discussion of the analytical methods used.

The chapter begins by presenting the parameters that will be regarded as independent of the heterogeneous-to-homogeneous design comparison. This subsection starts with a description of the overall design of the GCFR, followed by a presentation of the thermal-hydraulic constraints on assembly design. The set of assembly designs thereby established are then considered to be applicable, independent of the homogeneous-to-heterogeneous design comparison. The "optimum" homogeneous design is then taken to be the core using the best performing assembly from among the thermally and hydraulically constrained designs. Similarly, the "optimum" heterogeneous core is the most favorable

combination of acceptable fuel and internal blanket assembly designs.

The chapter proceeds to determine the optimum homogeneous design and explains the effects leading to an optimum. With the optimum core characteristics selected, the detailed analysis begins. It starts with a description of the fuel management scheme and the method used to establish an equilibrium core. With the equilibrium core modeled, a series of short sections presents the analysis techniques and the results for the mass flows and doubling time, power distributions, flux and fluence distributions, β_{eff} calculations, Doppler reactivity calculations, control rod requirements and worths, and material worths (fuel, clad, and helium). Finally, the chapter is summarized by a short discussion of the viability of the overall design.

3.2 Parameters Independent of the Homogeneous to Heterogeneous Design Comparison

In order for the homogeneous versus heterogeneous design comparison to be valid both cores must have viable thermal-hydraulic designs. This section will first describe the basic GCFR design selected for the present work. It will then discuss constrained fuel assembly design. Using the constraints established from this review, a series of viable assembly designs for fuel pin diameters ranging from 6 mm to 11 mm will be presented. Blanket assembly designs will also

be discussed and presented. The selection of the optimum homogeneous design will be limited to the selection of the best of the viable assembly designs. The selection of the optimum heterogeneous design will consist of finding the best arrangement (interspersed core layout) of viable fuel and blanket assemblies.

3.2.1 Basic GCFR Design Selection

The GCFR has been investigated since 1962, but the funding levels have always been low compared to those of the LMFBR. For this reason major design changes are still under consideration (S4). Consequently, the selection of a reference GCFR for the homogeneous-to-heterogeneous comparison was a non-trivial exercise, which therefore requires discussion.

In a GCFR the peak clad temperature is a major limiting criteria due to the modest heat transfer properties of helium relative to liquid coolants. However, if the prestressed concrete reactor vessel (PCRv) is sufficiently robust to allow a high operating pressure and/or the circulator power is sufficiently high to develop high coolant flow rates then the attainable heat transfer can allow the fuel (PuO_2/UO_2) to reach its maximum tolerable rating, KW/ft, when the clad reaches its maximum permissible temperature. A GCFR having these characteristics is within the realm of state-of-the-art technology, and thus will be used in the present work (T7, M4). It should be noted that a design of this type is non-conservative in some

respects, and has recently lost favor in some quarters (M3). The fundamental economic assumption underlying selection of this advanced core is that better neutronics can pay for the increased price of the PCRV and circulators. This aspect has been studied and it was found that the neutronic payoff and the increase in capital costs were fairly evenly balanced (M4). The present work deals mainly in neutronics, and it was desired that the thermal/hydraulic influence be kept subordinate. For that reason an aggressive core design has been selected. (The true benefits of this selection will not be apparent until Chapter IV.) The main consequence of this decision is that each fuel assembly design (for all pin diameters: 6 to 11 mm) meets the same KW/ft and peak clad temperature limits.

The key characteristics of the GCFR used in the present work are shown in Table 3.1. This precise core design is not published elsewhere, but it relies heavily on many other GCFR designs. For items not covered in Table 3.1 check references S4, G3, T6, D5 and G4. Figure 3.1 is included to show the basic primary system component layout, with flow directions indicated.

3.2.2 Constrained Assembly Design

From the neutronic point of view the only values needed from an assembly design are the volume fractions of structure, coolant, and heavy metal oxide, the dimensions of the assembly, and the maximum volumetric heat generation rate allowable.

Table 3.1
Key Characteristics of the GCFR Used in the
Present Work

Thermal Power	3600 MWt
Approximate Net Electrical Power	1200 MW _e
Number of Primary Coolant Loops	6
Main Turbine Steam Temperature	510°C (950°F)
Main Turbine Steam Pressure	132.4 bar (1920 psia)
Primary System Pressure	120. bar (1740 psi)
Primary Helium Circulation Direction	Up through the core
Core Inlet Temperature	302°C (575°F)
Fuel Material	PuO ₂ /UO ₂ mixed oxide
Structural Material for Fuel and Blanket Assemblies	HT-9
Reactivity Control	Fuel assemblies of enriched boron pins
Circulator Drives	Synchronous electric motors
Axial Blanket Length	60 cm each

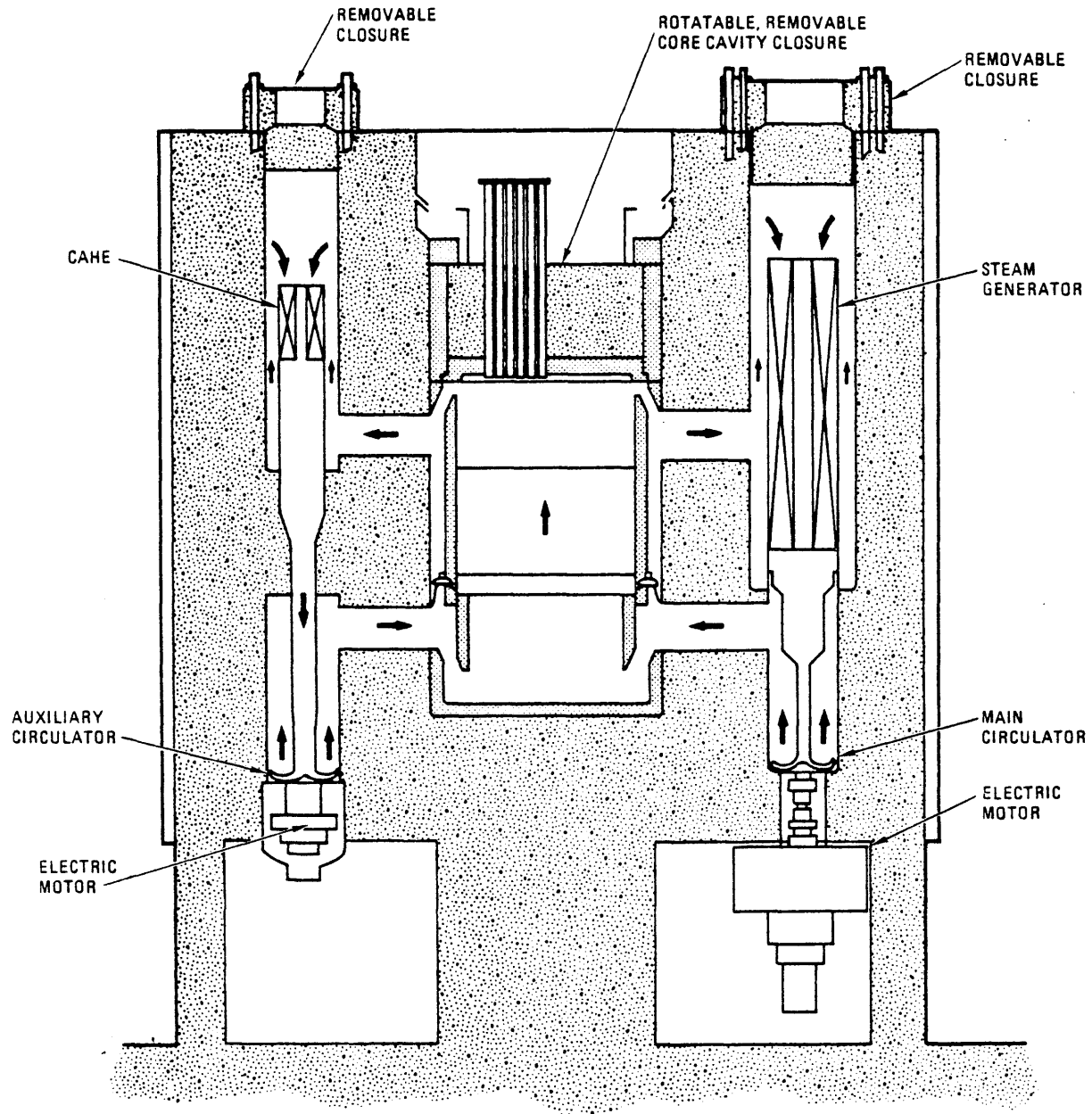


Fig. 3.1 Basic GCFR upflow core configuration (M3)

However, varying these values independent of any additional constraints would show an optimum which would correspond to an unrealistic engineering design. For that reason some thermal-hydraulic constraints must be chosen in order to assure that the optimum design is buildable.

The most obvious constraint is that the geometry of the assembly be maintainable throughout its life: this corresponds to preventing the fuel from melting and the clad from operating at a temperature so high it would lose its strength. In the present work a 15 Kw/ft limit has been set to prevent melting in the fuel and blanket pins. This limit leaves some margin for overpower and uncertainties. The selection of the peak clad temperature is not as clear cut, since the clad failure rate depends on fluence and stress as well as temperature. GA has selected 750°C as their peak clad temperature, and that value has been accepted for this work.

Constraining the clad temperature and the peak Kw/ft is enough to assure that the assembly will not undergo excessive distortion, but this does not insure that the design is buildable and otherwise reasonable. Buildable implies constraints such as a minimum clearance between fuel pins. Normally for a fuel assembly other obvious limits intervene before the "buildable" constraint, such as reasonable pressure drop, so that excessive powers are not consumed in the primary coolant circulators.

Expressing the totality of good engineering practice in a limited number of additional constraints is admittedly expedient. The preferred approach would be a simultaneous optimization considering both fuel cycle costs and plant capital costs and all of their determinants. This approach is being worked on at General Atomic, to be embodied in a code called SØFAST, but at this time no coupled optimization exists. As a result an arbitrary thermal-hydraulic constraint is usually added in GCFR design studies of the present genre. This constraint can be on circulator power, ΔT across the core, or ΔP through the core. The circulator power and the ΔT across the core are associated with high capital cost components; ΔP is not as directly related to a capital cost. ΔP , however, was the constraint selected for the present work. This was done so that neither the ΔT nor the circulator power would vary from assembly design to assembly design by an unacceptable amount. Using ΔP as a constraint also forces both the circulator power and ΔT to vary by roughly the same percentage as the fuel pin diameter is changed.

The detailed thermal-hydraulic design was done using CALIØP. The iterations performed by the code are described in Chapter II, Section 2.3.1, under the discussion of calculations of non-fixed geometries. The fuel assembly designs obtained using CALIØP are shown in Table 3.2. As can be seen from the table, a wide range of fuel volume fractions is covered. The circulator powers are all larger than the 23,000 hp circulators recommended for the first commercial GCFRs (M3), but are

Table 3.2
Compatible Fuel Assembly Designs for Various Fuel Pin
Diameters*

Fuel Pin Diameter** [mm]	6.	7.	8.	9.	10.	11.
Fuel Volume Fraction***	0.236	0.302	0.357	0.405	0.449	0.487
Structure Volume Fraction***	0.158	0.159	0.160	0.158	0.156	0.152
Helium Volume Fraction***	0.606	0.539	0.483	0.437	0.395	0.361
Assembly Pitch*** [cm]	16.22	17.29	18.51	19.88	21.23	22.67
Fuel Pin Pitch*** [mm]	9.01	9.62	10.32	11.10	11.87	12.69
Core Mass Flow Rate [^{lb} /sec]	6789.	6202.	5878.	5638.	5471.	5368.
Temperature Rise						
Across the Assembly (ΔT) [°C]	239.	260.	274.	285.	292.	297.
Total Circulator Power [MW _e]	178.	163.	155.	148.	144.	141.
Power Per Circulator [hp]	39,800	36,499	34,600	33,100	32,200	31,500

*Constraints: 15 KW/ft, 750°C maximum clad temperature, and 63.2 psi pressure drop

** Cold dimensions

*** Hot-full-power dimensions

all less than the maximum state-of-the-art power of 50,000 hp (T7). Table 3.2 also shows another important aspect: as the pin diameter gets larger, the thermal-hydraulic performance gets better. The determining factor is the increased film temperature drop associated with smaller fuel pins: This would normally drive the cladding temperature up but since it is fixed at 750°C a greater amount of flow must be used instead. This in turn decreases the ΔT and increases the circulator power. This characteristic behavior will turn out to be advantageous for the homogeneous core design.

3.2.3 Blanket Assembly Design

The traditional design goal for blanket assemblies has been to pack them with as much heavy-metal-oxide as possible. Because of their low power densities this was generally achievable without undue concern with respect to pressure drop. In brief, only the ability to fabricate the assemblies remained as a constraint. As a rule of thumb a 1 mm clearance between pins was all this required. General Atomic, therefore, determined that the tightest packing reasonable for their "advanced oxide" core design would have 91 pins per assembly and a fuel volume fraction of 0.5. These blanket assemblies were then orificed so that the peak clad temperature condition was met at the end of life for the assembly.

Unfortunately, since the peak power density of a radial blanket is roughly one third of that desired for an internal blanket, ignoring possible pressure drop problems no longer

seems reasonable. It is desired to have the maximum (un-orificed) pressure drop in the driver fuel assemblies, so some elementary calculations were done to compare the pressure drop across an internal blanket to that of a driver fuel assembly. It was found that using the General Atomic design with 91 pins per assembly (fuel volume fraction of 0.5) was reasonable up to a full 15 Kw/ft. Further, it was found that a design with 127 pins per assembly (fuel volume fraction of 0.5) would most likely be acceptable up to 15 Kw/ft. A more detailed examination of the thermal-hydraulic problems of the internal blankets is described in Chapter 4.

All of the blanket assemblies used for this work have the same volume fractions. They are 0.5, 0.106, and 0.395 for the fuel, structure, and coolant respectively. The volume fractions remain the same since they correspond to the as-tight-as-practicable design decision made by General Atomic for their "advanced oxide" core. The external dimensions of their blanket assemblies clearly must be the same as for the fuel assemblies. Thus, all the information needed for the neutronic calculations is given, except the assembly lifetime. General Atomic characteristically uses 6 years for its radial blanket assembly lifetimes. Since the conditions under which their optimizations were performed do not differ substantially from those in the present work, we also adopted this refueling interval. The results should not be sensitive to this choice: blanket optimization curves (fuel cycle cost versus exposure time) are

typically very flat near the optimum (Bl0, S5), and in any case, refueling is only possible in multiples of one year, the interval preferred by utilities for reactor refueling. The internal blanket assemblies were allowed to remain in the core until their Kw/ft limit was met, which was two years.

3.3 Optimum Core Design Selection

The selection of the optimum homogeneous core design has been reduced to the selection of the best performing assembly design from the set of thermally and hydraulically acceptable candidates developed by applying the screening procedure just described. Determining best performance, however, requires the selection of a figure of merit and an appropriate method for calculating its value. There are at least four figures of merit commonly used for optimization studies of the present type. They are, in order of increasing complexity:

- 1) Doubling Time,
- 2) Energy Growth Potential,
- 3) Fuel Cycle Costs, and
- 4) Power Generation Costs.


Each one of these figures of merit is evaluated for all of the acceptable assembly designs. The "optimum" core design is then selected. But before all the figures of merit are presented the following section describes the neutronics methods used to derive the required data.

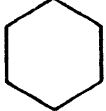
3.3.1 Neutronics Methods for the Optimization

For each fuel assembly design presented in Table 3.2, an R-Z analysis of the first cycle was done using 2DB. For each case an enrichment search followed by a burn of 256 full-power-days (FPD) was performed. This required a number of iterations in order to achieve proper power flattening and an end of cycle critical condition (assumed to be $k_{\text{eff}}=1.01$ to account for streaming (H4)). Figure 3.2 shows the basic core layout used for all the cases. This was translated into the R-Z model shown in Fig. 3.3.

The fuel assembly dimensions and volume fractions are shown in Table 3.2; the blanket volume fractions are given in Section 3.2.3; and the control rod and shield descriptions are given in Table 3.3. With this data in hand, the analysis was straightforward. The burnup was done with one time step but many zones, as shown in Fig. 3.3. Since the control channels provide a streaming path, the diffusion coefficient, D , in the channel was modified so that the axial leakage predicted by this model would agree with a transport calculation done by General Atomic. The modification of the diffusion coefficient was done only once based on the assembly size associated with the 8 mm fuel pins. As the assembly size varies so should this correction. Unfortunately, transport data was only available for the 8 mm case. Since the assembly dimensions do not vary greatly from the 18.51 cm assembly pitch of the 8 mm case the use of only one modified diffusion coefficient seems acceptable.

30° Symmetry Sector Shown

 Control Rod (P-primaries)
(S-secondaries)

 Fuel or Blanket Assembly

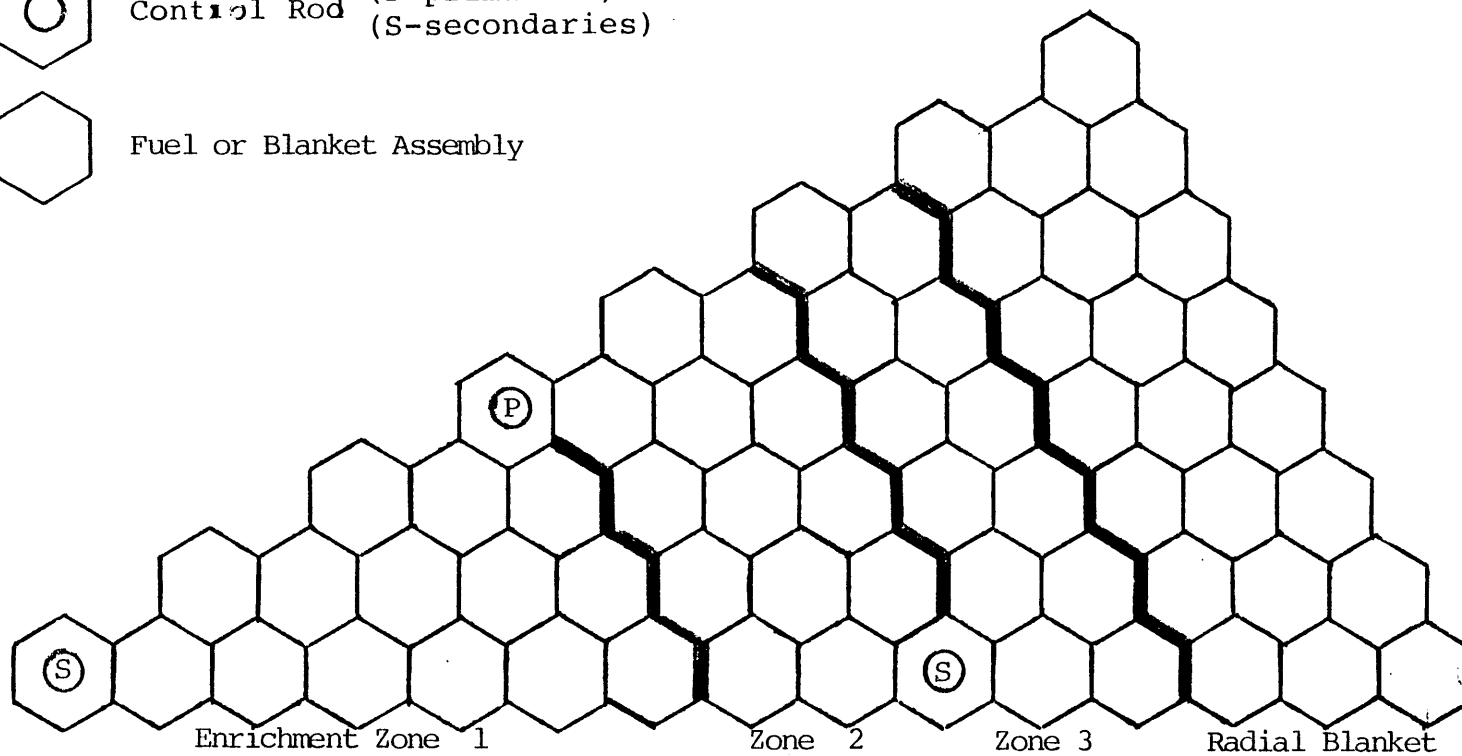


Fig. 3.2 Homogeneous Core Layout

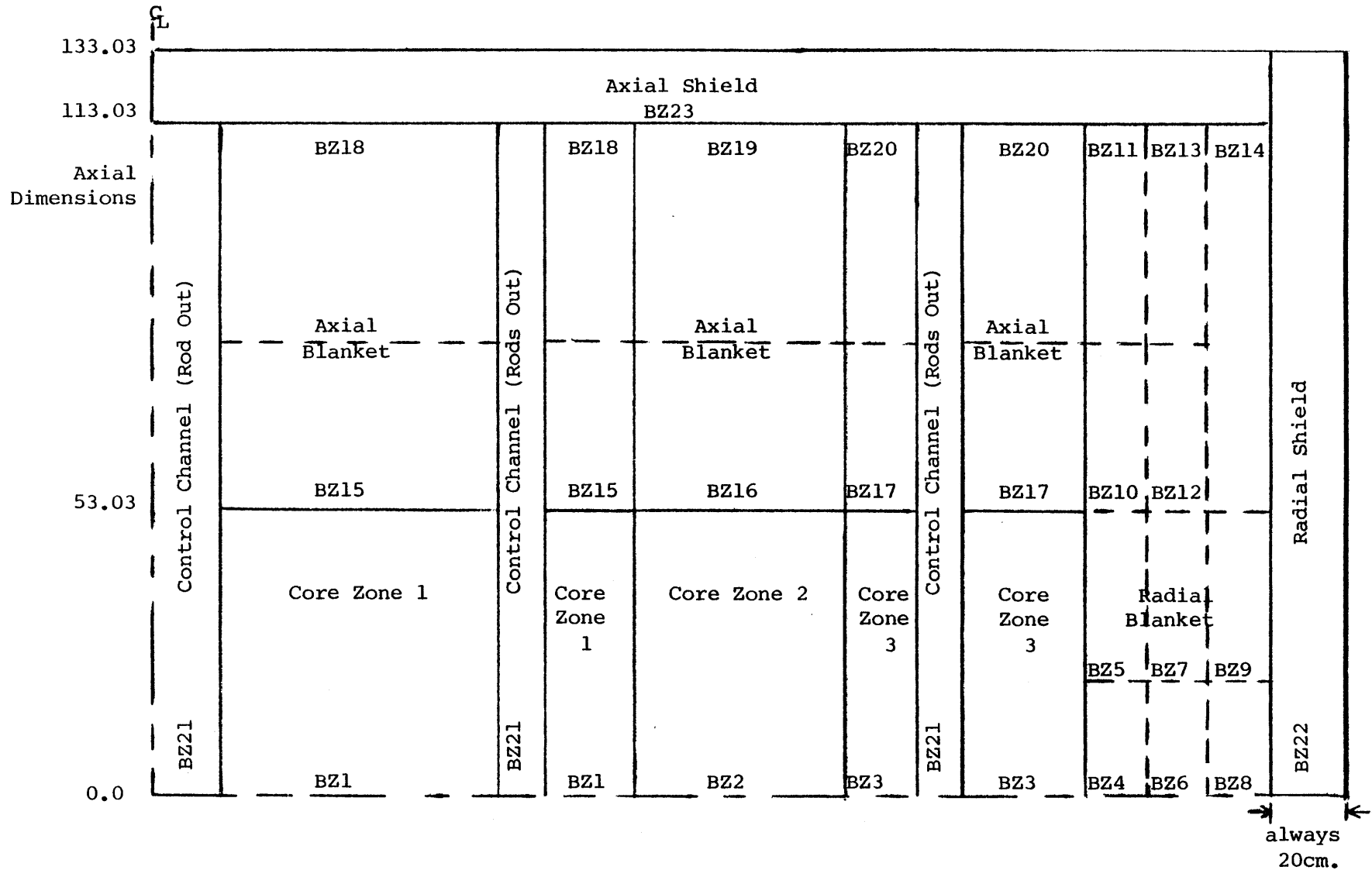


Fig. 3.3 R-Z model used for the homogeneous core analysis. (The designations of the form BZ_n identify the burnup zones. The axial dimensions are always the same as given here. The radial dimensions depend on the assembly pitch.)

Table 3.3
Control and Shield Compositions

	Atom Densities (nuclei/barn cm.)			
	Control out	Control in	Axial Shield	Radial Shield
He	0.00116	0.000595	0.00032	0.00015
C-12	--	0.0098	0.0073	0.0564
Fe	0.00444	0.0115	0.0172	0.00989
Cr	0.00065	0.0017	0.0041	0.0023
Ni	0.000026	0.000067	0.0029	0.00168
Mo	0.000029	0.000108	0.00038	0.00021
Mn	0.000026	0.000067	0.00052	0.00030
B-10	--	0.0197	0.0058	--
B-11	--	0.0197	0.0235	--

Plutonium Isotopic Composition (LWR recycle) (C9)

Pu-239	67.3%
Pu-240	20.2%
Pu-241	10.1%
Pu-242	2.4%

Uranium Isotopic Compositions (Depleted U)

U-238	99.8%
U-235	0.2%

The correction to the channel diffusion coefficient required a reduction of D by a factor of 2.8. Matching axial leakage in this manner also perturbs the radial diffusion of neutrons. The resulting radial effect was checked by comparing two hexagonal analyses of a homogeneous core with both having the same DB^2 but different Ds (possible through also changing B). The difference in the peak power density was less than 1%. The location of the peak power density did not change.

The preceding summarizes all the information needed to reproduce any of the calculations made for the optimization. At this stage the analysis is still scoping in nature, to locate the neighborhood of the optimum rather than to find the exact fissile inventories or fissile gains. In that spirit only the first cycle, as opposed to the ultimate equilibrium cycle, was examined to hold down the costs associated with multi-cycle burnup calculations. Based on experience, it is believed that the changes in performance indices from the first cycle to the equilibrium cycle will not change the existence or location of any minimum or maximum in these indices.

3.3.2 Doubling Time Optimization

Doubling time is traditionally used as an optimization parameter since it maximizes the material return on the fissile inventory commitment. The numerator of the doubling time equation is then physical "investment" in the inventory of the fissile material. The denominator is the annual "return" on

(production rate for) that investment; therefore, minimizing the doubling time is the same as maximizing the return on the fissile inventory investment. Since the fissile investment is the largest investment in the fuel cycle cost analysis, the shortest doubling time often indicates the lowest fuel cycle cost. Unfortunately doubling times of fissile material are generally not as fast as the doubling time of money invested in alternative projects, thereby making the fissile investment return a net loss. The magnitude of that loss depends on the quantity invested (the fissile inventory) and the rate of loss (proportional to the doubling time). In order to determine whether a low fissile inventory or a low doubling time is more important, the value of the fissile material and the time value of money (rate of return) must be specified. To avoid this complication, traditionally the lowest doubling time has been accepted as the key optimization parameter with an understanding that given equal doubling times the lower fissile inventory is preferred.

Although doubling time would appear to be a clear concept, there have been many different definitions (W4, L5, B8, B9, L6). The definition selected for this work is a combination of that used by WARD (L6) and ANL (B9). The definition is:

$$DT = \frac{\ln 2 * FI * OPF}{(FG - FL) * CPY} \quad (3.1)$$

where

DT is the doubling time (actually a compound system doubling time) in years,

FI is the fissile inventory in Kg,

OPF is the ot of pile factor, the ratio of all the fissile material committed to the reactor to the fissile material actually in the core,

FG is the net fissile material gained over a cycle
[Kg]

FL is the fissile material lost outside of the reactor
[Kg], and

CPY is the cycles per year [yr^{-1}]

Further definition is still required. For all the calculations of breeding ratio and doubling time in this work only Pu-239 and Pu-241 will be considered "fissile material," and both will be considered of equal neutronic and economic value. The uranium used in the present work is always depleted to 0.2% U-235, so the U-235 is not credited as a usable fissile fuel. The fissile inventory is the total fissile mass of the core and blankets. (This differs from the WARD definition.) The out-of-pile factor is defined as:

$$\text{OPF} = \frac{1+\text{CB}}{\text{CB}} \quad (3.2)$$

where

CB is the number of cycles a fuel assembly is burned
in core.

For all of the analysis in the present work the fuel assemblies are burned for 3 one-year cycles. This makes the

OPF = 1.333, which corresponds to a total of one year delay to accommodate interim on-site storage, transportation, reprocessing, and fabrication. The fissile material lost, FL, is defined for the present work by:

$$FL = 0.02 * \left(\frac{FL}{CB} \right) \quad (3.3)$$

WARD and ANL assign a combined 1% loss to reprocessing plus fabrication, and then debit Pu-241 decay for the out-of-pile time. The 2% used here is consistent with General Atomic usage. The out-of-pile decay of Pu-241 was ignored, since the effect was small (~ 0.5% of FI) compared to the uncertainties in the reprocessing and fabrication losses, and in any event a larger loss rate was assumed than the WARD or ANL conventions.

Using the fissile inventories and fissile gains from the R-Z analyses described in the previous section, the doubling times were calculated for a series of core designs with fuel pin diameters of 6 mm to 11 mm (the values for the 10 and 11 mm cases were found using CALIØP (one group) results and biasing them to agree with the 2DB R-Z (multigroup) results). Table 3.4 presents these results along with other parameters of interest. The doubling time results are plotted in Fig. 3.4. As can be seen from the figure, a minimum in the doubling time occurs between the 7 mm and 8 mm fuel pin cases. Figure 3.4 has been replotted as Fig. 3.5, with the fuel volume fraction as the independent variable rather than the fuel pin diameter, since earlier studies have shown that the

Table 3.4

Results of the Analysis of Homogeneous Cores Using Acceptable Thermal-Hydraulic
Assembly Designs*

Pin Diameter (mm)	6	7	8	9	10**	11**
Fuel Volume Fraction	0.236	0.302	0.357	0.405	0.449	0.487
Doubling Time (yr)	10.1	8.24	8.25	9.4	10.5	11.7
Fissile Inventory (Kg)	3255.	3744.	4345.	5201.	5992.	6842.
Breeding Ratio (BOCl)	1.36	1.54	1.65	1.69	1.72	1.74
Core Averaged, % Enrichment ($\frac{\text{fissile Pu}}{\text{U} + \text{Pu}}$)	16.4	12.9	11.1	10.2	9.3	8.5
Cycle Δk	-0.045	-0.0144	+0.0009	+0.0076	increasing	increasing
Core Volume (liters)	9280.	10,560.	12,080.	13,940.	15,900.	18,130
Core Surface Area (cm ²)	293,900.	326,100.	364,700.	410,300.	457,900.	511,400.
$\frac{1+\delta}{1+\alpha}$	1.038	1.062	1.077	1,088	--	--
Net Fissile Gain (Kg)	297.7	419.0	485.6	510.7	526.1	539.1

*Designs constrained to 15 KW/ft, 750°C peak clad temperature and 63.2 psi pressure drop across an assembly.

** Values from a CALIØP analysis, adjusted to agree with the R-Z analyses.

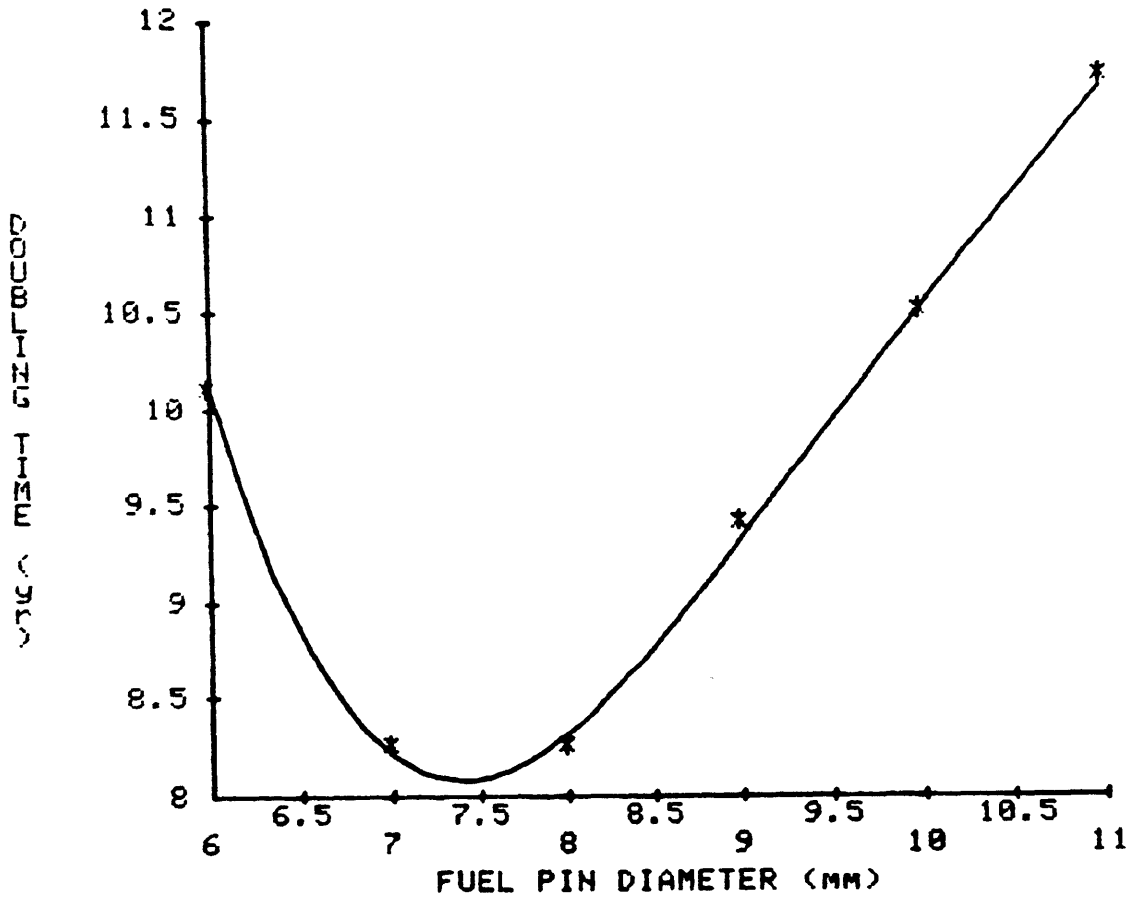


Fig. 3.4 Doubling time as a function of fuel pin diameter [Homogeneous core constrained by 15KW/ft peak linear power, 750° peak clad temperature, and 63.2 psi pressure drop across the assembly.]

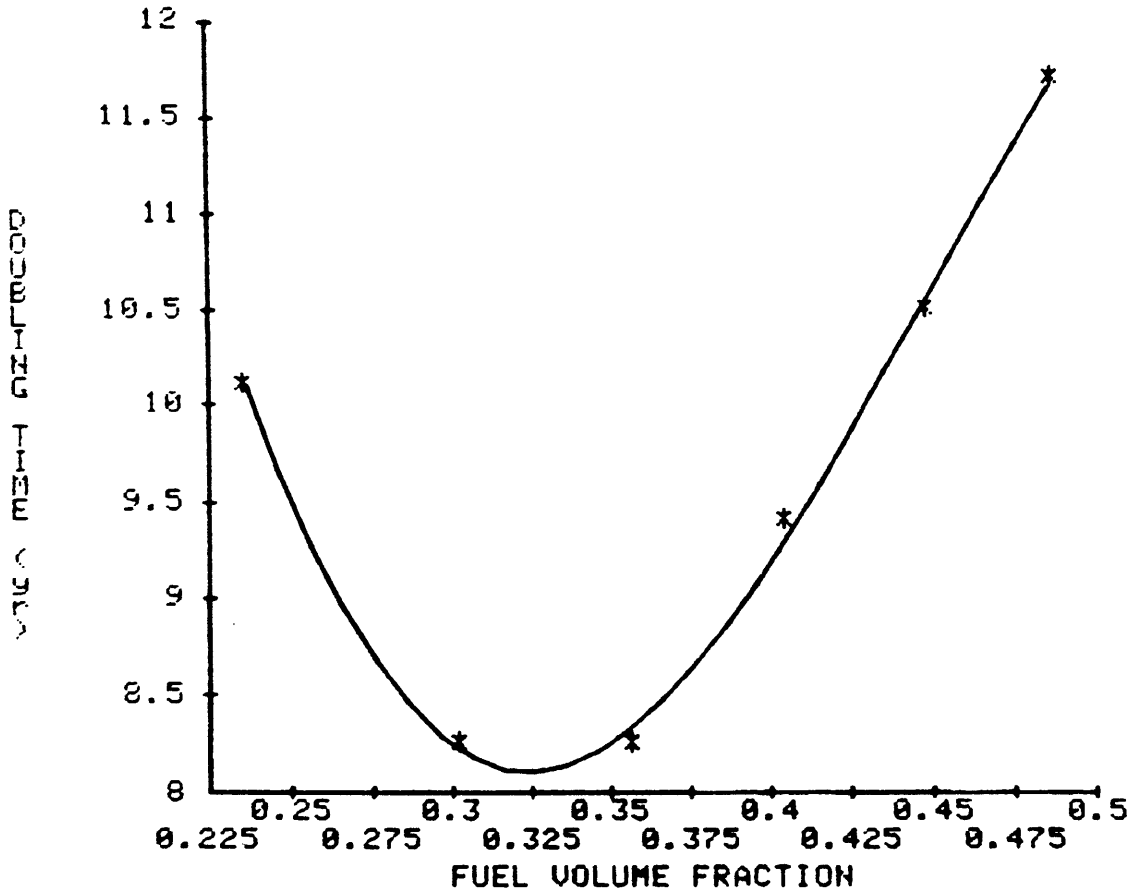


Fig. 3.5 Doubling time as a function of fuel volume fraction
[Homogeneous core constrained by 15KW/ft peak linear power, 750° peak clad temperature, and 63.2 psi pressure drop across the assembly.]

doubling time dependence on fuel volume fraction is the main reason for improved core performance in heterogeneous cores (C2, B2). The reason for a minimum in this curve must now be explored.

As a first step in examining this phenomenon, the doubling time is broken down into its components: fissile inventory and fissile gain. These are presented in Figs. 3.6 and 3.7, respectively. Since the fissile gain is roughly proportional to the breeding ratio minus one, the breeding ratio is plotted as a function of fuel volume fraction in Fig. 3.8. As can be seen from these figures the fissile inventory, fissile gain, and breeding ratio all increase with increasing fuel volume fraction. A minimum in the doubling time occurs because the rate of increase in the fissile gain decreases with increasing fuel volume fraction while the rate of increase in the fissile inventory increases with increasing fuel volume fraction.

Doubling time and its components plotted as a function of fuel volume fraction do not tell the whole story. In fact, if one believed that the effects shown were due to changes in the fuel volume fraction alone, the curves would be misleading. Each one of the points on all the curves shown so far comes from a constrained design where the assembly sizes as well as the volume fractions are changing.

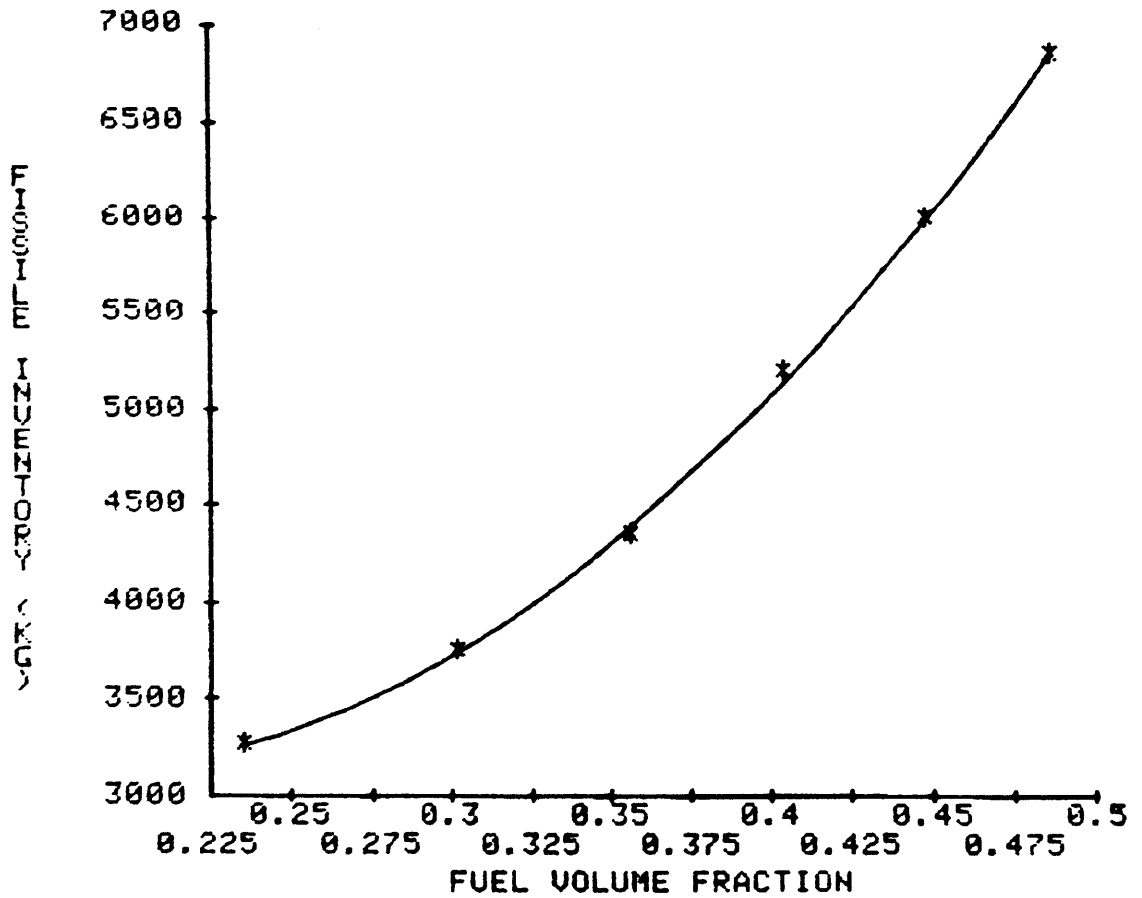


Fig. 3.6 Fissile inventory as a function of the fuel volume fraction
[Homogeneous core constrained by 15KW/ft peak linear power, 750° peak clad temperature, and 63.2 psi pressure drop across the assembly.]

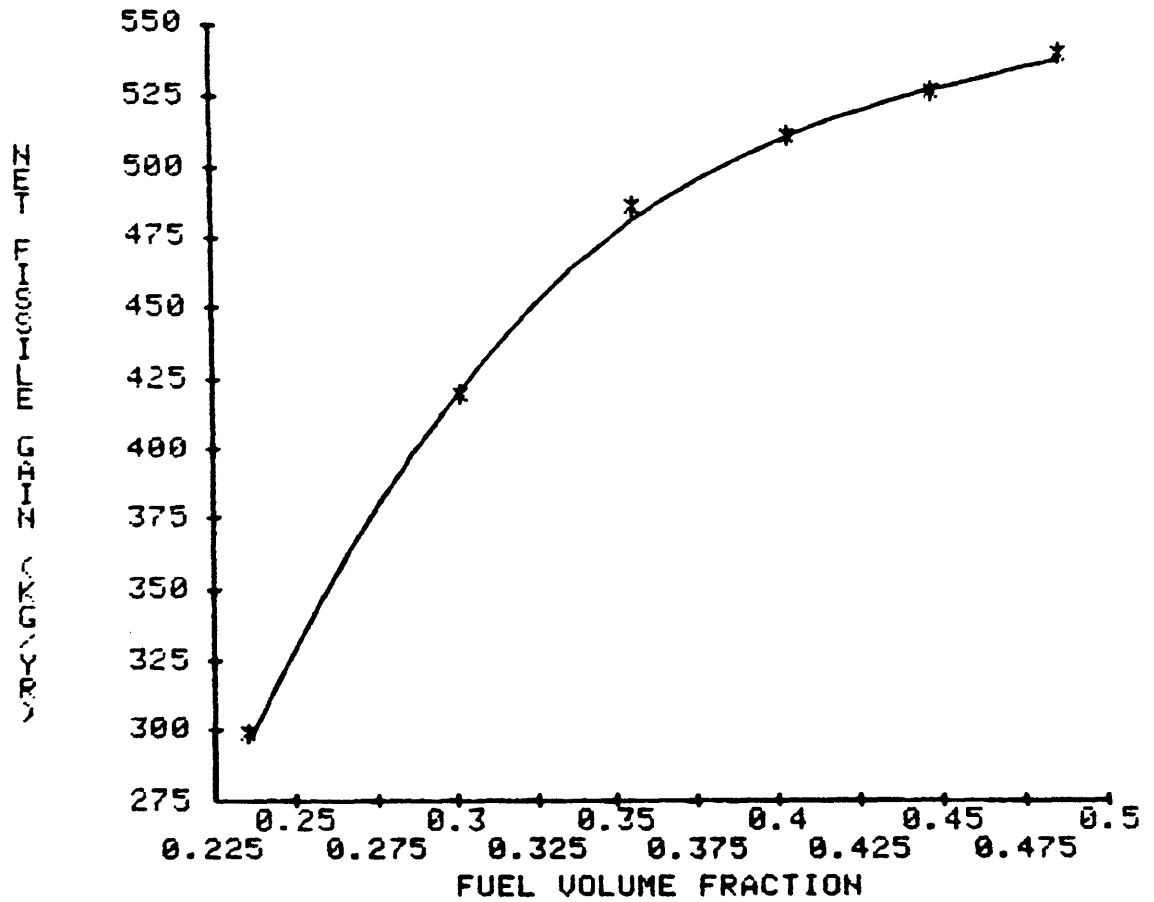


Fig. 3.7 Net Fissile Gain as a function of fuel volume fraction
[Homogeneous core constrained by 15KW/ft peak linear power, 750° peak clad temperature, and 63.2 psi pressure drop across the assembly.]

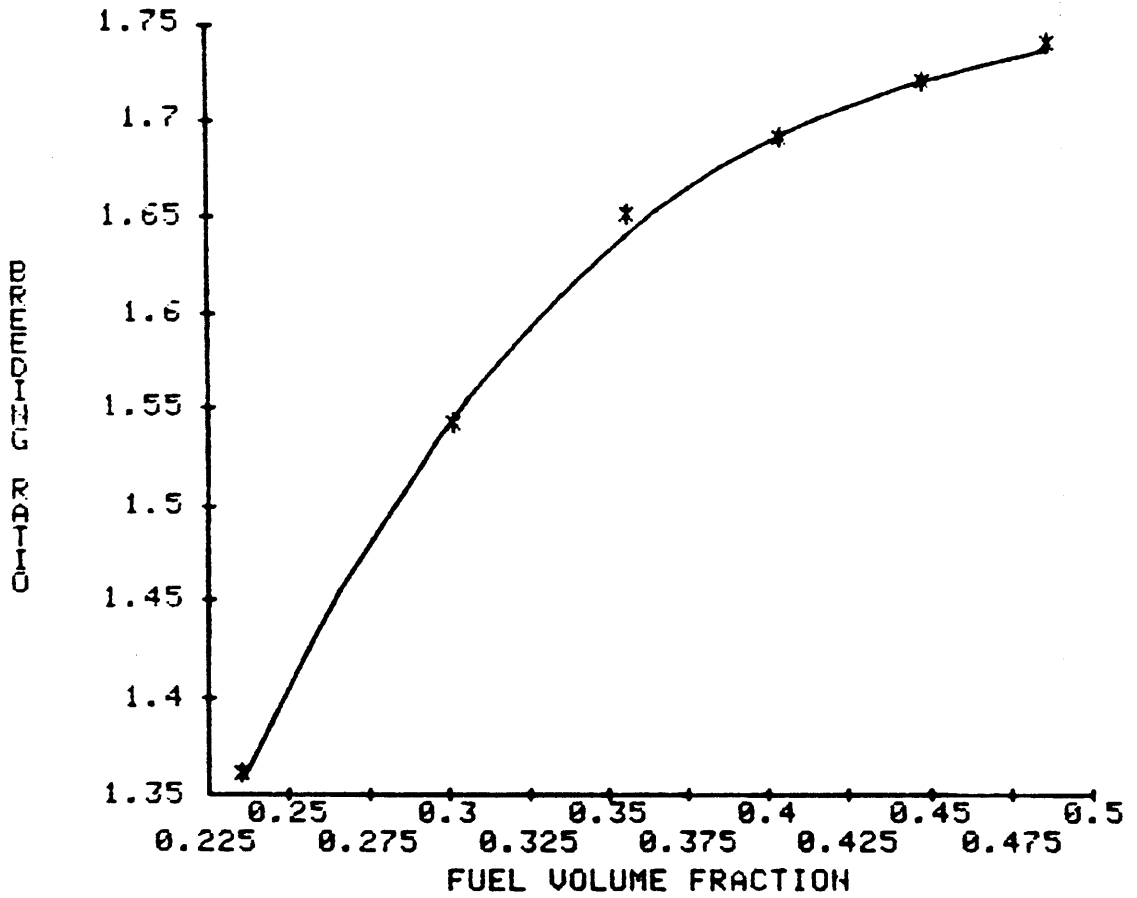


Fig. 3.8 Breeding ratio as a function of fuel volume fraction
[Homogeneous core constrained by 15KW/ft peak linear power, 750° peak clad temperature, and 63.2 psi pressure drop across the assembly.]

Table 3.4 shows how the corresponding core sizes are changing with the various pin diameter selections (or fuel volume fractions). It is possible to increase the fuel volume fraction without increasing the assembly size but this would require using higher circulator powers, higher primary system pressure, and/or lower core inlet or outlet temperatures. Just a small variation in fuel volume fraction without a corresponding change in assembly size would quickly yield unrealistic thermal-hydraulic conditions, but just for illustrative purposes, a series of analyses were performed where the fuel volume fractions were changed but the model geometry was not changed. (The assembly dimensions of the 6 mm pin case were used.) The results of these analyses are summarized in Table 3.5, and the doubling times are plotted on Fig. 3.9 along with the previously determined thermally and hydraulically constrained results. As can be seen from Fig. 3.9, eliminating the assembly size increase associated with larger fuel volume fractions (brought about by the imposition of thermal-hydraulic constraints) decreased all the doubling times and eliminated the rise in doubling time previously seen at larger fuel volume fractions.

The results in Table 3.5 indicate that as long as the k_{eff} was increasing over the cycle the fuel volume fraction had very little influence on the doubling time. This suggested investigating the impact of cycle Δk on the doubling time. To test this, the 6 mm and 7 mm pin cases shown in Table 3.5 were reanalyzed requiring only the start of cycle to be critical

Table 3.5

Analysis of Homogeneous Cores Without Thermal-Hydraulic Constraints*

Fuel Volume Fraction	0.236	0.302	0.357	0.405	0.487
Doubling Time (yr)	10.1	7.5	6.6	6.6	6.7
Fissile Inventory (Kg)	3255.	3341.	3465.	3645.	3963.
Net Fissile Gain (Kg/yr)	297.7	409.7	481.4	407.7	543.4
Breeding Ratio	1.36	1.53	1.64	1.69	1.75
Core Averaged, % Enrichment ($\frac{\text{fissile Pu}}{\text{U} + \text{Pu}}$)	16.4	13.2	11.6	10.7	9.7
Cycle Δk	-0.045	-0.018	-0.001	+0.007	+0.015
$\frac{1 + \delta}{1 + \alpha}$	1.038	1.062	1.080	1.092	1.111

* All analyses were done using the geometry corresponding to the 6 mm fuel pin assembly design (i.e. core volume = 9280 liters). This corresponds to unrealistic thermal-hydraulic conditions.

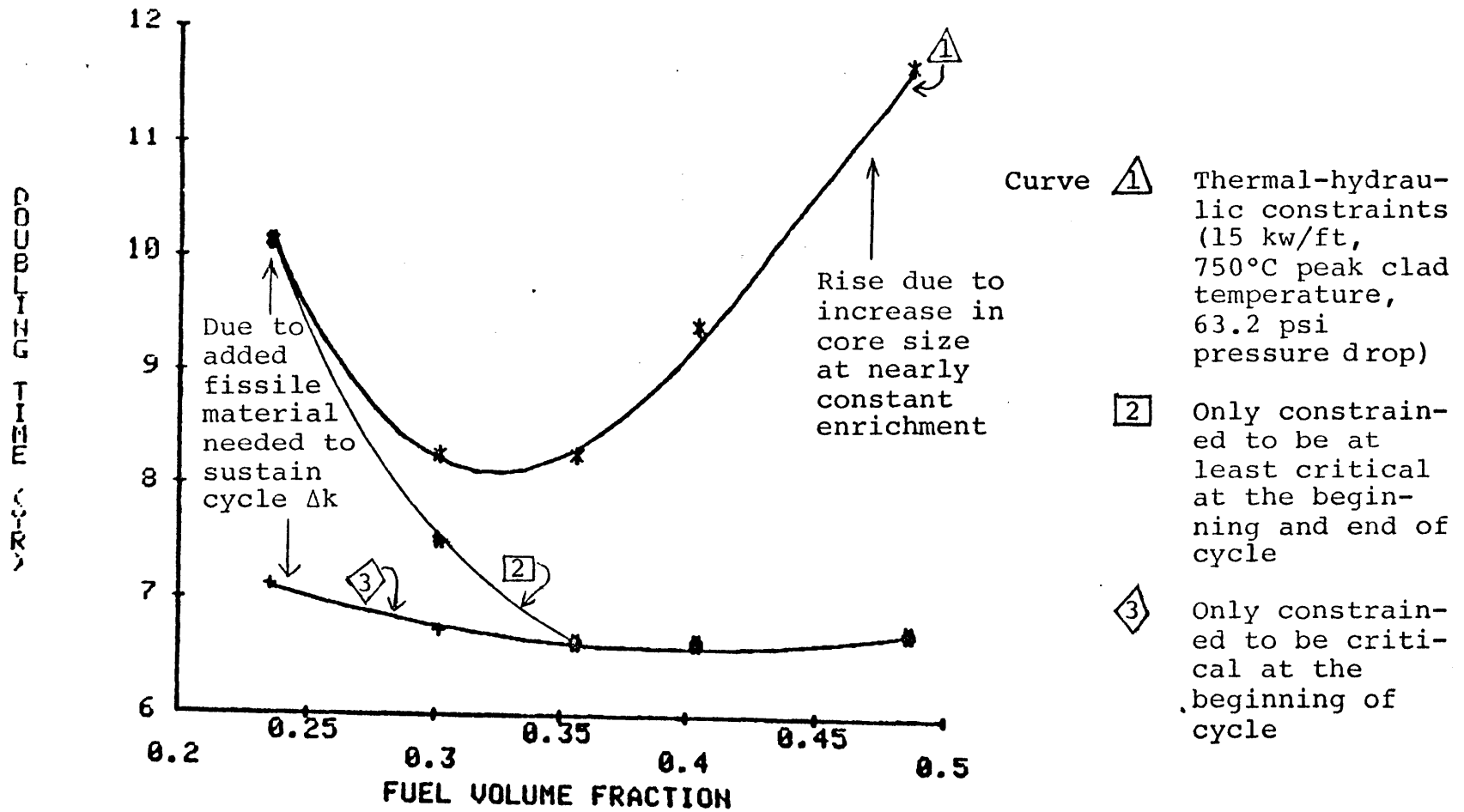


Fig. 3.9 DOUBLING TIME AS A FUNCTION OF FUEL VOLUME FRACTION UNDER VARIOUS CONSTRAINTS

(as opposed to an end of cycle constraint). These results are tabulated in Table 3.6, and the doubling times are plotted as curve 3 on Figs. 3.9. As can be seen from Fig. 3.9, the doubling time under these constraints has very little dependence on the fuel volume fraction.

Now that the two major effects that produce a doubling time optimum have been identified, further understanding of each effect is required. First the doubling time dependence on the cycle Δk will be explored, followed by an examination of the geometric effects.

On the surface the doubling time does not depend on where the plutonium is bred; whether it is bred in the blankets or in the core it all contributes to the same plutonium inventory after reprocessing. However, if the end of cycle must be critical the doubling time does depend on where the breeding is done. Plutonium bred in the blankets has a lower reactivity worth than that in the core. For small pin diameters (lower fuel volume fractions) more of the material is bred in the blankets, requiring a high initial inventory to overcome the subsequent reactivity deficit. This high inventory in turn results in a high doubling time. When the cycle Δk is positive then the doubling time dependence on pin diameter (or volume fraction) is eliminated because one no longer needs to augment the core inventory to provide excess beginning of cycle reactivity to sustain cycle burnup.

The geometric effect on the doubling time is a combination

Table 3.6

Analysis of Homogeneous Cores Without Thermal-Hydraulic Constraints and
Critical Only at the Beginning-of-Cycle*

Fuel Volume Fraction	0.236	0.302	0.357	0.405	0.487
Doubling Time (yr)	7.1	6.7	6.6	6.6	6.7
Fissile Inventory (Kg)	3002.	3240.	3465.	3645.	3963.
Net Fissile Gain (Kg/yr)	387.6	453.2	481.4	507.7	543.4
Breeding Ratio	1.48	1.58	1.64	1.69	1.75
Core Averaged, % Enrichment ($\frac{\text{fissile Pu}}{\text{U} + \text{Pu}}$)	15.1	12.8	11.6	10.7	9.7
Cycle Δk	-0.035	-0.014	-0.001	+0.007	+0.015
$\frac{1 + \delta}{1 + \alpha}$	1.046	1.066	1.080	1.092	1.111

* All analyses were done using the core geometry corresponding to the 6 mm fuel pin assembly design (i.e. core volume = 9280 liters). This corresponds to unrealistic thermal-hydraulic conditions. All analyses were searched to critical at beginning-of-life conditions and burned for one year.

of a change in leakage and a change in power density. Given two designs with the same volume fractions the critical enrichments depend on the leakage. Using the 9 mm case as an example, in going from Table 3.4 to Table 3.5, the core volume-to-surface-area ratio decreased 7.6% causing the critical enrichment to increase by 4.9%. This was a sufficiently small effect on compositions that the breeding ratio did not change noticeably. For the same example the fissile inventory decreased 30.1% as the core volume decreased 33.4%. It is this increase in the fissile inventory without a significant change in breeding that causes the doubling times to increase with increasing assembly sizes. In increasing the assembly size the power density was decreased. If the power density were maintained as the assembly size increased (by increasing the reactor power) the doubling time would have decreased only about 3% (Using $DT \propto \frac{FI}{P}$ from section 1.4 of Chapter 1) compared to the 42% decrease seen in Tables 3.4 and 3.5. Hence the key geometric effect, increasing doubling time with increasing core size, is due to the change in the power density.

This understanding of the physical processes leading to a minimum in the doubling time has serious implications to the homogeneous-versus-heterogeneous design comparison. Since internal blankets run at low power densities the core-averaged power density in a heterogeneous core will always be less, which, as just shown, leads to higher

doubling times. This suggests that the heterogeneous core will possess an inherent disadvantage. The heterogeneous core must make up for this detrimental attribute by exploiting some other phenomenon in its favor. An attempt to find such compensatory phenomena is saved for Chapter 4.

3.3.3 Energy Growth Potential Optimization

The amount of energy a breeder reactor system can produce in the future depends on the quantity of power the system can produce when started and the rate at which the system can grow. The rate at which the system can grow is determined by the doubling time. The amount of power the system can produce when started depends on the amount of fissile material available at that point and the fissile inventory required per reactor of a given rating. General Atomic uses an in-house computer program to determine the amount of energy a reactor system will generate as a function of time. They then identify a "critical energy year" and use the system energy produced in that year as a figure of merit (T_9). In the G.A. approach estimates of the fissile material available at the system start-up and the duration of a development period have to be supplied as program input. For the present work an even simpler approach is developed.

The installed power rating at a given time, t , of a system of breeder reactors can be symbolized by $P(t)$. If

the system is allowed to compound according to its characteristic rate, $\ln 2$ over the doubling time (DT), then the power available at some time, t , later would be:

$$P(t) = P_0 e^{(t/DT) \ln 2} \quad (3.4)$$

where P_0 is the initial power rating.

For the maximum power at any time P_0 should be as large as possible. This would occur if P_0 were all the fissile material available at time zero, FM_0 , divided by the fissile inventory of a breeder reactor, FI , multiplied by its power rating, PR . This transforms Eq. 3.4 to:

$$P(t) = \frac{PR \times FM_0}{FI} e^{(t/DT) \ln 2} \quad (3.5)$$

In comparing reactor designs the initial fissile material, FM_0 , is assumed independent of design so a relative power potential index, PPI , would be:

$$PPI(t) = \frac{PR e^{(t/DT) \ln 2}}{FI} \quad (3.6)$$

From this equation it becomes clear that as t goes to infinity the reactor design with the shortest doubling time has an advantage. But also from this equation it should be clear that in the early years a breeder with a longer doubling time but less fissile inventory may be preferred.

In order to use this power potential index a critical

energy year must be identified and the time elapsed between that critical year and the start of the breeder system must be calculated. This will give t in Eq. 3.6. With t selected the power that can be produced at that time with two reactor concepts can be compared using PPI from Eq. 3.6. For example, solving Eq. 3.6 for the 6 mm and 7 mm cases using the data from Table 3.4 yields 4.08 and 6.12, respectively, for the power potential index for a critical year $t = 35$ years after introduction of the system of breeders. This means that if the 7 mm pin case was selected, 50% more power could be produced at the critical time than if the 6 mm pin case was selected. However, if the critical year was 5 years after the introduction of the breeders, the power potential index for these two cases would be 0.516 and 0.492 respectively. This implies the 6 mm pin case would be favored by 6%. The power potential index has been plotted as a function of the fuel pin diameter for t equal to 5, 20, and 35 years as Fig. 3.10. The shape of the power potential index is due to the combined effects of the (inverse of the) fissile inventory curve shown in Fig. 3.6 and the doubling time curve shown in Fig. 3.4. As the time, t , changes, the relative importance of the fissile inventory or the doubling time changes. A maximum quickly develops at the 7 mm case since it has the shortest doubling time and still a fairly low fissile inventory.

The power potential index approach has its

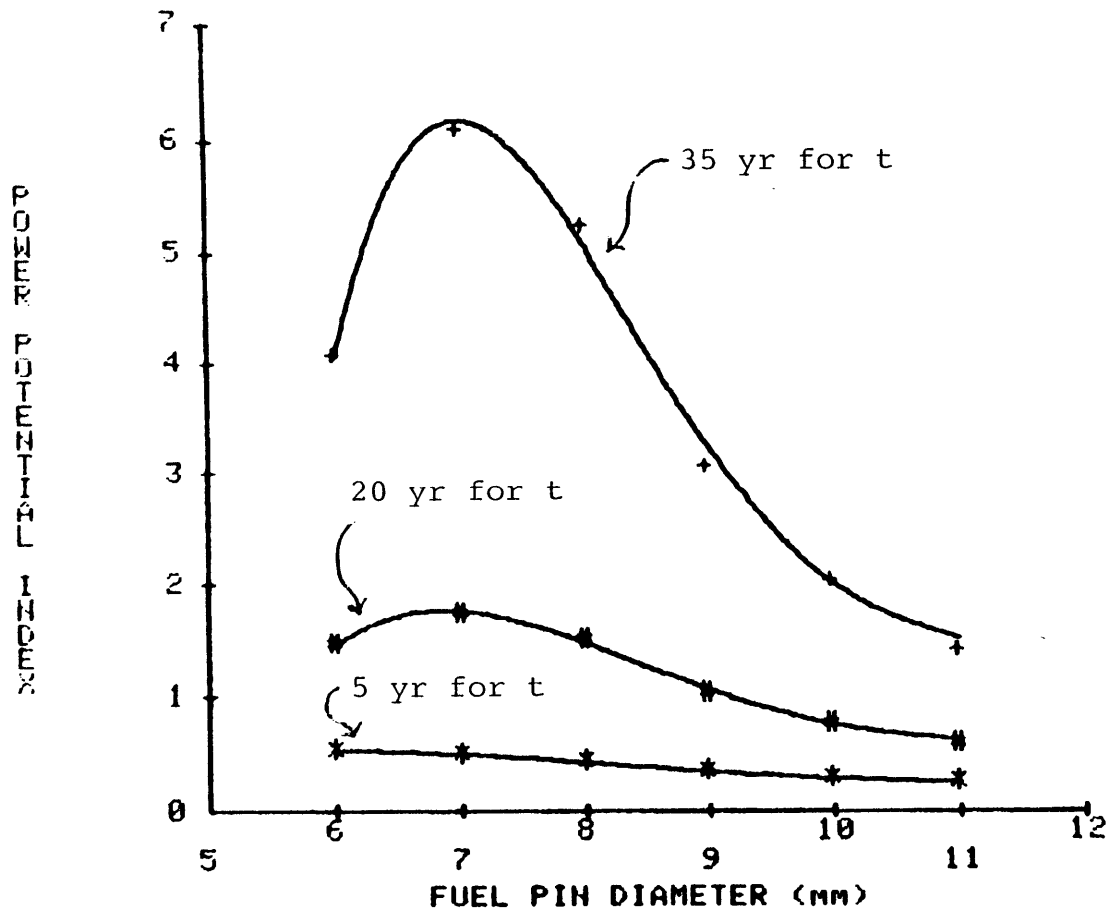


Fig. 3.10 Power potential index as a function of fuel pin diameter at various years after GCFR introduction

advantages and disadvantages. Its key advantage comes from recognizing the advantage of low fissile inventory cores. In fact just as the doubling time can be thought of as an economic parameter that measures the rate of return on the fissile investment, the power potential index can be viewed as a measure of the inefficient use of capital associated with large fissile inventories. The power potential index takes into account the rate of return on the fissile investment (the doubling time) and the size of that investment (the fissile inventory). The disadvantage of using the power potential index is the necessity of selecting a critical energy year, the year when it is desired to have the maximum power contribution from breeder reactors. The optimist would hope that the combination of fission, coal, oil, fusion, geothermal, wind, and solar energy would never produce a "critical energy year." This all but renders the index useless unless an arbitrary critical year is selected.

3.3.4 Fuel Cycle Cost Optimization

Fuel cycle costs have often been used to determine the optimum core design. This approach, however, has two problems. The first is related to the large number of assumptions required to permit the analysis. Values must be assumed for unit costs such as those for plutonium, fabrication, and reprocessing. The time value of money, tax rates, and depreciation policy must also be specified. The uncertainty in these assumptions and input data can

frequently obscure the resulting difference in fuel cycle costs between options. The second problem comes from the assumption that capital cost impacts are small compared to the fuel cycle impact. This is often not the case, and will be explored in the next subsection.

Since Chapter 5 is devoted to an economic analysis, all discussion of the values assumed in this subsection will be deferred until then. This subsection will merely list the assumed values and present the fuel cycle costs that result.

Table 3.7 shows the fuel cycle costs for the 6 mm through 11 mm fuel pin assembly designs along with the assumptions used to calculate these values. Figure 3.11 shows the fuel cycle costs as a function of the fuel pin diameter. As can be seen from this curve, the cheapest fuel cycle costs occur with a 6 mm fuel pin diameter. This is because the 6 mm pin diameter has the lowest reprocessing costs. This result is actually an artifact of the way the analysis was done. For this study all of the cores were burned the same number of full-power-days although the cases all had different amounts of heavy metal loaded in the core. (The number of cycles burned was also the same for each case.) This implies that the smaller pin diameter cases (with less heavy metal loaded into the core) were given higher burnups (MWD/MTHM). If all the cores were given the same amount of burnup and produced the same amount of power (thus

Table 3.7

Fuel Cycle Costs for Various Homogeneous Core Designs

Fuel Pin Diameter	6 mm	7 mm	8 mm	9 mm	10 mm	11 mm
Fissile Material	0.8	0.6	0.7	0.9	1.4	1.8
Fabrication	3.3	3.3	3.3	3.3	3.3	3.3
Reprocessing	1.1	1.6	2.1	2.7	3.3	4.1
Total	5.2	5.5	6.1	6.9	8.0	9.2

Cost Assumptions

Fissile Material	\$27/gm
Reprocessing Charges (Includes waste storage and shipping)	\$500/KgHM
Discount rate (no inflation or escalation)	4%
Tax rate	50%
Fabrication (includes shipping)	\$150,000/core assembly 30,000/blanket assembly

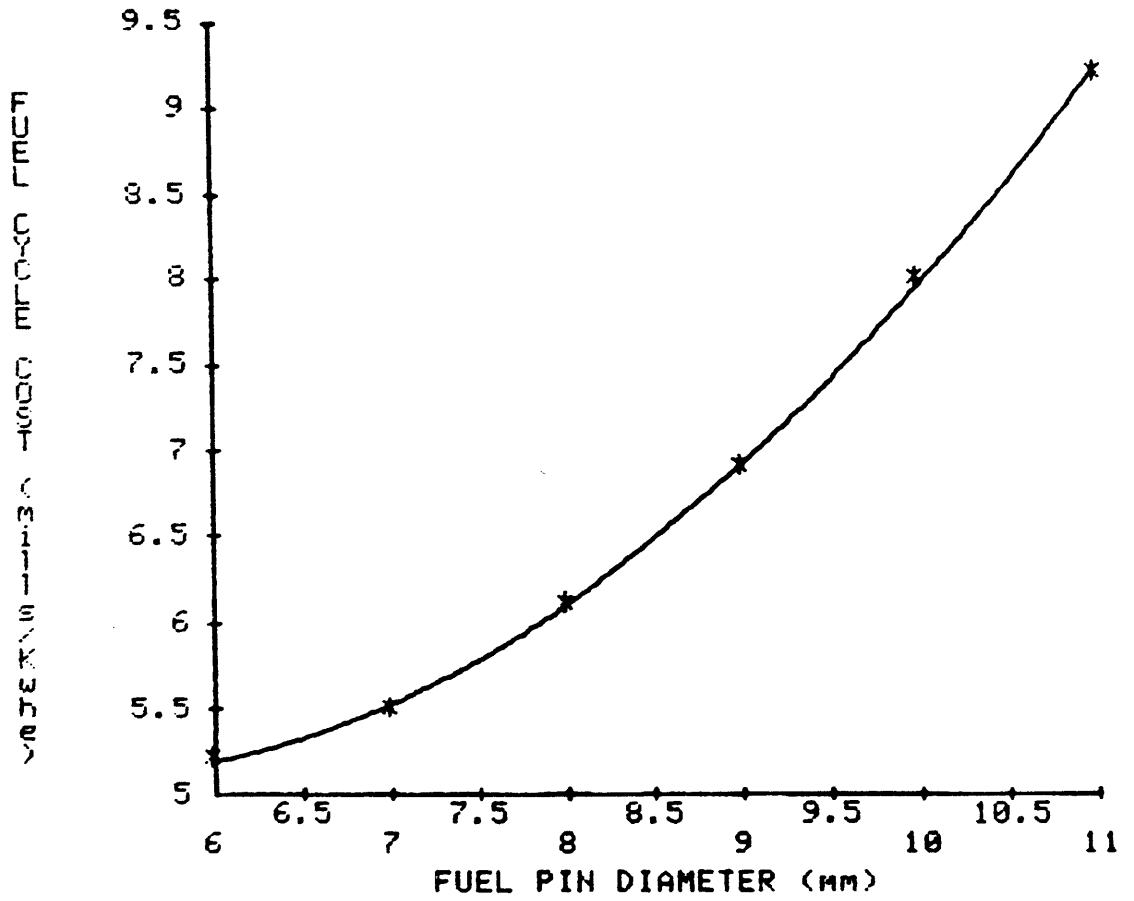


Fig. 3.11 Fuel cycle cost as a function of fuel pin diameter

the same MTHM) then the reprocessing charges would be the same for each case (if the charge were on a per MTHM basis).

A common assumption for optimization studies (as adopted in the present work) is that the reactor power, the number of full-power-days, and the number of burnup cycles remain constant (C8, B11) but GA (partly due to the construction of CALIØP) generally uses a constant burnup assumption. To test the impact of the constant burnup assumption as opposed to the assumptions used in the present work a number of CALIØP runs were made. Table 3.8 shows the results including the doubling times, the power potential index (at 30 yrs), and the fuel cycle costs predicted by CALIØP. As can be seen from this table, the optimum pin diameter for doubling time and power potential is not changed by going to the constant burnup assumption. The optimum pin diameter using fuel cycle costs as the figure of merit has changed from 6 mm to near to 10 mm.

The change in results associated with changing burnup stands as an example of how sensitive the fuel cycle costs are to a change in assumptions. It has been difficult to achieve consensus as to whether the GA constant burnup assumption or the assumptions used in the present work (and by others including ANL (B11)) are more appropriate, hence the optimum pin diameter with regard to fuel cycle costs will be said to range from 6 mm to 10 mm. This lack of definitude helps explain why doubling time is so often

Table 3.8
Results of Analyses Using A Constant Burnup Assumption*

Pin Diameter (mm)	6	7	8	9	10	11
Cycle Time (FPD)	139	200	272	356	450	555
Doubling Time (yr)**	10.3	8.7	8.6	9.6	10.7	11.7
Fissile Inventory (Kg)	2942	3580	4335	5340	6374	7519
Power Potential Index (t = 35 yr)	0.0036	0.0045	0.0039	0.0023	0.0015	0.0011
Fuel Cycle Cost (mills/KW hr)	8.8	6.7	5.7	5.4	5.4	5.6

* All of these results come from CALIØP which used one-group neutronics; hence these results are less precise than most of the other analyses in the present work.

** The out-of-pile factor changed from case to case since a one year waiting period outside the reactor was used for each cycle. See Eq. 3.2.

used for fuel pin optimization.

3.3.5 Power Generation Cost Optimization

In designing assemblies with 6 mm to 11 mm fuel pin diameter it was necessary to vary the circulator power, the core outlet temperature, and the reactor cavity volume in the PCRV. All of these have an impact on the capital cost of a GCFR. In order to find the lowest power generation costs these capital costs must be included in the evaluation of an optimum. To do this some rough estimates of the magnitude of these costs were obtained from General Atomic (M5). The following is a crude equation for these cost impacts relative to the 8 mm fuel pin case:

$$\begin{aligned} \text{CCD} = 30 \left[\left(\frac{\text{CP}}{155} \right)^{0.7} - 1 \right] + 1.1 \left[\frac{\text{CP} - 1.55}{0.9} \right] + 2.3 (\text{CD} - 27.7) \\ + 0.43 (561.2 - \text{OT}) \end{aligned} \quad (3.7)$$

where

CCD is the capital cost difference in millions of dollars for the design under consideration compared to the 8 mm case,

CP is the circulator power in MW,

CD is the core cavity diameter in the PCRV in feet,

and

OT is the core outlet temperature in degrees Fahrenheit.

Table 3.9 tabulates the capital cost differences for each pin diameter. These capital cost differences were then transformed into a cost/Kwhr and added to the fuel cycle costs calculated in the previous subsection. This parameter should then have a minimum at the optimum pin diameter with regard to power generation costs.

As can be seen from Fig. 3.12, the optimum fuel pin diameter is between 7 mm and 8 mm. This agrees very well with the optimum predicted by the doubling time criterion. This optimum, however, is very flat, and the uncertainties in its determination are very large. In order to develop this curve assumptions as to the value of plutonium, the time value of money (inflation, tax, and depreciation rates), capital cost estimates, and fuel management schemes have been made. The uncertainties in these data are large enough to change the optimum fuel pin diameter determined. It is the desire to avoid the ambiguity associated with this approach that makes doubling time optimization attractive.

3.3.6 Homogeneous Core Optimization; Summary

Four different ways of selecting an optimum pin diameter have been investigated. The results are summarized in Table 3.10. All things considered, the 8 mm pin is selected as representing an optimum homogeneous core. As can be seen from Table 3.10, the 7 mm pin could have been selected equally as well. However, the 8 mm pin also

Table 3.9

Power Generation Cost Optimization

Pin Diameter (mm)	6	7	8	9	10	11
Circulator Power (MW)	178	163	155	148	144	141
Core Cavity Diameter (ft)	25.6	26.6	27.7	29.0	30.2	31.6
Core Outlet Temperature (°F)	526.4	547.6	561.2	572.1	580.4	585.7
Capital Cost Difference (\$10 ⁶)	41	14.	0	-11	-17	-20
Capital Cost Difference in Power Generation Costs (mills/KWhr)*	1.1	0.4	0	-0.3	-0.5	-0.6
Fuel Cycle Cost (mills/KWhr)	5.2	5.5	6.1	6.9	8.0	9.2
Power Generation Cost Differential (mills/KWhr)	6.3	5.9	6.1	6.6	7.5	8.6

* Using 20% as the annual fixed charge rate.

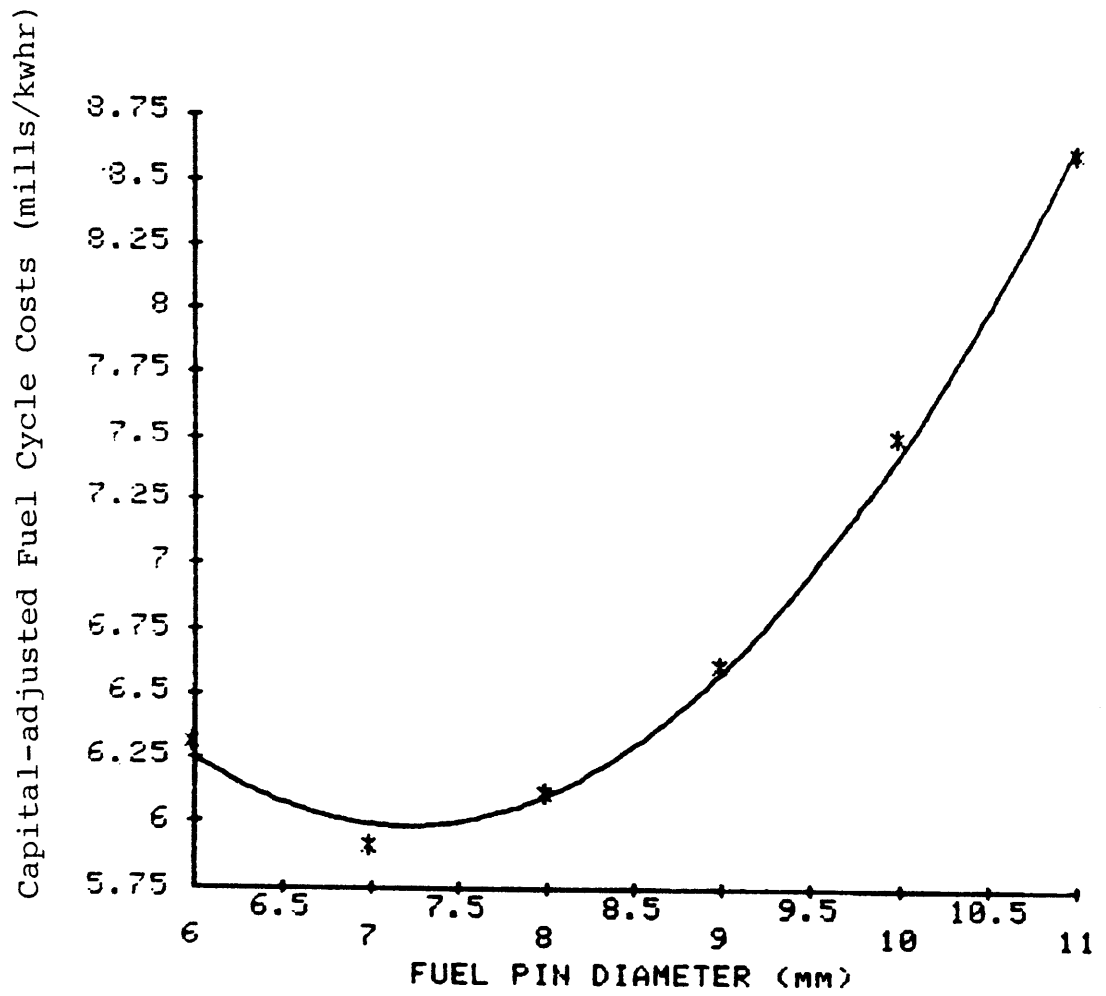


Fig. 3.12 Fuel cycle costs adjusted for capital cost differences as a function of fuel pin diameter

Table 3.10

Homogeneous Core Optimization Summary

<u>Figure of Merit</u>	<u>Optimum Pin Diameter</u>
Doubling Time	7 mm - 8 mm
Energy Potential Index	7 mm
Fuel Cycle Costs	6 mm - 10 mm
Power Generation Costs	7 mm - 10 mm

corresponds to the assembly design most studied by General Atomic. It was also the pin diameter used in the NASAP analysis (D5). Finally as mentioned in Section 3.2 of this chapter the thermal-hydraulic conditions of the GCFR under consideration in the present work are aggressive, and due to that have recently lost favor in some quarters. The 8 mm pin case has slightly less challenging thermal-hydraulics than the 7 mm case, making the 8 mm pin diameter an easy selection from this point of view as well.

It should be pointed out that the doubling time optimization gave results which were in good agreement with the power generation cost optimization. This observation will be helpful in the heterogeneous core optimization process, addressed in the next chapter.

3.4 Fuel Management and Burnup Analysis

For a valid comparison of core designs, both should be compared in their equilibrium cycles. Unfortunately, as the economic environment evolves, the characteristics of the sought-for equilibrium cycle change. Also, since a complete analysis of every cycle leading up to this "equilibrium cycle" would be prohibitively expensive, a number of simplifying assumptions must be made. This section will first describe the fuel loading and shuffling pattern to be used and then select the "equilibrium cycle." The analytical methods used to arrive at the equilibrium cycle will then be described.

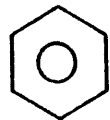
Finally, all the details needed for neutronic modeling of the "equilibrium" cycle will be presented.

3.4.1 Fuel Loading and Shuffling Scheme

The goal of the core fuel loading and shuffling scheme is to provide a flat power distribution and to burn the fuel to roughly 100,000 MWD/MT peak burnup. The number of enrichment zones and the number of hexagonal rows per zone were investigated using CALIØP. It was found that the addition of more than three radial enrichment zones made very little impact. With three enrichment zones the zone pattern shown in Fig. 3.2 was found to give optimal performance. (Generally less than a 1% variation in the doubling time was found among the candidate cores investigated). The determining variable turned out to be the enrichment of the third zone. With two rows as compared to one row for the last enrichment zone the peak enrichment was much less, without degrading the doubling time or increasing the fissile inventory. To reach ~100,000 MWD/MT peak burnup requires a three year burnup. This is accomplished through annual reloading of one third of the core. For the present work 30° symmetry was desired to keep down the calculation costs. Figure 3.13 shows a 30° sector of the core and the loading pattern used.

The goal of the radial blanket loading and shuffling scheme is quite different. The length of time a radial blanket is allowed to be irradiated should be an economic

30° Symmetry Sector Shown



Control Rod (P-primaries)
(S-secondaries)

- A loaded years 2 and 5
- B loaded years 3 and 6
- C loaded year 4
- E moved in even numbered years
- O moved in odd numbered years

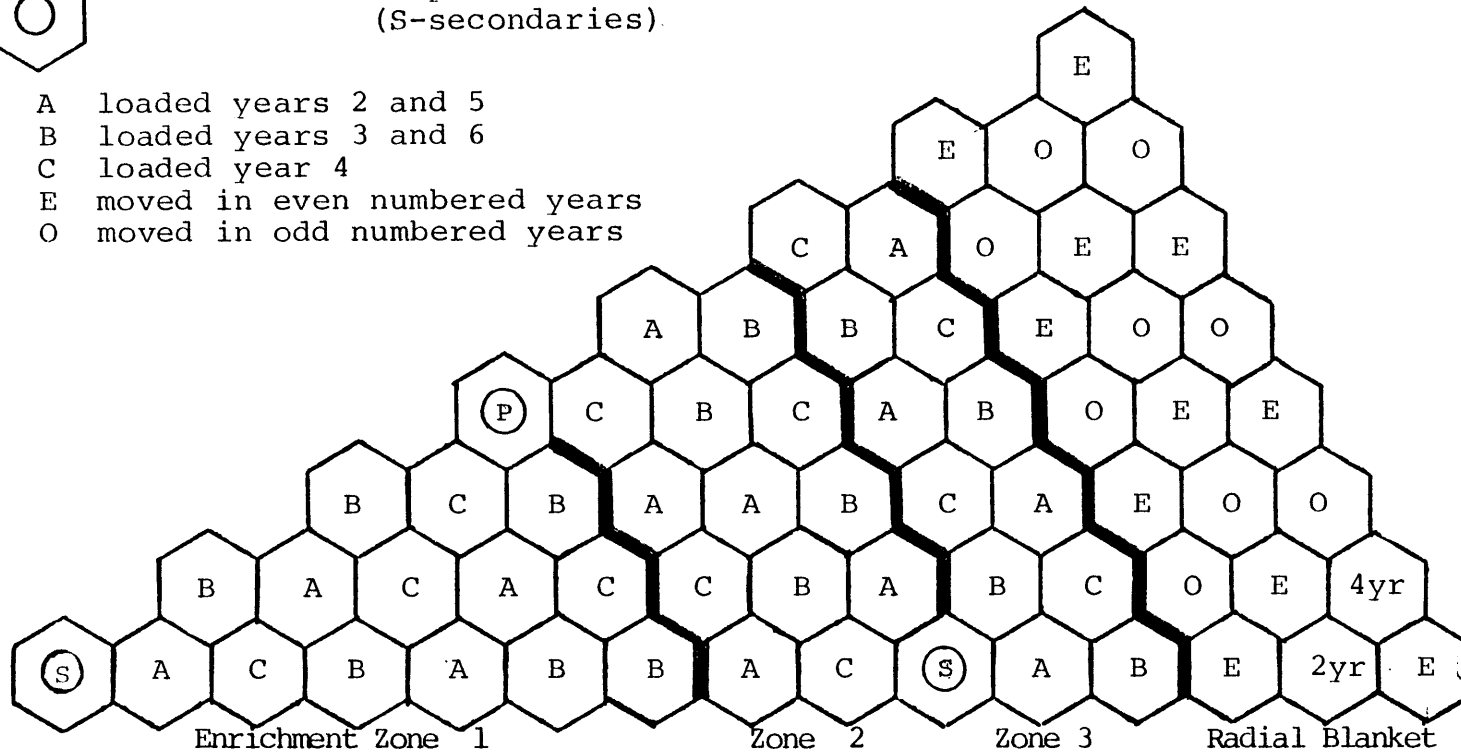


Fig. 3.13 Fuel Loading Pattern for the Reference Homogeneous Core

optimum, that comes from consideration of fabrication costs, the time and reactivity value of the plutonium bred in the blanket and the ability to shield the core barrel. Since this optimization is not expected to impact on the homogeneous-vs-heterogeneous comparison, the blanket irradiation time of six years which General Atomic uses was selected. The shuffling pattern used was an out-in-out scheme, where the clean blanket assemblies are loaded into the third row, moved to the first row after two years, moved to the second row after two more years, and then, after a total of six years moved out of the core. There are 12 and 6 additional assemblies in the third and second rows, respectively, that cannot fit into this shuffling scheme. These assemblies remain in the third row four years and then get moved to the second row for two years. (For computational purposes these assemblies are kept in their original positions for all 6 years, since the fuel loading scheme just described does not have 30° symmetry.) The blanket loading pattern was also modeled in 30° symmetry, and is also shown in Fig. 3.13. This blanket shuffling scheme should yield the best combination of reactivity contribution and shielding.

The sixth cycle has been selected as the "equilibrium" cycle. This is the first cycle in which none of the blanket assemblies took a shorter path to their location (i.e. to get to the second row radial blanket in a position to be removed at the end of the cycle requires five previous

cycles). The sixth cycle, however, is only an approximate "equilibrium" cycle since the fluence history of the second row radial blankets is not the same in this cycle as it would be for a later cycle. (This is due to the absence of plutonium in the second row of the radial blanket when these assemblies were in the third row, and other such effects.) This approximation is acceptable since the core driver assemblies dominate the economics and they are in a good "equilibrium" condition. This can be seen in Table 3.11, which shows that k_{eff} does not change from cycle to cycle when a constant feed enrichment is used.

3.4.2 Analytical Techniques Used to Arrive at the Equilibrium Cycle

The approach employed to arrive at the equilibrium cycle involves a number of steps. They are:

- 1) Use PERT-V to determine the zone dependent bucklings from the R-Z model used for the optimization study.
- 2) With these bucklings use a 30° symmetry 2DB hexagonal model to determine the relative zone enrichments which will yield the same peak power density in each zone.
- 3) Using these relative enrichments perform a concentration search in a 2DB R-Z model to determine the critical feed enrichments. Burn these compositions for three years.

Table 3.11

Eigenvalues* at the Start and End of the First Six
Cycles for Fixed Assembly Feed Compositions

<u>Time in Life</u>	<u>k_{eff}</u>
BOC1	1.015
EOC1	1.017
BOC2	1.013
EOC2	1.013
BOC3	1.011
EOC3	1.011
BOC4	1.011
EOC4	1.011
BOC5	1.011
EOC5	1.011
BOC6	1.010
EOC6	1.011

BOC \equiv Beginning of Cycle

EOC \equiv End of Cycle

* Eigenvalues from hex analysis, then biased by RZ analysis to account for the change in buckling as the cycle proceeds.

- 4) Use PERT-V and the fluxes from step 3 to determine bucklings for one, two, and three-year burned assemblies.
- 5) With the bucklings from step 4 and the feed enrichments from step 3 use a hexagonal 2DB analysis with 30° symmetry to model the feeding, burning, and shuffling to the beginning of cycle 6.

These five steps yielded all the information needed for the determination of the "equilibrium" cycle conditions. The R-Z analysis of the equilibrium cycle, however, requires assumptions with respect to axial burnup effects. (For the R-Z model see Fig. 3.3.) For the axial blankets the number densities after one cycle burnup from step 3 were employed since the average burnup of a fuel assembly at the beginning of an equilibrium cycle is one year. The axial buildup of plutonium in the radial blankets was simulated differently. First, the hexagonal number densities were assumed to be the mean over the active core height. Second, zone axial shape factors for each isotope were determined from the R-Z analysis of step 3. The zone axial shape factor is the ratio of the number density of a given isotope in a particular zone to the active-core-height-averaged values. Finally, these shape factors with hexagonal number densities were combined to form the R-Z zone number densities. Radial homogenization of each core zone and each blanket row was also

carried out to form the R-Z equilibrium model. The hexagonal model of the equilibrium core corresponded to conditions pertaining at the beginning of cycle six from step 5, but the axial bucklings were updated to correspond to the beginning of equilibrium cycle R-Z model just described.

This technique worked remarkably well. The beginning of equilibrium cycle eigenvalue determined using the R-Z analysis was 1.010 which was exactly the desired value. (The 1% excess in k_{eff} is to account for streaming.) Of most concern in this procedure was the assumption of constant feed number densities, which was required since the 2DB version then in use could not handle shuffling search parameters. (For the heterogeneous core this coding change had to be made.) As can be seen from the eigenvalues in Table 3.9, the use of constant feed number densities was quite adequate. This implies that the negative reactivity of the fission product buildup in the core was directly compensated by the positive reactivity effect of the buildup of plutonium in the radial blankets. Another concern was over the method used to determine the number densities for the equilibrium R-Z model. Since the R-Z analysis k_{eff} of 1.01 matched the hexagonal model k_{eff} of 1.01 the reactivity error associated with the determination of these number densities was small. Reactivity worth was chosen as the figure of merit since actual comparison of burned number densities would require a complex and expensive six cycle R-Z analysis or a 3DB burnup analysis.

3.5 Analysis of the Optimized Homogeneous Core Equilibrium Cycle

In this section all of the parameters needed to represent the homogeneous core in the assessment of using internal blankets in a GCFR will be determined. There will be many subsections describing the analysis techniques and results. The section begins with an analysis of the mass flows and doubling time. This is followed by a reporting of the power, burnup, flux, and fluence distributions. Next β_{eff} and other delayed neutron parameters are investigated. This is followed by the determination of the Doppler coefficients, and the control rod requirements and worths. Finally, material worths are presented for helium, clad, and fuel. The economic analysis is saved for Chapter 5.

3.5.1 Mass Flows and Doubling Time

To permit a complete economic analysis of core performance all of the mass flows would be desired for every cycle. Using the hexagonal burnup analysis described in subsection 3.4.2, and the same type of zone axial shape factors as described in that subsection, the mass flows for the first six cycles were calculated. These mass flows are recorded in Table 3.12. This table provides all of the physical information required for even the most complex economic analysis.

The doubling time, although a measure of the rate of buildup of plutonium, cannot be found directly from the mass

Table 3.12
Mass Flows for the Homogeneous Core
Kilograms Removed

Cycle Time:	EOC1	EOC2	EOC3	EOC4	EOC5	EOC6
Fuel Assemblies						
U-235	44.4	41.1	34.5	34.6	36.3	34.5
U-238	25,056.	25,807.	24,182.	24,182.	25,357.	24,184.
Pu-239	1,394.	1,594.	1,647.	1,649.	1,722.	1,647.
Pu-240	394.	434.	441.	441.	459.	440.
Pu-241	162.	148.	127.	128.	133.	127.
Pu-242	48.5	53.3	53.0	53.1	55.2	53.0
Fission Products	287.	561.	857.	853.	884.	854.
Number of Assemblies*	126.	132.	126.	126.	132.	126.
Blanket Assemblies						
U-235	21.2	20.5	19.6	18.7	18.6	28.6
U-238	10,907.	10,875.	10,788.	10,724.	10,724.	16,147.
Pu-239	27.2	60.2	104.	161.	162.	212.
Pu-240	0.1	0.6	1.7	4.2	4.1	5.9
Fission Products	1.5	4.4	12.0	23.9	23.5	30.6
Number of Assemblies*	36.	36.	36.	36.	36.	54

*84 Kg of HT-9 per fuel assembly, 55 Kg of HT-9 per blanket assembly

Table 3.12

(continued)

Cycle Time:	Kilograms Fed					
	BOC1	BOC2	BOC3	BOC4	BOC5	BOC6
Fuel Assemblies						
U-235	154.	50.5	52.9	50.5	50.5	52.9
U-238	77,720.	25,502.	26,716.	25,502.	25,502.	26,716.
Pu-239	3,774.	1,238.	1,297.	1,238.	1,238.	1,297.
Pu-240	1,138.	373.	391.	373.	373.	391.
Pu-241	571.	187.	196.	187.	187.	196.
Pu-242	136.	44.6	46.8	44.6	44.6	46.8
Number of Assemblies	384.	126.	132.	126.	126.	132.
Number of Blanket Assemblies*	234.	36.	36.	36.	36.	36.

* 304 Kg of heavy metal per blanket assembly.

flows. Instead, the fissile inventories at the beginning and end of the equilibrium cycle must be determined. In order to do that the R-Z equilibrium model was burned for one year (256 FPD) using the model shown in Fig. 3.3. From this the inventories were derived, and the doubling time for the equilibrium cycle of the optimum homogeneous core was thereby determined to be 10.9 years. Table 3.13 contains all the relevant data for the calculation of this doubling time. It is difficult to identify the uncertainty in this value but the sources of uncertainty can be assigned to one of two classifications: the errors due to model simplification, and iteration convergence error. Contributing to the first category are assumptions such as: the use of 1.01 for the critical eigenvalues, modeling the control rods as being all the way out of the core and axial blankets, and the use of LIB-IV cross sections for the analyses. These simplifications are believed to introduce errors which are independent of the homogeneous-to-heterogeneous comparison, and hence will not influence the relative doubling times. From experience, these uncertainties can add (or subtract) a number of years to (from) this doubling time. At this point it is also important to point out that the 10.9 year doubling time applies to an aggressive GCFR design, and the value should not be compared freely to doubling times quoted for a conservatively-designed LMFBR. The second category of errors is associated with the

Table 3.13
Homogeneous Core Doubling Time

BOEC Fissile Inventory (Kg)	5095.9
EOEC Fissile Inventory (Kg)	5559.3
BOEC Breeding Ratio	1.57
EOEC Breeding Ratio	1.51
Approximate Mean Core Neutron Energy	160 KeV
$\frac{1 + \delta}{1 + \alpha}$	1.063
Doubling Time (yr)	10.9

BOEC \equiv Beginning of Equilibrium Cycle

EOEC \equiv End of Equilibrium Cycle

level of accuracy of the methods used in the present work. This includes the determination of the number of cross section sets collapsed-to in SPHINX, the convergence tolerance specified for the power flattening iterations, and the end of cycle eigenvalue convergence. The uncertainty due to these effects is estimated as plus or minus a maximum of one year. It is this uncertainty that is recommended for use in evaluating the significance of doubling time differences in the present work.

3.5.2 Power, Burnup, Flux, and Fluence Distributions

The power, burnup, flux, and fluence distributions are derived from the combination of radial and azimuthal distributions from a 2DB hexagonal analysis (30° symmetry) and axial shape factors from an R-Z analysis. The R-Z model used is shown in Fig. 3.2 and the number densities for this equilibrium model were discussed in subsection 3.4.2. The hexagonal model is shown in Fig. 3.13 and also discussed in subsection 3.4.2.

The power densities at any location in the reactor can be calculated from the following prescription:

$$PD_{i,j,k} = \frac{POCH}{(HP)(12)(CH)} (HPD)_{i,j} (LTA)_k \quad (3.8)$$

where

$PD_{i,j,k}$ is the power density at position i,j,k ,

POCH is the total power of the core and radial blankets integrated over the active core height (i.e.: excluding the axial blankets and radial blanket extensions), derived from the R-Z analysis,

HP is the power normalization used in the hexagonal model (must be a 30° sector to agree with the factor of 12 in the denominator),

CH is the active core height (fissile fueled region excluding axial blankets) in cm,

HPD_{ij} is the hex power density for point i,j, and

LTA_k is the ratio of local to active core plane at height averaged power density at height K.

All this equation does is multiply a hex power density by an axial shape factor, but it assures that the hex power normalization is correct. Under normal circumstances $\frac{POCH}{(HP)(12)(CH)}$ is close to 1.0, but since the power in the axial blankets changes with burnup this correction to the hexagonal model's power normalization is often needed.

Equation 3.8 implies the assumption of separability of axial and hexagonal (radial) power shapes. If they were truly separable then only one axial shape function, LTA(k), would be needed. To test the separability, axial power density traverses normalized by the average power density over the active core height, LTAs from the R-Z analyses, were

compared. The peak to average power density ratios (largest LTAs) for all active core zones were found to vary from 1.95 to 1.231 for all radial locations and for all amounts of burnup (zero to three cycles). This would imply that using a single axial shape function, $LTA(K)$, with a peak to average power density ratio of 1.21 would hold the error in peak power density to within 2%, which is acceptable for core design at this level. The axial shape function, $LTA(K)$, used for the active core zones is shown in Fig. 3.14. The power densities from a three-year-burned axial blanket was used to introduce a degree of conservatism if this shape function is later used for thermal-hydraulic analysis. The LTAs for blanket assemblies vary more, with the peak values ranging from 1.25 to 1.32. For that reason a separate axial shape function is plotted for each row of the radial blanket in Fig. 3.15. Rather than give the radial power distribution in terms of power densities, the values have been converted to peak Kw/ft per assembly. These values are found in Fig. 3.16 for BOC and Fig. 3.17 for EOC. The data comes from a six mesh per hex model, and the side of the hex nearest to the calculated peak Kw/ft is marked with a dot. As can be seen from the figures, the peak fuel Kw/ft is 13.7 for BOC and 14.0 for EOC. The peak blanket Kw/ft is 6.8 at end of cycle. To convert any of these to peak power densities (Kw/cm^3) divide the core Kw/ft by 33.4 and the blanket Kw/ft by 99.4. Thus the

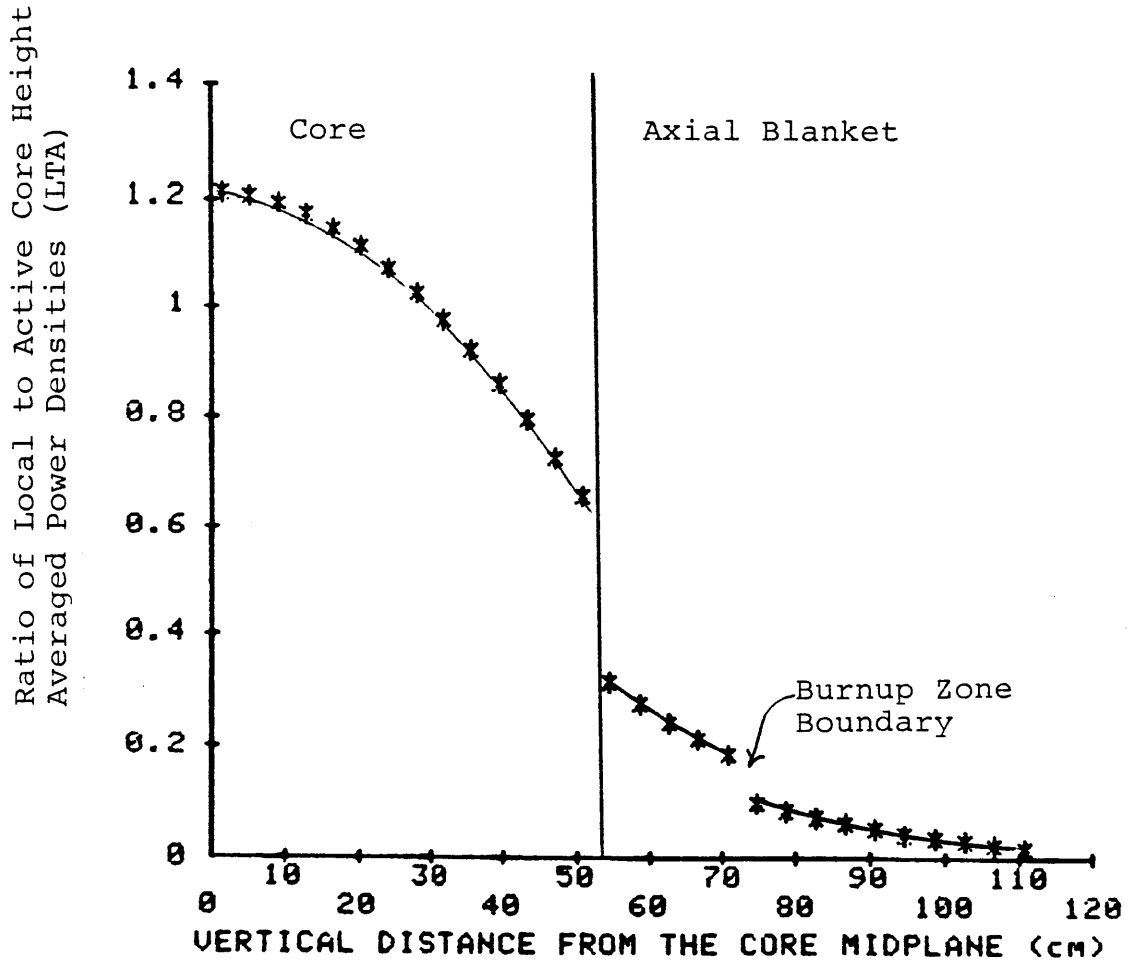


Fig. 3.14 The ratio of the local power density to the active core height averaged power density (LTA) as a function of the vertical distance from the core midplane.

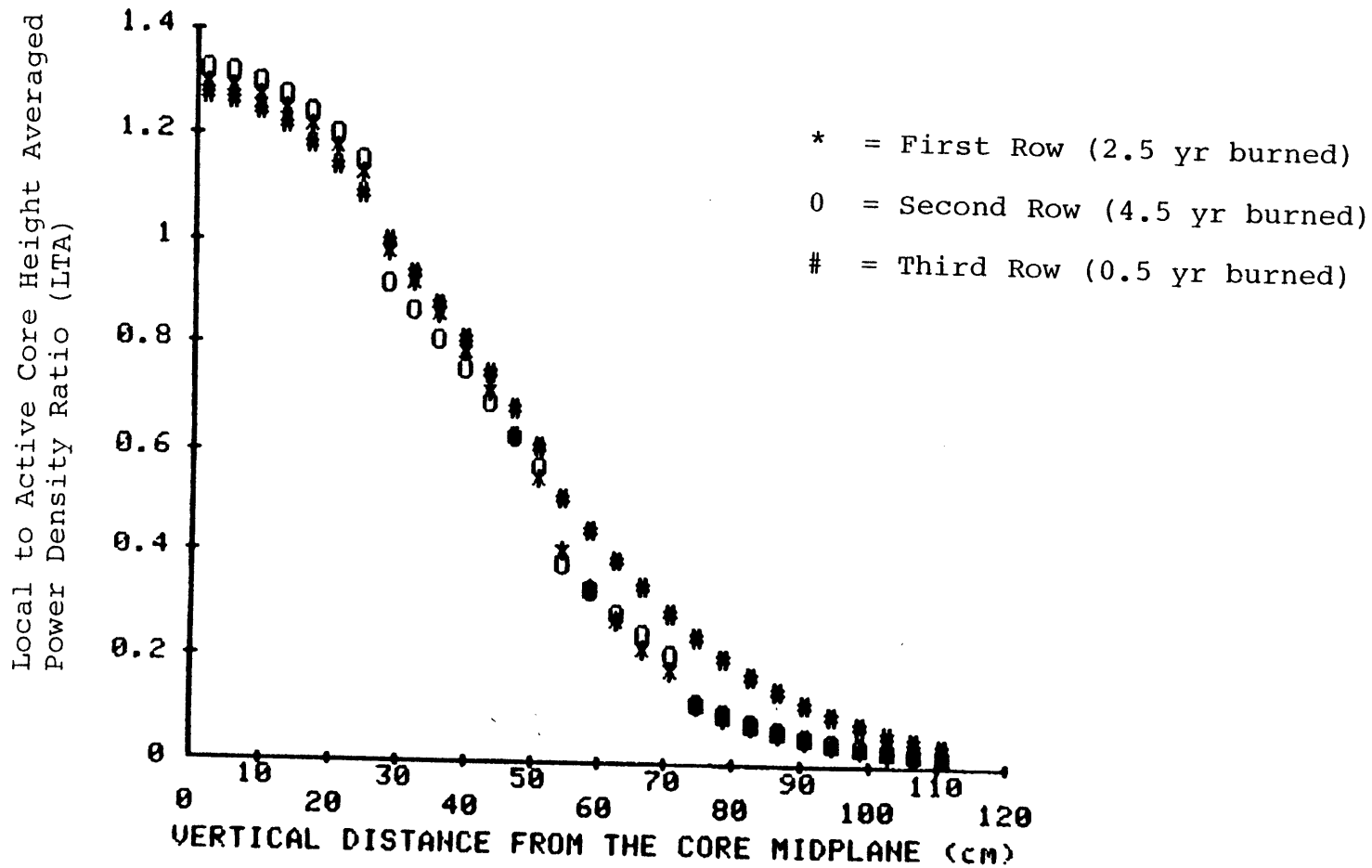


Fig. 3.15 The ratio of the local power density to the active core height averaged power density (LTA) for each of the radial blanket rows. [Note: The discontinuities in the curves are caused by the burnup zoning.]

30° Symmetry Sector Shown

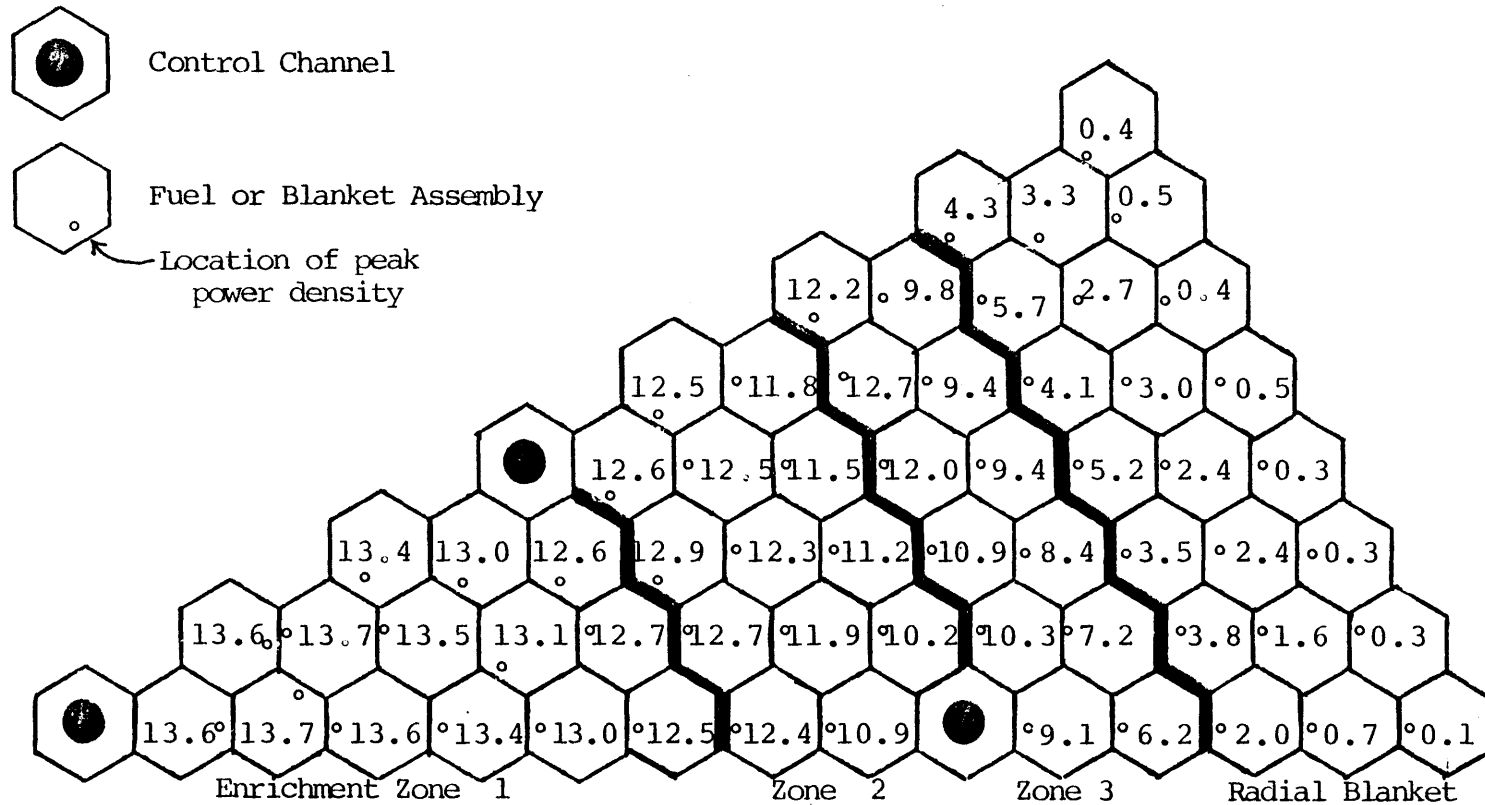


Fig. 3.16 Peak kw/ft at BOEC for the Reference Homogeneous Core

30° Symmetry Sector Shown

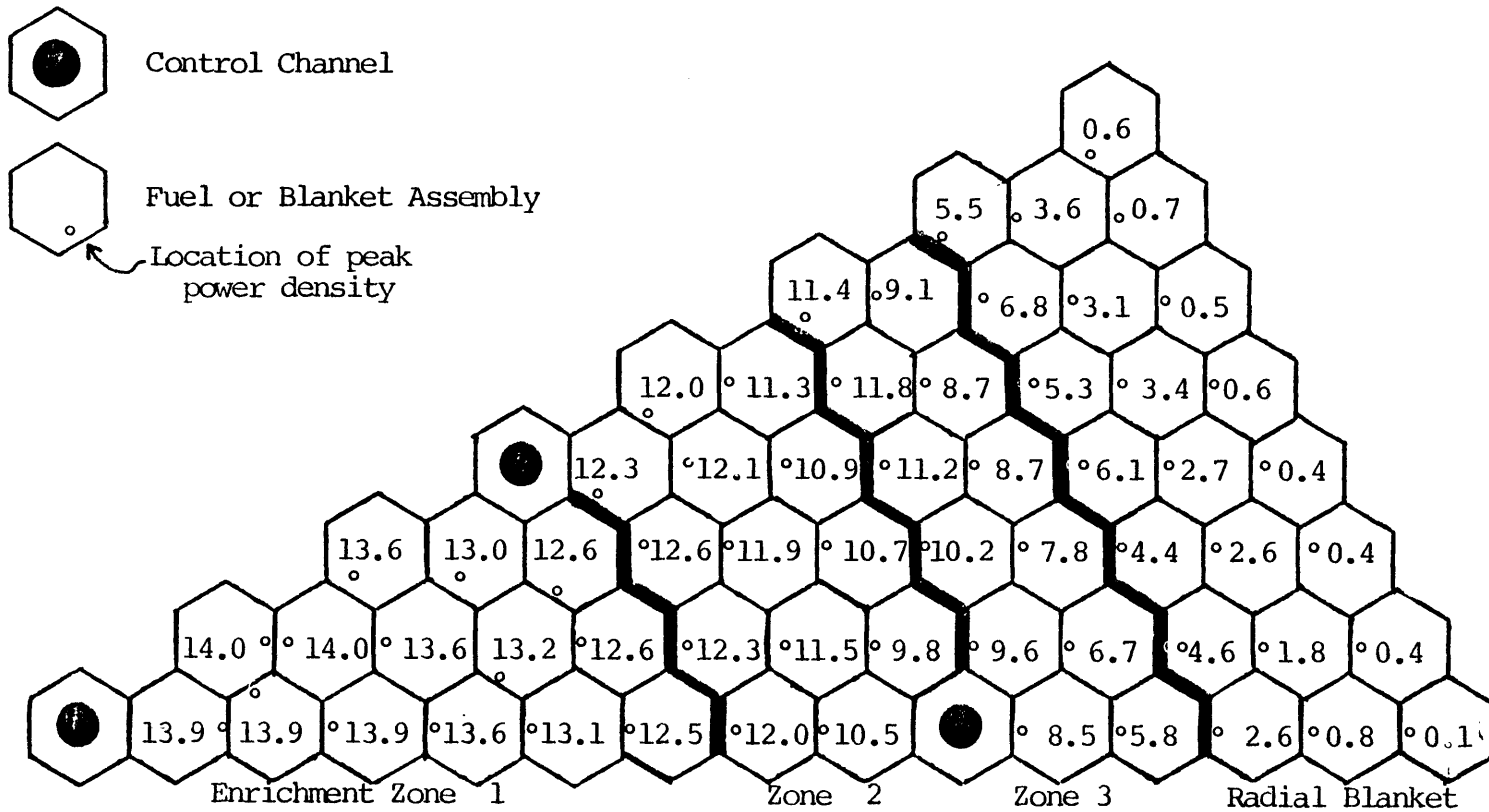


Fig. 3.17 Peak kw/ft at EOEC for the Reference Homogeneous Core

core peak power densities are 0.41 Kw/cm^3 and 0.42 Kw/cm^3 at BOC and EOC, respectively. The blanket peak power density is 0.07 Kw/cm^3 . One final figure of merit is the radial peak-to-average power density for the fuel assemblies, since this is an indication of the effectiveness of the enrichment zoning. This ratio is 1.23 and 1.29 for BOC and EOC respectively.

The burnup distribution could be calculated much the same way as the power distribution. However, since the breeding ratio in the core is close to 1.0 there is no significant change in assembly power as burnup progresses. Thus, the burnup distribution is essentially the same as the power distribution, except for a constant. The core burnups can be found by taking the EOC distributions found in Fig. 3.17 and multiplying them by 7115 to get the peak burnup in MWD/MT. Using this approach the peak core burnup is found to be 99,000 MWD/MT; and the average burnup is $99,000 / (1.29 \times 1.21) = 64,000 \text{ MWD/MT}$. The blanket assembly burnup cannot be calculated quite as simply, but using the burnup analysis previously carried out to devise the equilibrium core, the peak blanket burnup is found to be roughly 10,000 MWD/MT.

The flux and fluence distributions were generated in the same manner as the power and burnup distributions. The flux distributions at the core mid-plane at BOC and EOC are shown in Figs. 3.18 and 3.19, respectively. The axial shape function (LTA's) for the active fuel regions is the same as

shown in Fig. 3.13. For the axial blanket a smooth extrapolation of the curve in Fig. 3.13 could be used if needed. For the radial blanket the shape factors from Fig. 3.14 can be used as an approximation. As can be seen from the figures the peak flux is 6.4×10^{15} neutrons/cm² sec, and the peak total fluence is 4.2×10^{23} neutrons/cm². Since the "fast" fluence is of greatest importance to the assembly damage function the fraction of the total fluence that is above 0.1 MeV must be determined. Figure 3.20 shows the normalized zone averaged flux as a function of energy for each core zone. (Shown only for BOC; the EOC spectrum is very similar except for slightly fewer neutrons at the lower energies). From these curves the fraction of the flux above 0.1 MeV was determined to be 0.56. Therefore the peak fast fluence is 2.4×10^{23} neutrons/cm².

3.5.3 β_{eff} and Delayed Neutron Parameters

β is the fraction of neutrons produced in fission that are delayed. β_{eff} , then, is the importance-weighted value of β . Calculations were performed to find β_{eff} for BOEC and EOEC. The flux and adjoint were obtained from 2DB R-Z analyses and PERT-V was used to do the weighting. Everything is straightforward in such a calculation except that the selection of the input data must be specified.

The data used for the present analysis comes from the ENDF/B-IV evaluation done by Cox (C7). Six delayed neutron

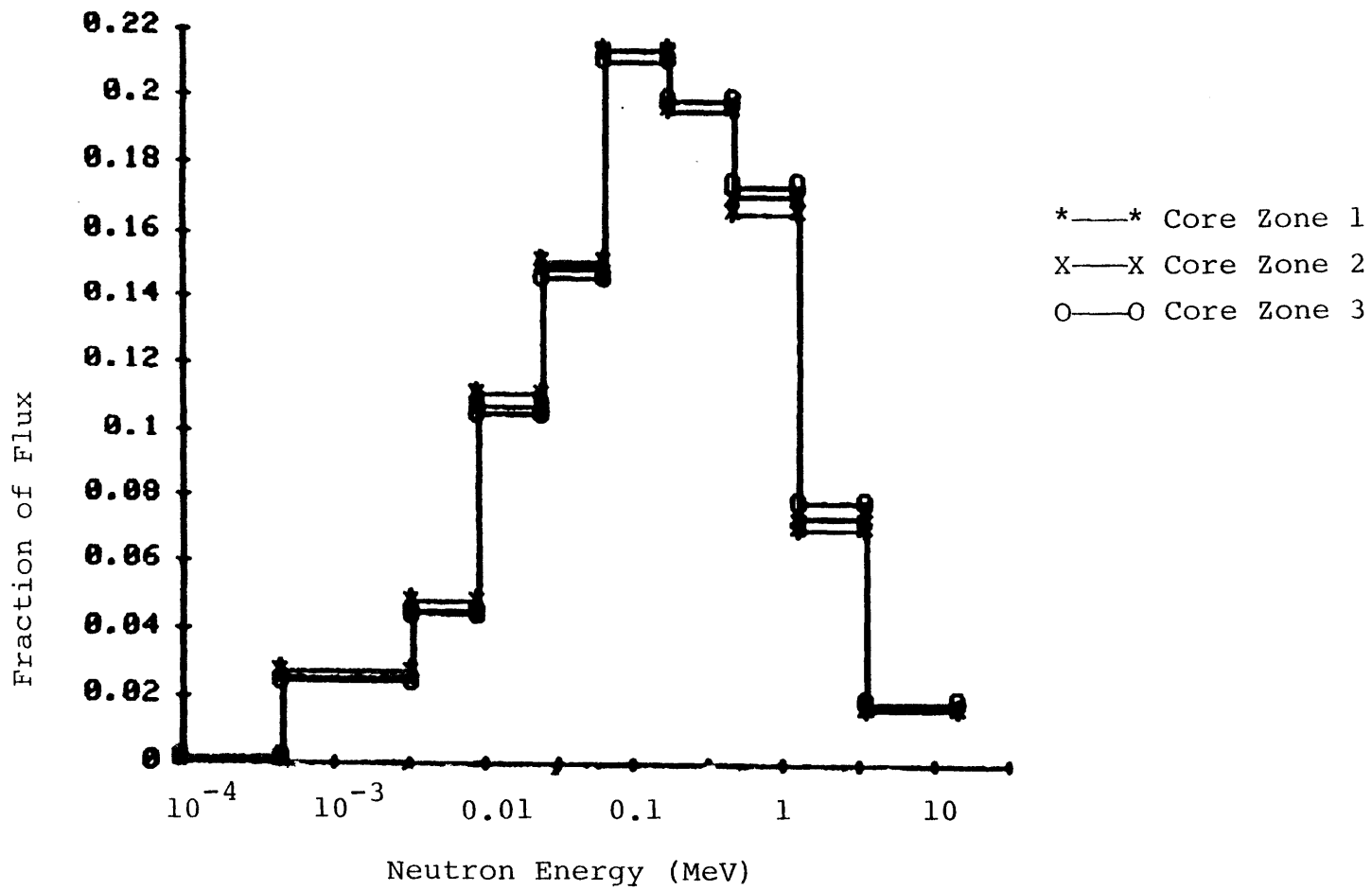


Fig. 3.20 Homogeneous core neutron energy spectrum.

group data for U-235, U-238, Pu-239, Pu-240, and Pu-241 were available, and used. For Pu-242 fission 1×10^{-2} was used for the absolute total delayed neutron yield per fission and the relative group yields of Pu-241 were used. Only one set of half lives for the delayed groups was used: a fission rate weighted average of the U-238 and Pu-239 half lives. Only one delayed fission spectrum was used: the delayed chi for Pu-239 for each delayed group weighted by its fractional yield. The selection of the delayed fission spectrum is important. If, for example, the prompt fission spectrum were used β_{eff} would increase by 25%!

The results of the β_{eff} calculation are shown in Table 3.14.

3.5.4 Control Rod Analysis

In this subsection we will address the question of whether there are enough control rod positions in the present design (see Fig. 3.13). To do this estimates must be obtained of the control rod requirements and worths. It will be assumed that some flexibility exists in the present design by way of varying the B-10 enrichment. Since all of the analysis has been done with all rods out, only the number of control positions needed and their location impact the homogeneous-to-heterogeneous comparison.

3.5.4.1 Control Rod Requirements

The purpose of the control rod systems is to provide

Table 3.14

β_{eff} and Delayed Neutron Parameters for the
Reference Homogeneous Core

Delayed Group	Half Life (sec)	Effective Delayed Neutron Fraction	
		BOEC	EOEC
1	53.7	8.1 - 5	8.1 - 5
2	22.2	7.6 - 4	7.5 - 4
3	5.2	7.1 - 4	6.9 - 4
4	2.0	1.4 - 3	1.4 - 3
5	0.50	7.0 - 4	6.8 - 4
6	0.19	2.1 - 4	2.1 - 4
Total		3.9 - 3	3.8 - 3

for reactivity control throughout normal operation and to provide for a highly reliable shutdown system for off-normal events. To meet these requirements two independent systems are normally used, each with its own appropriate reactivity requirements. The primary system is used for normal reactivity control and must be able to handle the temperature-reactivity defect from room temperature to hot-full-power (HFP) conditions at the time in any cycle which has the highest excess reactivity. The primary system must do this without use of its highest worth rod, and the system is assumed to have a reactivity fault of 0.01 in Δk . The secondary system must be able to do the same, but it is not required to handle the temperature-reactivity increment from room temperature to the hot-standby condition. Finally, both systems must be able to do their task at a 99.7% confidence level (3σ).

It is not the point of this subsection to determine accurately the control requirements but rather to get an estimate that can be used in the homogeneous-to-heterogeneous comparison. In most fast reactor calculations the Doppler effect is roughly 80% or more of the temperature defect (T_2 , R_1). The uncertainty on the Doppler reactivity is roughly 15% (1σ) (R_1). For the homogeneous core in the present work the cycle Δk is zero. With this in mind the control reactivity worth requirement will be estimated as the Doppler reactivity

times 1.8 plus 0.01 Δk for the reactivity fault. (1.8 comes from the Doppler reactivity plus three sigma divided by 80%).

3.5.4.2 Doppler Coefficients and Temperature Defects

The Doppler reactivity feedback was calculated for a temperature change of 700°K for the fuel and 300°K for the structure. (Helium has basically no Doppler feedback.) This was done using the fluxes and adjoint fluxes from 2DB R-Z analyses of the beginning and end of the equilibrium cycle. The temperature-induced difference in the cross sections was obtained from SPHINX using the hot and cold cross section sets described in Chapter 2. The first order perturbation theory embodied in PERT-V was used to calculate the reactivities for every mesh point in the core and blankets due to the change in temperature in the fuel and structure separately. These reactivities were converted to Doppler coefficients and are tabulated by zone in Table 3.15. These Doppler coefficients are larger than those previously published for a 300 MWe design (T10), due to the lower enrichment in the larger core. For added insight, two traverses of the Doppler coefficient are plotted as Figs. 3.21 and 3.22 (radial and axial traverses, respectively). If needed, combining the radial Doppler coefficients from Fig. 3.21 with a normalized axial factor from Fig. 3.22 would yield a good representation of the overall Doppler effect.

To determine the temperature defect, temperatures must

Table 3.15

Homogeneous Doppler Coefficients

Doppler Coefficient $(-T \frac{dk}{dT} \times 10^{-4})$

Region	<u>Fuel</u>		<u>Structure</u>	
	BOEC	EOEC	BOEC	EOEC
Core Zone 1	29.7	28.3	1.6	1.6
Zone 2	24.4	22.4	1.3	1.3
Zone 3	9.1	8.4	0.4	0.4
Total	<u>63.2</u>	<u>59.1</u>	<u>3.3</u>	<u>3.3</u>
Radial Blanket				
1st Row	2.1	2.1	--	--
2nd Row	0.5	0.5	--	--
3rd Row	0.1	0.1	--	--
Extensions	0.2	0.2	--	--
Total	<u>2.9</u>	<u>2.9</u>	<u>0.06</u>	<u>0.07</u>
Axial Blanket	<u>7.3</u>	<u>8.4</u>	<u>0.2</u>	<u>0.3</u>
Total	73.4	70.4	3.6	3.7

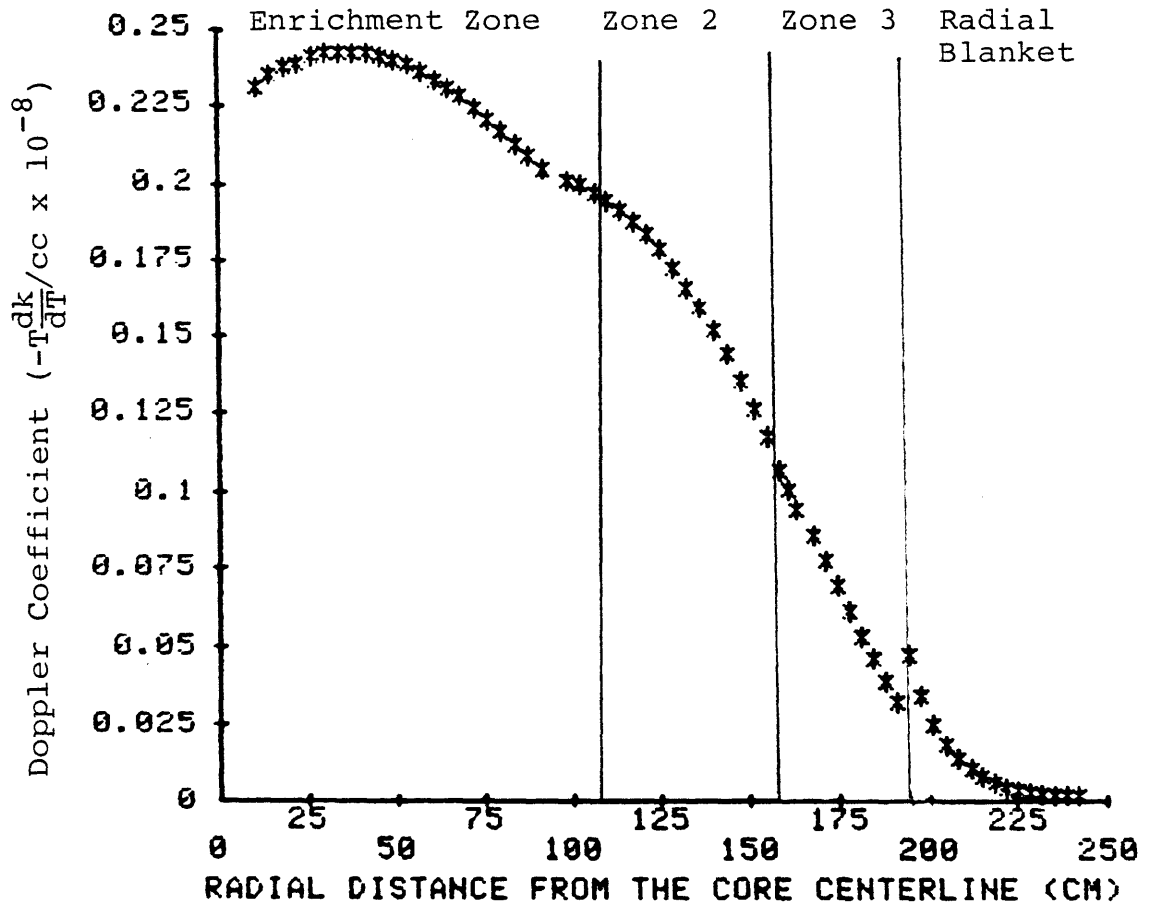


Fig. 3.21 Doppler coefficient at the core midplane for the reference homogeneous core.

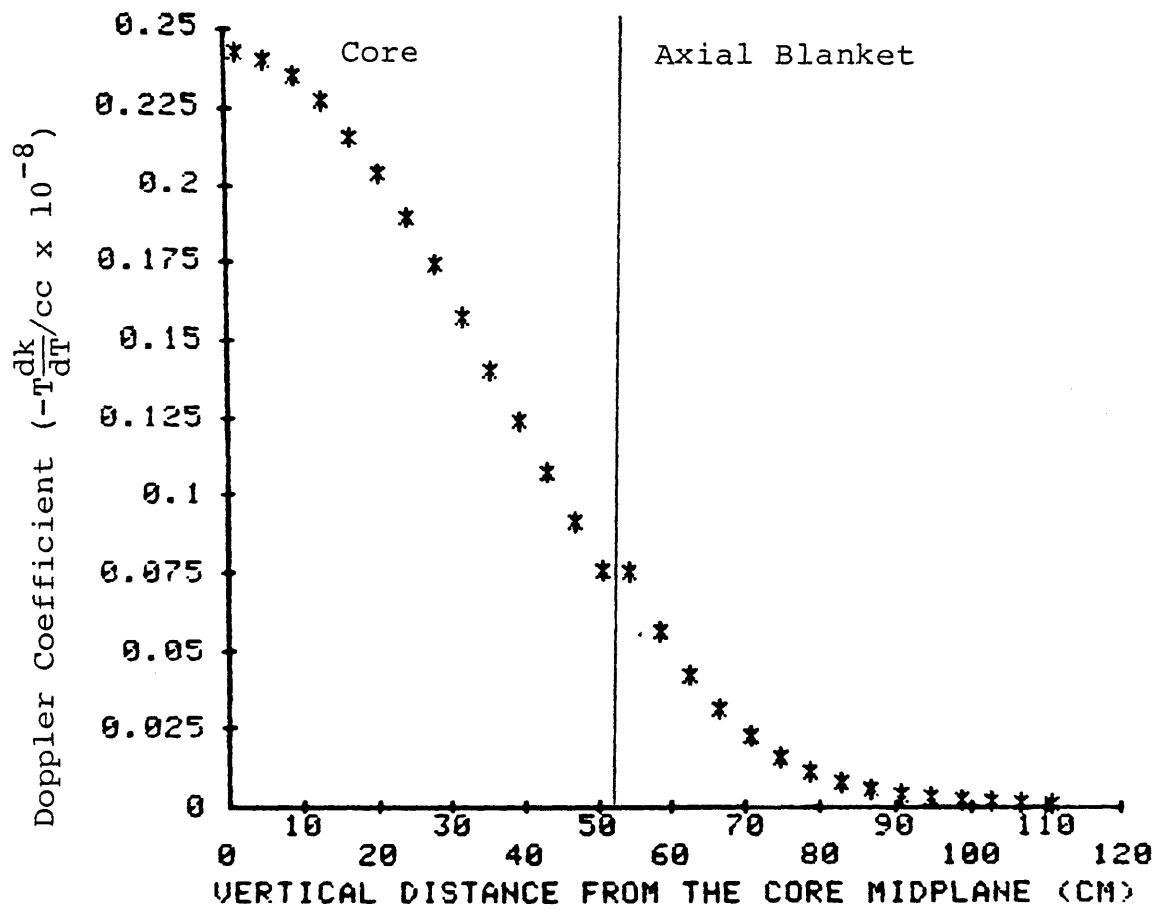


Fig. 3.22 Axial traverse of the Doppler coefficient for the reference homogeneous core.

be known for the hot-full-power and hot-standby conditions. Using CALIØP the pellet temperatures at HFP are estimated to be 1500°C for the driver fuel and 1000°C for the blankets. At HFP all the structure will be assumed to be at 600°C. The hot-standby temperatures will be assumed to be the core inlet temperature of 300°C, and everything will be assumed to be at that temperature. Using these temperatures the reactivity worth needed for startup has been found and is recorded in Table 3.16.

3.5.4.3 Control Rod Worths

The control rod worths were calculated using 2DB's hexagonal 30° symmetry model. Eigenvalue calculations were done at the beginning and end of the equilibrium cycle for an all-rods-out case, a case with all the primaries in, and, finally, a case with all the secondaries in. In order to calculate cases with one stuck rod out a full core analysis would be needed. This was avoided to save computational costs, and since this detailed an analysis is not needed for present purposes. Furthermore, one can assume as an approximation that the stuck rod has the average worth of the set of rods. Thus, one sixth of the primary and one seventh of the secondary worth is neglected in the comparison of the control rod worths and their requirements.

Table 3.17 summarizes the control rod worth calculations and compares the worths to the requirements.

Table 3.16

Temperature Defect and Control Requirements for the
Reference Homogeneous Core

PuO ₂ /UO ₂	Δk/k	
	BOEC	EOEC
Core		
Room Temp. to 300°C	-0.0042	-0.0040
300°C to 1500°C	-0.0071	-0.0067
Blankets		
Room Temp. to 300°C	-0.0007	-0.0008
300°C to 1000°C	-0.0008	-0.0009
Structure		
Room Temp. to 300°C	-0.0002	-0.0002
300°C to 600°C	-0.0002	-0.0002
Cold to HFP	-0.0132	-0.0128
Hot-Standby to HFP	-0.0081	-0.0078
Primary Requirements	-0.034 (\$8.72)	-0.033 (\$8.68)
Secondary Requirements	-0.025 (\$6.41)	-0.024 (\$6.15)

Table 3.17

Control Rod Worths and Requirements* for the Reference
Homogeneous Core

<u>Capabilities</u>	BOEC	EOEC
Δk Primaries*	0.0321	0.0324
Δk Secondaries*	0.0196	0.0190
Worth with One Stuck Rod*		
Primaries	\$6.86	\$7.11
Secondaries	4.31	4.29
<u>Requirements</u>		
Primaries	8.72	8.68
Secondaries	6.41	6.15

*The control rods used here are only 50% enriched in B-10. Clearly, since the worths do not meet the requirements, a higher enrichment would be used.

3.5.4.4 Summary of the Control Rod Analysis

Looking at Table 3.17 may lead one to believe that more control positions are needed. This may not be the case since the boron enrichment used for this analysis was only 50% B-10. The maximum deviation from the desired worth was ~50% for the secondaries at BQEC. The B-10 content, however, could be increased 100%. This may be enough to increase the rod worths to meet their requirements. The rod worths and rod requirements are sufficiently close for the purpose of this analysis. Further investigation would be required, however, if this design is continued beyond the present work.

3.5.5 Material Worths

This subsection presents the calculation of the material worths for helium, HT-9, and fuel. These worths along with other parameters from other subsections, such as the Doppler coefficient, aid in determining the inherent safety of the reactor design. Ultimately the achievement of an appropriate level of safety depends on the engineering of reliable protection systems designed to mitigate off-normal events.

The calculation of the material worths was done using first order perturbation theory (PERT-V). This required the flux and adjoint flux from 2DB R-Z analyses and the change in the macroscopic cross sections due to removal of the material under consideration. The analysis was done for both the beginning and end of the equilibrium cycle. A regionwise compilation of the results is found in Table 3.18. Caution

Table 3.18

Material Worths for the Reference Homogeneous Core

Material Worths, $\Delta k/kg$

Region	Helium*		HT-9		Fuel**	
	EOEC	BOEC	BOEC	EOEC	BOEC	EOEC
Core						
Zone 1	-2.0-4	-2.1-4	-6.1-6	-6.4-6	9.4-6	9.5-6
Zone 2	-1.4-4	-1.4-4	-4.2-6	-4.3-6	8.1-6	7.6-6
Zone 3	-4.8-5	-4.8-5	-8.2-7	-8.8-7	6.1-6	5.5-6
Average	-1.3-4	-1.3-4	-3.7-6	-3.8-6	7.8-6	7.5-6
Axial Blanket						
First 20 cm	-1.6-5	-1.9-5	+3.9-7	+2.7-7	8.6-8	2.5-7
Remaining 40cm	-2.1-6	-2.5-6	+5.5-8	+6.0-8	1.5-9	1.1-8
Average	-6.8-6	-8.0-6	+1.7-7	+1.3-7	2.9-8	8.7-8
Radial Blanket						
1st row	-3.3-6	-3.7-6	+1.9-7	+1.6-7	8.2-8	9.8-8
2nd row	-9.0-7	-9.8-7	+2.8-8	+2.8-8	2.3-8	2.5-8
3rd row	-1.0-7	-1.2-7	+4.5-9	+4.9-9	5.1-10	6.6-10
Average	-1.4-6	-1.6-6	+7.3-8	+6.3-8	3.5-8	4.1-8

* $\Delta k/\Delta\psi$; core plus blanket total is 3.9-6 and 4.0-6 for BOEC and EOEC respectively.

** Fuel worth is the worth of the pellet material normally at the given position.

should be taken in using this table since it assumes a uniform removal or addition of material in the entire region. The region-averaged $\Delta k/Kg$ is not necessarily a good indicator of reactivity changes due to the addition or removal of material during specific accident scenarios, since wide spatial variations in reactivity worth (even in the sign of the reactivity) is common inside many zones.

The most common way of addition or removal of helium is through a change in pressure. Therefore, it is more appropriate to use a Δk per psi change in pressure for this constituent. For this core the $\Delta k/\text{psi}$ change is $3.9E-6$ and $4.0E-6$ for the beginning and end of the equilibrium cycle respectively. This makes the reactivity worth of depressurization 0.0067 and $0.0070 \Delta k$, or $\$1.71$ and $\$1.83$ for BOEC and EOEC, respectively. These depressurization worths may seem high at first but this is due to the high operating pressure employed (2.21 times the system pressure used in reference (T10), where the helium depressurization worth was determined to be 55¢ in a 300 MWe reactor). The removal of helium contributes positive reactivity, since by removing it the spectrum is hardened. In order to aid in understanding the spectral effects the importance (i.e. adjoint flux) as a function of energy is plotted in Fig. 3.23.

The cladding worth is important in many accident scenarios. A conservative approach to a set of HCDA accidents has the cladding removed from the core and freezing just inside

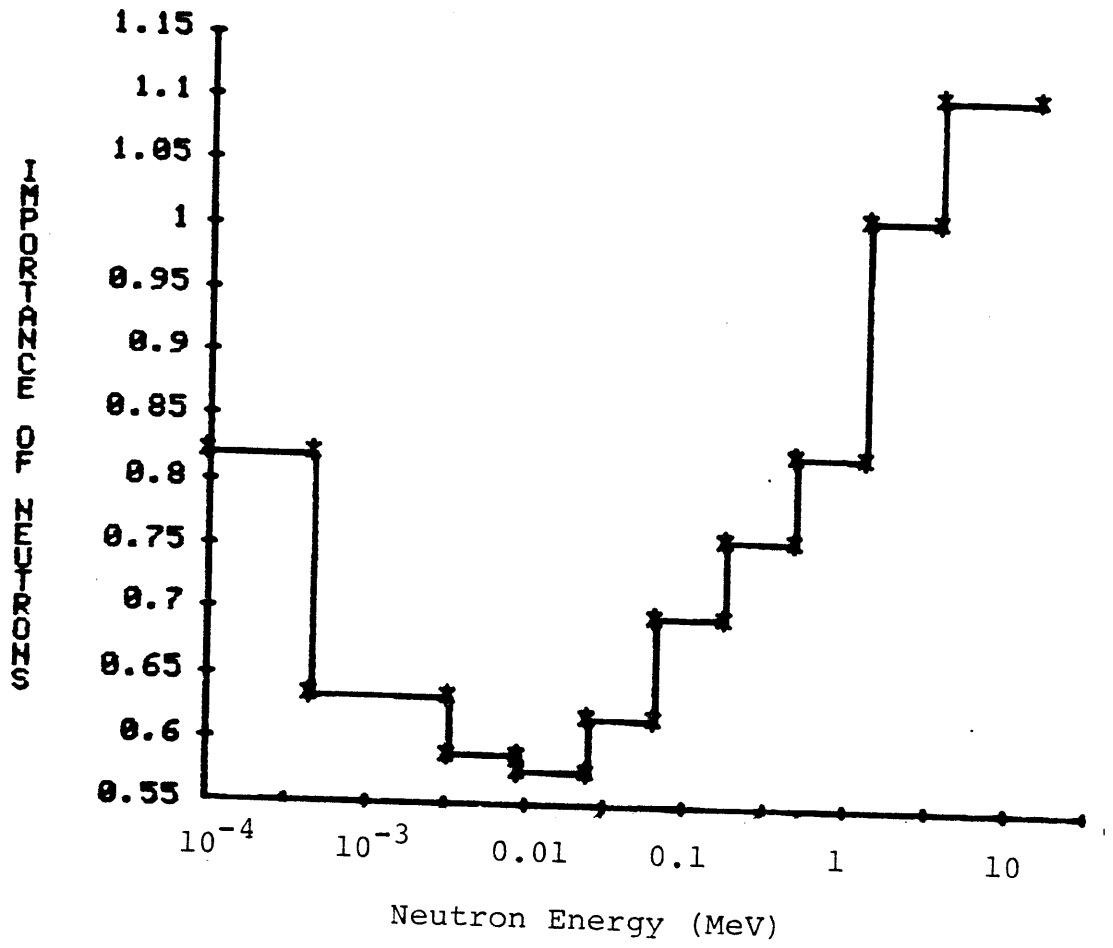


Fig. 3.23 Adjoint spectrum for the homogeneous core.

the axial blankets. For this core the reactivity worth of such a movement would be \$9.77 and \$9.98 for the beginning and end of the equilibrium cycle, respectively. These values are low compared to other GCFR studies due to the relatively low absorption cross section of HT-9 (in fact the moderation worth is larger than the absorption worth). In moving the cladding from the core to the axial blanket the worth goes from negative to positive. This is due to the dominant effect of HT-9 in the core where it acts as a moderator, more efficiently than in its role as a reflector in the axial blanket. In order to illustrate this reactivity effect, Fig. 3.24 is presented.

The fuel worth is needed to estimate the worth of fuel compaction or expansion. Figures 3.25 and 3.26 show a radial and axial traverse respectively. One can estimate the worth of small core expansions or contractions by comparing the worth of the fuel at the edge of the core to that of the average core worth. Doing this, the axial and radial expansion coefficients become roughly 3¢/mm and 5¢/mm respectively.

The reactivity worths and coefficients calculated in this subsection are the ingredients for the more detailed safety analyses carried out on specific GCFR designs. Therefore, the reactivity worths and coefficients reported here can be compared to those of the heterogeneous core design to indicate the relative potential of each to meet

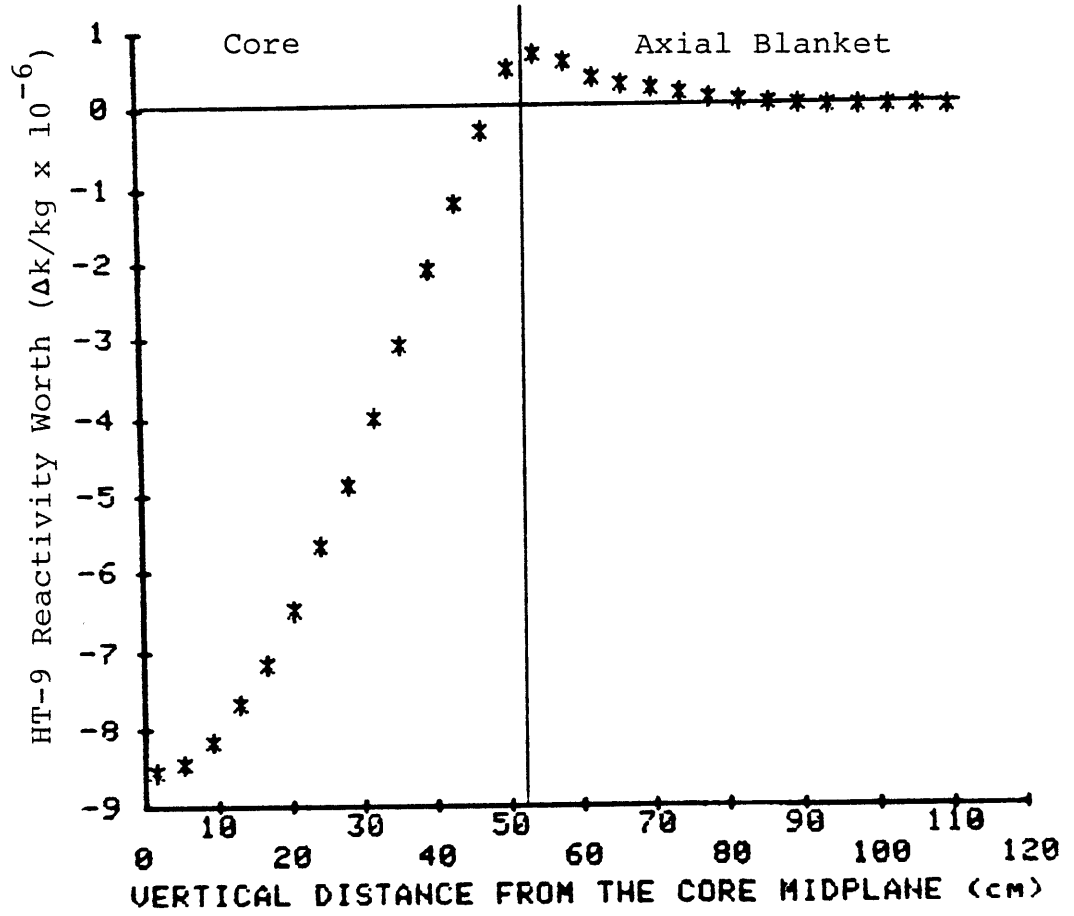


Fig. 3.4 Axial traverse of the HT-9 reactivity worth for the reference homogeneous core.

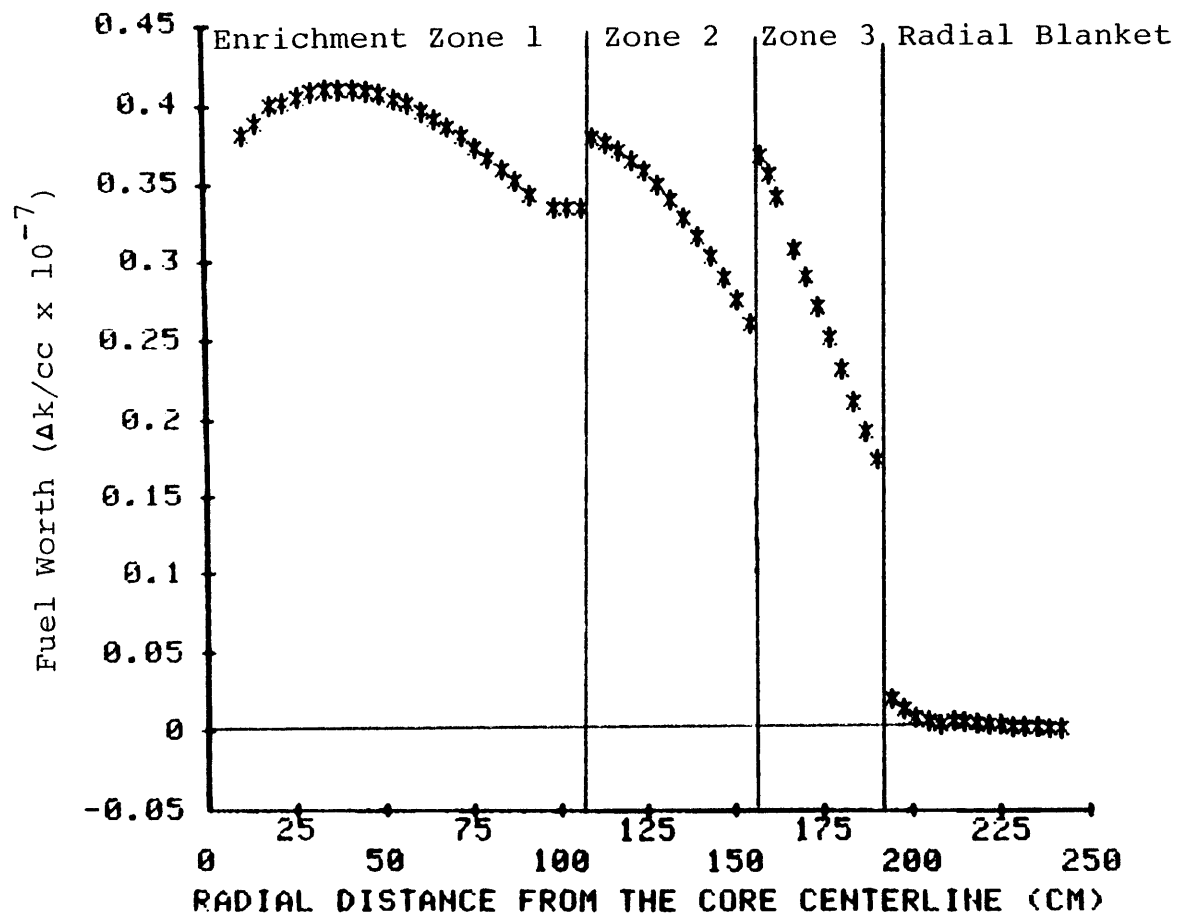


Fig. 3.25 Fuel worth as a function of radial position for the reference homogeneous core.

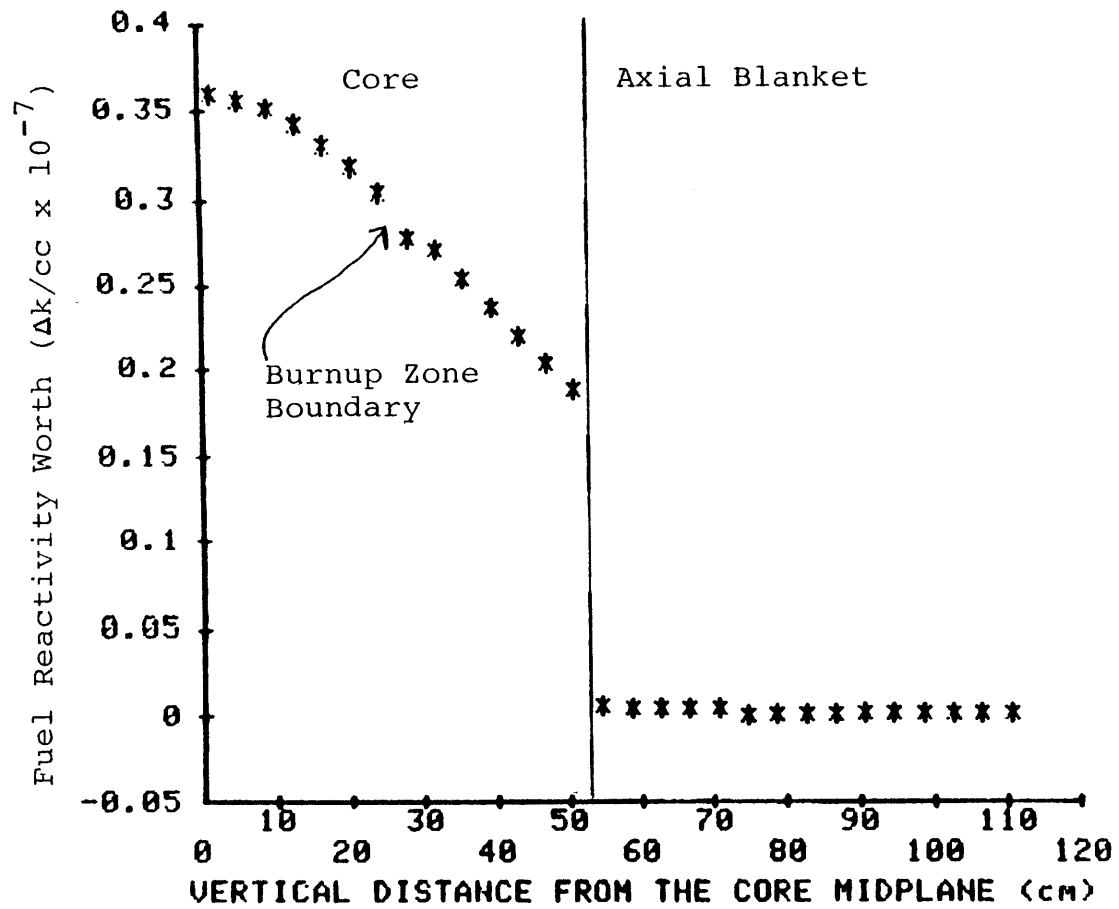


Fig. 3.26 Fuel reactivity worth as a function of axial position for the reference homogeneous core.

safety criteria and to assess the relative difficulty of designing safety systems for each to provide appropriate margins between normal, transient, and accident conditions, and core damage.

3.5.6 Summary of the Homogeneous Core Analysis

This section has described the neutronic analysis of the optimum homogeneous core. The design meets state-of-the-art power, burnup, and fluence limits. The design is projected to have sufficient allowance for neutronic control, but more work would be recommended to verify adequate control worth. The reactivity worths for key materials correspond to those expected for a large GCFR.

3.6 Summary

In this chapter the constraints of the homogeneous-to-heterogeneous design comparison were discussed, the optimum homogeneous core design was found, the fuel management and burnup of the optimum homogeneous core from start up to equilibrium cycle conditions was performed, and finally, the equilibrium cycle of the optimum homogeneous core was fully analyzed neutronically.

This homogeneous core, which will be used as a reference for the comparison to a heterogeneous core, has undergone thorough thermal-hydraulic and neutronic examination. The thermal-hydraulic analysis was done using CALIØP. The neutronic analysis was done using 2DB and PERT-V.

Overall the design is aggressive and optimistic rather than conservative. Some of the aggressive assumptions are:

- 1) PCRV pressure of 120 bar,
- 2) Circulators of 35,000 hp each,
- 3) Cladding and duct material is HT-9,
- 4) All-rods-out neutronic analysis, and
- 5) Only 13 control rod positions.

This aggressive approach does not impact on the homogeneous-to-heterogeneous design comparison since both designs are done under the same constraints.

The optimization of the homogeneous core was done by selecting the best performing pin diameter meeting thermal-hydraulic constraints. A set of four different optimization parameters were investigated to give confidence in the selection of the optimum. The 8 mm pin diameter was selected, since it performed well for most of the figures of merit investigated. In the investigation of the optimum doubling time it was found that increasing core size had a large negative impact on the doubling time. This forbodes possible difficulties for the heterogeneous core, which will always be larger than a homogeneous core due to the low power density of its internal blankets.

This chapter has developed the methods of analysis and determined the key parameters for the homogeneous core. The next chapter will use these methods to develop the optimum heterogeneous core and compare it to the homogeneous core analyzed here.

CHAPTER 4

HETEROGENEOUS CORE ANALYSIS

4.1 Introduction

The heterogeneous core has been variously attributed with a higher breeding ratio, lower doubling time, decreased fast fluence, cheaper fuel cycle costs, better power flattening, and improved safety compared to a conventional, homogeneous core. Most of these claims have been hotly debated, as Chapter 1 has already noted. This chapter will help to resolve that debate by not only presenting results, but also by explaining the reasons for the observed effects. Much of the reason for the continuing debate has come from inconsistent analysis of the heterogeneous/homogeneous core concepts. This may take the form of comparing a fully optimized design to an unoptimized design or, even worse, comparing a constrained design to another design which does not meet the constraints. Chapter 3 has set the constraints and optimization level of the present work. This chapter will investigate the heterogeneous core under those constraints. Thus, with the conclusion of this chapter both the heterogeneous and homogeneous core designs will have been investigated in a fair and unbiased manner, thereby permitting identification of the real effects of heterogeneity.

The chapter begins by determining the optimum heterogeneous core which meets the constraints established in Chapter 3. This is actually done by finding the optimum arrangement of core and blanket assemblies from a set of thermally and hydraulically acceptable assembly designs. Both the optimum fuel volume fraction and core arrangement are studied. The key figure of merit for these studies is the doubling time; however, the impact on other figures of merit is discussed.

Following the selection of the optimum heterogeneous core is a section describing the fuel management scheme and the analysis needed to determine the equilibrium cycle. Care was taken to use, as close as possible, the same methods as were used for the homogeneous core.

With the optimum equilibrium core identified, it is analyzed using the methods described in Chapter 3 for the homogeneous core analysis. The analysis includes mass flow rates and doubling time, power, burnup, flux, and fluence distributions; calculation of β_{eff} ; control rod analysis, including Doppler coefficients; and, material worths. As each parameter is analyzed a comparison will be made to the homogeneous core results and a discussion presented explaining the reasons for the differences.

The chapter is then summarized, and the key weaknesses and strengths of the heterogeneous design are pointed out.

4.2 Heterogeneous Core Optimization

In order to match the constraints placed on the homogeneous design, the optimum heterogeneous design will be limited to the best performing combination of thermally and hydraulically acceptable core and blanket designs described in Section 3.2 of Chapter 3. This constraint should be fair to the heterogeneous core since it allows selection of pin diameters from 6 to 11 mm and fuel volume fractions in the driver assemblies of 0.24 to 0.49. The heterogeneous designs are allowed any number and arrangement of internal blanket assemblies, using any of the six thermally and hydraulically acceptable assembly designs. The investigation of the optimum heterogeneous design will be carried out in two steps. The first step will be to determine which fuel driver pin diameter to use and how many internal blanket assemblies to use with it. This establishes the effective fuel volume fraction. With this done an investigation as to the optimum arrangement will be carried out.

4.2.1 Determination of the Driver Pin Diameter and the Number of Internal Blanket Assemblies

As can be seen from the optimization of the homogeneous core (Section 3.3 of Chapter 3), an optimum fuel volume fraction exists. As suggested by Chang, et al. (C2) an optimum effective fuel volume fraction exists for the heterogeneous core as well. The effective fuel volume fraction defined by Chang, et al., for a heterogeneous core is the

volume weighted average fuel volume fraction of the driver and internal blanket assemblies (i.e.: If a core design had 100 internal blanket assemblies having a fuel volume fraction of 0.5 and 300 driver assemblies with a fuel volume fraction of 0.2 the effective fuel volume fraction would be

$\frac{100 * 0.5 + 300 * 0.2}{400}$, or 0.275). In this subsection the use of an optimum effective fuel volume fraction of this type will be explored.

For a given driver fuel pin diameter any effective fuel volume fraction between the driver's fuel volume fraction and the internal blanket's fuel volume fraction can be obtained by varying the number of internal blankets. This means that the optimum effective fuel volume fraction for each driver fuel pin diameter could be found simply by studying a series of designs having an increasing number of internal blanket assemblies. The optimum heterogeneous core design would be the best performing design selected from the optimum designs at each pin diameter. (This assumes that the effective fuel volume fraction effects dominate over the arrangement effects. This is explored in the next subsection.) Indeed, in the present work a series of heterogeneous designs with an increasing number of internal blanket assemblies were analyzed.

4.2.1.1 Technique for Determining the Optimum Effective Fuel Volume Fraction

To determine the optimum effective fuel volume fraction for each driver pin diameter a set of six heterogeneous core arrangements with an increasing number of internal blanket assemblies was laid out. These six arrangements are presented as Figs. 4.1 to 4.6. The major goal in each of these layouts was to attain the greatest practicable separation between internal blanket assemblies. (For a discussion of core patterns see the next subsection, 4.2.2.) Each one of these designs was then "ringed" to form the R-Z models shown as Figs. 4.7 to 4.12. The ringing of the assemblies was done preserving volume and the mean distance from the core center. An enrichment search to an eigenvalue that would maintain end-of-cycle criticality (presumed to be $k_{\text{eff}} = 1.01$ to account for streaming), followed by a burnup of 256 full-power-days (FPD) (one year at 70% capacity factor), was performed for each case studied. Iteration on relative zone enrichments was done to achieve the same peak power density in all enrichment zones.

Since an approximate optimum effective fuel volume fraction was known from the homogeneous study of the previous chapter only the 6, 7, and 8 mm driver pin diameters were investigated; further, not all six arrangements were analyzed for each driver pin case. However, the procedure described in the preceding paragraph was performed for a total of 15 heterogeneous cases.

30° Symmetry Sector Shown

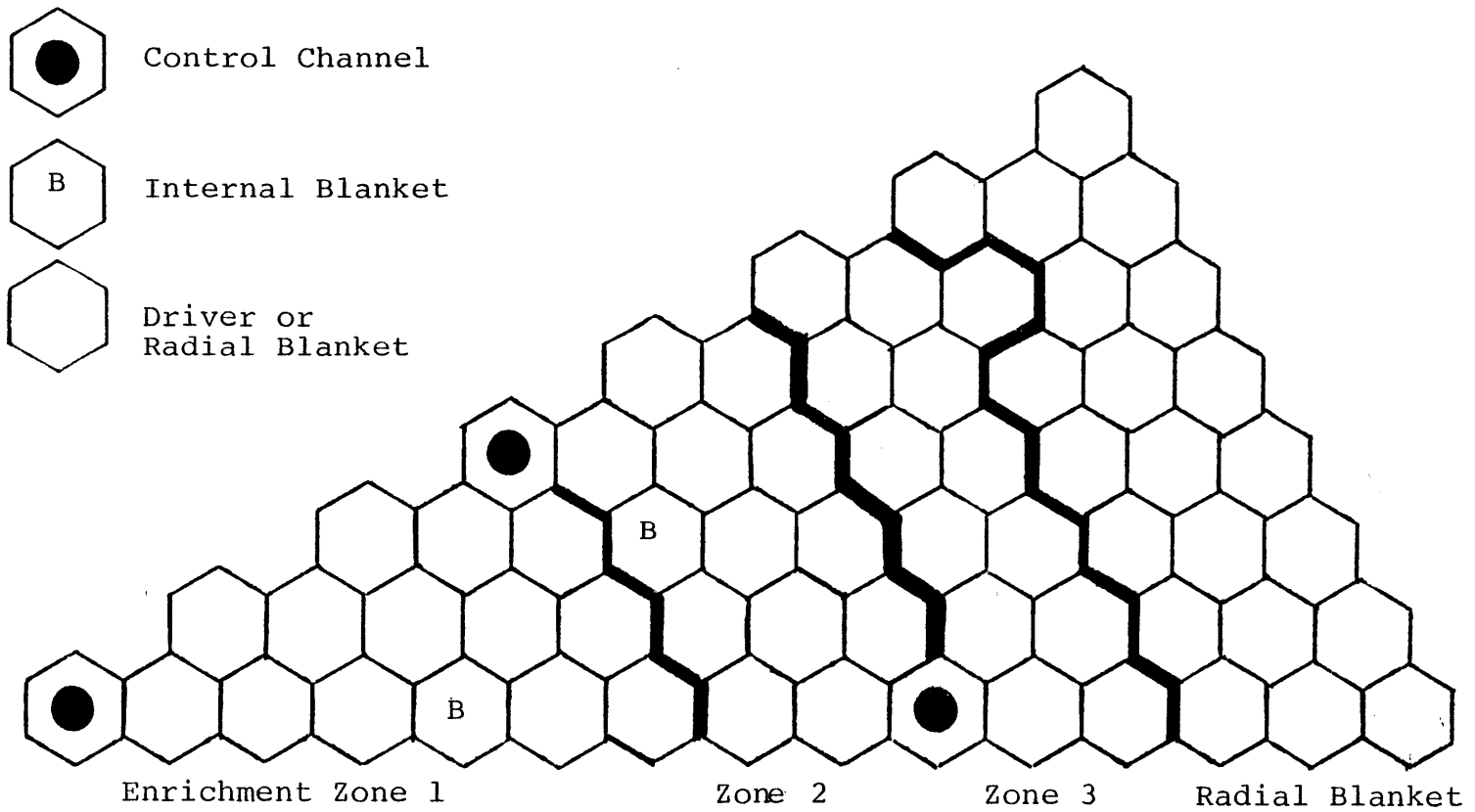


Fig. 4.1 Heterogeneous core I with 18 internal blanket assemblies and 378 fuel assemblies

30° Symmetry Sector Shown

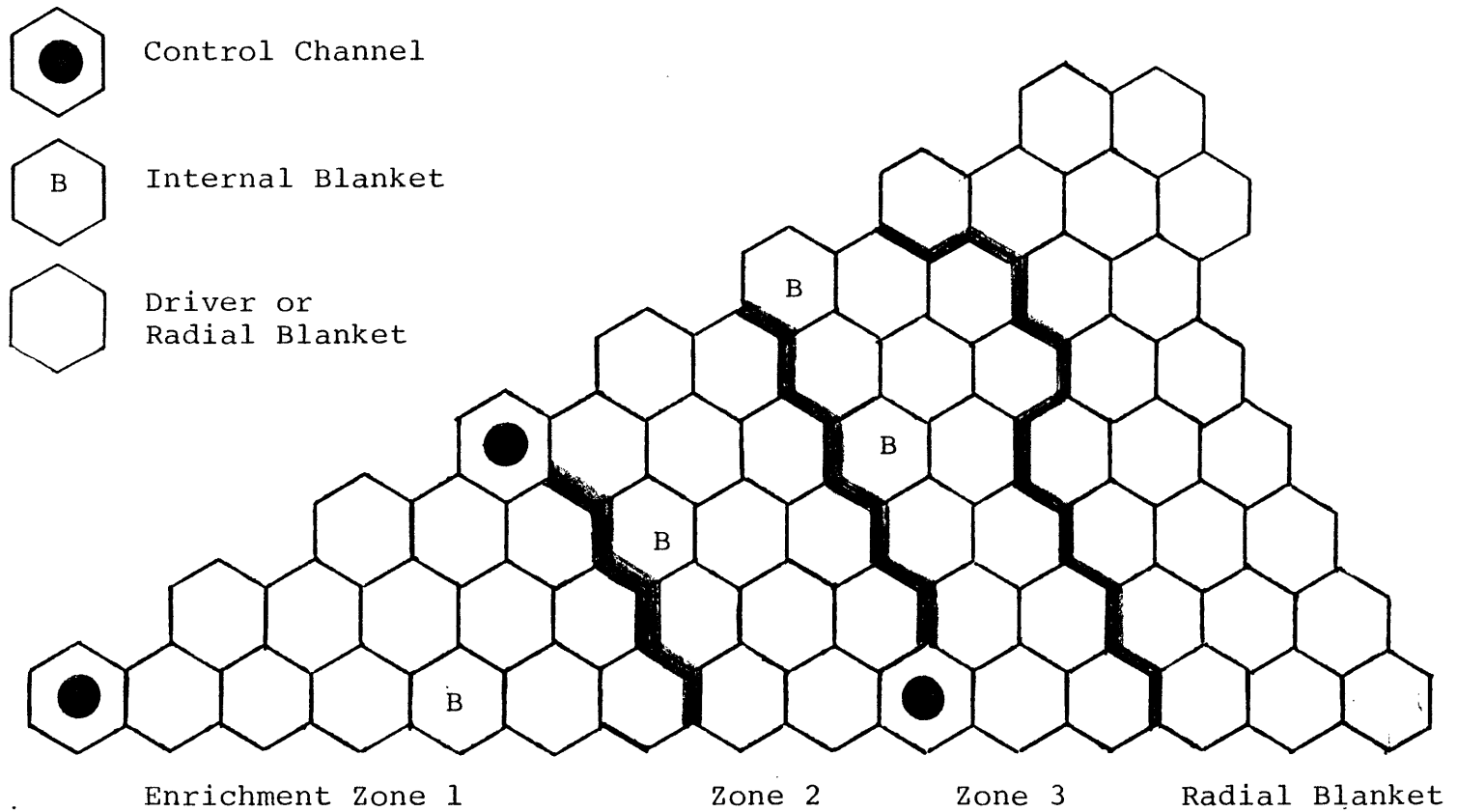


Fig. 4.2 Heterogeneous core II with 36 internal blanket assemblies and 372 fuel assemblies

30° Symmetry Sector Shown

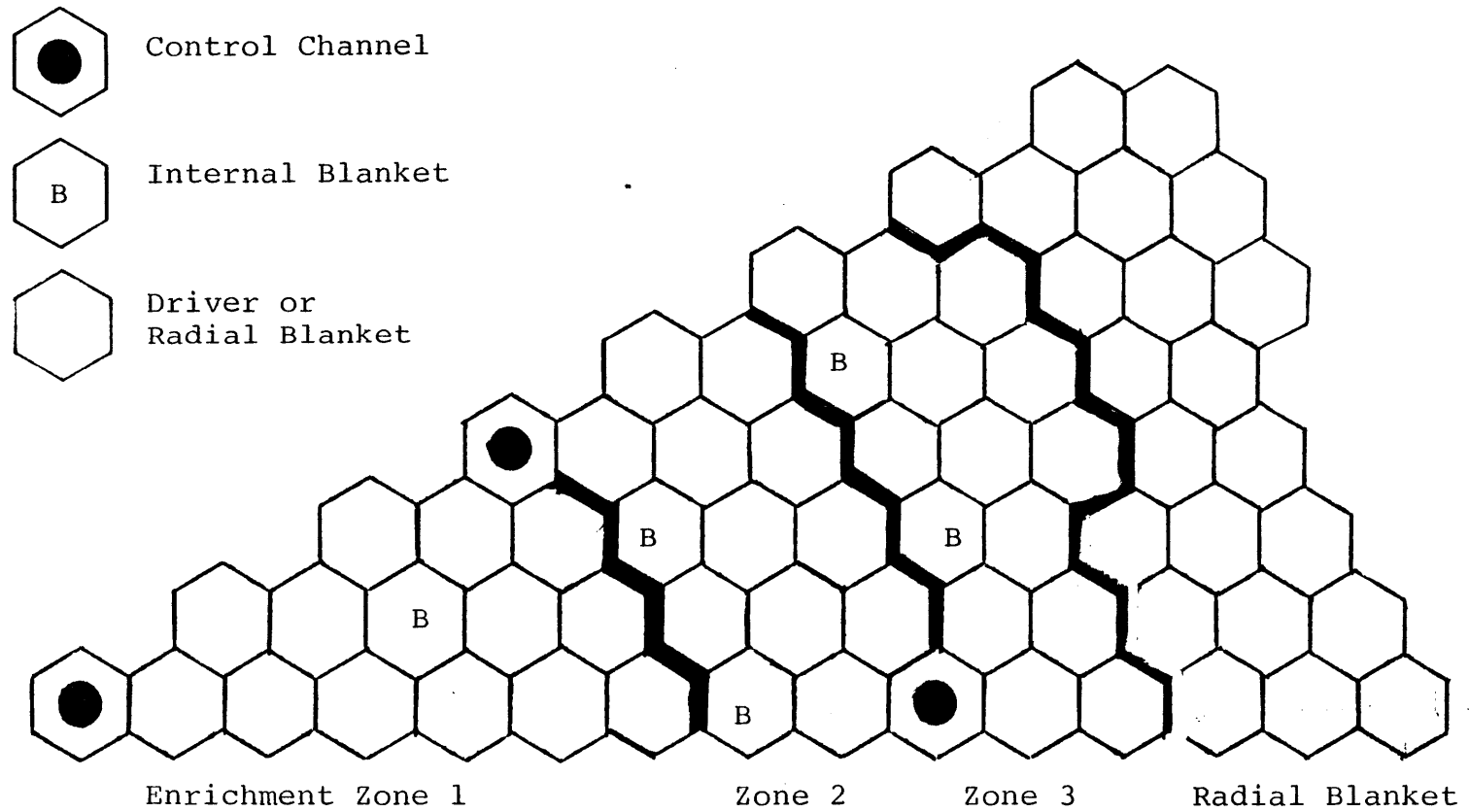


Fig. 4.3 Heterogeneous core III with 54 internal blanket assemblies and 366 fuel assemblies

30° Symmetry Sector Shown

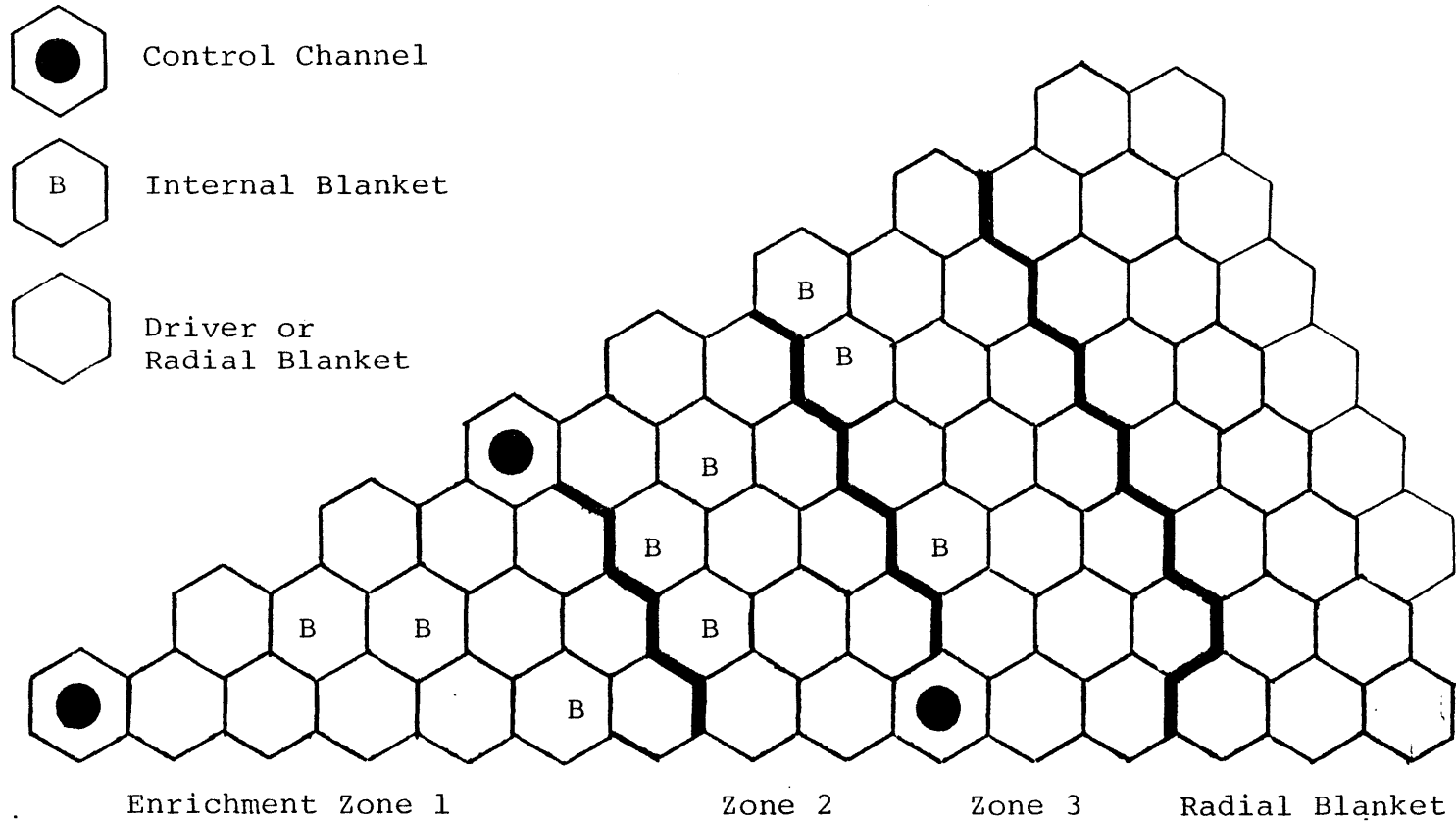
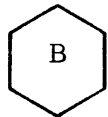


Fig. 4.4 Heterogeneous core IV with 96 internal blanket assemblies and 354 fuel assemblies

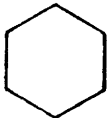
30° Symmetry Sector Shown



Control Channel



Internal Blanket



Driver or
Radial Blanket

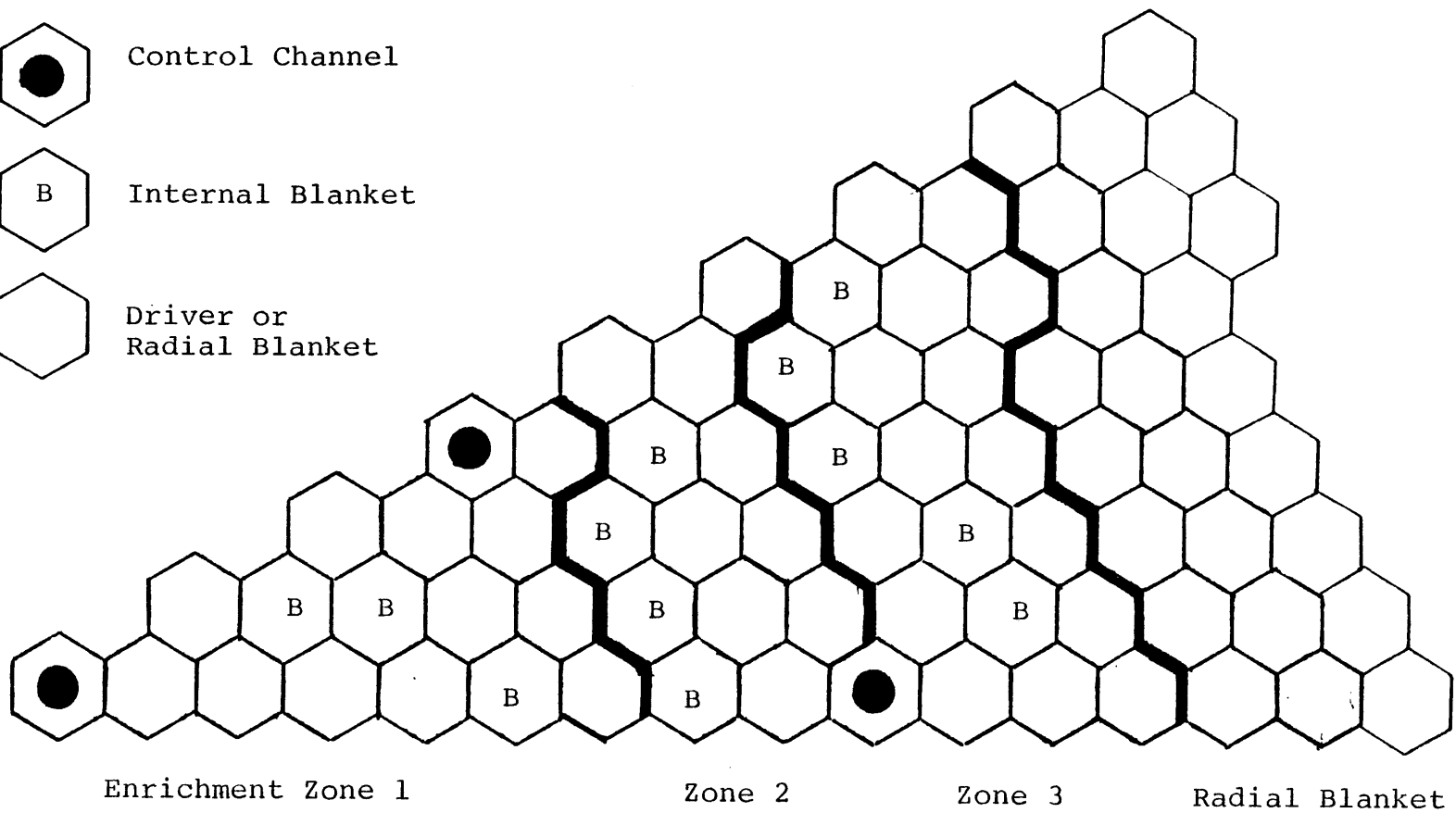


Fig. 4.5 Heterogeneous core V with 132 internal blanket assemblies and 348 fuel assemblies

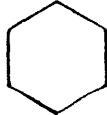
30° Symmetry Sector Shown



Control Channel



Internal Blanket



Driver or
Radial Blanket

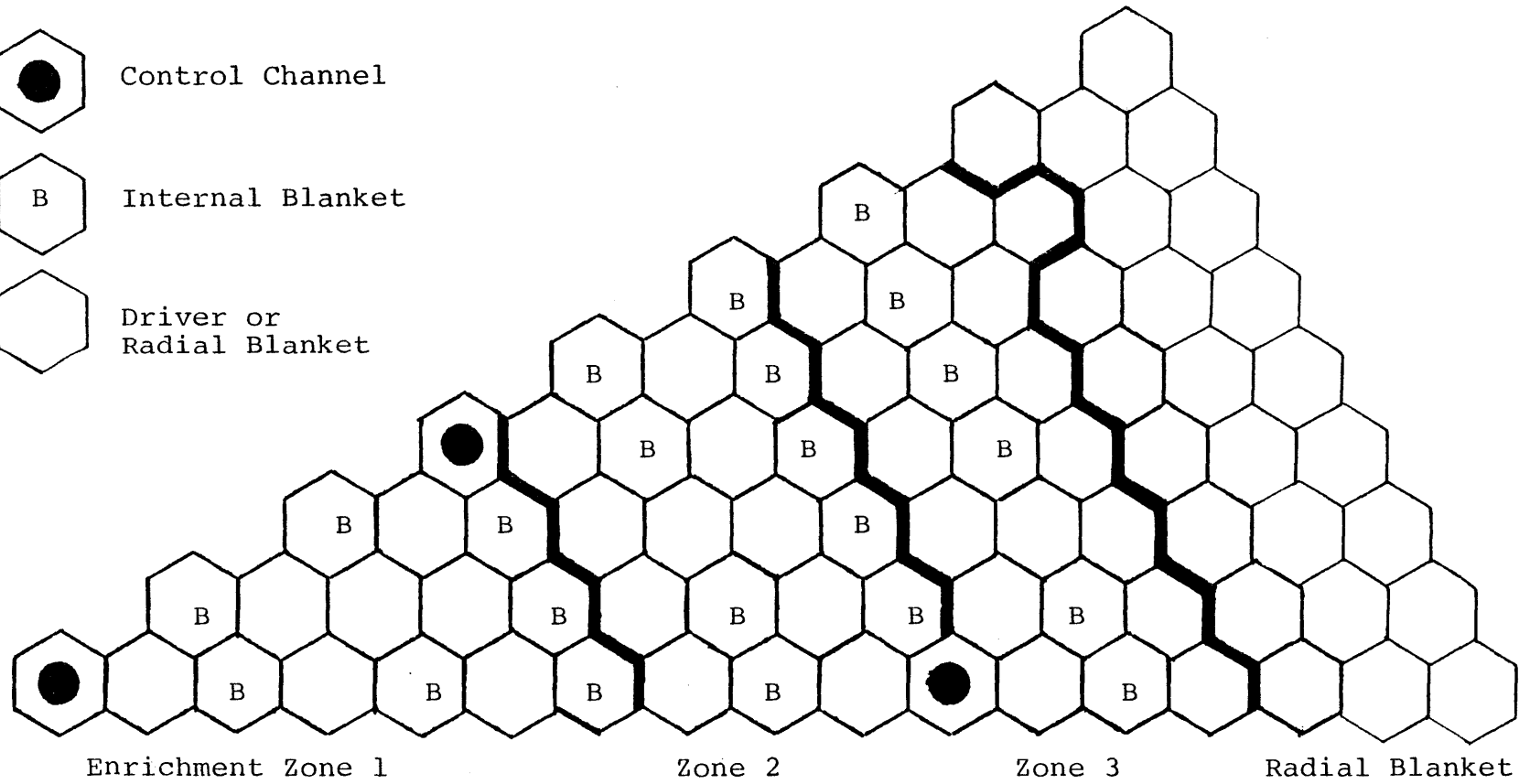


Fig. 4.6 Heterogeneous core VI with 204 internal blanket assemblies and 342 fuel assemblies

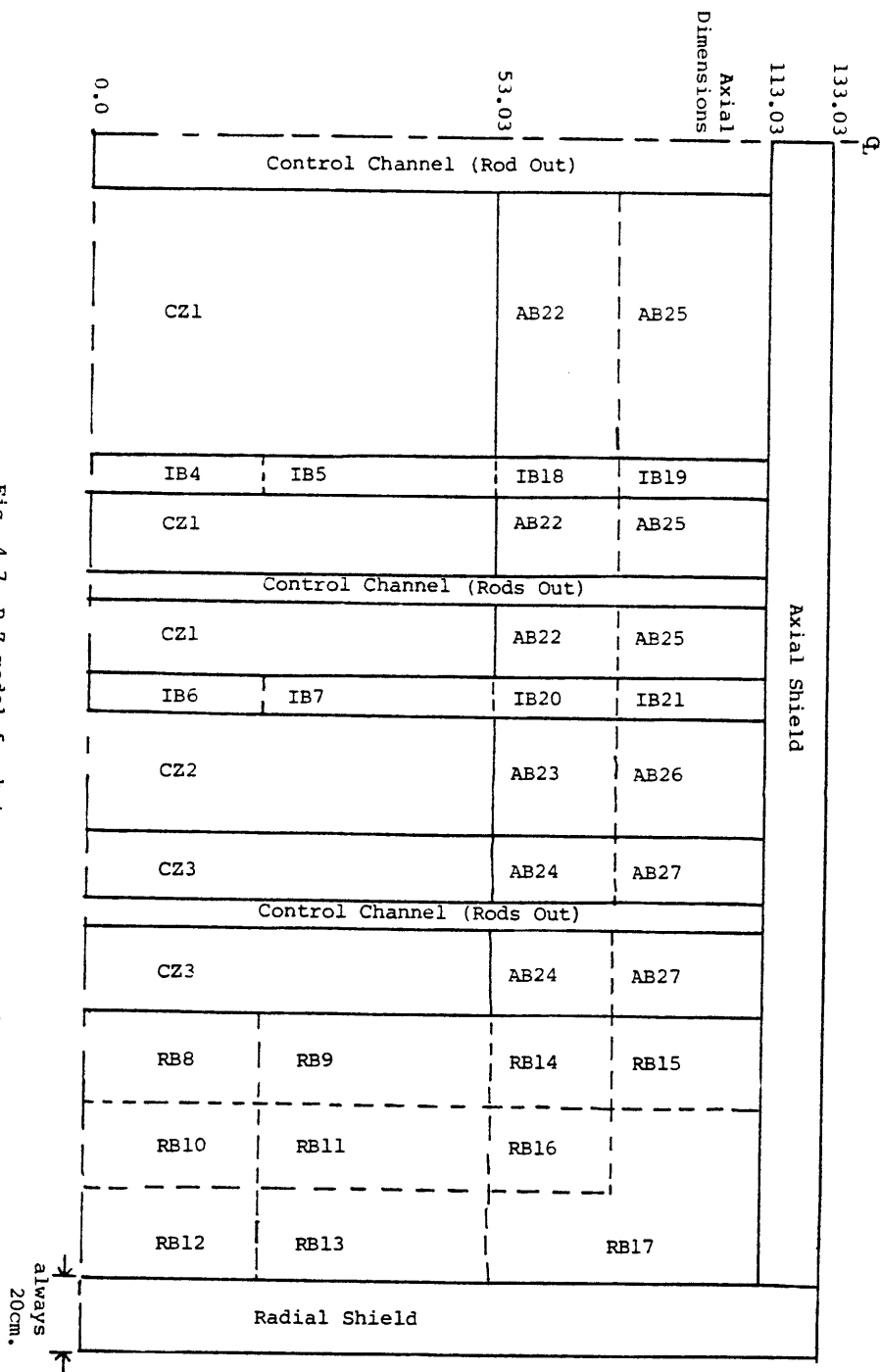


Fig. 4.7 R-2 model for heterogeneous core I

CZ = Core Zone
 IB = Internal Blanket
 AB = Axial Blanket
 RB = Radial Blanket

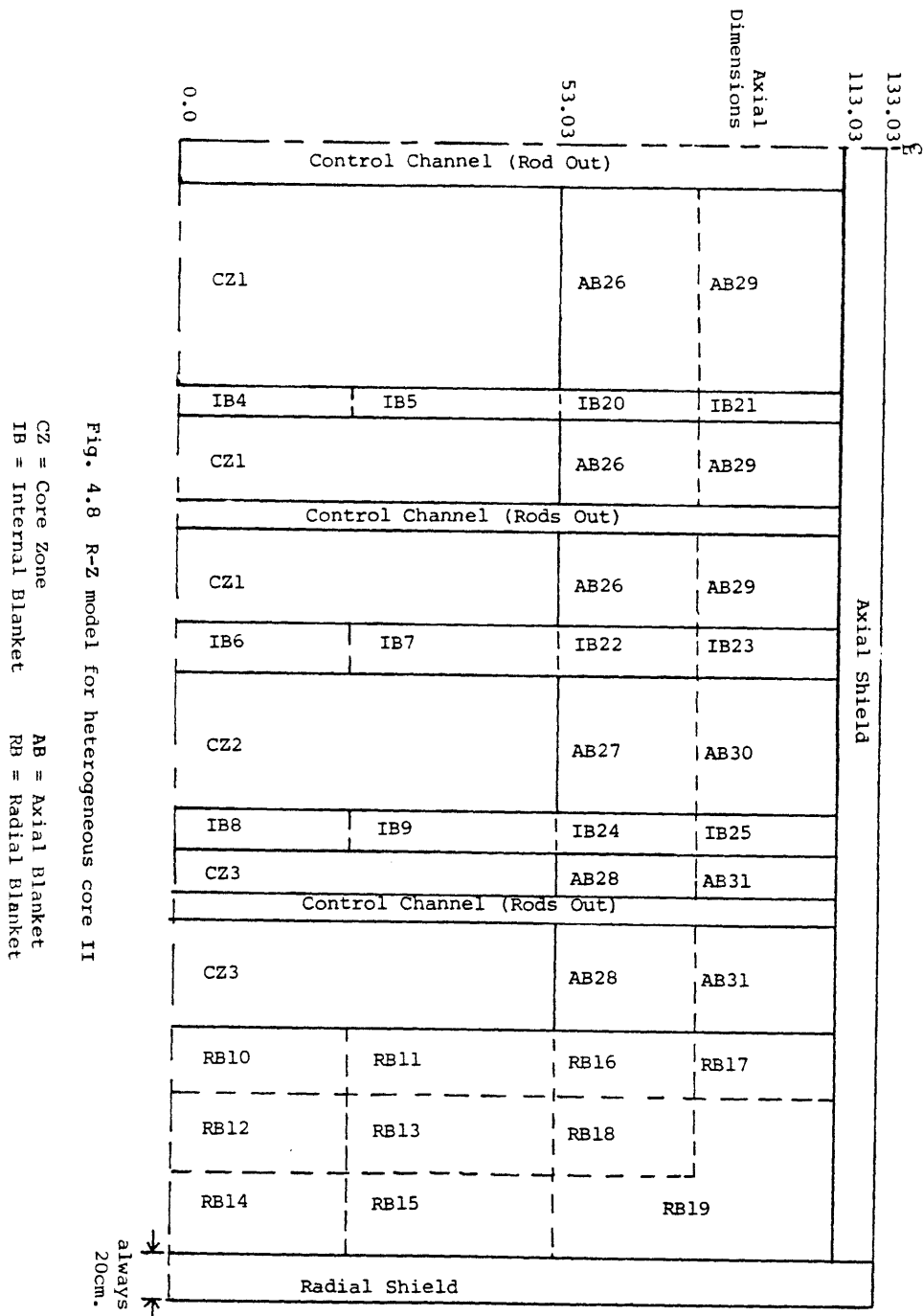


Fig. 4.8 R-Z model for heterogeneous core II

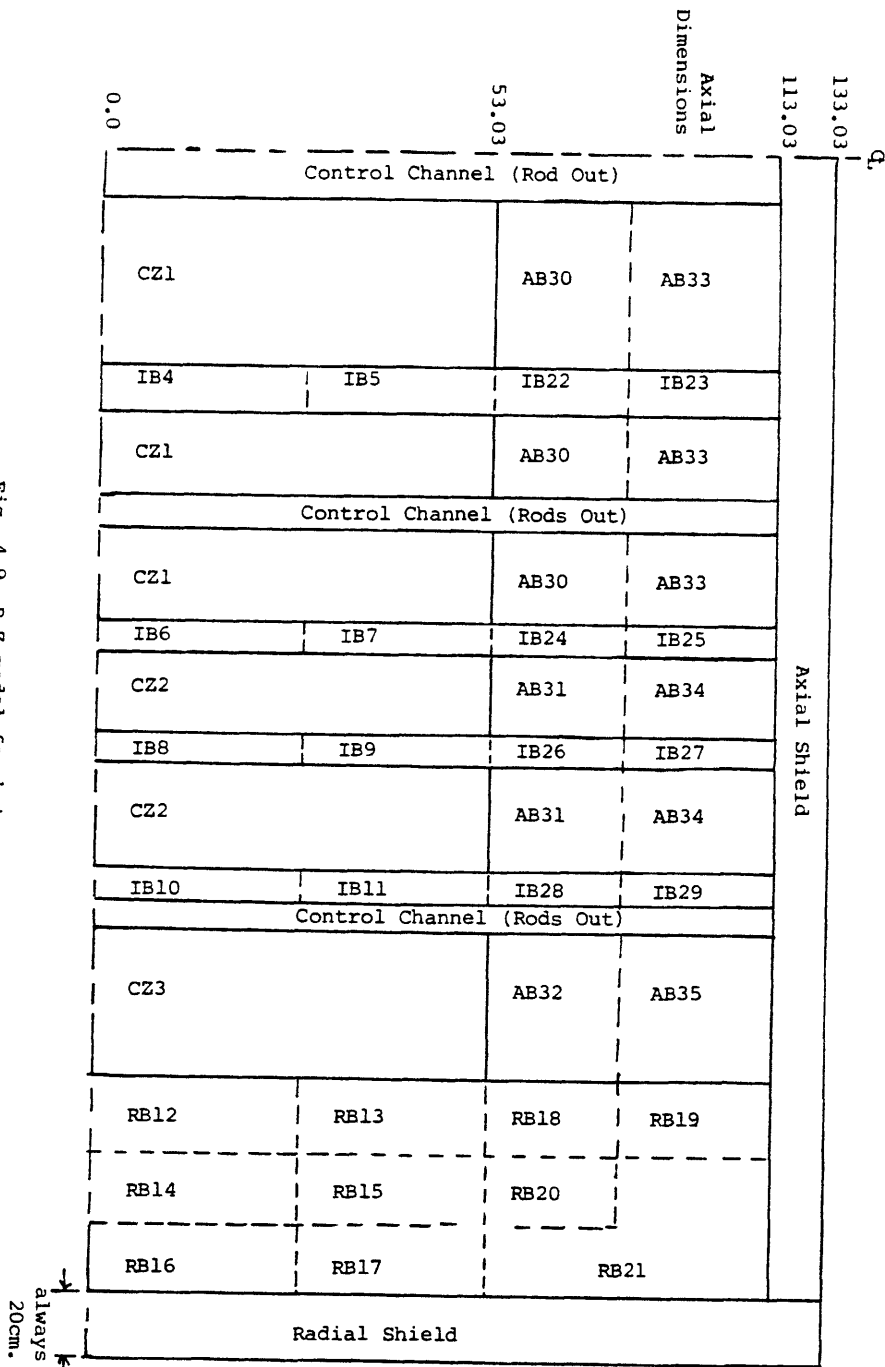


Fig. 4.9 R-Z model for heterogeneous core III

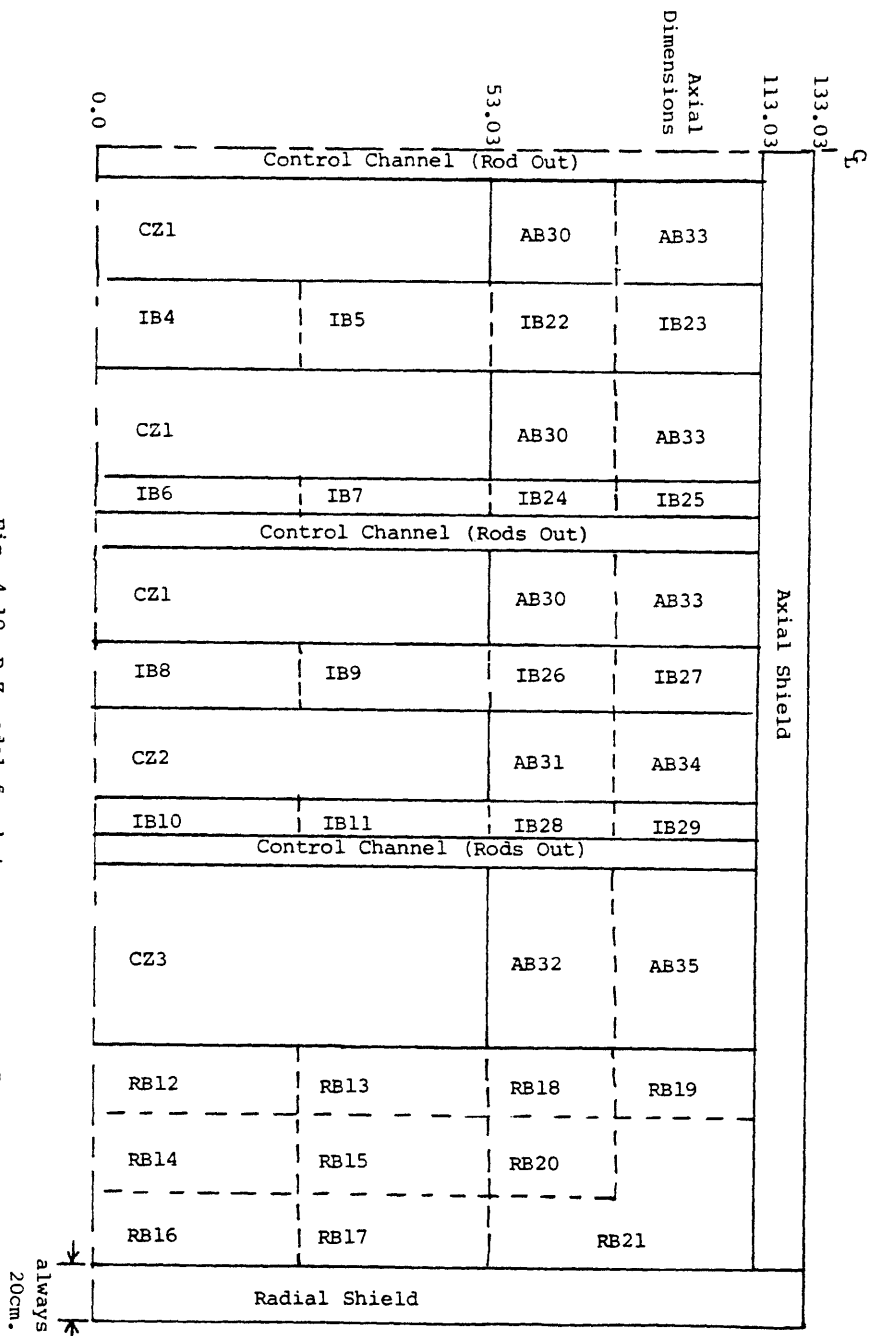


Fig. 4.10 R-Z model for heterogeneous core IV

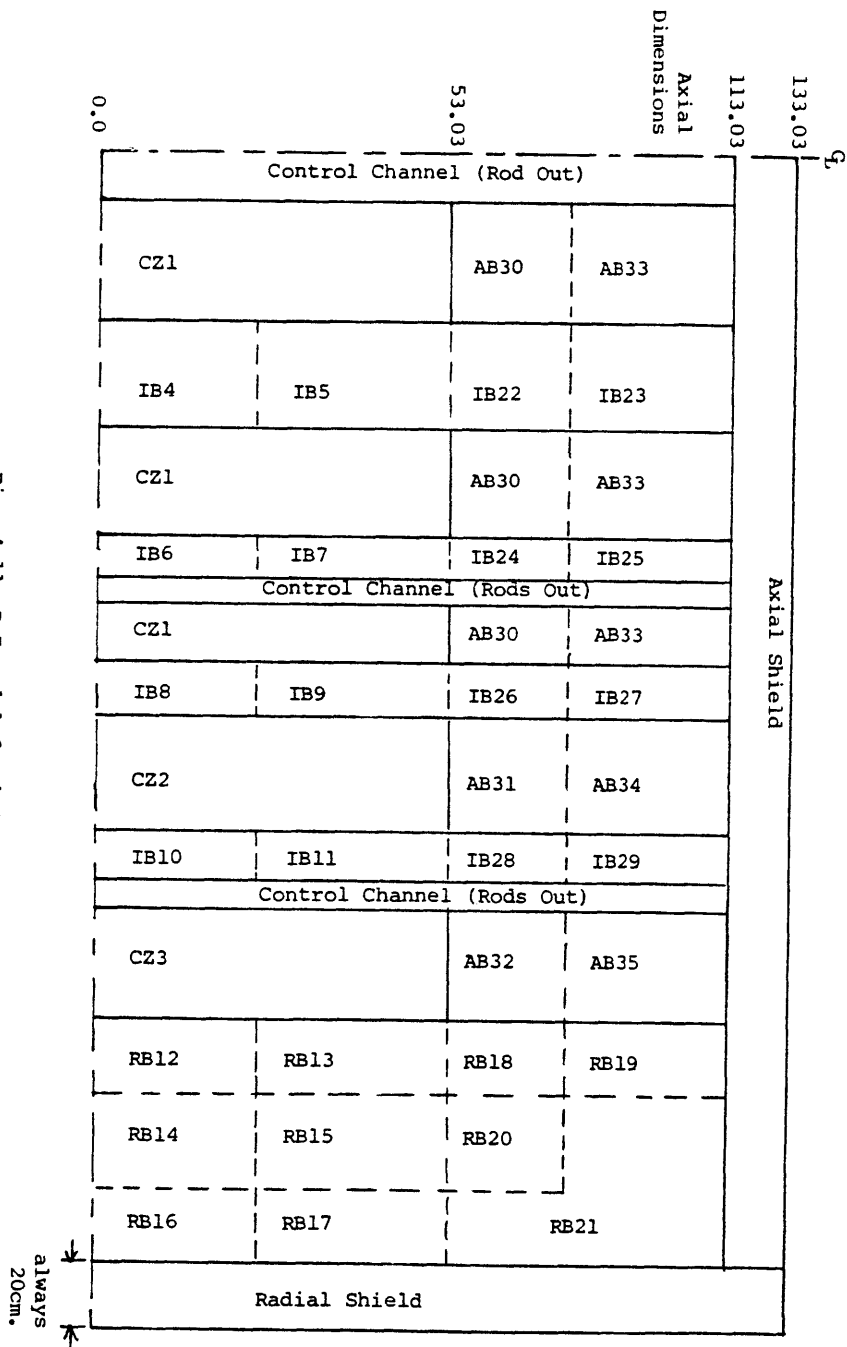
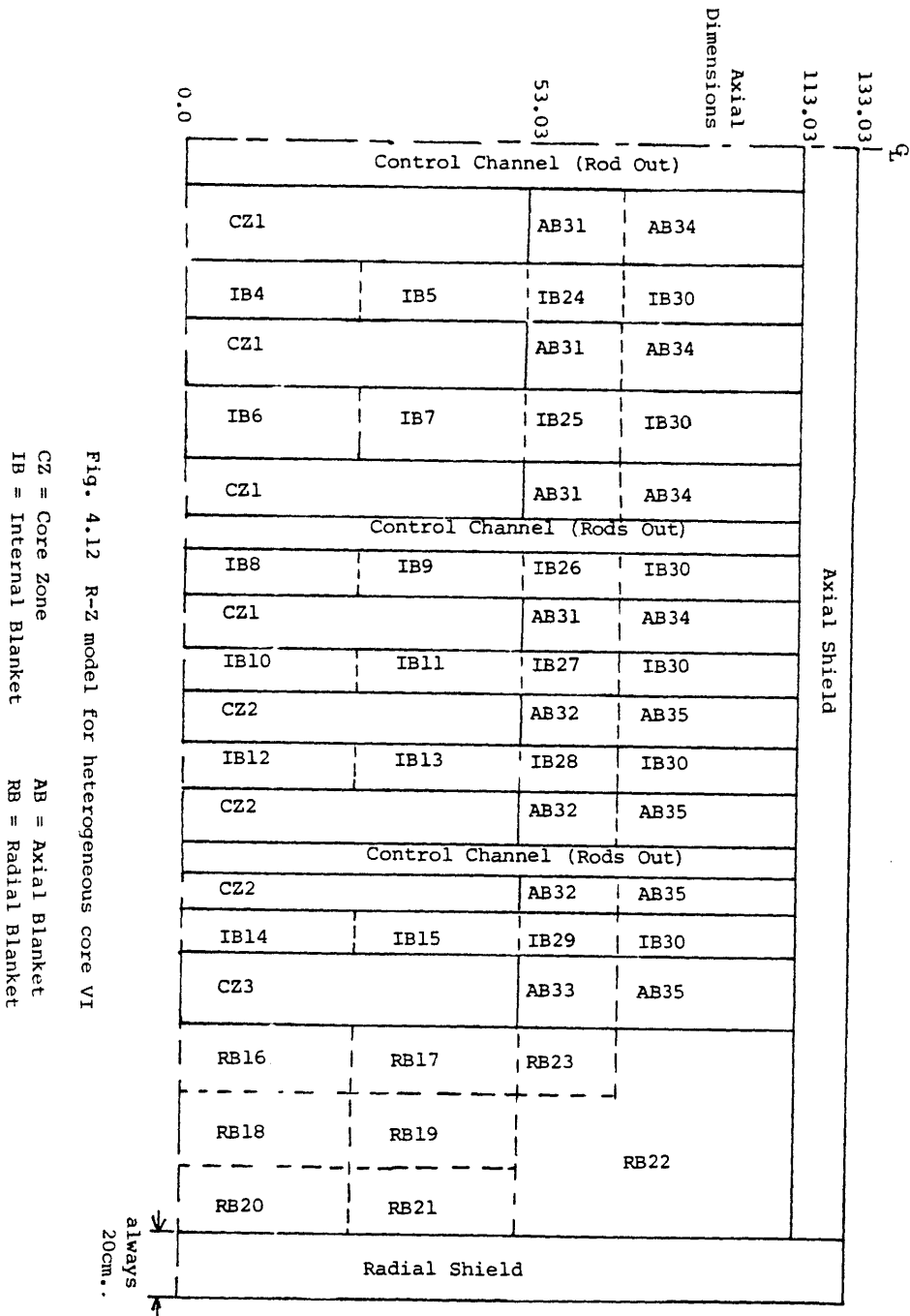


Fig. 4.11 R-Z model for heterogeneous core V

CZ = Core Zone
 IB = Internal Blanket
 AB = Axial Blanket
 RB = Radial Blanket

always
 20cm.



4.2.1.2 Optimum Effective Fuel Volume Fraction:

Results and Discussion

The key results of the analysis of the heterogeneous cores are shown in Table 4.1. This table also includes the zero internal blanket cases from the homogeneous core analysis. The doubling times for all cases are plotted in Fig. 4.13. As can be seen from this figure the homogeneous core always has a shorter doubling time than any heterogeneous core which has the same effective fuel volume fraction. This result is as expected, since the heterogeneous core always has a lower average power density in its active core region. (The active core region is defined as that region bounded by the inside of the radial and axial blankets.) The implication of this figure is that the optimum number of internal blanket assemblies to add to a homogeneous core would be zero.

In order to verify the understanding as to why the heterogeneous core always has a longer doubling time, four pairs of cases with roughly the same effective fuel volume fraction were investigated a bit further. Table 4.2 shows key characteristics for these four pairs of cases. Roughly speaking, if the effective fuel volume fraction is the same, the effective enrichment and breeding ratio is nearly the same. The key difference between each case in these pairs is a higher power per kilogram of heavy metal in the smaller (fewer internal blanket assemblies) core. If the more highly

Table 4.1
Key Results of Heterogeneous Core Analyses

Case Number	1	2	3	4	5
Heterogeneous Core Design	0	III	IV	V	VI
Driver Fuel Pin Diameter (mm)	6	6	6	6	6
Number of Internal Blanket Assemblies	0	54	96	132	204
Number of Fuel Assemblies	384	366	354	348	342
Effective Fuel Volume Fraction	0.236	0.270	0.292	0.309	0.334
Peak KW/ft	12.6	12.8	13.1	12.8	12.8
Fissile Inventory (Kg)(BOCI)	3255	3633	3890	4276	4937
Net Fissile Gain (Kg/yr)	298	368	422	456	478
Breeding Ratio	1.36	1.48	1.56	1.61	1.65
Doubling Time (yr)	10.1	9.10	8.50	8.64	9.53
Effective Enrichment (%)*	16.4	14.6	13.5	13.1	12.3
Cycle ΔK	-0.045	-0.021	-0.014	-0.007	+0.002
Power Per KgHM**	60.3	48.2	41.6	36.9	30.0
Core Volume (liter)***	9,280	10,150	10,875	11,600	13,200
Core Surface Area (m ²)***	29.4	31.5	33.3	35.1	38.9

Table 4.1 (Continued)

Case Number	6	7	8	9	10	11	12
Heterogeneous Core Design	0	I	II	III	IV	V	VI
Driver Fuel Pin Diameter(mm)	7	7	7	7	7	7	7
Number of Internal Blanket Assemblies	0	18	36	54	96	132	204
Number of Fuel Assemblies	384	378	372	366	354	348	342
Effective Fuel Volume Fraction	0.302	0.311	0.319	0.327	0.344	0.356	0.376
Peak KW/ft	13.1	13.4	13.1	13.1	13.4	13.7	13.7
Fissile Inventory (Kg)(BOC1)	3744	3815	4018	4167	4479	4856	5740
Net Fissile Gain (Kg/yr)	419	430	452	463	488	504	512
Breeding Ratio	1.54	1.56	1.59	1.61	1.65	1.68	1.70
Doubling Time (yr)	8.24	8.18	8.19	8.29	8.46	8.89	10.33
Effective Enrichment* (%)	12.9	12.4	12.4	12.2	11.6	11.4	11.2
Cycle ΔK	-0.014	-0.012	-0.005	-0.004	-0.002	+0.004	+0.004
Power Per KgHM** (KWe/Kg)	41.4	39.0	36.9	35.0	31.0	28.1	23.4
Core Volume (liters)***	10,560	10,890	11,220	11,550	12,380	13,200	15,020
Core Surface Area (m ²)***	32.6	33.4	34.2	35.0	37.0	39.0	43.2

Table 4.1 (Continued)

Case Number	13	14	15	16	17	18	19
Heterogeneous Core Design	0	I	II	III	IV	V	0
Driver Fuel Pin Diameter (mm)	8	8	8	8	8	8	9
Number of Internal Blanket Assemblies	0	18	36	54	96	132	0
Number of Fuel Assemblies	384	378	372	366	354	348	384
Effective Fuel Volume Fraction	0.357	0.364	0.370	0.375	0.388	0.396	0.405
Peak KW/ft	13.4	14.0	14.0	14.0	14.3	14.3	13.9
Fissile Inventory (Kg)(B0C1)	4345	4479	4750	4964	5231	5692	5201
Net Fissile Gain (Kg/yr)	486	492	503	511	517	530	511
Breeding Ratio	1.65	1.66	1.66	1.67	1.70	1.72	1.69
Doubling Time (yr)	8.25	8.40	8.70	8.95	9.33	9.90	9.40
Effective Enrichment*(%)	11.1	10.9	11.0	11.0	10.5	10.5	10.2
Cycle ΔK	+0.001	+0.001	+0.002	+0.003	+0.003	+0.006	+0.008
Power Per KgHM** (KWe/Kg)	30.6	29.1	27.8	26.7	24.1	22.1	23.4
Core Volume (liters)***	12,080	12,460	12,840	13,210	14,160	15,100	13,940
Core Surface Area (m ²)***	36.5	37.4	38.3	39.2	41.4	43.6	41.0

Notes for Table 4.1

- * The effective enrichment is the fissile inventory divided by the total heavy metal in the active core region, which is defined as the region inside of the radial blankets and axial blankets.
- ** The kilogram basis for this analysis is the kilograms inside the active core.
- *** These are the active core volumes and surface areas i.e. that volume bounded radially by the inside (core/blanket interface) of the radial blanket and axially by the inside of the axial blankets.

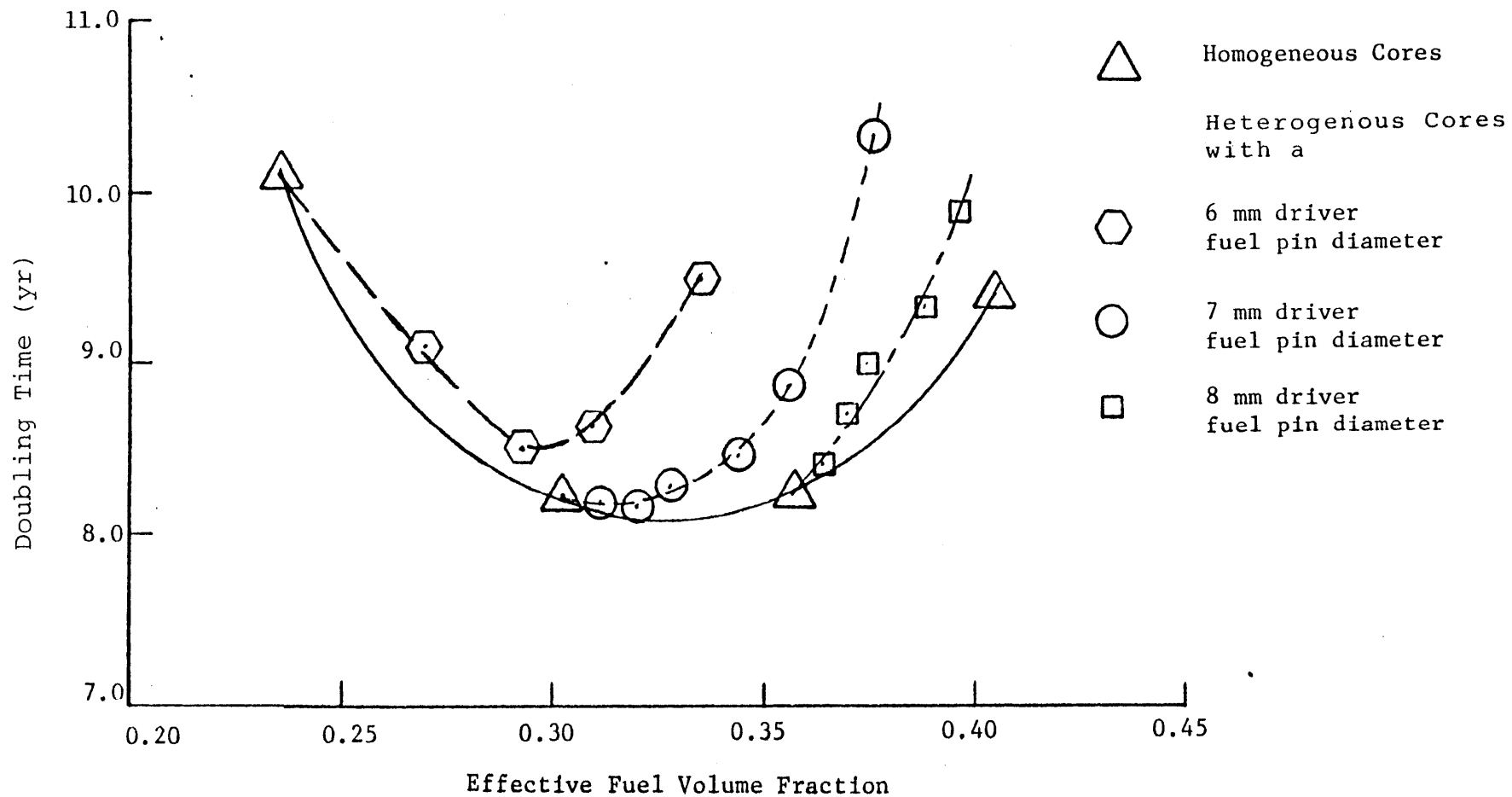


Fig. 4.13 Doubling Time as a Function of the Effective Fuel Volume Fraction for Various Homogeneous and Heterogeneous Designs

Table 4.2

Comparison of Cores with the Same Effective
Fuel Volume Fraction but Different Numbers
of Internal Blanket Assemblies

Case Numbers	4/7	5/9	11/13	12/16
Number of Internal Blanket Assemblies	132/18	204/54	132/0	204/54
Effective Fuel Volume Fractions	0.309/0.311	0.334/0.327	0.356/0.357	0.376/0.375
Effective Enrichment (%)	13.1/12.4	12.3/12.2	11.4/11.1	11.2/11.0
Core Volume (liters x 10 ³)	11.6/10.9	13.2/11.6	13.2/12.1	15.0/13.2
Fissile Inventory (Kg)	4276/3815	4937/4167	4856/4345	5740/4964
Power Per Kg of Heavy Metal (KWe/Kg)	36.9/39.0	30.0/35.0	28.1/30.6	23.4/26.7
Doubling Time (yr)	8.64/8.18	9.53/8.29	8.89/8.25	10.33/8.95
% Difference in Doubling Time	5.6	15.0	7.8	15.4
Adjusted Doubling Time for Equal Specific Powers	8.17/8.18	8.17/8.29	8.16/8.25	9.05/8.95
% Difference in Adjusted Doubling Times	0.1	1.5	1.0	1.1

heterogeneous cores were allowed to increase in power to the same power per kilogram of heavy metal as the more compact cores, then most of the doubling time difference would be eliminated, as shown in Table 4.2. This, however, is never possible since internal blanket assemblies always must start at low power densities due to their lack of fissile material at the beginning of cycle. (Gains in power density in the driver assemblies due to the use of smaller pin diameters or due to possibly improved power flattening never in practice make up for the low power density of the internal blankets.) Thus the assertion that heterogeneous cores will always have longer doubling times due to their lower average power densities is confirmed.

In Fig. 4.13 and Tables 4.1 and 4.2 there is no mention of uncertainties. However, throughout the calculational procedure attempts were made to ascertain the impact on doubling time of various possible errors. For example, it was ascertained that an error in the power flattening methodology which caused the peak power density in one zone to be 25% higher than that in the other core zones would lead to on the order of a 0.1 year error in doubling time. As another example, an error of 0.1% in the beginning of cycle k_{eff} causes roughly an error of 0.1 years in doubling time. Careful attention was paid to such effects to hold the error in doubling time to below 0.1 year for any given source of error. Of course, some systematic errors which depend on the



Room 14-0551
77 Massachusetts Avenue
Cambridge, MA 02139
Ph: 617.253.2800
Email: docs@mit.edu
<http://libraries.mit.edu/docs>

DISCLAIMER

MISSING PAGE(S)

Page 92

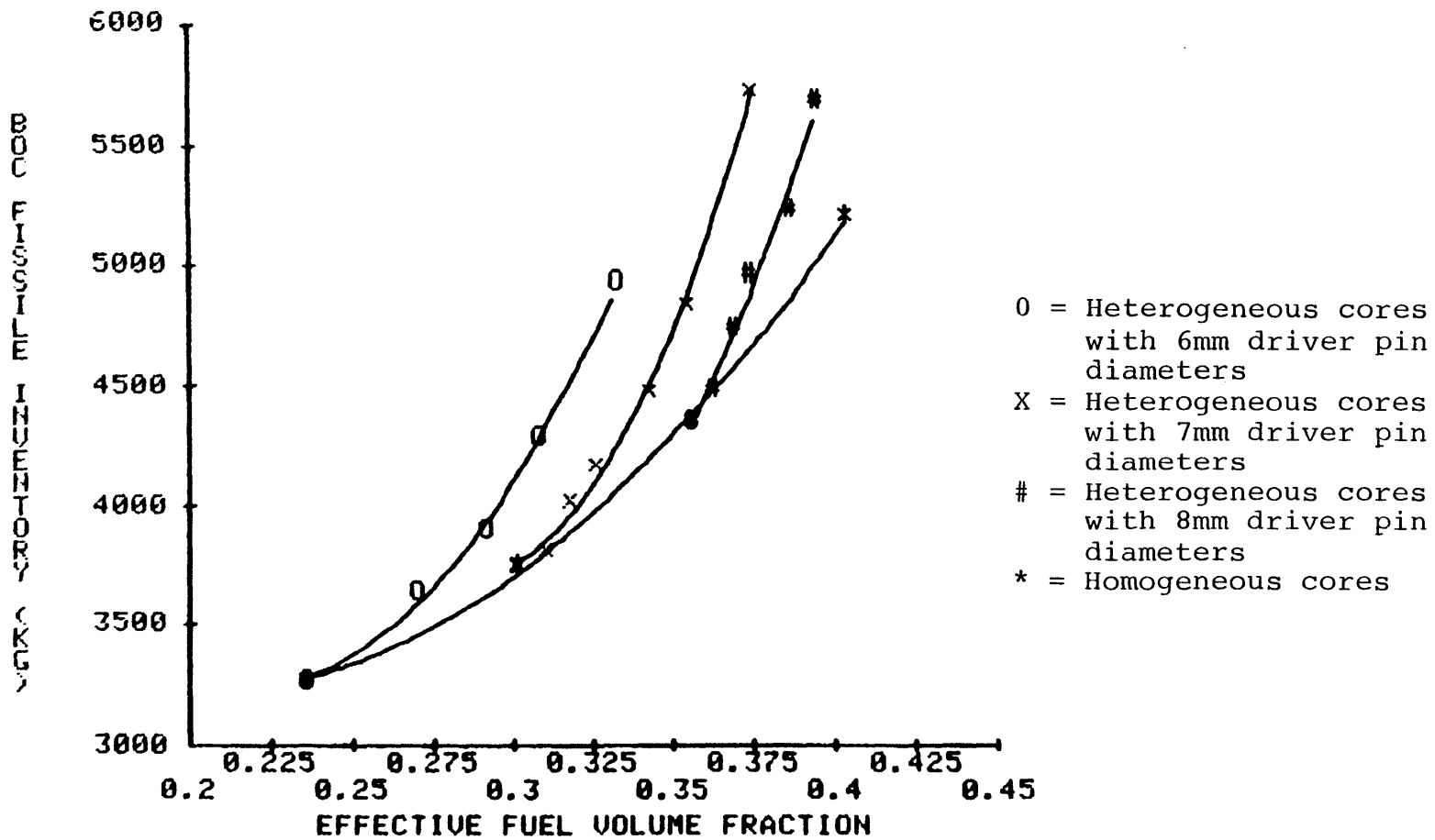


Fig. 4.14 Fissile inventory as a function of effective fuel volume fraction.

pin diameter than a homogeneous core.) The detailed economic analysis is saved for Chapter 5, but using the information in Table 3.9 of Chapter 3 the magnitude of this disadvantage can be found. Thus for all the figures of merit it appears that the optimum number of internal blanket assemblies is zero.

4.2.1.3 Summary of the Determination of the Driver Fuel Pin Diameter and the Number of Internal Blanket Assemblies

The conclusion that the optimum number of internal blanket assemblies is zero may seem to contradict the results that were obtained for the CRBR when it was changed from a homogeneous to a heterogeneous core. In that case, however, the fuel volume fraction was increased by the addition of internal blankets, and the initial fuel volume fraction for the homogeneous core was too low. What happened to the CRBR is analogous to starting with the 6 mm (actually 5.8 mm for the CRBR) pin diameter homogeneous core (case 1 in Table 4.1, or 0.236 effective fuel volume fraction on Fig. 4.13) and adding about one hundred internal blanket assemblies (76 in the case of the CRBR). For this scenario the GCFR doubling time would improve about 15% (CRBR's change was much larger due to the non-linearity of the doubling time dependence on breeding gain. See Table 1.2 of Chapter 1).

Since the optimum number of internal blanket assemblies is zero the decision as to which heterogeneous core to analyze further becomes somewhat arbitrary, however, it was



Room 14-0551
77 Massachusetts Avenue
Cambridge, MA 02139
Ph: 617.253.2800
Email: docs@mit.edu
<http://libraries.mit.edu/docs>

DISCLAIMER

MISSING PAGE(S)

Page 195

30° Symmetry Sector Shown

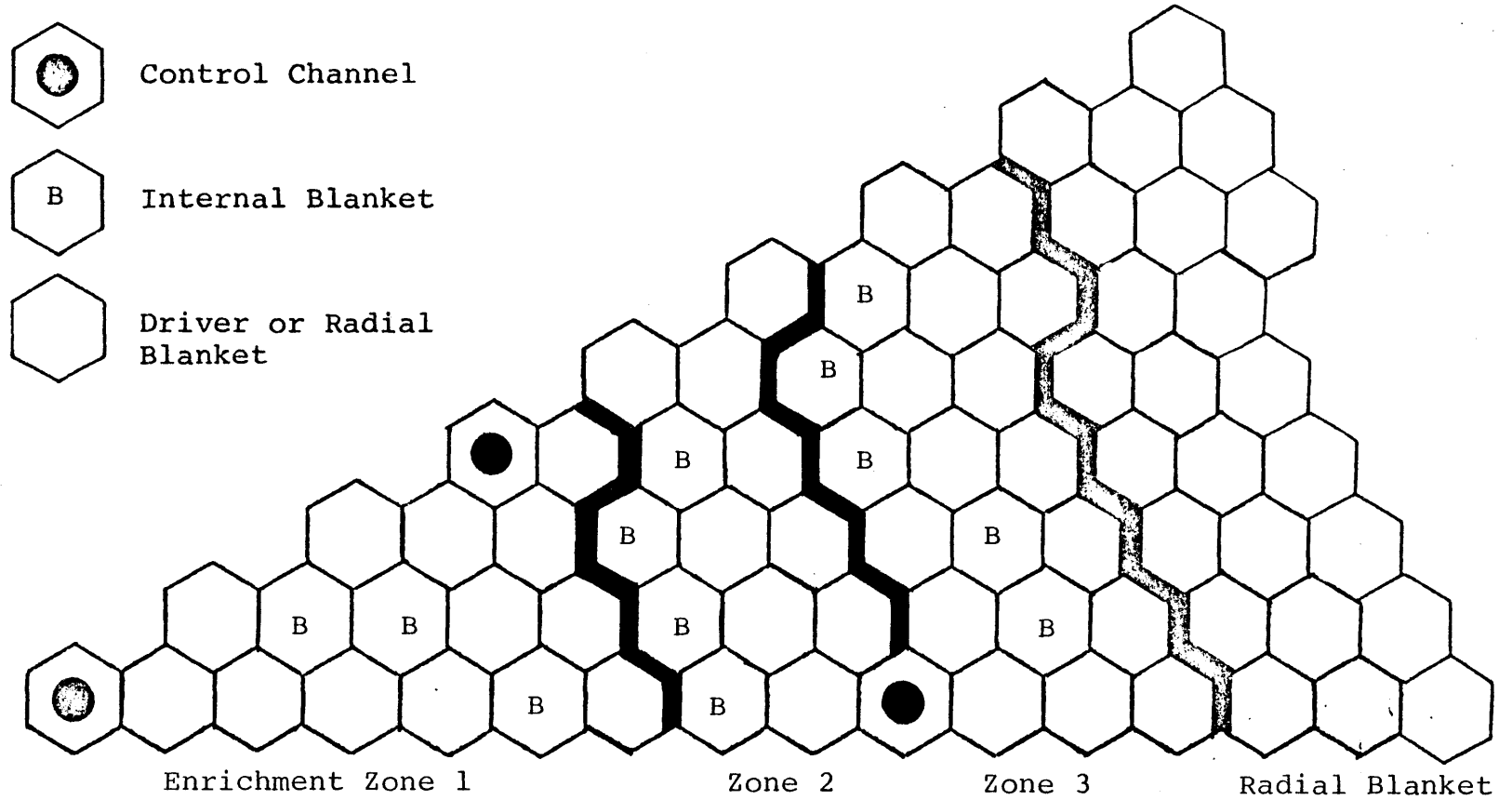


Fig. 4.15 Heterogeneous core arrangement V A

30° Symmetry Sector Shown

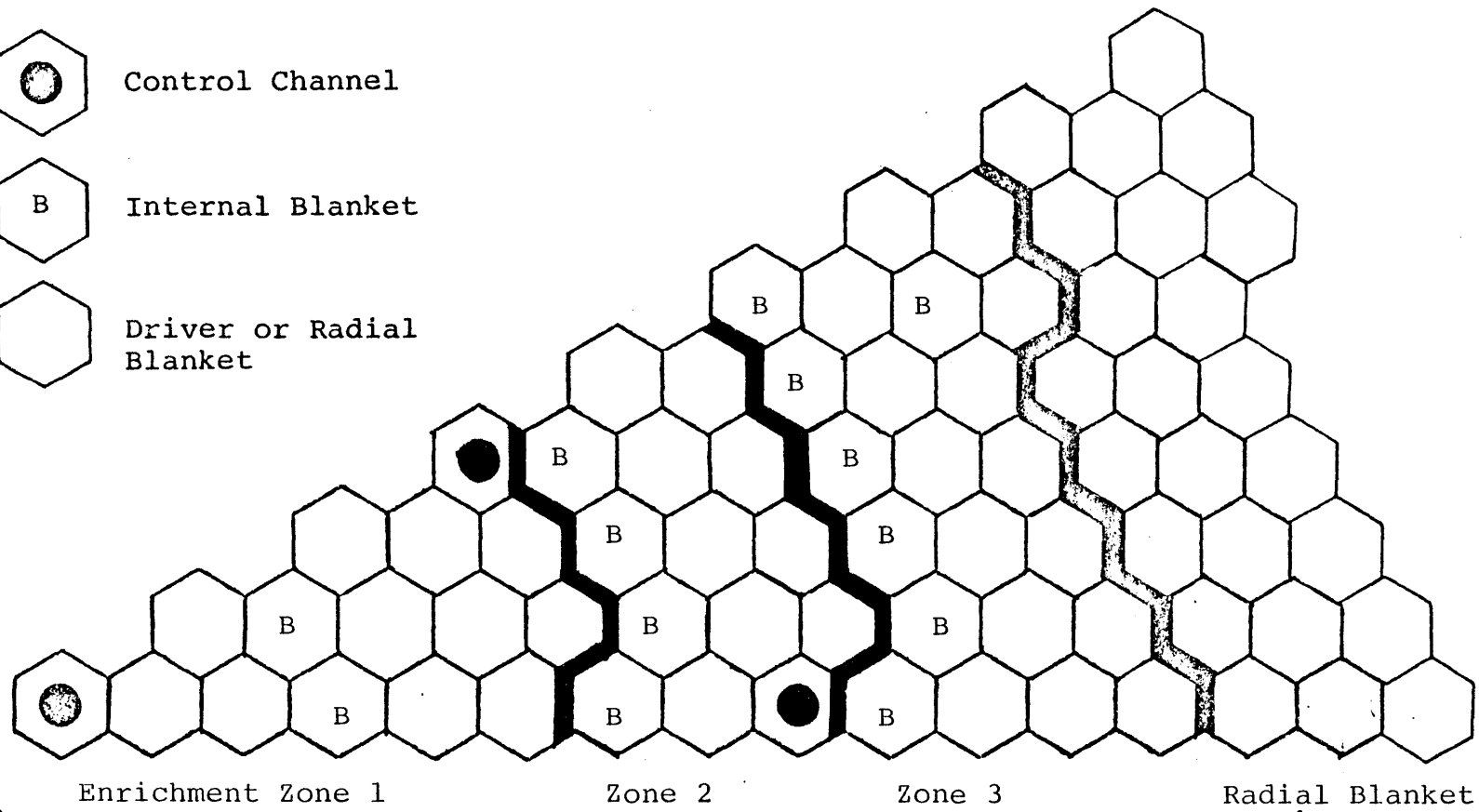
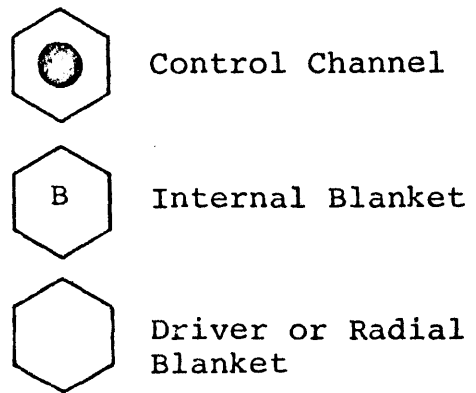


Fig. 4.16 Heterogeneous core arrangement V B

30° Symmetry Sector Shown



Control Channel



Internal Blanket



Driver or Radial
Blanket

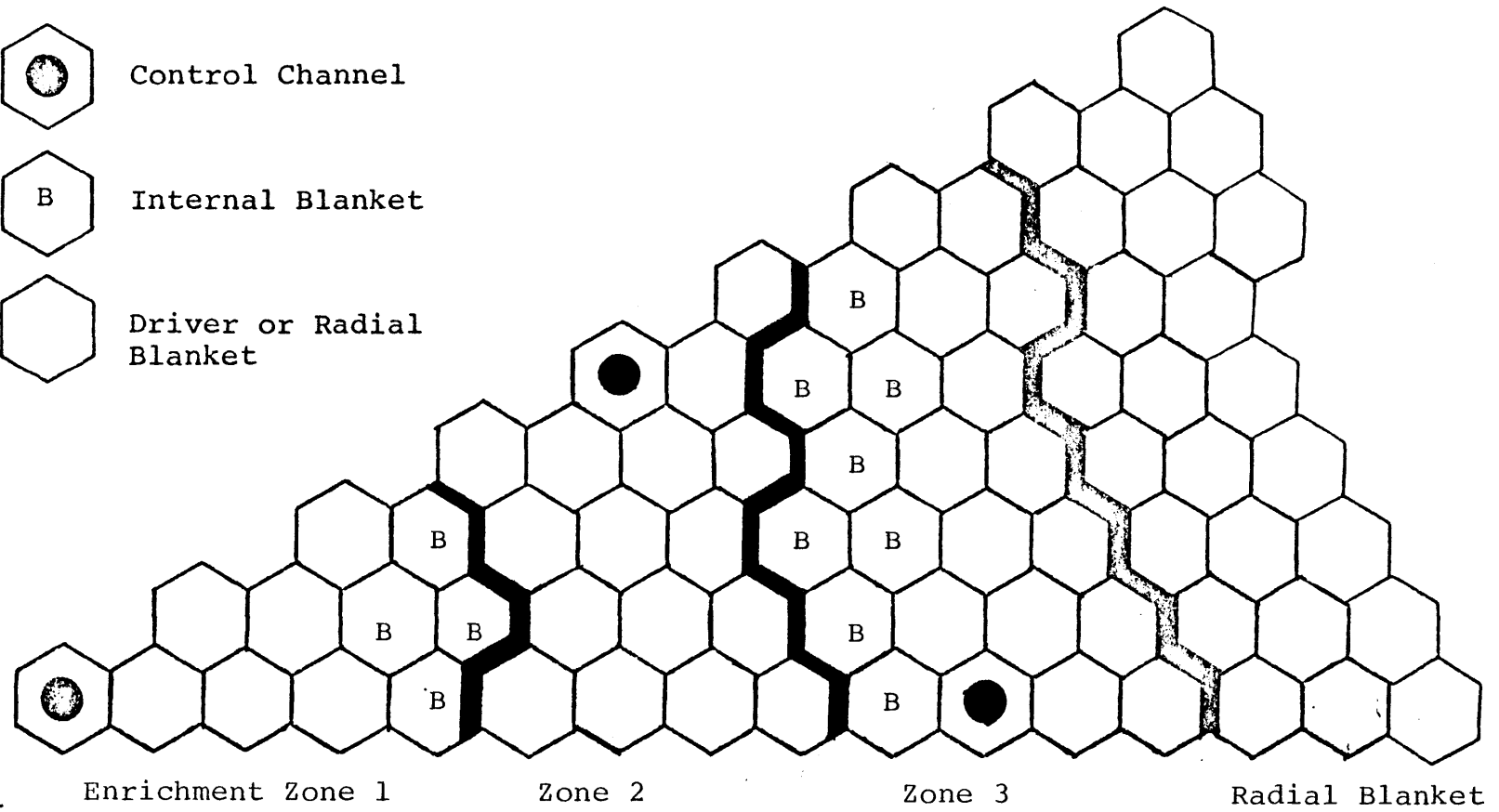


Fig. 4.17 Heterogeneous core arrangement V C

30° Symmetry Sector Shown

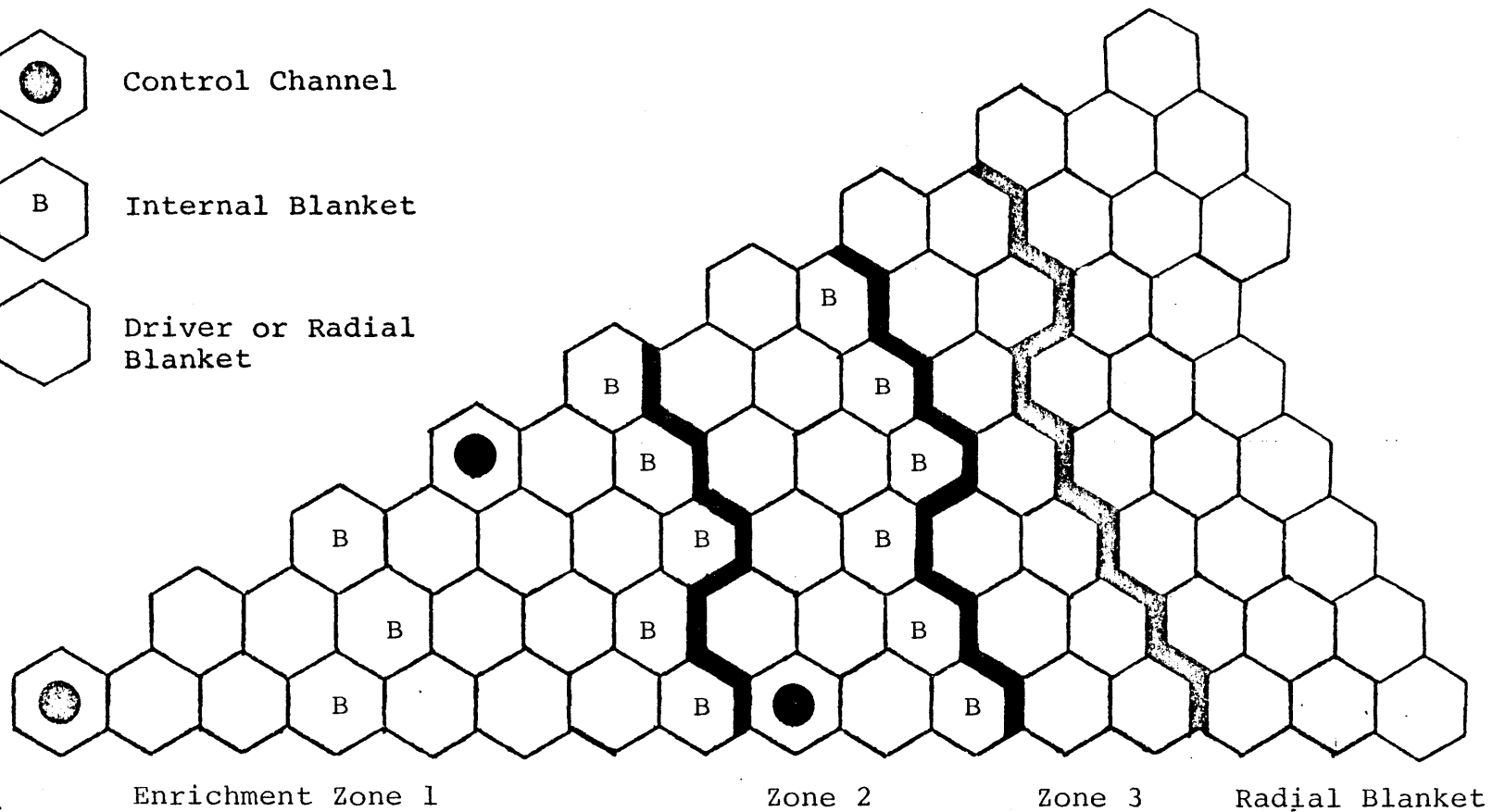
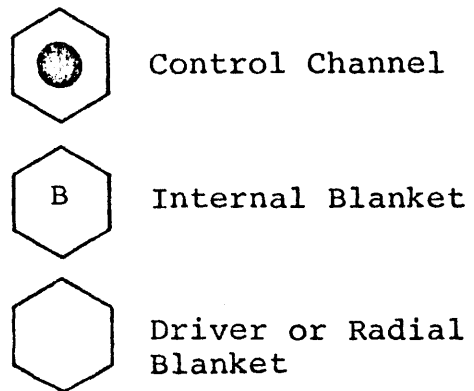


Fig. 4.18 Heterogeneous core arrangement V D

30° Symmetry Sector Shown

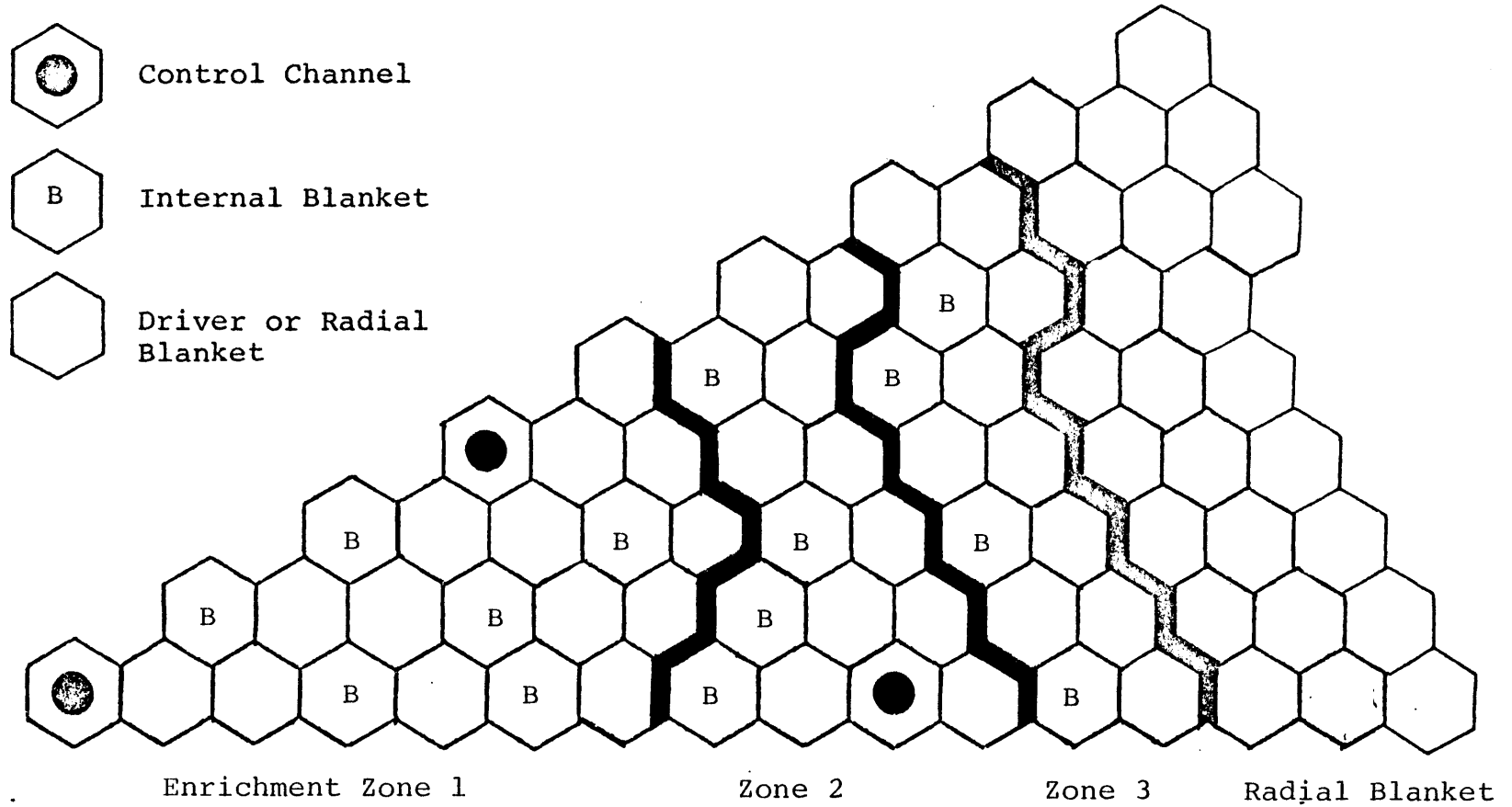


Fig. 4.19 Heterogeneous core arrangement V E

30° Symmetry Sector Shown

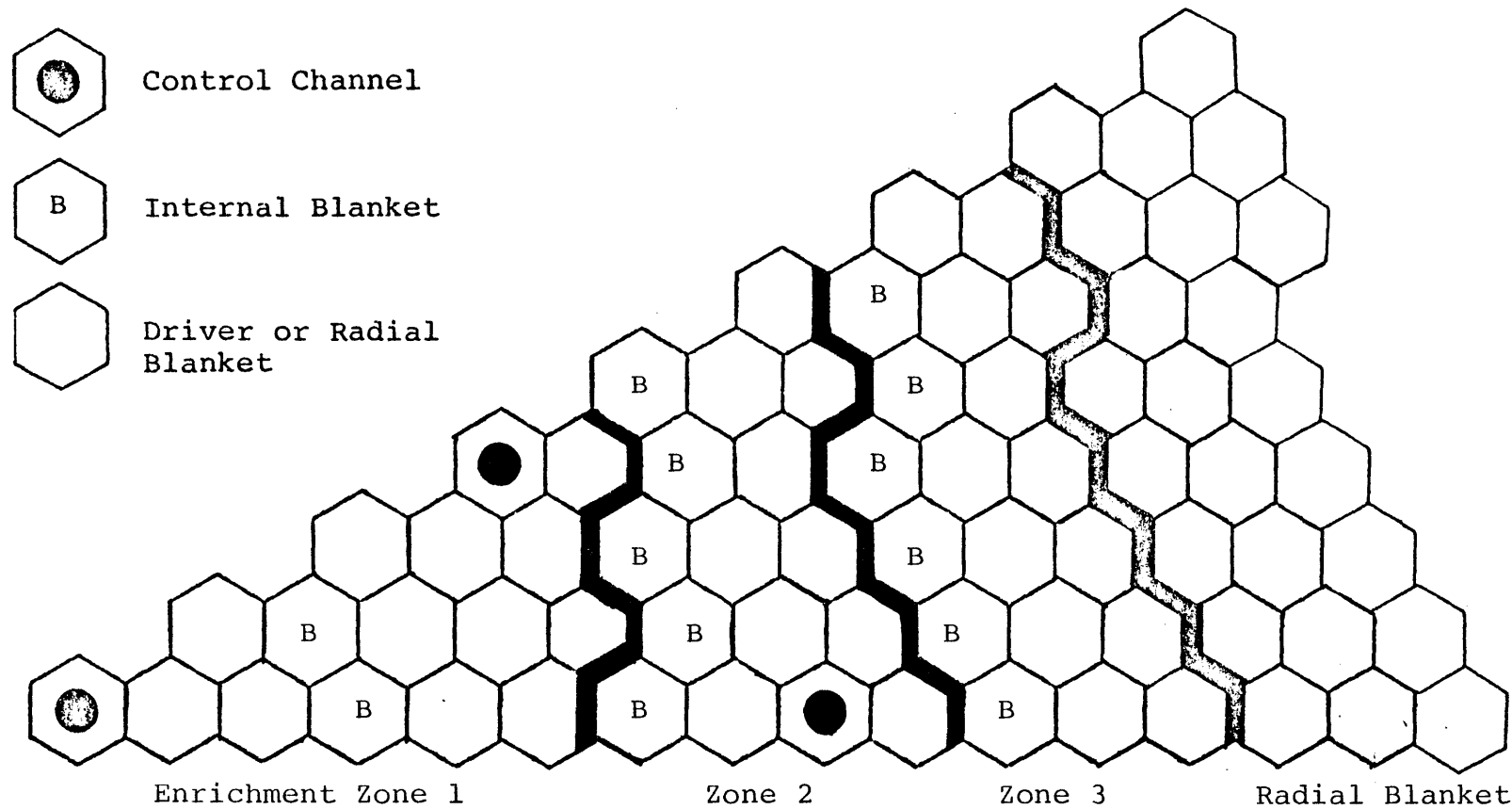


Fig. 4.20 Heterogeneous core arrangement V F

factor). Iteration was required to determine the correct relative enrichments for the enrichment zones. The axial bucklings for all cases were the same and were derived from the R-Z model of case 11 of Table 4.1.

To calculate the fissile inventories the hexagonal atom densities were assumed to be the average over the entire active core height. The fissile gain per year in the axial blankets and extensions was taken from the same R-Z analysis as the bucklings and was assumed the same for all cases. These steps allowed calculation of the doubling time and other key parameters, which are found in Table 4.3.

As can be seen from Table 4.3, the doubling times of all six cases are virtually indistinguishable. Assuming the same axial fissile gain for each case actually makes the uncertainty in the doubling times larger than the variation shown in Table 4.3. In that case, other criteria must be used to decide which case yields optimum performance.

The basis for arrangement selection in an LMFBR is considerably different than for a GCFR. In an LMFBR the key figure of merit for a heterogeneous core arrangement is the sodium void worth. This suggests that an LMFBR designer would prefer to deploy his internal blankets in the center of the core. In a GCFR, with no sodium void worth problems, center blankets are to be avoided. Placing internal blankets in the center of the core creates a situation where the flux tends to move toward the core center as burnup progresses.

Table 4.3

Performance of Heterogeneous Core Arrangements
Having the Same Driver Fuel Pin Diameter and
Number of Internal Blanket Assemblies

Arrangement Number	VA	VB	VC	VD	VE	VF
Doubling Time (yr)	8.2	8.2	8.3	8.3	8.2	8.3
BOC Fissile Inventory (Kg)	4700	4800	4800	4800	4800	4800
Maximum Power Increase over a cycle in a Driver Fuel Assembly (%)	0.8	3.0	0.0	0.9	0.0	6.0

This flux movement can cause driver fuel assemblies in the center of the core to increase in power from the beginning of cycle to the end of cycle. This increase in power forces beginning of cycle overcooling which lowers the mixed-mean core outlet temperature and thus decreases thermodynamic efficiency. Cases VB and VF have enough internal blanket assemblies close to the core center to draw the flux inward as the cycle proceeds. This flux movement causes 3% and 6% increases in power in a central driver assembly for cases VB and VF, respectively. For this reason these two cases were eliminated.

In an LMFBR a decoupled core, such as case VC, is often investigated since it produces low sodium void worths. However, such decoupled cores have other safety concerns associated with their susceptibility to radial and azimuthal power tilts. Once again, since the GCFR designer does not have to worry about sodium void worths a decoupled core leads to unneeded trouble, and as can be seen from Table 4.3, no benefits. Thus core VC is eliminated.

This leaves cores VA, VD and VE, all of which have essentially the same level of performance. Cores VA and VE have isolated internal blankets, but core VD has all its internal blanket assemblies in rings. This suggests that core VD is more amenable to R-Z analysis. Since much of the analysis done for the present work must be performed in R-Z geometry, core VD was selected.

4.2.3 Summary of the Selection of an Optimum Heterogeneous Core

Fifteen different heterogeneous cores were analyzed in the process of selecting an optimum driver fuel pin diameter and the number of internal blanket assemblies. All of these cores exhibited longer doubling times than homogeneous cores with the same effective fuel volume fraction. The dominant reason shown to cause this behavior comes from the lower average power per kilogram of heavy metal (at the same effective average enrichment). This lower average power density is an inherent trait of a heterogeneous core, making the optimum heterogeneous design the design with the least number of internal blanket assemblies (i.e. a homogeneous core). In order to allow further analysis of heterogeneous core effects a heterogeneous core with roughly one quarter of its active assemblies in the internal blankets, and an effective fuel volume fraction essentially the same as the optimum homogeneous core analyzed in Chapter 3, was focused upon. This heterogeneous core uses a 7 mm driver fuel pin diameter and 132 internal blanket assemblies.

Six different arrangements of the candidate heterogeneous core were investigated. It was found that the core arrangement had very little effect on the doubling time performance. The core arrangement shown on Fig. 4.18 was selected as the reference heterogeneous core for further study since it did not exhibit strong flux shifts with

burnup and since it was neutronically tightly coupled and easy to analyze.

4.3 Fuel Management and Burnup Analysis

As mentioned in Chapter 3, it is important that core designs be compared in their "equilibrium" condition. This section will describe the equilibrium cycle selection, the fuel management scheme, and the accompanying burnup analysis to arrive at the equilibrium cycle. Close attention will be paid to assure that the fuel management scheme and burnup analysis used for the heterogeneous core will be as similar as possible to those used for the homogeneous core so as not to yield one an undue advantage over the other. Therefore, this section will reference extensively the corresponding section for the homogeneous core (Section 3.4 of Chapter 3).

4.3.1 Fuel Loading and Shuffling Scheme

The objectives of the fuel loading and shuffling scheme for the heterogeneous core were the same as for a homogeneous core: a flat power distribution and roughly 100,000 MWD/MT peak burnup. Since the homogeneous core was allowed three enrichment zones, the heterogeneous core was allowed the same number. During the core arrangement analysis of Section 4.2.2 of this chapter, care was taken to avoid strong power peaking in any one assembly position in an enrichment zone. (The placement of the internal

blankets often adds a strong azimuthal power dependence to the normal radial dependence, which can cause single assemblies to have abnormally high or low-power densities when compared to other assemblies in the same zone.) With this tendency taken into account, the enrichment zones were apportioned in much the same manner as in the homogeneous case: ~ 2 rows of assemblies for the outermost enrichment zone, ~ 2 rows for the next zone in, and all of the rest of the assemblies in the center enrichment zone. The zoning is shown in Fig. 4.18.

The cycle length is normally determined by the burn-up limit and practical considerations such as the utility's annual peak load history. If the same cycle length was used for the heterogeneous core as was used for the homogeneous core the heterogeneous core would have a higher peak burnup (MWD/MT). This is because the 7 mm pins of the heterogeneous core have 35% less heavy metal per pin than the 8 mm pins used for the homogeneous core, while both pin sizes run at the same peak power level (15kw/ft). This would imply that a slightly shorter cycle time should be used for the heterogeneous core. However, since the GCFR fuel is vented, the assembly lifetime depends more heavily on fast fluence than burnup. The heterogeneous core has a roughly 17% lower fast flux than the homogeneous core. Since the burnup criterion and the flux criterion

compensate for each other it was decided that the same in-pile-time would be used for the heterogeneous driver assemblies as was used for the homogeneous assemblies. Hence, annual cycles (256 FPD) with one third of the driver assemblies being replaced every cycle will be used for the heterogeneous core. For the loading pattern see Fig. 4.21.

It was found in the early rounds of the analysis that an internal blanket assembly with 128 pins per assembly would reach close to 15 kw/ft in two years of burnup. If longer cycle times are desired more pins per assembly would be required. This would result in a decrease in the fuel volume fraction of the blanket assembly, which would in turn force the use of more internal blanket assemblies to achieve a given effective fuel volume fraction. The addition of more internal blanket assemblies would then hurt the core neutronic performance (See Section 4.2.1 of this chapter). An optimization could be performed to determine the best internal blanket assembly in-pile-time by balancing the cheaper blanket fabrication costs (due to less pins) and the time value of the plutonium in the blanket assemblies against the degradation in the neutronic performance. This is beyond the scope of the present work, and moreover, the impact of such an optimization is expected to be quite small. Thus for the present

30° Symmetry Sector Shown

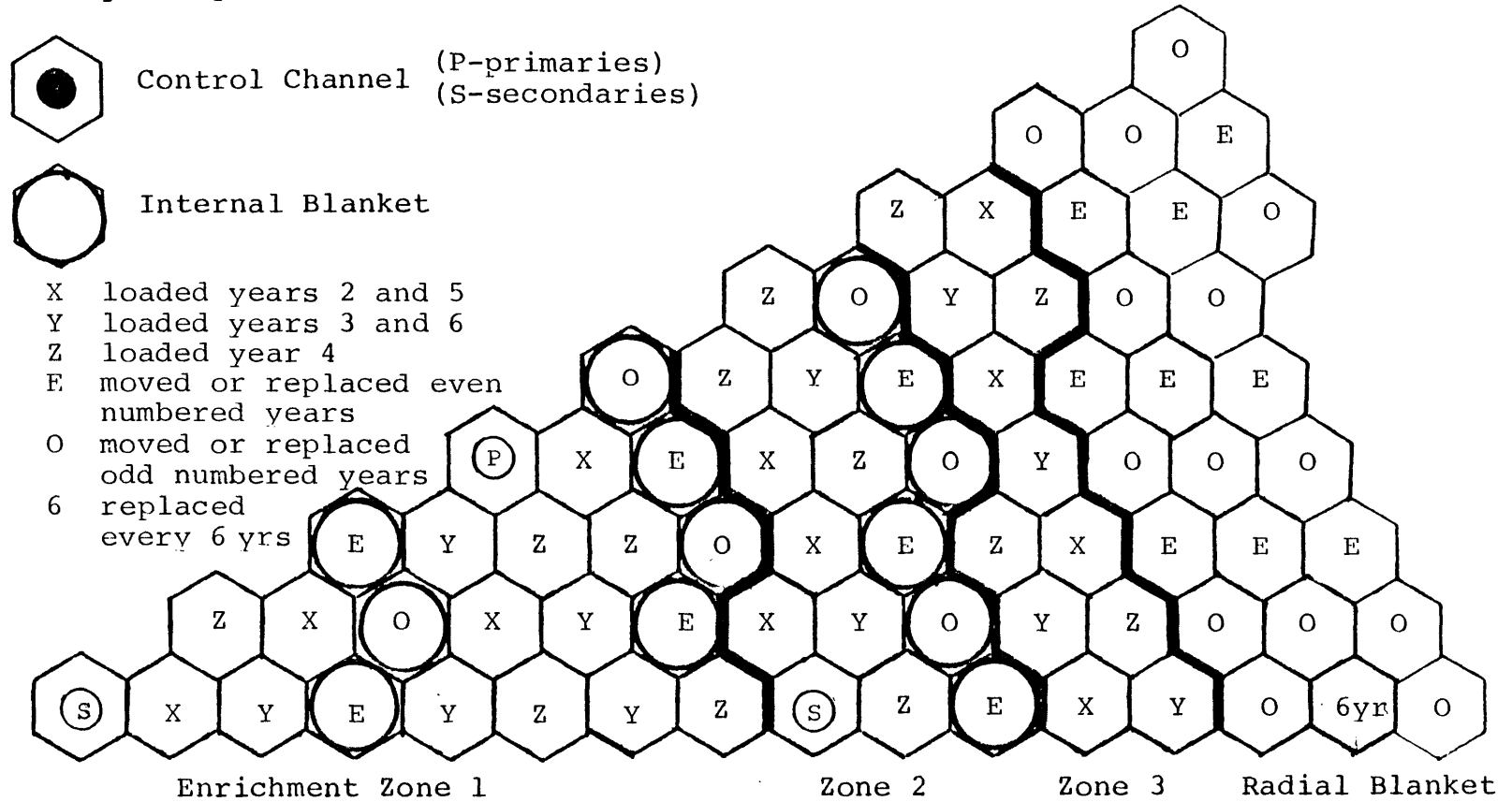


Fig. 4.21 Fuel Loading Pattern for the Reference Heterogeneous Core

work a two-year in-core residence period will be employed with half of the internal blanket assemblies replaced every cycle. For the loading scheme see Fig. 4.21.

The radial blanket fuel management scheme used for the homogeneous core was also used for the heterogeneous core (i.e., an in-out-in shuffling scheme with each radial blanket assembly in-pile for six cycles). The radial blanket loading and shuffling scheme is also shown on Fig. 4.21.

To allow the radial blanket assemblies to approach an equilibrium cycle condition the sixth cycle was selected as the equilibrium cycle. This corresponds to the same cycle as chosen for the homogeneous core. For the homogeneous core the sixth cycle was shown to be an acceptable equilibrium cycle by presenting the beginning and end of cycle eigenvalues obtained for the first six cycles when a constant feed enrichment was used. For the heterogeneous core constant feed enrichments were not acceptable, so a feed search was required for each cycle. Table 4.4 shows the resulting feed enrichments and the end of cycle k_{eff} for each cycle. As can be seen from this table, variations in the feed enrichments still exist by cycle six, but the cycle Δk no longer changes from cycle to cycle. Part of the variation in the feed enrichments is due to the non-existence of a true equilibrium cycle, since each of the three driver reload batches is different. For example,

Table 4.4
Heterogeneous Core Feed Enrichments and
End of Cycle k_{eff} for the First Six Cycles

Cycle	Feed Enrichment For Enrichment Zone 1	End of Cycle k_{eff}
1	15.0%	1.013
2	15.8%*	1.012
3	15.7%	1.011
4	15.2%	1.011
5	15.9%*	1.011
6	15.5%	1.011

Note: Each cycle has a beginning of cycle k_{eff} of 1.01.

*12 fewer feed assemblies than the other cycles.

one of the reload batches has twelve less driver assemblies than the other two. (This was required to permit 30° symmetry modeling). The variations in feed enrichments will be viewed as an addition to the calculational uncertainties.

4.3.2 Analytical Techniques Used to Arrive at the Equilibrium Cycle

The analytical approach employed in this subsection is very similar to that followed for the homogeneous core and described in Subsection 3.4.2 of Chapter 3. Thanks to the core arrangement study (Subsection 4.2.2 of this chapter) the relative zone enrichments to produce a flat power distribution have already been calculated. Thus the steps needed to find the equilibrium cycle conditions are only:

- 1) Using the relative enrichments calculated for the core arrangement study for case VD perform an enrichment search in a 2DB R-Z model to determine B₀C₁ critical feed enrichments. Burn these compositions for three years.
- 2) Use PERT-V and the fluxes from step 1 to determine axial bucklings for one, two, and three-year burned assemblies.
- 3) With the bucklings from step 2 use a hexagonal 2DB analysis with 30° symmetry and perform an enrichment search, followed by a burn for one cycle, then followed by shuffling to the start of the next cycle's conditions. Do this for the first five cycles.

Using the same approach described in Chapter 3 Subsection 3.4.2, the hexagonal number densities can be converted, with the aid of axial burnup distributions from the R-Z analysis of step 2, into the input for an equilibrium

cycle R-Z model. The equilibrium cycle hexagonal model is merely an extension of step 3 with updated bucklings from the equilibrium cycle R-Z analysis.

Once again, as for the homogeneous core, this technique was shown to work well, as evidenced by the R-Z equilibrium k_{eff} at the beginning of cycle: 1.0120, which is close to the 1.01 value targeted. For the heterogeneous core analysis different feed enrichments were required for each cycle, but only one feed enrichment set was required for the homogeneous core analysis. This difference arose because the conversion ratio of the driver assemblies in the heterogeneous core is less than one, but in the homogeneous core the conversion ratio is just enough above one to make the reactivity worth of a feed assembly and a burned assembly the same. The feed enrichments of the heterogeneous core also depend on the combination of internal blanket and driver assemblies in a particular loading pattern.

With the "equilibrium" cycle models determined, the analysis of a reference heterogeneous core which can be compared to the reference homogeneous core can now begin.

4.4 Analysis of the Optimized Heterogeneous Core Equilibrium Cycle

This section will perform a complete neutronic analysis of the heterogeneous core equilibrium cycle. All of the parameters previously calculated for the homogeneous core in Section 3.5 of Chapter 3 will be calculated here for the heterogeneous core and compared to the homogeneous core values. Since all the analytical methods used in this section have already been discussed in Chapter 3 the emphasis in this section will be on describing the reasons for the differences observed between the heterogeneous and homogeneous cores.

4.4.1 Mass Flows and Doubling Time

The mass flows for the first six cycles are listed in Table 4.5. They were calculated using the same technique employed to arrive at the equilibrium cycle R-Z model (see previous section). A comparison of this table with the corresponding table for the homogeneous core would show that the heterogeneous core in general has larger mass flows due to its lower power density. However, if the number of fuel assemblies involved is important due to an emphasis on fabrication costs or proliferation-related concerns it should be recognized that the heterogeneous core requires fewer fuel assemblies, due to the power production in the internal blankets.

Table 4.5
Mass Flows For the Heterogeneous Core

Cycle Time:	Kilograms Removed					
	EOC1	EOC2	EOC3	EOC4	EOC5	EOC6
<u>Fuel Assemblies</u>						
U-235	27.5	27.7	25.3	22.6	25.1	25.
U-238	15,113.	16,561.	16,342.	14,601.	16,245.	16,318.
Pu-239	1,301.	1,420.	1,409.	1,309.	1,444.	1,423.
Pu-240	414.	473.	483.	457.	504.	490.
Pu-241	176.	173.	157.	148.	163.	159.
Pu-242	51.2	59.6	61.5	58.3	64.3	62.4
Fission Products	240.	518.	734.	668.	765.	736.
No. of Assemblies**	108.	120.	120.	108.	120.	120.
<u>Blanket Assemblies*</u>						
U-235	55.1	45.4	50.0	42.2	48.6	45.5
U-238	29,910	26,417	29,486	26,281	29,398	27,797
Pu-239	267.	476.	561.	577.	633.	621.
Pu-240	3.6	15.6	17.9	18.6	21.4	21.5
Fission Products	47.3	110.	130.	138.	146.	148.
No. of Assemblies**	114	102	114	102	114	108

*Internal and Radial Blanket Assemblies.

**72 kg of HT-9 per fuel assembly, 48 kg of HT-9 per blanket assembly.

Table 4.5 (continued)

Cycle Time:	Kilograms Fed					
	BOC1	BOC2	BOC3	BOC4	BOC5	BOC6
<u>Fuel Assemblies</u>						
U-235	99.	30.4	33.8	34.0	30.4	33.9
U-238	49,236.	15,176.	16,880.	16,946.	15,144.	16,909.
Pu-239	427.	1,397.	1,541.	1,496.	1,404.	1,521.
Pu-240	1,288.	421.	464.	451.	423.	458.
Pu-241	647.	211.	233.	226.	212.	230.
Pu-242	155.	50.7	55.8	54.2	50.9	55.1
No. of Assemblies	348.	108.	120.	120.	108.	120.
No. of Blanket Assemblies*	390.	114.	102.	114.	102.	114.

*265 kg of heavy metal per internal or radial blanket assembly.

Most of the debate over heterogeneous cores versus homogeneous cores has centered on which type has the lowest doubling time. As shown in the optimization analysis of Section 4.2 of this chapter, the heterogeneous core appears to always have longer doubling times. All of that analysis however was done using clean first-cycle cores. It was assumed that the effect of burnup on the equilibrium cycle would be nearly the same for all cores. The homogeneous core doubling time changed from 8.25 years for a clean core to 10.9 years for the equilibrium core. By analyzing the equilibrium R-Z model for the heterogeneous core a doubling time of 11.4 years was determined. This is 2.5 years longer than that of a clean (B0C1) core, essentially the same as for the homogeneous core, for which the increase was 2.6 years. Hence, the assumption of comparable burnup effects is borne out.

The doubling time difference between the heterogeneous and homogeneous cores can now be analyzed in depth. Table 4.6 shows many of the key parameters in the determination of the doubling time for both the homogeneous and heterogeneous cores. As pointed out in a previous section (4.2), the key reason for longer doubling times for the heterogeneous core is the lower average power density. Both heterogeneous and homogeneous cores (with the same effective fuel volume fraction) require approximately the

Table 4.6

Comparison of Parameters Determining the
Doubling Time of the Reference Equilibrium
Homogeneous and Heterogeneous Cores

	Homogeneous Core	Heterogeneous Core
BOEC Fissile Inventory (Kg)	5096.	5617.
Net Fissile Gain (Kg/yr)	430.	454.
BOEC Breeding Ratio	1.57	1.61
EOEC Breeding Ratio	1.51	1.54
Reaction Rate Averaged Fissile η (BOEC)	2.37	2.39
Reaction Rate Averaged Pu-239 ν (BOEC)	2.94	2.94
Fast Fission Fraction (BOEC)	24.6 %	25.1 %
(EOEC)	24.1 %	24.7 %
Core Averaged Enrichment (BOEC)	13.0 %	13.2 %
Core Volume (liters x 10 ³)	12.1	13.2
Approximate Mean Core Neutron Energy (BOEC)	160 keV	170 keV
$\frac{1 + \delta}{1 + \alpha}$ (BOEC)	1.063	1.080
Power per Kg HM (kw_e /Kg)	28.1	20.6
Doubling Time (years)	10.9	11.4

BOEC \equiv Beginning of Equilibrium Cycle,

EOEC \equiv End of Equilibrium Cycle.

same average enrichment (13.2% and 13.0% for the heterogeneous and homogeneous core, respectively) but the heterogeneous core produces less power per kilogram of heavy metal. If this were the only effect the heterogeneous core doubling time would be 10% longer than that of the homogeneous core; however, there is only a 5% net difference. In other words, the heterogeneity was able to compensate for half of the lower power density effect by facilitating a better breeding gain. In order to help understand why the breeding gain is enhanced, a detailed neutron balance for the beginning of equilibrium cycle of both the heterogeneous and homogeneous cores is presented as Table 4.7. As can be seen from this table the increase in breeding is due mainly to the increase in neutron production due to an improved η and more fast fission. Both of these effects are due to the hardening of the spectrum seen by the plutonium. This comes from separating the fissile material from the fertile material (into driver assemblies and internal blankets). The increase in fast fission is actually due to an increase in Pu-240 fission. The U-238 fast fission in the heterogeneous core is very slightly less than that in a homogeneous core. In order to increase these beneficial effects of heterogeneity more internal blanket assemblies would be needed; but this would further decrease the average power density and the net result would be a longer doubling time.

Table 4.7
 Detailed Neutron Balance for BOEC Reference
 Heterogeneous and Homogeneous Designs

	Homogeneous Design	Heterogeneous Design
Neutron Production (per fissile absorption)		
Fissile Material	2.365	2.386
Fertile Material	<u>0.731</u>	<u>0.759</u>
Total	3.096	3.145
Neutron Losses (per fissile absorption)		
Fissile Absorption	1.000	1.000
Structure*	0.109	0.100
Leakage	0.077	0.090
Fission Products and Pu-242	0.048	0.041
Control**	0.031	0.031
Fertile Fission	0.261	0.271
Fertile Capture (=BR)	<u>1.570</u>	<u>1.612</u>
Total	3.096	3.145

*Oxygen absorption is included in this term.

**This accounts for $k_{eff} \neq 1.0$.

Since the difference between the homogeneous and heterogeneous doubling times is so small (5% or 0.5 years) concern over whether this margin will hold as the core design changes is valid. The procedure followed in this work varies from that adopted in some other recent work (M3) in that it allows the circulator power to vary among designs. If a constant circulator power were used in the present work the heterogeneous core's doubling time would be made longer, since it requires more circulator power due to the smaller pin diameters of its driver assemblies. A constant circulator power constraint would lower the heterogeneous core's average power density and further increase the doubling time difference between it and the homogeneous core. Another design feature in the present work that may differ from the work of others involves the selection of the cladding material. In this work HT-9 was selected for all structural material. This results in a 26% lower absorption loss to structure than that if SS-316 were used. Since the homogeneous core has a higher effective volume fraction of structural material than does the heterogeneous core (0.160 versus 0.144, respectively) the heterogeneous core's doubling would benefit relatively if SS-316 were used instead. From the detailed neutron balance in Table 4.7, the effect can be estimated to be less than a 0.5% change in the relative doubling times.

An important generic question is whether or not the doubling time difference seen in the present work would indicate that homogeneous LMFBR_S would have shorter doubling times than heterogeneous LMFBR_S. Before addressing this question it is important to recall that current LMFBR design practice involves the use of sodium void worth as a dominant figure of merit. If the design approach used for the present work were applied to an LMFBR, the homogeneous core would have a larger sodium void worth -- and if measures were taken to reduce it, neutronic performance would suffer. It should be pointed out that in the recent past it was considered that large-scale sodium voiding was sufficiently unexpected (and that plausible voiding patterns were sufficiently incoherent in space and time) that the maximum positive sodium void worth should not be used as a design constraint (H1). Sodium voiding has reappeared as a controlling design constraint only in the last five years, and may once again fade in importance in the future. Neutronically, a GCFR and an LMFBR are very similar, so that many of the same parametric trends for the doubling time are to be expected. Addition of internal blankets to an LMFBR decreases the power per kilogram of heavy metal just as it does for the GCFR. Further, the effective fuel volume fraction dominates the critical enrichment determination for the LMFBR just as it does for the GCFR. Thus the dominating effect which causes the heterogeneous GCFR

to have a longer doubling time than a homogeneous design is still controlling for an LMFBR. The beneficial effects of heterogeneity which help compensate for the insertion of low power internal blanket assemblies are also expected to be similar for an LMFBR. Therefore, qualitatively, one would expect a homogeneous LMFBR to have a lower doubling time than a heterogeneous LMFBR. On a quantitative basis the argument is a more difficult one, since the difference in doubling times is so small. In fact, the uncertainties in the doubling time analysis for the GCFR make it difficult to quantitatively support an unqualified assertion that a homogeneous GCFR is inherently superior to a heterogeneous GCFR; but, on the other hand, there is no known reason to expect that the heterogeneous core would outperform a homogeneous core. Thus it is expected that in LMFBR's, as in GCFR's, a homogeneous core will have a shorter doubling time than a comparably constrained and optimized heterogeneous core.

4.4.2 Power Analysis Distributions

Power distributions were calculated for the heterogeneous core using the same techniques described in Chapter 3, Subsection 3.5.2 for the homogeneous core, i.e., a hexagonal analysis having 30° symmetry was used for the radial and azimuthal distribution, and axial shape factors

from an RZ analysis were used to describe the axial dependence.

As for the homogeneous design, the number of axial shape functions needed to accurately calculate the power distribution was investigated. For the driver fuel assemblies the peak power density divided by the average power density divided by the average power density over the active core height varied between 1.19 and 1.24. The bounds of this range are determined by a three-year-burned assembly next to the central control rod for the low value (1.19), and the last radial position in the outer core zone at the start of the first cycle for the high value (1.24). It was decided that using one shape function with a peak-to-average power density of 1.22 would provide sufficient accuracy for this analysis. The shape function is shown on Fig. 4.22. The use of the shape function shown in Fig. 4.22 for the axial blanket yields power densities typical of the end of the third cycle (a convention adopted for the sake of conservatism).

The internal blanket axial power distributions were similarly investigated. It was found that for clean internal blankets the peak-to-average power density varied from 1.25 to 1.26. The internal blankets burned for one to two years had peak-to-average power densities ranging from 1.28 to 1.31. It was decided to use two axial shape functions for the internal blankets: one for the clean

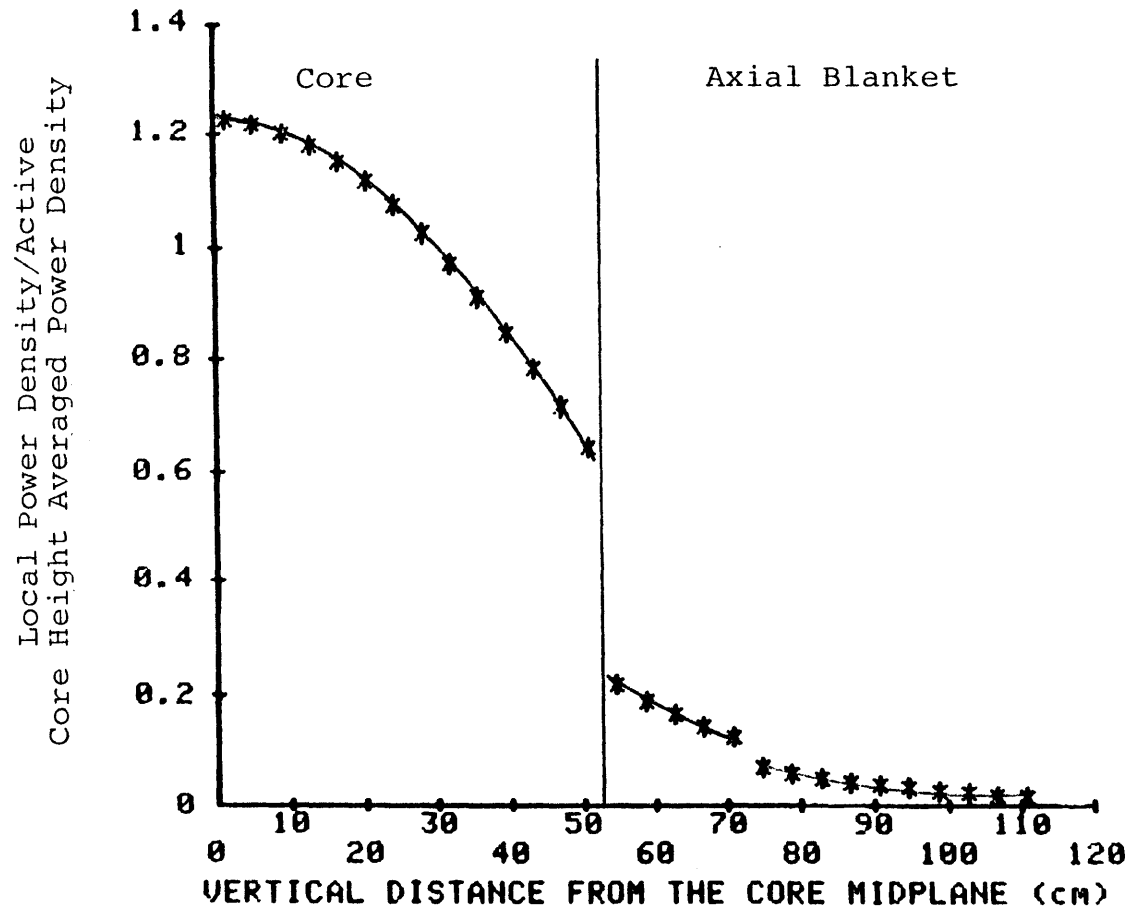


Fig. 4.22 Normalized axial power shape for the driver assemblies of the reference heterogeneous core.

internal blanket (1.25) and one for the burned internal blanket (1.31). These shape functions are shown on Fig. 4.23. The axial power distributions in the radial blanket assemblies were also investigated. It was found that the peak-to-average power density varied by position and time in cycle from 1.30 to 1.33, from 1.339 to 1.341, and from 1.28 to 1.31 for the first, second, and third row of the radial blanket, respectively: single effective peak values of 1.33, 1.34, and 1.31 were used for the three rows, respectively. Since the basic shape of these axial shape functions is very similar to that for the homogeneous core the reader is referred to Fig. 3.15 for a detailed display.

Using these axial shape functions and the radial-azimuthal distribution from the hexagonal analysis the peak kw/ft for each assembly can be calculated. Figures 4.24 and 4.25 show the peak kw/ft for each assembly at the beginning and end of the equilibrium cycle, respectively. To convert any of these values to peak power densities (kw/cm^3) divide the driver kw/ft by 29.12, the internal blanket kw/ft by 62.14, and the radial blanket kw/ft by 86.72. The power densities (or kw/ft) at any given position can be calculated with the shape functions previously given, and Figs. 4.24 and 4.25.

From Figs. 4.24 and 4.25 the peak kw/ft is seen to be 13.5 kw/ft and 14.0 kw/ft for the beginning and end of equilibrium cycle, respectively. This compares to

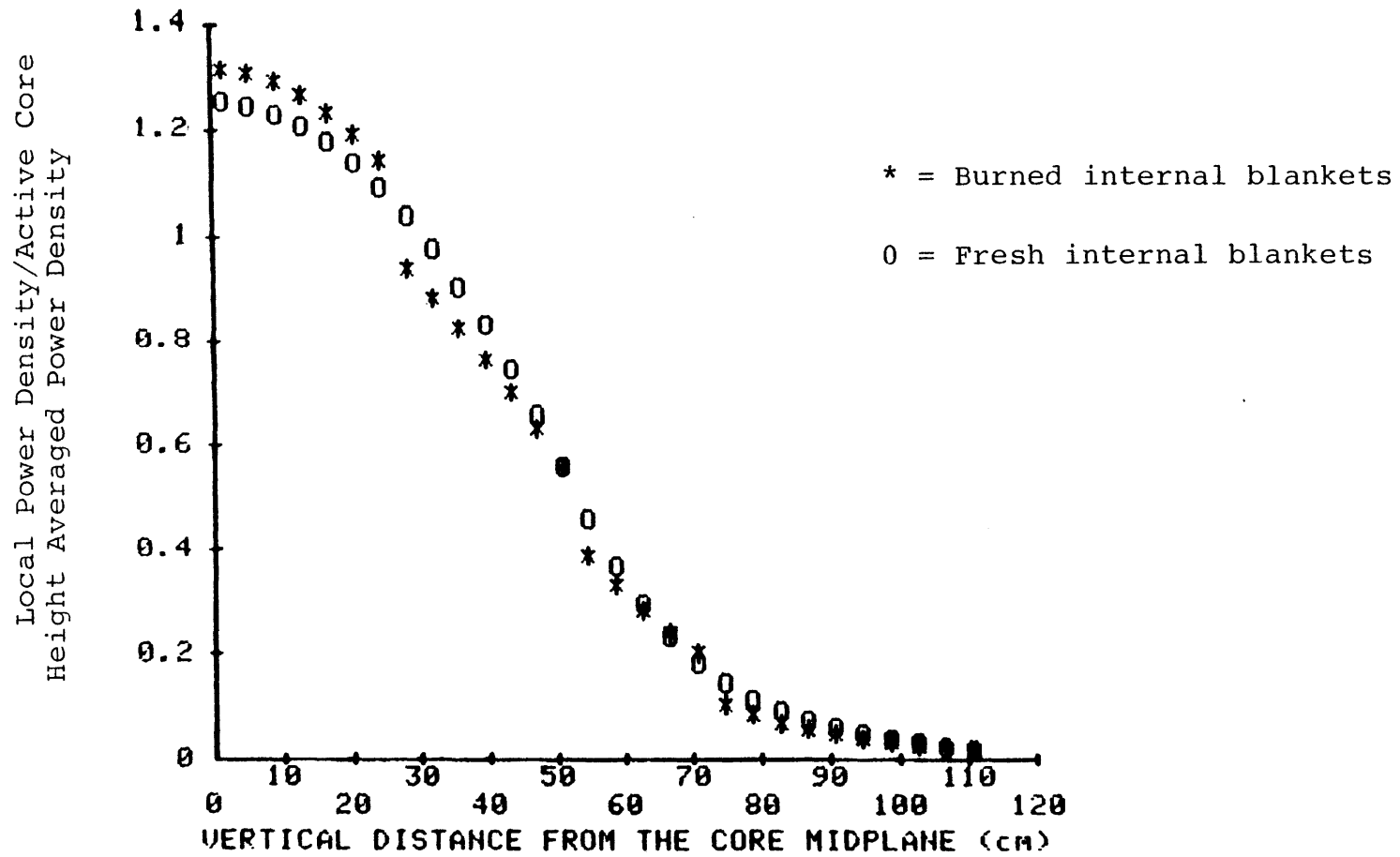


Fig. 4.23 Normalized axial power shapes for the burned and fresh internal blankets for the reference heterogeneous core.

30° Symmetry Sector Shown

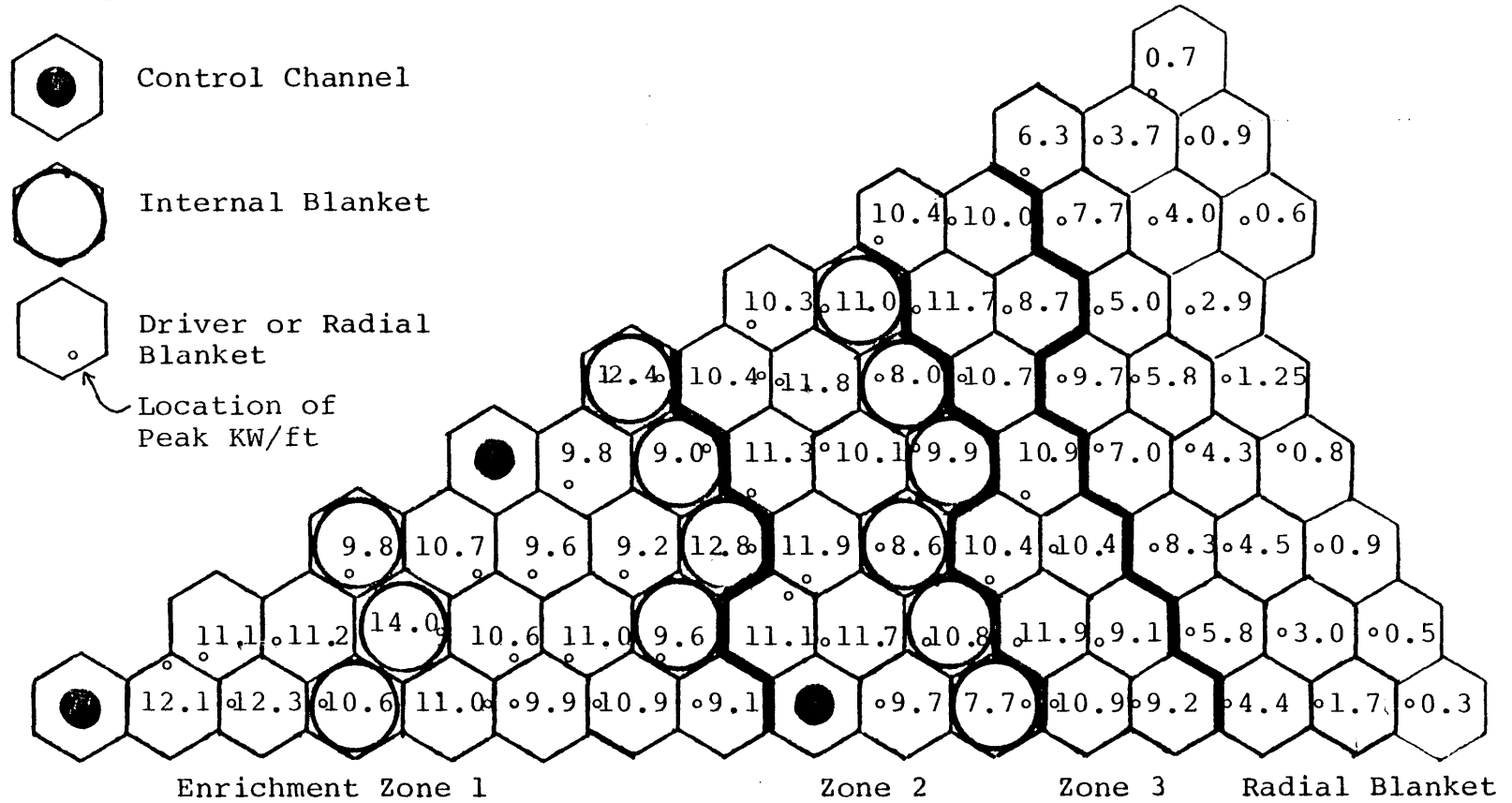


Figure 4.25 Peak KW/ft for assemblies at EOEC for the reference heterogenous core.

13.7 kw/ft and 14.0 kw/ft, respectively, for the homogeneous core. As evidenced by these values, neither core was given an advantage in the form of a higher peak kw/ft rating. To further check for equivalence, the radial power flattening must be compared. For the heterogeneous core the radial peak-to-average power densities (of the driver fuel assemblies) are 1.21 (and 1.32) for the beginning (and end) of the equilibrium cycle. The corresponding homogeneous core values are 1.23 and 1.29, respectively. Since the doubling time is inversely proportional to power, it is reassuring to confirm that both the peak kw/ft and the power flattening of the heterogeneous and homogeneous cores are essentially the same, implying that the difference in the doubling times can not be attributed to either the pin power or the enrichment zoning.

The peak linear power rating for an internal blanket assembly was found to be 14 kw/ft. This is below the centerline melting criterion of 15 kw/ft, but more analysis must be performed to ascertain whether the pressure drop across the core provides enough cooling capability. The first step is to find the pin diameter that yields a volume fraction fuel of 0.5 using 127 pins in the same size assembly as the core assemblies. The pellet diameter calculation is straightforward, yielding a value of 11.4 mm. A constant pellet diameter to pin diameter (OD of clad) ratio

was assumed, producing an internal blanket pin diameter of 12.1 mm. Assuming the same thickness of the duct wall, the same interassembly gap as for a fuel assembly, and equal spacing between all pins and the duct wall the pitch was determined to be 13.14 mm. With the geometry known, and the pressure drop across the core known, it was possible with the aid of some correlations supplied by General Atomic (T11) to determine an approximate mass flow rate per pin. The value computed in this manner was 154 lb_m/hr. At this mass flow rate the peak midwall clad temperature (including an allowance for hot spot factors) would be about 850°C. This is 100°C over the design limit. This blanket assembly design, however, will be considered acceptable for the present work since for the following reasons, the impact of a redesign of the internal blankets would be small:

- 1) A decrease of only 6% in the internal blanket fuel volume fraction would allow the design to meet the 750°C midwall clad temperature constraint. This would result in an effective fuel volume fraction of 0.348 as opposed to the 0.356 used in the present work. This would produce (roughly) a 0.2 year (2%) change in the doubling time
- 2) It may be possible to redesign the internal blanket assemblies without any impact on the neutronics at all. By making the combination of the duct wall and interassembly gap thickness only 10% thinner, the cross sectional flow area per pin would be increased enough to allow adequate cooling (peak midwall clad temperature equal to 750°C).

- 3) With a reduction in the uncertainties in the calculated temperature and/or the manufacturing and construction tolerances it may be possible to show that even the current design is capable of adequate cooling. The present design without hot spot factors makes the 750°C limit. A reduction in the hot spot factors may be possible through exploitation of the fact that the hottest pins in the blankets are where the best cooling occurs: i.e., next to the duct wall.
- 4) Since the internal blanket assemblies experience a lower fast fluence and a much lower burnup than the driver assemblies it may be possible to justify a higher peak clad temperature.

Based on the above arguments, the analysis of the heterogeneous core having internal blanket assemblies with 127 pins, and a fuel volume fraction of 0.5, continues.

A review of the kw/ft ratings given in Figs. 4.24 and 4.25 shows that the internal blanket assemblies increase in power dramatically in one cycle (roughly doubling in the first year, and increasing another 50% in the second year). Because of this the internal blankets are overcooled initially so that there is enough cooling capability for the end of cycle. This is not exclusively a problem for heterogeneous cores since the radial blanket of the homogeneous core has the same problem (but to a much lesser extent). Through variable orificing it would be possible to eliminate this concern, but a complex system of this type would add to the capital cost of the GCFR and pose unique safety problems. For the present work two approaches will be evaluated. In the first, the internal blanket assemblies will be orificed each year to permit matching the maximum

clad temperature at the end of each year, thus producing the maximum allowable ΔT across each internal blanket assembly at the end of every cycle. For the second case, the internal blankets will be orificed only when they are initially placed in the core and thereby only meet their maximum ΔT across the assembly after two cycles. The second approach is believed to be more realistic. For these analyses the maximum temperature rise across the internal blanket assemblies was taken to be 300°C at the end of the cycle for case one or upon assembly removal for case two. (The temperature rises across the fuel assemblies are given in Table 3.2 of Chapter 3). The loss in the mixed mean outlet temperature can be approximated using the relation:

$$\Delta T_i = \Delta T_f \frac{Q_i}{Q_f} \quad (4.1)$$

where

ΔT is the temperature rise across the blanket assembly,

Q is the power generated in the assembly, and the subscripts i and j stand for the initial and final conditions, respectively.

The above equation is valid as long as the mass flow rate is constant. The ratio of powers $\frac{Q_i}{Q_f}$ for the internal blanket assemblies spatially averaged over all assembly positions are 0.62 and 0.36 using approaches one and two respectively. Using 300°C as the final ΔT , the average ΔT across the internal blankets is 186°C and 112°C for

one and two, respectively. Assuming the zone-wise coolant mass flow rate is proportional to the power (and also assuming that the ΔT across the radial blankets is the same for the homogeneous and heterogeneous cores and that both have the same amount of bypass flow) the mixed-mean whole-core outlet temperature of the heterogeneous core is 21°C (case 1) or 39°C (case 2) less than that in the homogeneous core. From Eq. 3.7 of Chapter 3, this brings about a capital cost penalty of \$16.3 million (case 1) or \$30.2 million (case 2).

In this subsection the power distributions for the heterogeneous core have been presented, followed by an analysis of the attendant problems. Strictly speaking, the present design of the internal blanket assemblies does not meet the same thermal constraints imposed on the fissile-fueled assemblies: notably the 750°C peak clad temperature. However, it was concluded that the effect of the changes needed to meet this requirement were small enough not to affect strongly the conclusions of the present work. The power distributions were shown to involve a loss in the mixed mean outlet temperature, attributable to the internal blankets of the heterogeneous core design. This loss in the mixed mean outlet temperature was estimated and the associated capital cost penalty was quantified. The flux, fluence, and burnup distributions also come from the same

set of calculations, and will be presented next.

4.4.3 Flux, Fluence, and Burnup Analysis

The flux and fluence distributions are revealed in the analysis done to obtain the power distributions of the previous subsection. The flux and fluence distributions, however, require the use of different axial shape factors in the blanket assemblies than those prescribed for the power distributions. It was found that although the power shape for the blankets differs from that of the driver assemblies their flux shape is the same. Therefore, for both the internal blankets and driver fuel assemblies the axial shape shown on Fig. 4.22 is adequate. Spatially, the flux shape gradually becomes slightly more peaked as one moves out radially until a peak-to-average value of 1.24 is reached in the last row of the radial blanket. For the present work the axial shape shown in Fig. 4.22 was used for all driver and internal blanket assemblies; for the radial blanket a peak-to-average of 1.24 was used. (For this work only the peak-to-average values were needed. If a full set of shape factors is needed in the radial blanket Fig. 4.22 could be used with a little modification). Using a 30° symmetric 2DB equilibrium hexagonal model and the peaking factors of 1.22 and 1.24 described above, Figs. 4.26 and 4.27 were prepared. They show the peak flux distributions for the beginning and end of the equilibrium cycle.

30° Symmetry Sector Shown

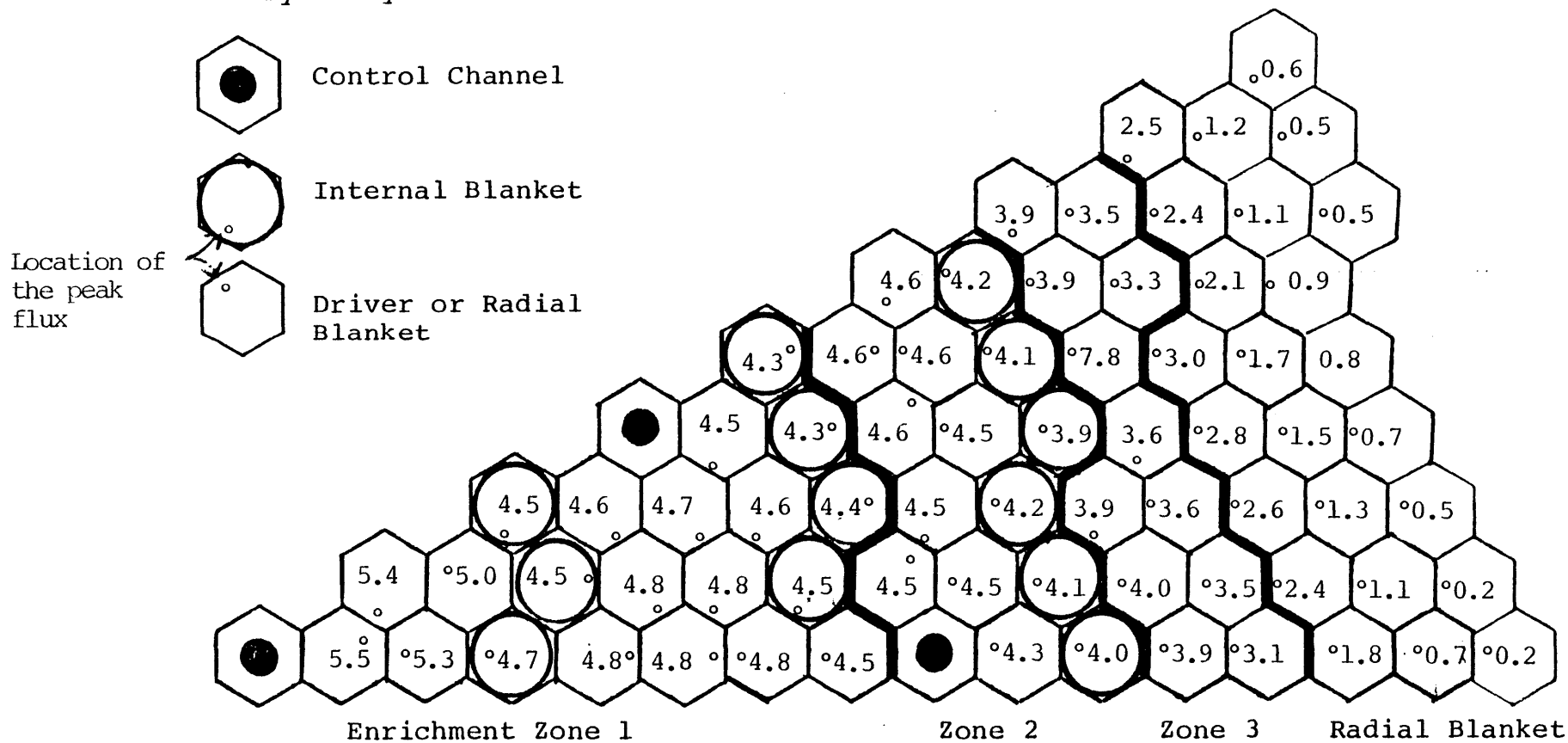


Figure 4.26 Peak flux (neutrons/cm²sec x 10¹⁵) for BOEC for the reference heterogeneous core.

30° Symmetry Sector Shown

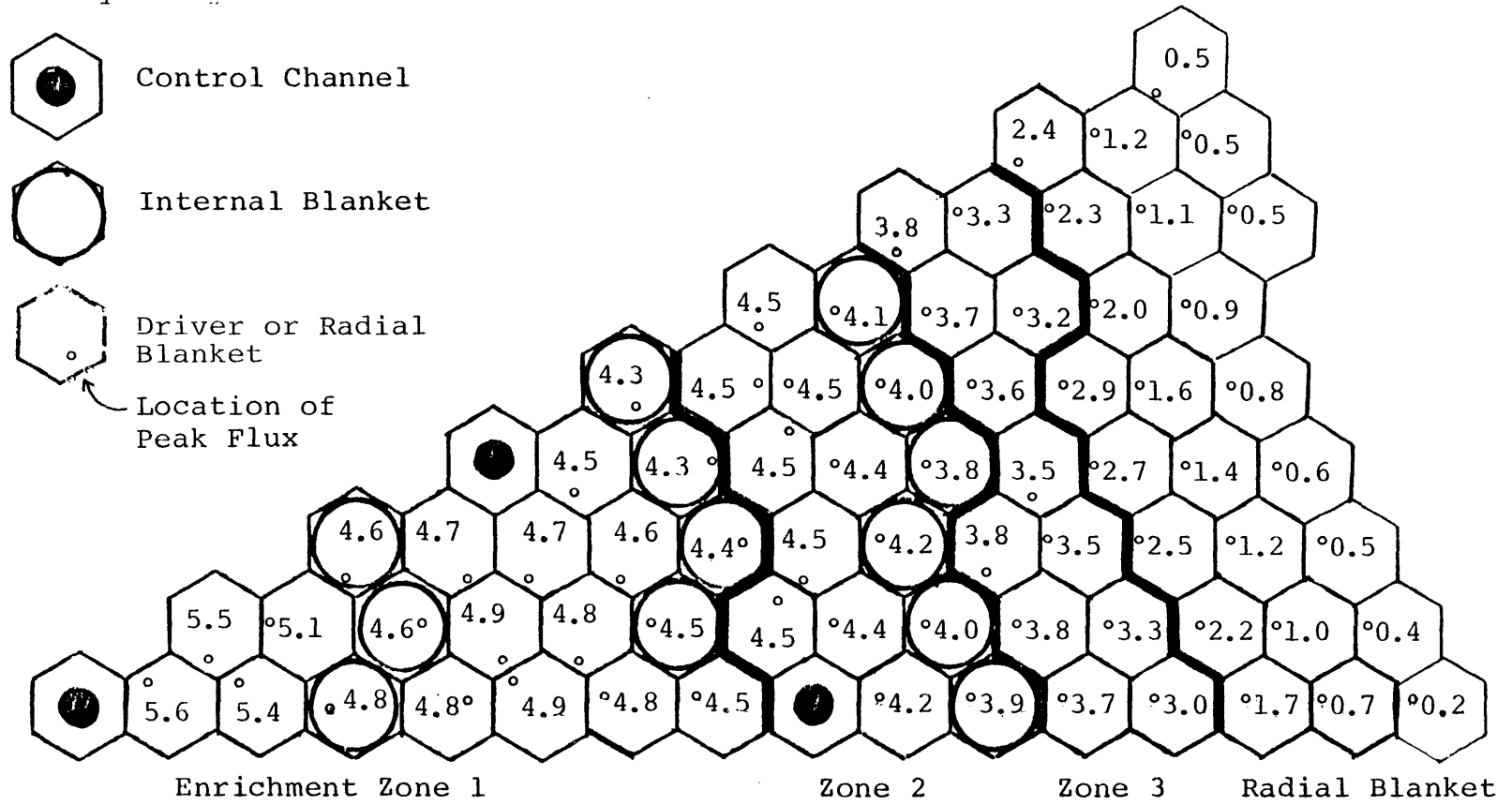


Figure 4.27 Peak flux (neutrons/cm²sec x 10¹⁵) for EOEC for the reference heterogeneous core.

The peak flux for the heterogeneous core is 5.6×10^{15} neutrons per $\text{cm}^2\text{-sec}$. This compares to 6.4×10^{15} neutrons per $\text{cm}^2\text{-sec}$ for the homogeneous core. Since the flux maps shown in Figs. 4.26 and 4.27 do not vary significantly with time, the total fluence can be calculated for each position by multiplying the flux by the time spent in that position. The driver assemblies spend 6.6×10^{-7} full-power seconds in the core, making their peak total fluence 3.7×10^{23} neutrons per cm^2 (versus 4.2×10^{23} for the homogeneous core). The neutron energy spectrum for each driver zone is shown in Fig. 4.28, and for the average internal blanket in Fig. 4.29. From these spectra the fraction of the neutron flux above 0.1 MeV can be found to determine the "fast" fluence. The peak fast fluence determined in this manner is 2.1×10^{23} neutrons/ cm^2 . For the homogeneous core the peak fast fluence was 2.4×10^{23} neutrons/ cm^2 .

At first glance this difference in the fast fluence may seem small. The CRBR project achieved a 43% reduction in fast fluence by changing to a heterogeneous design, while a reduction of only 14% is attained in the present work. Thus some explanation is required. The flux is usually normalized by the power, so that:

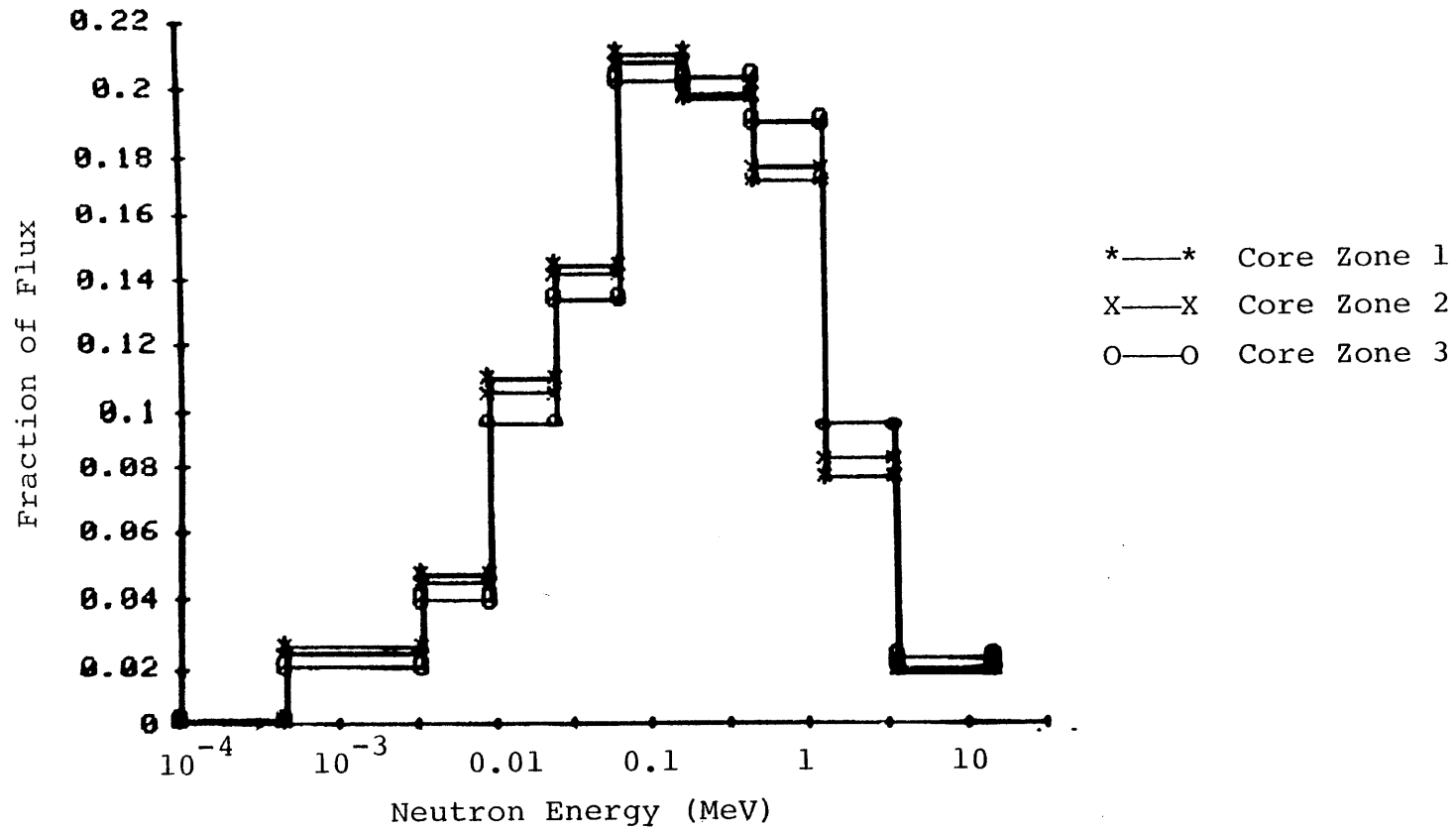


Fig. 4.28 Neutron energy spectrum in the driver fuel regions of the reference heterogeneous core.

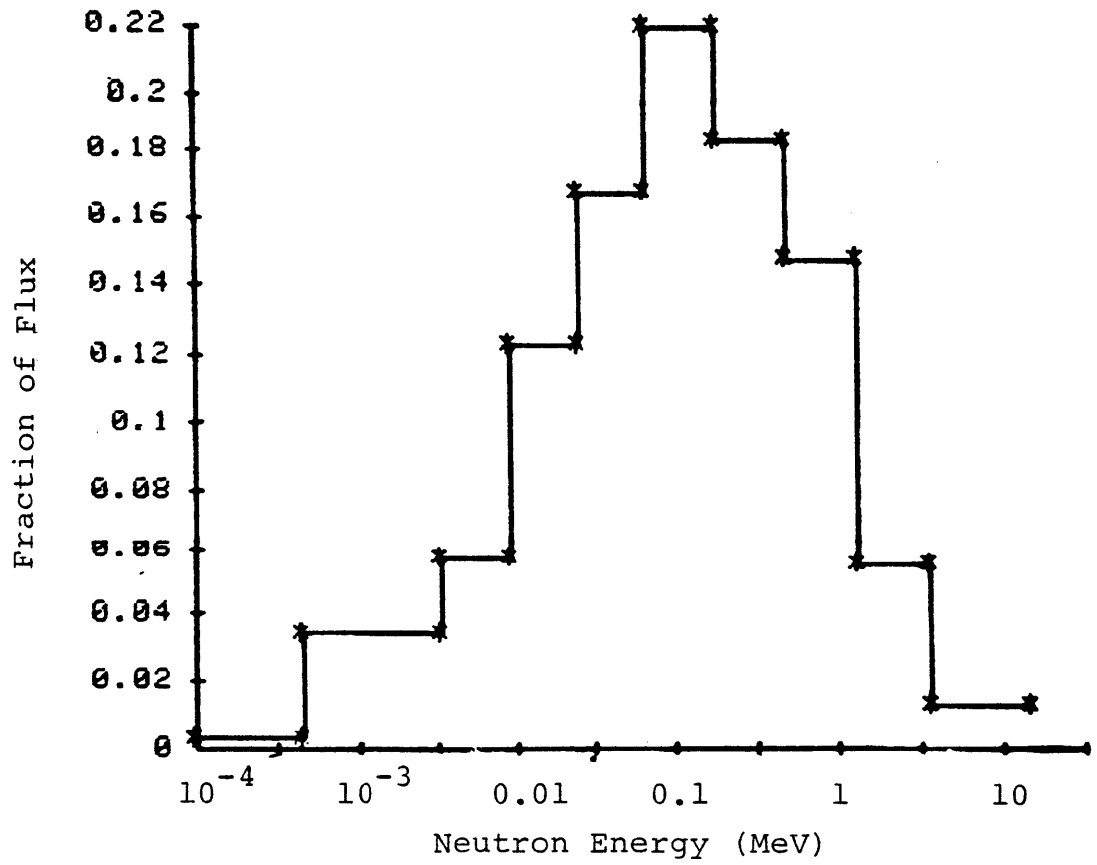


Fig. 4.29 Neutron energy spectrum in an internal blanket assembly of the reference heterogeneous core.

$$\phi = \frac{P}{a \Sigma_f V} \quad (4.2)$$

where

- ϕ is the volume-averaged one group flux,
- P is the power,
- a is a constant to convert the fission rate into the units of power
- Σ_f is the one-group spatially-averaged macroscopic fission cross section, and
- V is the volume over which the averaging was done.

Because all of the driver fuel assemblies in the present work were designed to produce the same power, the flux depends only on their volume and macroscopic fission cross-section and therefore enrichment. Adding internal blanket assemblies increases the enrichment in the driver fuel assemblies thereby causing a decreased flux. This is a real effect of heterogeneity. However, it is associated with a decrease in the average power/KgHM which (as shown in Section 4.2) will cause a longer doubling time (if no fuel volume fraction effect is present). Because internal blanket assemblies normally have a higher fuel volume fraction than driver fuel assemblies, the addition of internal blankets increases the fuel volume fraction. Indeed, for the CRBR studies the fuel volume fraction increased 15% as the flux decreased 43%. For the present work the effective fuel volume fraction of the heterogeneous and homogeneous cores are the same. Thus, the driver fuel assembly design for the

heterogeneous core has a smaller fuel volume fraction and a smaller total volume. The smaller volume of the assembly counteracts somewhat the increased enrichment caused by the heterogeneity. Thus for the present work only a 14% reduction in the flux was observed.

The amount of damage done to the clad and duct, which determines the length of time an assembly can stay in the core, is dominated by the fast fluence. In LMFBRs, which retain their fission product gases in the fuel pins (as opposed to GCFRs which have vented fuel), the burnup in MWD/MT is also a key constraint on fuel lifetime. Burnup also controls fuel swelling, thus in both GCFRs and LMFBRs it is of some concern with respect to fuel-cladding interaction. The peak burnup in the heterogeneous core is 123,000 MWD/MT. This is to be compared to 99,000 MWD/MT for the homogeneous core. The heterogeneous core has a higher burnup because of its smaller pins, which provide less heavy metal to absorb the same amount of energy. Based on the fluence comparison, the heterogeneous driver fuel assemblies should be able to burn for 14% more full power days than the homogeneous driver assemblies; but based on the burnup comparison they should be allowed 24% fewer full power days. Due to these compensating effects, the in-pile-time used for the heterogeneous and homogeneous cores was assumed to be the same (768 FPDs).

The in-pile-time for the internal blankets is determined by plutonium buildup and the maximum power limits. The peak fast fluence in an internal blanket assembly is only 1.1×10^{23} neutrons/cm². The peak burnup is only 15,000 MWD/MT. It is this low fast fluence and low burnup which may make it possible to increase the peak clad temperature for an internal blanket pin above the driver clad limit of 750°C.

This subsection has presented the flux distribution and explored its implications. The heterogeneous core does operate at a lower 14% flux (and fluence) than the homogeneous core, but the burnup is 24% higher. Although the analysis in this subsection did not confirm the sizeable benefits earlier reports had indicated for heterogeneity, the analysis of the core will continue with the focus now shifted to potential safety advantages. This quest starts in the next subsection with the β_{eff} analysis.

4.4.4 β_{eff} and Delayed Neutron Parameters

The delayed neutron fractions and β_{eff} for the equilibrium heterogeneous core are shown in Table 4.8. The method of calculation has been previously described in subsection 3.5.3 of Chapter 3. As can be seen by comparing this table with Table 3.14, which contains the homogeneous core values, the heterogeneity has very little effect on β_{eff} . This is the expected result, since the relative isotopic fission rates vary only slightly with heterogeneity. This can be deduced from Table 4.6, which shows the heterogeneous core has a 0.5% increase in fertile fissions (importance weighting decreases even this insignificant effect). It is possible to produce a heterogeneous core with a higher β_{eff} than the homogeneous core if the effective fuel volume fraction is not kept constant, but then this would not be truly a "heterogeneous" effect.

4.4.5 Control Rod Analysis

This subsection presents the analysis of the control rod requirements and worths for the heterogeneous core. It follows the same form as subsection 3.5.4 of Chapter 3 in which a similar analysis was performed for the homogeneous core. It is also in this subsection that the Doppler coefficients are presented, since they are needed to determine the control rod requirements. Other reactivity coefficients and worths, however, are saved for subsection 4.4.6.

Table 4.8

β_{eff} and Delayed Neutron Parameters
for the Reference Heterogeneous Core

Delayed Group	Half Life (sec)	Effective Delayed Neutron Fraction	
		BOEC	EOEC
1	53.7	8.1-5	8.1-5
2	22.2	7.7-4	7.5-4
3	5.2	7.0-4	6.9-4
4	2.0	1.4-3	1.4-3
5	0.50	6.9-4	6.8-4
6	0.19	2.0-4	2.0-4
Total β_{eff}		3.8-3	3.803

4.4.5.1 Control Rod Requirements

The requirements of the primary and secondary control systems were specified in Subsection 3.5.4.1 of Chapter 3. It was concluded in that subsection that the requirements of the secondary system could be defined as 1.8 times the Doppler reactivity from the hot-standby condition (300°C) to hot-full-power plus 0.01 ΔK . The requirement for the primaries was defined to include all Doppler reactivity from room temperature (300°K) to the hot-full-power condition. The hot-full-power temperatures are assumed to be 1500°C for the driver pellets, 1200°C for the internal blanket pellets, 1000°C for the radial blanket and axial blanket pellets, and, finally, 600°C for all structural material. These temperatures are the same as assumed for the homogeneous core (except, of course, for the added condition needed for the internal blanket). In actuality the 7 mm pins of the heterogeneous driver assemblies do have a hotter average temperature than the 8 mm pins of the homogeneous core, but only by ~4%, which is quite small compared to the uncertainties in this analysis.

4.4.5.2 Doppler Coefficients and Temperature Defects

The method used to calculate the Doppler coefficients was previously described in Subsection 3.5.4.2 of Chapter 3. Table 4.9 presents the Doppler coefficients by zone for both the beginning and the end of the equilibrium

Table 4.9

Heterogeneous Core Doppler Coefficients

Region:	Doppler Coefficient $-T \frac{dk}{dT} \times 10^{-4}$			
	Fuel		Structure	
	BOEC	EOEC	BOEC	EOEC
Zone 1	14.5	14.9	0.9	1.0
Zone 2	10.4	9.6	0.7	0.7
Zone 3	<u>7.9</u>	<u>6.8</u>	<u>0.5</u>	<u>0.4</u>
Subtotal	32.8	31.3	2.1	2.1
Internal Blankets*				
1st Ring	6.3	7.5	0.1	0.2
2nd Ring	11.6	12.5	0.2	0.3
3rd Ring	<u>15.8</u>	<u>15.3</u>	<u>0.3</u>	<u>0.4</u>
Subtotal	33.7	35.3	0.7	0.9
Radial Blanket*				
1st Row	5.2	4.9	---	---
2nd Row	1.3	1.3	---	---
3rd Row	<u>0.4</u>	<u>0.4</u>	<u>---</u>	<u>---</u>
Subtotal	6.9	6.6	0.1	0.2
Axial Blanket	<u>4.3</u>	<u>5.0</u>	<u>0.1</u>	<u>0.2</u>
Total	77.7	78.2	3.0	3.4

*Full length including extensions.

cycle. Table 4.10 shows the temperature defects that result from these coefficients, and also the resulting primary and secondary control requirements.

Comparing these results for the heterogeneous core to those of the homogeneous core (Tables 3.15 and 3.16) suggests some interesting safety differences between the cores. Although the total Doppler reactivity increment that would occur if all the fuel and blanket pellets were raised one degree in temperature is roughly the same for the heterogeneous and homogeneous cores, fast transients can occur which would yield a much lower Doppler reactivity feedback for the heterogeneous core than for the homogeneous core, as will be shown. Table 4.11 shows the time constants for each pin diameter for both cores. The time constant is the time it takes for the fuel to increase or decrease in average temperature above ambient by a factor of e . From these time constants one can see that fast transients -- those which run their course in a second or so -- will be controlled by the "power" (power density weighted) Doppler, since energy is trapped inside the fuel pin where it originates. Because the driver pins have much higher power densities than internal or radial blanket pins, the driver pin Doppler dominates the reactivity feedback. The following helps to quantify this effect.

If it is assumed that none of the heat generated in the transient is removed from the pellets the following

Table 4.10

Temperature Defect and Control Requirements
for the Reference Heterogeneous Core

PuO ₂ /UO ₂	$\Delta k/k$	
	BOEC	EOEC
Core		
Room Temperature to 300°C	-0.0021	-0.0020
300°C to 1500°C	-0.0037	-0.0035
Internal Blankets		
Room Temperature to 300°C	-0.0022	-0.0023
300°C to 1200°C	-0.0032	0.
Radial and Axial Blankets		
Room Temperature to 300°C	-0.0007	-0.0008
300°C to 1000°C	-0.0009	-0.0009
Structure		
Room Temperature to 300°C	0.	-0.0002
300°C to 600°C	-0.0001	-0.0001
Cold to HFP	-0.0131 (\$3.45)	-0.0131 (\$3.45)
Hot-Standby to HFP	-0.0079 (\$2.08)	-0.0078 (\$2.05)
Primary Requirements	0.034 (\$8.95)	0.034 (\$8.95)
Secondary Requirements	0.024 (\$6.32)	0.024 (\$6.32)

Table 4.11

Time Constants for the Heterogeneous and
Homogeneous Fuel and Blanket Pins*

Homogeneous Core	Pellet Diameter (mm)	Time Constant (seconds)
Fuel Pins	7.06	2.4
Radial Blanket Pins	14.4	10.0
Heterogeneous Core		
Driver Pins	6.06	1.8
Internal Blanket Pins	11.4	6.3
Radial Blanket Pins	13.5	8.8

$$\text{*Time constant**} = \frac{\rho C_p D^2}{597.1 k} = 0.048D^2$$

where ρ is the fuel density (640 lb_m/ft³),
 C_p is the heat capacity of UO₂ (0.081 Btu/lb_m°F),
 D is the pin diameter (mm), and
 k is the thermal conductivity of UO₂ (1.8 Btu/hr-ft°F),

**This comes from assuming separability in the time dependent heat equation and the use of a T(at the pellet O.D.)= 0 boundary condition.

expression can be formulated:

$$PF_j \int P(t) dt = m_j c_p (T_f - T_i)_j \quad (4.3)$$

where $P(t)$ is the reactor power as a function of time, t ,

PF_j is the power fraction for region j ,

m_j is the mass in region j ,

c_p is the specific heat of UO_2 ,

T is the average temperature, initially i , and finally f .

To use this relation for comparative purposes assume

$$\int \frac{P(t) dt}{C_p} = 1.0 \text{ and then, knowing the mass,}$$

power fraction, and initial average temperatures of a region, T_f can be calculated. This T_f and the initial hot-full-power temperatures can be used to yield a Doppler feedback reactivity increment for both the heterogeneous and homogeneous cores. From this type of calculation it can be shown that the homogeneous core provides 41% more reactivity feedback for a fast transient (at BOEC). (Notice since $P = q'''V$, Eq. 4.3 is equivalent to making the zonewise ΔT 's proportional to their q''' , i.e: a power density weighted Doppler feedback).

During very slow transients (e.g., a gradual rise in the isothermal temperature level) the heterogeneous and homogeneous cores would have roughly the same Doppler feedback. For example, in going from room temperature to hot-full-power conditions the Doppler reactivity feedback seen by the heterogeneous core is within several percent of that of the homogeneous core. The same is true of going from the hot-standby temperature to the hot-full-power condition. (This can be seen by comparing Tables 4.10 and 3.16).

4.4.5.3 Control Rod Worths

Calculations of the control rod worths were performed using the techniques described in Subsection 3.5.4.3 of Chapter 3. Table 4.12 shows the Δk 's caused by the insertion of the entire bank of primary or secondary control rods. As for the homogenous core, an estimate of the bank worths with one stuck rod was made by removing one rod of average worth. This assumption is even less valid for a heterogeneous core but is adequate for the present work.

Once again, as for the homogeneous core, the heterogeneous core's control rods of 50% B-10 are not sufficient to meet the requirements. It is again projected that further enrichment of the control rods would supply enough rod worth. However, the key objective for present purposes of an equal-handed comparison of homogeneous and heterogeneous cores is met, since the difference between rod

Table 4.12

Control Rod Worths and Requirements*
for the Reference Heterogeneous Core

<u>Capabilities</u>	BOEC	EOEC
Δk primaries*	0.0293	0.0339
Δk secondaries*	0.0208	0.0223
Worth with One Stuck Rod*		
Primaries	\$6.43	\$7.43
Secondaries	4.69	5.03
<u>Requirements</u>		
Primaries	\$8.95	\$8.95
Secondaries	6.32	6.32

*The control rods used here are only 50% enriched in B-10. Clearly, since the worths do not meet the requirements, a higher enrichment would be used.

worths and rod requirements is remarkably similar for the two cores (See Tables 4.12 and 3.17).

4.4.6 Material Worths

As for the homogeneous core, the material worths for helium, HT-9, and fuel have been calculated for the heterogeneous core. The calculational method has been previously described in Subsection 3.5.5 of Chapter 3. Table 4.13 shows the resulting material worths by region for the beginning and end of cycle for the equilibrium heterogeneous core. The corresponding values for the homogeneous core are to be found in Table 3.18.

The helium worth for the heterogeneous core is very nearly the same as for the homogeneous core. The $\Delta k/\text{psi}$ values for depressurization are within 8% of each other at BOEC and within 3% at EOEC. For full depressurization the loss of helium would introduce \$1.64 and \$1.78 at the beginning and end of the equilibrium cycle, respectively. Most of the differences in helium worth between the heterogeneous and homogeneous cores seem to be due to the power shape differences, which depend on the relative zone enrichments more than heterogeneity per se. This is expected, since helium worth comes from moderation, and the adjoint energy shape is virtually the same for the homogeneous and heterogeneous cores. (The adjoint energy shape depends primarily on the average composition which is essentially the same when the effective (core-averaged) fuel

Table 1.13
Material Worths for the Reference Heterogeneous Core

Region:	Material Worths ($\Delta k/kg$)					
	Helium*		HT-9		Fuel**	
	BOEC	EOEC	BOEC	EOEC	BOEC	EOEC
Driver Fuel						
Zone 1	-1.2-4	-1.4-4	-3.7-6	-4.2-6	+1.3-5	+1.3-5
Zone 2	-1.2-4	-1.3-4	-3.6-6	-3.7-6	+1.8-5	+1.6-5
Zone 3	-6.2-5	-6.1-5	-1.3-6	-1.3-6	+1.7-5	+1.3-5
Average	-9.9-4	-1.1-4	-2.8-6	-3.0-6	+1.6-5	+1.4-5
Internal Blanket						
1st Ring	-1.3-4	-1.5-4	-4.1-6	-4.8-6	-5.4-6	-4.0-6
2nd Ring	-1.4-4	-1.5-4	-4.3-6	-4.7-6	-5.9-6	-4.0-6
3rd Ring	-1.2-4	-1.2-4	-4.0-6	-3.8-6	-5.1-6	-3.2-6
Extensions	-8.5-6	9.5-6	-4.7-8	-6.3-8	-2.3-7	-1.9-7
Axial Blanket						
First 20 cm	-8.8-6	-1.2-5	+7.1-7	+6.0-7	+3.8-7	+4.5-7
Remaining 40 cm	-1.5-6	-1.8-6	+9.0-8	+8.3-8	+2.9-8	+3.7-8
Average	-3.9-6	-5.2-6	+3.0-7	+2.6-7	+1.5-7	+1.7-7
Radial Blanket						
1st Row	-6.4-6	-7.0-6	+4.2-7	+3.0-7	+2.3-7	+2.4-7
2nd Row	-2.5-6	-2.5-6	+7.5-8	+6.4-8	+7.2-8	+7.3-8
3rd Row	-3.7-7	-4.0-7	+2.1-8	+2.0-8	+3.6-9	+4.3-9
Average	-3.1-6	-3.3-6	+1.7-7	+1.3-7	+1.0-7	+1.1-7

*The whole-core $\Delta k/psi$ is 3.6-6 and 3.9-6 for the BOEC and EOEC, respectively.

**Fuel worth is the worth of the pellets normally at the given position.

volume fraction is maintained constant -- as it was for this study).

In comparing the cladding (HT-9) worth of the heterogeneous and homogeneous cores one notices a lower clad worth in the heterogeneous core. This is due to leakage effects. The clad worth when HT-9 is used as the cladding is dominated by the moderation term in the center of a driver region and by the leakage term at the edge of a driver region. This is analogous to sodium worth in an LMFBR. Due to the number of low worth areas (internal blankets) near the active fuel zones the leakage term is enhanced in the heterogeneous core. Thus the clad worth is less. If all the cladding in the driver core zone was removed and placed in the first 30 cm of the axial blankets, reactivity insertions of \$6.66 and \$6.84 would result at the beginning and end of the equilibrium cycle, respectively. This is approximately a 50% decrease from the homogeneous core values. However, if the cladding in the internal blankets was also moved from the core to the same axial height an additional \$1.50 would result, reducing the difference between the homogeneous and heterogeneous cores to 20%. Thus, the heterogeneous core appears to have a slight safety advantage with respect to this parameter; however, it is only of value when extremely severe core disruption is in progress, and accidents of this magnitude

are projected to be extremely rare for the GCFR.

The fuel worths for the heterogeneous core are higher than those for the homogeneous core. This is due to the higher enrichments in the driver fuel assemblies. This implies that the heterogeneous core may have more problems in fuel melting scenarios that involve compaction. Further analysis of the safety implications would require more detailed delineation of a specific step-by-step accident scenario, which is beyond the scope of the present work.

The material worths presented in this subsection do not indicate that either core design has a significant safety advantage over the other. Both have roughly the same reactivity insertion due to helium depressurization. The heterogeneous core has an advantage in the form of lower cladding worth, but has the disadvantage of higher fuel worth. Although the material worths do not strongly favor one core over the other, the Doppler coefficients strongly favor the homogeneous core. Therefore, with respect to safety the homogeneous core seems to have the edge.

4.4.7 Summary of the Equilibrium Heterogeneous Core Analysis

This section has presented the analysis of the equilibrium heterogeneous core and compared the results to the homogeneous core values. It was found that the heterogeneous core has a longer doubling time (11.4 years versus 10.9

years), a lower mixed mean outlet temperature (by 21° to 39°C), a lower fluence (by 14%), a higher peak burnup (by 24%), a lower driver core Doppler coefficient (by a factor of two), lower clad removal worth (about 20%), and a higher driver fuel worth (by about a factor of two) than the homogeneous core. From this analysis there seems to be little to recommend the heterogeneous core. It seems to be less favorable with respect to economics, energy growth potential, and safety. It should be pointed out, however, in almost all aspects the heterogeneous and homogeneous cores perform similarly, and most of the differences observed are not large. A more quantitative economic penalty will be calculated in Chapter 5.

4.5 Summary

This chapter documents the analysis of the heterogeneous core examined in the present work. It started with an optimization of the driver pin diameter and the number of internal blanket assemblies. It was concluded from this optimization study that the optimum number of internal blanket assemblies would be zero if the fuel pin diameter of the driver assemblies is optimized. The reasons for this result were analyzed and explained. Of course, if the driver pin diameter is too small it was found that the addition of internal blankets could enhance performance.

In order to continue the study a heterogeneous core with the same effective (core-averaged) fuel volume fraction as the optimum homogeneous core was selected; this core had the same relative proportion of internal blanket assemblies as current LMFBR heterogeneous core studies.

With the driver pin diameter and the number of internal blanket assemblies selected, the optimum arrangement was explored. It was found that as long as three enrichment zones were used the arrangement of the internal blankets had little effect on most performance parameters. The arrangement selected for the present work was basically annular in configuration to facilitate analysis.

This core was then burned for six cycles to yield (for all practical purposes) an equilibrium core on which a detailed analysis was performed. In this analysis it was found that the heterogeneous core maintained its inferior doubling time performance, and realized only one minor safety advantage (lower clad worth), while incurring two disadvantages: much lower Doppler feedback in rapid transients, and much higher driver fuel worth. However, in most aspects the heterogeneous core performed quite similarly to the homogeneous core. In the next chapter we will quantify the cost differences between the heterogeneous and homogeneous designs to determine whether any important advantage or disadvantage can be claimed in this important aspect of overall concept evaluation.

CHAPTER 5

ECONOMIC ANALYSIS

5.1 Introduction

For two comparable GCFR units built to produce power at the same level of safety, one with a homogenous and the other with a heterogenous core design, the cost of the electric energy generated should be the deciding factor in the selection of the preferred alternative. The previous chapter suggests, with some key reservations, that a heterogenous core could be built with roughly the same level of safety as a homogenous core; this chapter will deal with the relative energy generation costs.

This chapter begins with an analysis of the fuel cycle costs. For this the simple model proposed by Abbaspour (A4) was used. This model is presented, discussed, and then used with a conventional set of economic assumptions. These data are then varied one at a time to ascertain the sensitivity of the analysis to each assumption.

With the fuel cycle costs known, the capital cost differences associated with the design decisions are estimated. These capital cost differences are then annualized, and added to the fuel cycle costs to arrive at the power generation cost difference between the homogenous and heterogenous cores.

Finally, the chapter is summarized, including a commentary on the uncertainty in the overall difference in the power generation costs.

5.2 Fuel Cycle Costs

In this section the fuel cycle costs of both the heterogeneous and homogenous cores will be calculated. The sensitivity of these costs to the input data is then examined. For this analysis the simple model presented by Abbaspour (A4) will be used.

5.2.1 Fuel Cycle Cost Model

The fuel cycle cost model was tested by Abbaspour (A4) and found to be in good agreement with more complex models such as MITCØST-II (C10). This model is based on a number of simplifications. The first is that restriction of the analysis to steady state reload batches is adequate. This assumption was found to have the largest impact on the results (accounting for 2/3 of the error for the PWR cases studied). Even so, the attendant error was only on the order of one percent (A4) on an absolute basis, and even less between consistently-evaluated alternatives. The second major approximation was that the revenue and depreciation accrue at a constant rate. (This version of the model is actually a modification proposed by Atefi (A2).) This assumption is quite good for fissile fuel assemblies or the core considered as a whole, but may not be appropriate for blanket assemblies, whose power level and plu-

tonium content vary widely over their in-core history. Finally, the version of the model used in the present work assumes the fuel is depreciated rather than expensed, which is generally considered appropriate for a recycle mode fuel cycle. The following abbreviated description of the model closely follows the development outlined by Atefi (A2).

The levelized fuel cycle cost, e (mills/kwhe), derived using the simple model approximations can be written in the form:

$$e = \frac{1}{E} \sum_i M_i C_i F_i G_i \quad (5.1)$$

where the index i , is over all fuel cycle transactions for a given batch and,

E is the total electricity generated by a batch of fuel (or blanket) during its residence in the reactor, (Mwhe)

M_i is the mass flow in stream i , (Kg)

C_i is the unit cost of the material in step i , (\$/Kg)

F_i is a "financial weighting factor", and for the case in which all fuel cycle expenses, and credits, are capitalized and depreciated is given by

$$F_i = \left[\frac{t_r}{1-\tau} \frac{(P/F, x, t_i)}{(P/\bar{A}, x, t_r)} - \frac{\tau}{1-\tau} \right] \quad (5.2)$$

τ is the tax rate

x is the discount rate, and is given by

$$x = (1 - \tau)r_b f_b + r_s f_s \quad (5.3)$$

r_b is the fraction of the total investment from bonds

r_s is the rate of return to the stockholders

f_s is the fraction of the total investment from stocks;

$$f_s + f_b = 1.0$$

t_i is the lag or lead time for transaction i , measured from the beginning of the batch irradiation, (yr)

t_r is the total residence time for a batch of fuel (or blanket) in the reactor, (yr)

$(P/F, x, t)$ is the present worth factor for transactions which occur t years from the reference time (the beginning of batch irradiation in the present calculations)

$(P/\bar{A}, x, t)$ is the present worth factor for a uniform cash flow of magnitude \bar{A} over the period t

G_i is the escalation factor, given by

$$G_i = \frac{(P/\bar{A}, y, t_r) \left[1 - \frac{(P/F, x, N \cdot t_c)}{(P/F, y_i, N \cdot t_c)} \right] \left[1 - \frac{(P/F, x, t_c)}{(P/F, y, t_c)} \right]}{(P/F, y_i, t_i) t_r \left[1 - \frac{(P/F, x, N \cdot t_c)}{(P/F, y, N \cdot t_c)} \right] \left[1 - \frac{(P/F, x, t_c)}{(P/F, y_i, t_c)} \right]}$$

(5.4)

y is the escalation rate allowed by the rate commission for the price of electricity

y_i is the escalation rate for transaction i

N is the total number of batches of fuel (or blanket) that will be irradiated throughout the life of the plant

t_c is the cycle duration, and is the time between successive refuelings of a batch of fuel (or blanket) assemblies. Assuming the escalation rate for the price of electricity is equal to the escalation rate for other transactions, i.e., $y_i = y$, G_i reduces to:

$$G_i = \frac{(P/\bar{A}, y, t_r)}{(P/F, y, t_i)t_r} \quad (5.5)$$

For the present work, both y and y_i will be assumed to be zero (i.e., no inflation). This means that $G_i = 1.0$. To be consistent, uninflated values for x are used. The effect of this simplification is addressed in Subsection 5.2.6.

From this simple model it is possible to calculate the mills/Kwhe for fuel, internal blanket, and radial blanket assemblies. The total fuel cycle cost is then the energy-weighted average of the contributions by the various types of assemblies in the reactor design under consideration.

5.2.2 Fuel Cycle Costs for the Heterogenous and Homogenous Designs using Nominal Cost Assumptions

The fuel cycle costs for the homogenous and heterogenous cores are presented in Tables 5.1 and 5.2, respectively, with each transaction itemized. The bottom line of each table

Table 5.1

Fuel Cycle Costs for the
Reference Homogenous Core

Homogenous Core Fuel Assemblies					
Transaction	Time (y _r)	C _i (\$/Kg)	M _i (Kg)	F _i	(CMF); X10 ⁶ (\$)
1. Plutonium Purchase	-1	27,000	1930.	1.25	65.1
2. Fabrication	-0.5	150,000*	132*	1.21	24.0
3. Reprocessing	4.0	500	28,700	0.85	12.2
4. Plutonium Credit	4.0	-27,000	2370.	0.85	<u>-54.4</u> 46.9

$$e_{\text{driver}} = \frac{46.9 \times 10^9 \text{ mills}}{7.35 \times 10^9 \text{ Kwhe}} = 6.38 \text{ mills/Kwhe}$$

Homogenous Core Blanket Assemblies					
Transaction	Time	C _i (\$/Kg)	M _i (Kg)	F _i	(CMF); X10 ⁶ (\$)
1. Fabrication	-0.5	30,000*	54*	1.34	2.17
2. Reprocessing	7.0	500	16,400	0.73	5.99
3. Plutonium Credit	7.0	-27,000	218	0.73	<u>-4.30</u> 3.86

$$e_{\text{radial blanket}} = \frac{3.86 \times 10^9 \text{ mills}}{0.341 \times 10^9 \text{ Kwhe}} = 11.3 \text{ mills/Kwhe}$$

$e_{\text{homogenous}} = (e \cdot \overline{PF})_{\text{driver}} + (e \cdot \overline{PF})_{\text{blanket}}$, where \overline{PF} is the lifetime-averaged power fraction for the region noted.

Table 5.1
(contd)

$$e_{\text{homogenous}} = 6.38(0.967) + 11.3(0.0334) = 6.55 \text{ mills/Kwhe}$$

* On a per assembly basis rather than a per Kg basis

Table 5.2

Fuel Cycle Costs for the
Reference Heterogenous Core

Heterogenous Core Driver Assemblies

Transaction	Time (y _r)	C _i (\$/Kg)	M _i (Kg)	F _i	(CMF); x10 ⁶ (\$)
1. Plutonium Purchase	-1	27,000	2230.	1.25	75.3
2. Fabrication	-0.5	150,000*	120*	1.21	21.8
3. Reprocessing	4.0	500	19,200	0.85	8.2
4. Plutonium Credit	4.0	-27,000	2130	0.85	<u>-48.9</u> 56.4

$$e_{\text{driver}} = \frac{56.4 \times 10^9 \text{ mills}}{6.33 \times 10^9 \text{ Kwhe}} = 8.91 \text{ mills/Kwhe}$$

Internal Blanket Assemblies

Transaction	Time (y _r)	C _i (\$/Kg)	M _i (Kg)	F _i	(CMF); x10 ⁶ (\$)
1. Fabrication	-0.5	30,000*	66*	1.16	2.30
2. Reprocessing	3.0	500	16,900	0.88	7.44
3. Plutonium Credit	3.0	-27,000	415	0.88	<u>-9.86</u> -0.12

$$e_{\text{internal blanket}} = \frac{-0.12 \times 10^9 \text{ mills}}{0.855 \times 10^9 \text{ Kwhe}} = -0.14 \text{ mills/Kwhe}$$

Table 5.2
(contd)

Heterogeneous Core Radial Blanket Assemblies

Transaction	Time (Y _r)	C _i (\$/Kg)	M _i (Kg)	F _i	(CMF); X10 ⁶ (\$)
1. Fabrication	-0.5	30,000*	42*	1.34	1.69
2. Reprocessing	7.0	500	11,100	0.73	4.05
3. Plutonium Credit	7.0	-27,000	227	0.73	$\frac{-4.47}{1.27}$

$$e_{\text{radial blanket}} = \frac{1.27 \times 10^9 \text{ mills}}{0.389 \times 10^9 \text{ Kwhe}} = 3.26 \text{ mills/Kwhe}$$

$$e_{\text{heterogeneous}} = (e * \overline{\text{PF}})_{\text{driver}} + (e * \overline{\text{PF}})_{\text{internal blanket}} + (e * \overline{\text{PF}})_{\text{radial blanket}}$$

where $\overline{\text{PF}}$ is the lifetime-averaged power fraction for the region noted.

$$e_{\text{heterogeneous core}} = (8.91)(0.830) + (-0.14)(0.116) + (3.26)(0.054) = 7.56 \text{ mills/Kwhe}$$

* On a per assembly basis rather than a per Kg basis.

shows the net fuel cycle cost for each core design. As can be seen from these tables, the fuel cycle costs are 6.55 mills/Kwhe and 7.56 mills/Kwhe for the homogenous and heterogenous designs, respectively. The mass flows used for this analysis come from Tables 3.12 and 4.5, but the lifetime-averaged power fractions had not been previously reported. The input to these calculations included: mass flow values which came from the neutronic analysis; a set of assumed prices for the unit costs of each item; and the time value of money. Each one of these assumed values will be discussed in the subsection which follows.

5.2.3. Sensitivity to Plutonium Value

The plutonium value used for the reference cost analysis (Subsection 5.2.2.) was \$27 per gram. This value comes from the indifference value of fissile plutonium in light water reactors for a yellowcake price of \$40 per pound and \$100 per kilogram of separative work (for more detail see page 191 of reference A2). Values from zero to \$100 per gram have been proposed by some economists (A2,S6). In fact, Saragossi (S6) maintains that the value of plutonium should depend on the reactor design since it affects the scarcity of the limited resource of plutonium. To show the impact of the price of plutonium on the heterogenous versus homogenous decision, Figure 5.1 is presented, in which the fuel cycle cost for both core designs is plotted as a function of the plutonium value (everything else is maintained at the nominal values). As can be

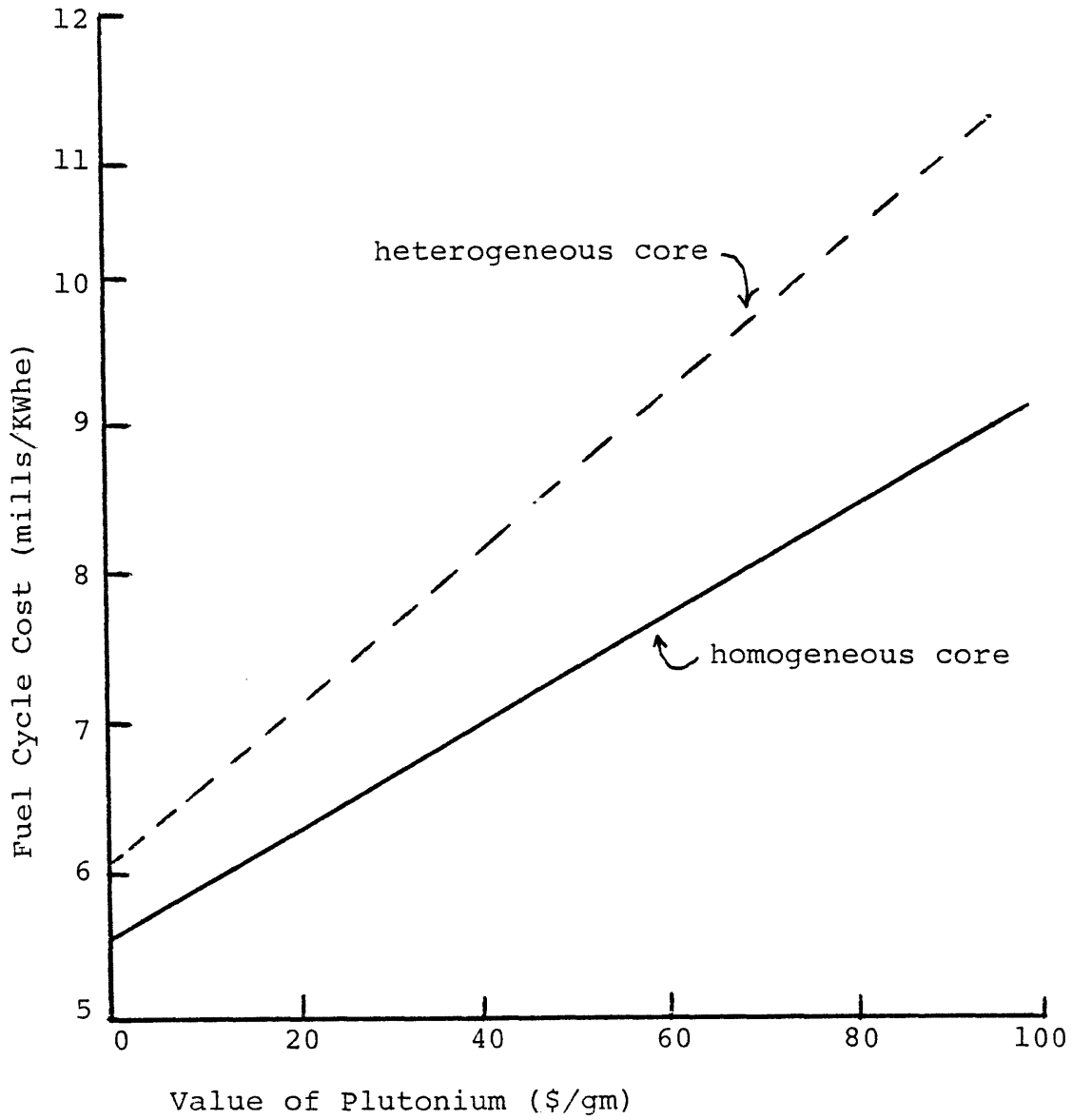


Fig. 5.1 Sensitivity of fuel cycle cost to the value of plutonium.

seen from this figure, the heterogeneous core's fuel cycle cost is more sensitive to the value of plutonium, and as plutonium value increases the cost penalty of heterogeneity increases. Even if the value of plutonium were zero, however, the homogeneous core would still be cheaper, by almost 10%.

5.2.4. Sensitivity to Fabrication Costs

The fuel fabrication costs used for the nominal analysis were \$150,000 per driver fuel assembly and \$30,000 per blanket assembly. These values come from a fabrication cost analysis performed in CALIØP, which depends on the number of pellets per assembly, the amount of heavy metal, the extent of clad roughening needed, and the length of the rod. Under common practice, a cost per kilogram would be used. The \$150,000 per driver fuel assembly translates into \$691/Kg and \$938/Kg for the homogeneous and heterogeneous cores, respectively. The key reason the unit cost of the heterogeneous fuel is higher lies in its use of a larger number of smaller diameter pellets.

These values for fabrication cost are high compared to the values reported in the NASAP report of \$580 to \$650 per kilogram for fast breeder reactors (D6), but since GCFRs require clad roughening and use venting, the higher costs are plausible. To show the sensitivity of fuel cycle costs to the driver assembly fabrication cost, Figure 5.2 is presented. From a careful inspection of the figure, it can be seen that the heterogeneous core is slightly less sensitive to the driver fuel fabrication cost. In fact, at the absurdly high price of

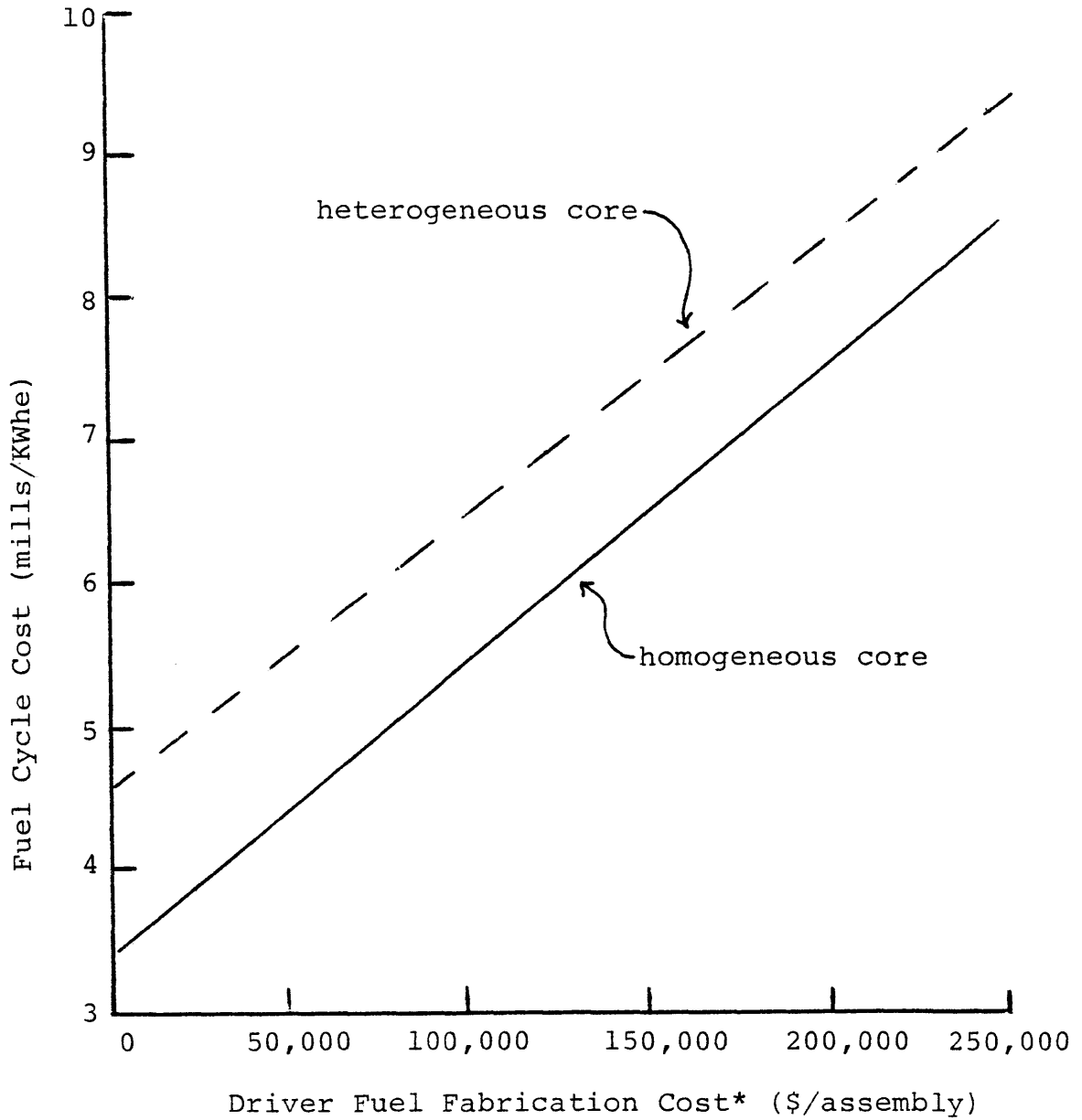


Fig. 5.2 Sensitivity of the fuel cycle cost to the driver fuel fabrication cost.

*These values can be converted to \$/kg by dividing by 217 and 160 for the homogeneous and heterogeneous cores, respectively.

\$663,000 per assembly the heterogeneous and homogeneous cores have the same fuel cycle costs; but, until that point the homogeneous core is favored.

So far the discussion has been centered on the driver fuel fabrication, but the fuel cycle costs are also somewhat sensitive to the blanket fabrication costs. The \$30,000 per blanket assembly converts to \$99/Kg and \$113/Kg for the homogeneous and heterogeneous cores, respectively. These values are lower than the \$140/Kg value reported in NASAP (D6). Figure 5.3 shows the sensitivity of the fuel cycle cost to the blanket fabrication cost. As can be seen from these curves the heterogeneous core is more sensitive to blanket fabrication costs. However, even if a zero fabrication cost was assumed, the heterogeneous core would always yield higher fuel cycle costs.

The discussion in this subsection so far has been based on the same cost per assembly fabricated for both the homogeneous and heterogeneous cores. This corresponds to a different cost per kilogram fabricated. It is believed that the latter difference is justifiable, but it is of some interest to recalculate the difference in the fuel cycle costs if a constant cost per kilogram were used. Using the cost per kilogram of the homogeneous core (\$691/Kg and \$99/Kg for the driver and blanket assemblies, respectively) the fuel cycle cost of the heterogeneous core is lowered to 6.73 mills/Kwhe, or only 0.18 mills (3%) more than the fuel cycle cost of the homogeneous core.

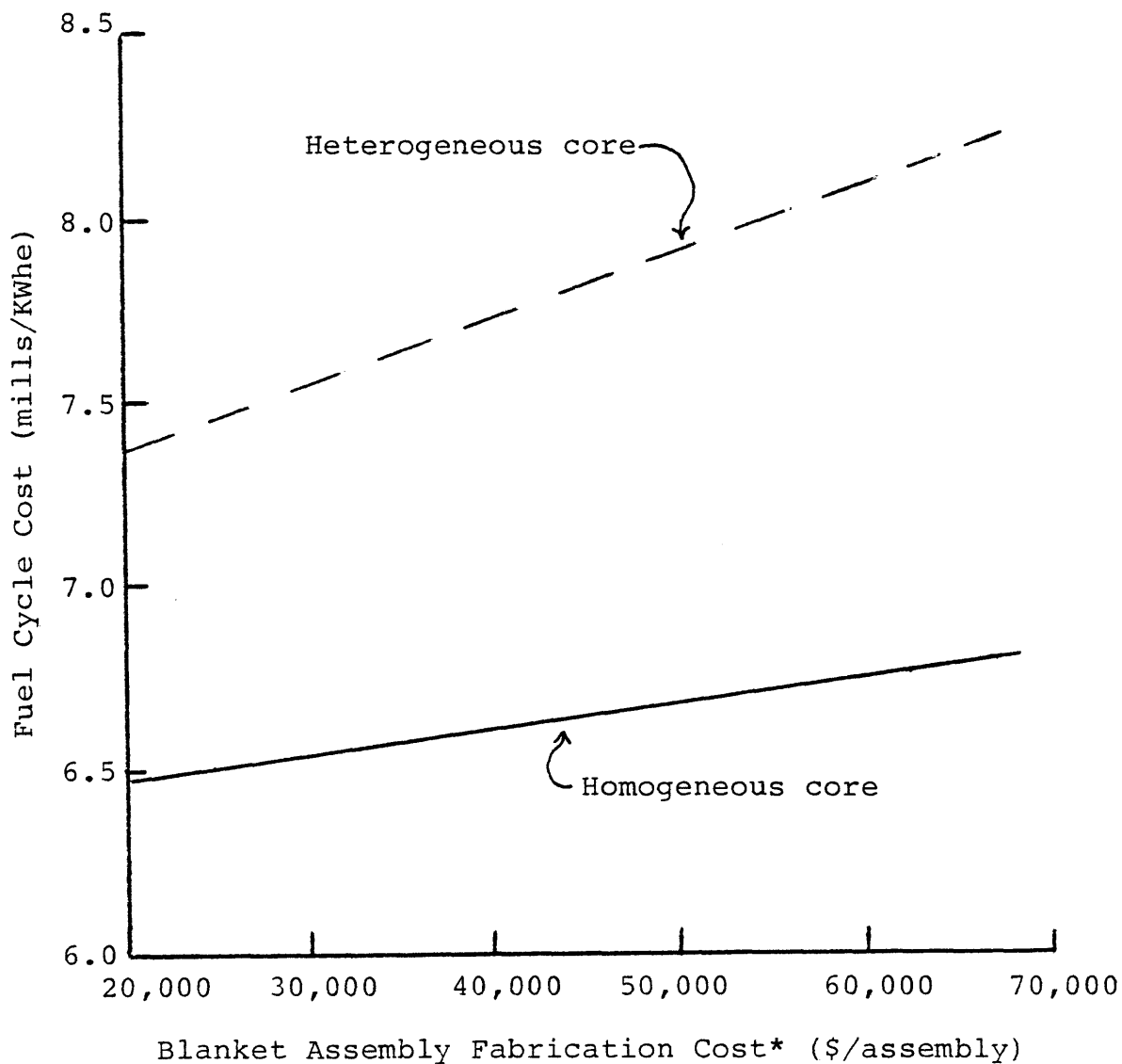


Fig. 5.3 Sensitivity of the fuel cycle cost to the blanket fabrication cost.

*These values can be converted to \$/kg by dividing by 304 and 265 for the homogeneous and heterogeneous cores, respectively.

A final note is that shipping of the freshly fabricated fuel to the reactor is relatively inexpensive, and it is assumed that this is included in the fabrication costs.

5.2.5. Sensitivity to Reprocessing Costs

For the present work the spent fuel shipping, reprocessing and waste shipping and storage costs are combined under one transaction labelled "reprocessing" costs. A value of \$500 per kilogram was used as the reference price for this transaction. No distinction was made between fuel and blanket assembly reprocessing costs for this work. The NASAP value (D6) for this composite transaction (reprocessing, etc.) ranges from \$565/Kg to \$665/Kg for LMFBR fuel assemblies and \$485/Kg to \$605/Kg for LMFBR blanket assemblies. Due to the absence of sodium, it is believed that the GCFR values should be slightly less; therefore, the rounded figure of \$500/Kg was selected. Figure 5.4 shows the sensitivity of the fuel cycle cost to the reprocessing cost. The heterogeneous core is more sensitive to the reprocessing costs than the homogeneous core; yet even at zero reprocessing charges the homogeneous core has the lower fuel cycle cost.

5.2.6. Sensitivity to the Time Value of Money

For the present work a discount rate of 4% (deflated) was used. Using a deflated discount rate avoids estimating the inflation rate into the future when a commercial sized GCFR will be built. The discount rate using NASAP (D6) values for bond

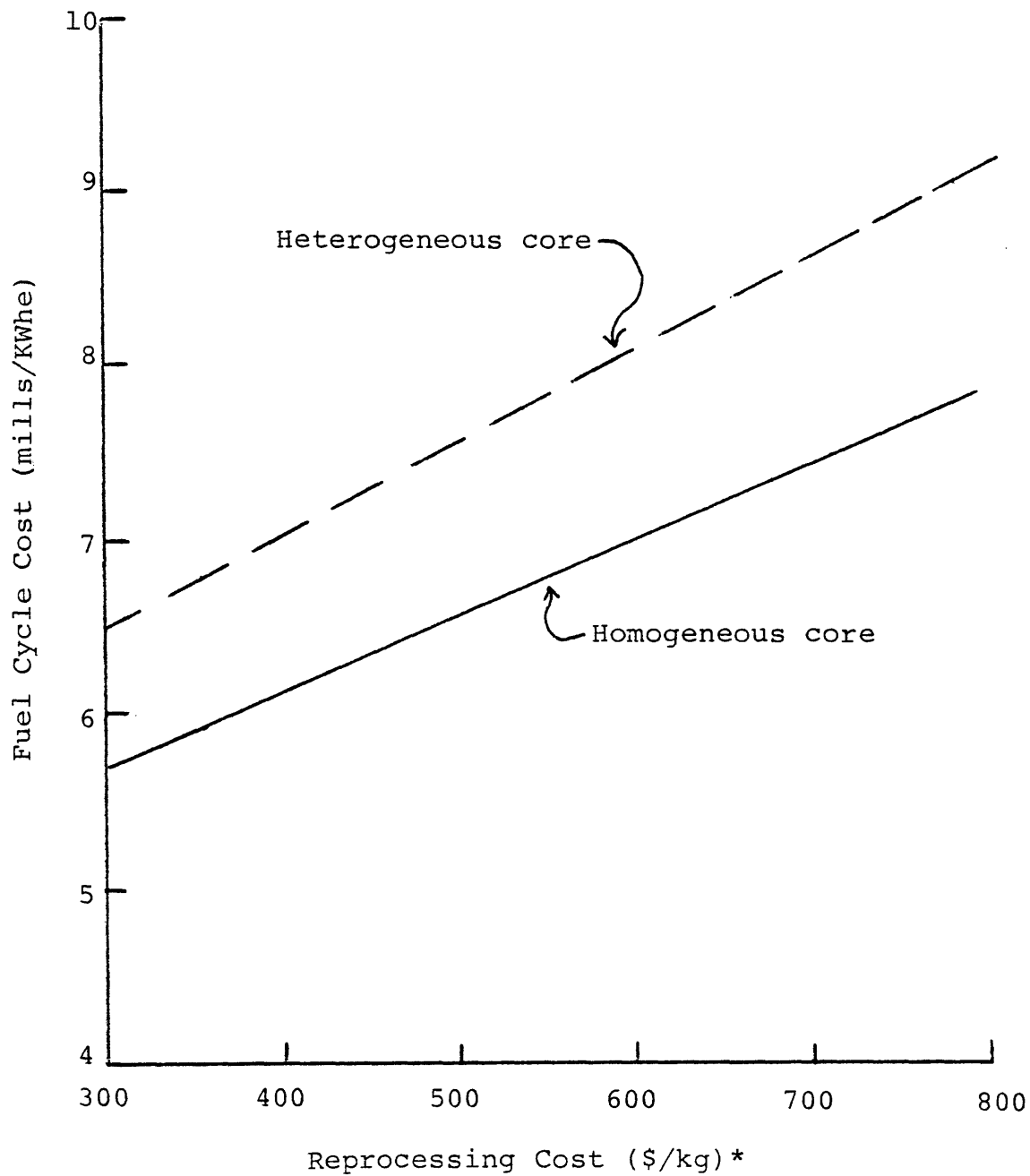


Fig. 5.4 Sensitivity of the fuel cycle cost to the reprocessing cost.*

*This includes spent fuel shipping, reprocessing, waste shipping, and waste storage.

and stock interest rates and the bond fraction would be 3.8%. (For the present work, as well as for the NASAP work, a tax rate of 50% was used.) The variation in the fuel cycle cost as a function of the discount rate is shown in Figure 5.5. As can be seen from this figure, the heterogeneous and homogeneous cores exhibit about the same sensitivity to the discount rate but the heterogeneous core is slightly more affected. Once again the homogeneous core's fuel cycle costs are less for all values of the parameter of interest.

5.2.7. Fuel Cycle Cost Summary

The fuel cycle cost for the homogeneous core was found to be 6.55 mills/Kwhe. This was 1.01 mill/Kwhe less than the value determined for the heterogeneous core, or 13% less. The sensitivity of this conclusion to the assumed economic parameters was investigated and it was found that the heterogeneous core had a higher fuel cycle cost in all cases where only one parameter at a time was varied over a wide range. This one mill/Kwhe margin translates into a seven million dollar saving per year if the homogeneous core is used.

The reader should be reminded that if the traditional cost per kilogram fabricated rather than the cost per assembly fabricated were kept constant the difference in the fuel cycle cost is decreased to 0.18 mills/Kwhe, which is only 3% of the fuel cycle costs of the homogeneous core. However, the homogeneous core still has the lower fuel cycle cost.

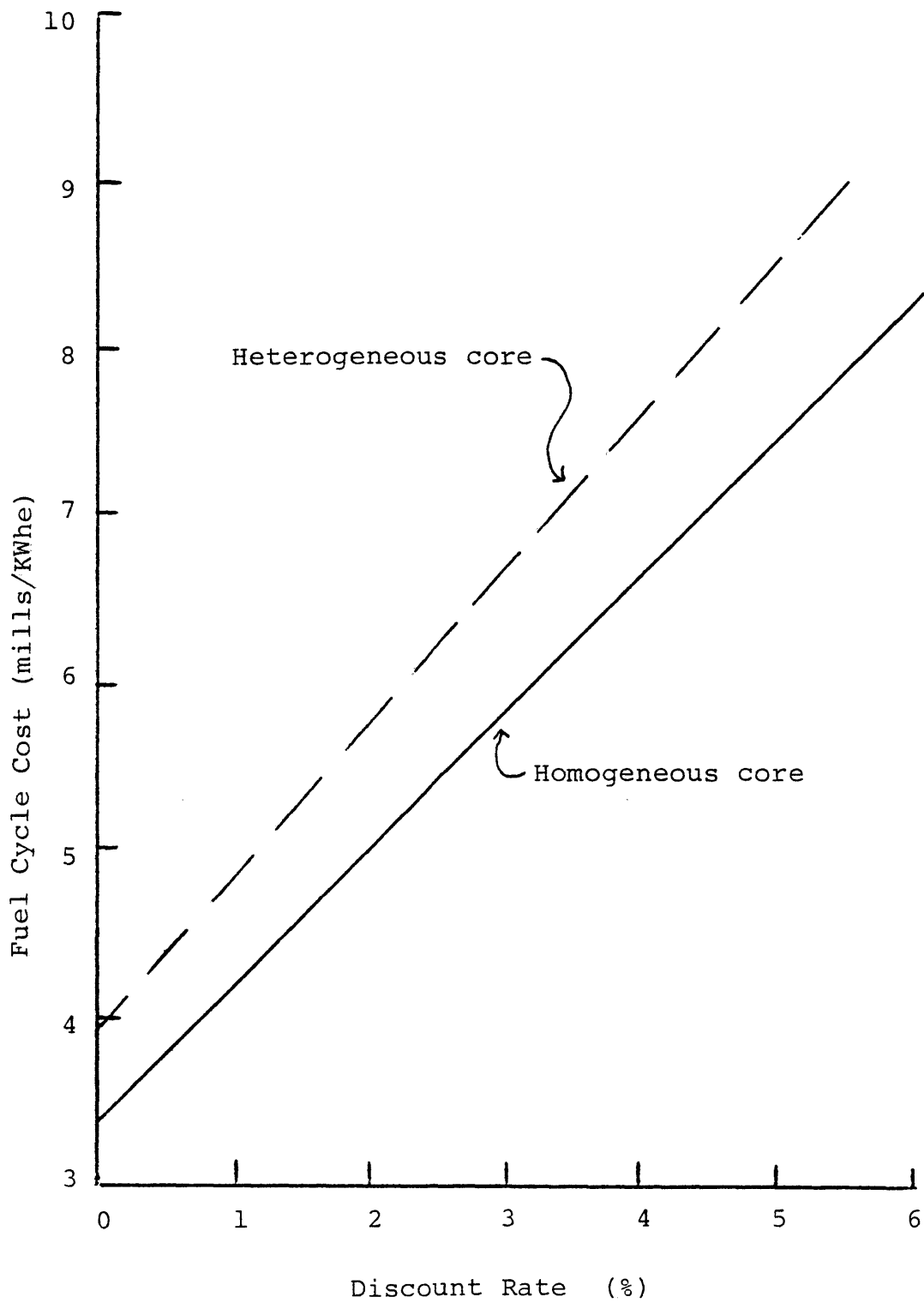


Fig. 5.5 Sensitivity of the fuel cycle cost to the discount rate.

5.3 Capital Cost Differences

The use of a heterogeneous core design not only changes the fuel cycle costs, but also impacts on the capital cost of the GCFR. The key capital cost effects are due to a larger core diameter and a lower mixed-mean core outlet temperature. The outer diameter of the radial blanket of the heterogeneous core is only 9.3 cm larger than that of the homogeneous core; however, in order that the flux at the core barrel be the same, another 14 cm of shielding is needed, which increases the diametrical difference to roughly 23 cm. Using estimates from General Atomic, this would increase the capital cost of the heterogeneous core about \$1.8 million over that for the homogeneous core. (See Section 3.3.5. of Chapter 3.)

The core diameter effect is small compared to the impact of a lower core outlet temperature. As calculated in Section 4.4.2. of Chapter 4, the mixed-mean outlet temperature of the heterogeneous core will be 21°C to 39°C less than that for the homogeneous core. If the 21°C drop in core outlet temperature is used it implies a more difficult refueling operation since 66 internal blanket assemblies would have to be reorificed each refueling. The 39°C drop requires no reorificing. These changes in the core outlet temperature imply a change in the circulator power as well. The circulator power would increase 8.3% for the 21°C drop in outlet temperature and 15% for the 39°C change. The capital cost difference resulting from this change in circulator power and the loss in the outlet tempera-

ture is substantial. Using Eq. 3.7 from Chapter 3, the effect may be as high as \$60 million; however, it is believed that cost estimates from the referenced prescription for an effect this large are no longer valid, since a complete system redesign could probably lower this cost impact. A ceiling on the penalty due to outlet temperature degradation could also be established by the installation of thermostatic or continuously variable orificing.

Although it is difficult and beyond the scope of the present work to establish the actual capital cost differences due to a 15% drop in the temperature rise across the core and a 5% increase in the core diameter, they can confidently be said to be large. If the total is actually near the \$60 million suggested by the values extrapolated from General Atomic's relation for small changes in ΔT , circulator power, and core cavity diameter, then an additional penalty of about 0.7 mill/Kwhe would result. This makes the total cost penalty predicted for the heterogeneous core 1.7 mills/KWhe.

5.4 Summary

The fuel cycle costs of the reference homogeneous and heterogeneous cores have been compared. The heterogeneous core design incurred a 13% penalty in fuel cycle costs. Varying the fabrication cost assumption (from a per fuel assembly basis to a per kilogram basis) can reduce this to a 3% penalty. The sensitivity of these results to all the cost assumptions was investigated, and it was found to be quite difficult to find

a plausible set of input data for which the heterogeneous core would have a lower fuel cycle cost.

The capital cost differences caused by the adoption of a heterogeneous core in place of a homogeneous core were also considered. The heterogeneous core could require up to 15% more circulator power due to the lower ΔT across the core, which results from the overcooling of the internal blanket assemblies at the start of life. An effect this large challenges the extrapolatability of the simple cost sensitivity relations provided by General Atomic, but for lack of better information these prescriptions were used and the heterogeneous core was found to incur a 60 million dollar penalty in capital costs. This converts to roughly 0.7 mill/Kwhe, making the total cost penalty 1.7 mills/Kwhe. This produces a new effective fuel cycle cost for the heterogeneous core which is 25% higher than that for the homogeneous core.

CHAPTER 6

SUMMARY, CONCLUSIONS, AND RECOMMENDATIONS

6.1 Introduction and Background

In the mid 1970's reactor designers began to pay increased attention to the use of internal blanket assemblies in fast breeder reactors. Initial studies identified impressively large increases in breeding ratio, and reductions in fissile inventory doubling times (M1). Subsequent analyses by many investigators have yielded inconclusive results: a review of 22 major studies carried out as part of the current research showed that only half concurred that the use of internal blankets improved the doubling time. Before it was resolved whether internal blankets improved or degraded the doubling time the LMFBR design community decided to accept the new designs to improve the sodium void worth. In fact, the CRBR reference design was changed to a heterogeneous core (one with internal blankets) in 1979 (C11). Many researchers have pointed out that some of the purported advantages of either heterogeneous or homogeneous designs have been due to inconsistent optimization (C2). It has been a major objective of the present work to resolve the controversy over doubling time improvements through thorough and consistent optimization of heterogeneous and

homogeneous cores designed to power the same basic gas cooled fast reactor (GCFR).

The debate over improved doubling time is important to GCFRs since there is clearly no sodium void worth advantage in a gas cooled reactor. Prior to the present work only one other study had been done on a GCFR with internal blankets, and it included no attempt at optimization (W1). The present work therefore centered on determining if the insertion of full length internal blanket assemblies would have advantages in a GCFR. In the present work, as with all recent LMFBR studies, attention is focused on so-called "radial" heterogeneity in which full length blanket assemblies, akin to those of the radial blankets, are interspersed amid fissile-fueled driver assemblies in the core proper. We have not considered axially heterogeneous cores, such as the internal axial "parfait" blankets examined by Ducat (D1).

A considerable amount of the present work was devoted to developing a consistent method for optimization of the two core designs. The next section will provide an overview of the procedures followed in the present work.

6.2 Overview of Procedure

To carry out a useful comparison of heterogeneous and homogeneous designs, a number of steps were required: establishing a set of given conditions describing the environment

sustaining the cores, determining the controlling design constraints, identifying the independent variables available to the designer, and selecting the objective functions/criteria governing the optimization process. The strategy employed is flow-charted in Fig. 6.1, and described in the paragraphs which follow.

First, the parameters characterizing a representative commercial-sized GCFR were established. Some of the salient features are noted in Table 6.1. Associated with this GCFR were a set of constraints used to arrive at the design of the fuel assemblies and the selection of primary loop thermal/hydraulic conditions. These constraints were evaluated to assess their impact on the heterogeneous/homogeneous design comparison. The selection of some of the constraints is very important. In the CRBR design effort, for example, one constraint was to keep to the same fuel pin diameter as the FFTF. This constraint created favorable conditions for the introduction of a heterogeneous core. Recent GCFR studies (M3) have constrained the circulator power and primary system pressure. These constraints favor large diameter fuel pins, which concedes the homogeneous core an advantage. Although there are many constraints imposed during the design process, three dominate with regard to this study; they are:

- 1) The peak linear heat generation rate is limited to 15 KW/ft,

Fig. 6.1
Flow Chart for the Comparison
of Heterogeneous and Homogeneous Cores

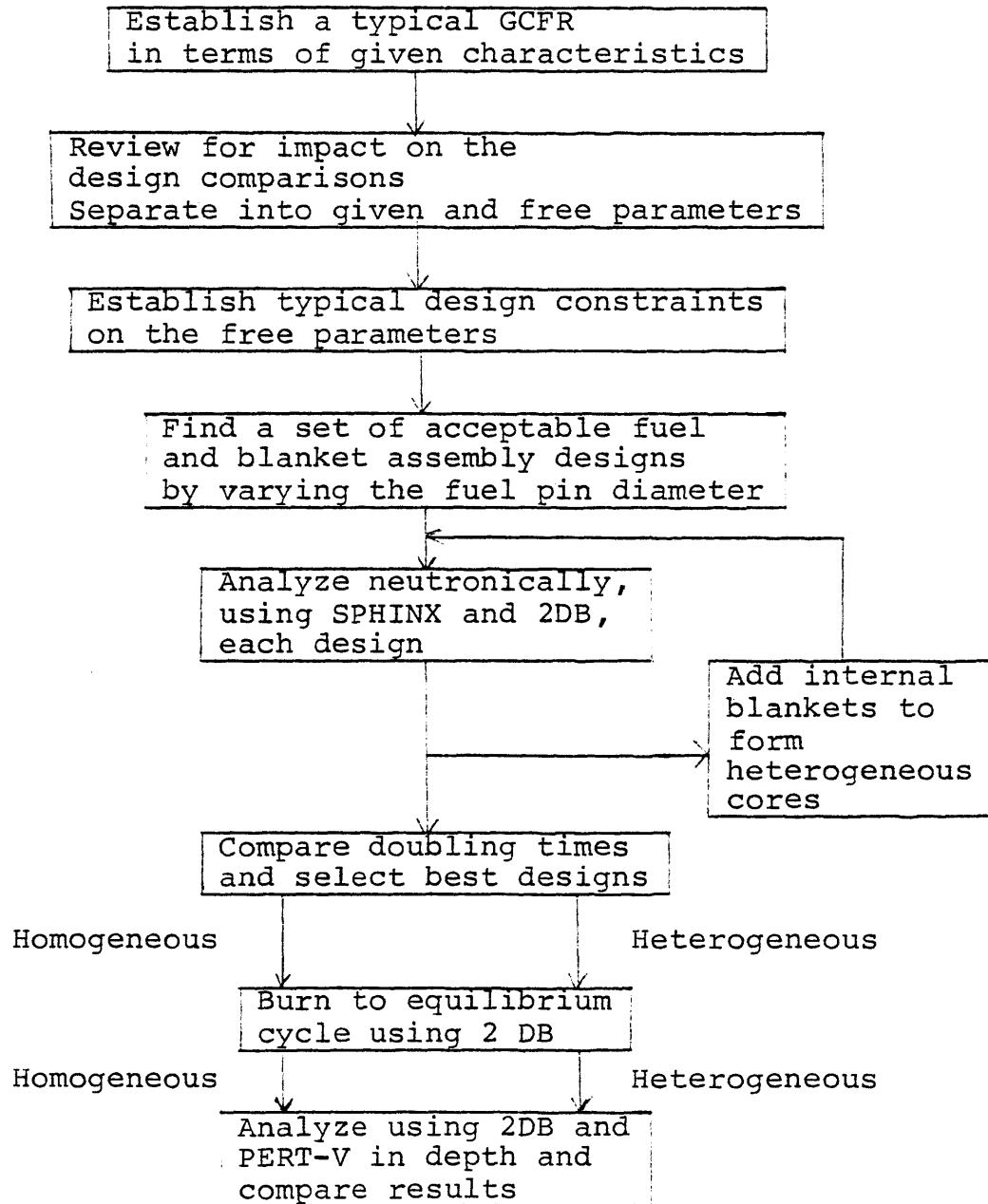


Table 6.1

Some Important Characteristics of the GCFR Adopted
as "Given Conditions" for the Present Work

Reactor Power (MW_e)	1200
Primary System Pressure (psi)	1740
Core Inlet Temperature ($^{\circ}C$)	302
Pins per Driver Fuel Assembly	271
Pins per Radial Blanket Assembly	91
Pins per Internal Blanket Assembly	127
Structural Material	HT-9
Axial Blanket Length (cm)	60
Circulator Power (hp) (per loop for each of six loops)	31,500 to 39,800
Approximate Active Core Length (cm)	106
Cycle Length (full-power-days)	254

- 2) The peak clad temperature must not exceed 750°C,
and
- 3) A peak unrorificed pressure drop of 63 psi is allowed
across an assembly (inlet to outlet)

It is these constraints that establish the fuel pin pitch and thereby the fuel volume fraction.

With the typical GCFR environment and constraints established, a series of fuel and blanket assembly designs meeting those constraints were developed. The independent variable in determining these designs was the fuel pin diameter. The dependent variables include the assembly volume, fuel pin pitch and core ΔT . With the designs established, they were neutronically analyzed in a homogeneous arrangement to determine the optimum homogeneous design. The optimum heterogeneous design was determined by adding an increasing number of internal blanket assemblies to each homogeneous design and identifying the best-performing of all the heterogeneous designs. The identification of the optimum core design required the selection of a figure of merit. Doubling time was selected since it was the least ambiguous and subsumes other figures of merit. Just the same the energy growth potential, fuel cycle cost, and capital-cost-adjusted fuel cycle costs were analyzed.

The optimum homogeneous design had a fuel pin diameter of 8 mm. The optimum "heterogeneous" design in principle

would include no internal blankets at all (i.e.: a homogeneous design is to be preferred). Rather than stop the analysis at this point a heterogeneous core with the same fuel volume fraction as the optimum homogeneous core was selected. This "reference" heterogeneous core had a fuel pin diameter of 7 mm and roughly one quarter of the assemblies in the active core region were internal blanket assemblies.

With the reference cores selected, a more detailed analysis of each was performed. This included a six cycle burnup analysis to determine their equilibrium conditions, followed by a detailed analysis of:

- 1) Doubling times,
- 2) Mass flow rates,
- 3) Power distributions,
- 4) Flux, fluence, and burnup,
- 5) β_{eff} and delayed neutron parameters,
- 6) Control rod worth and requirements,
- 7) Doppler coefficients, and
- 8) Material worths

All of these data were used to evaluate the true effects of heterogeneity.

Based on this analysis recommendations pertinent to both the GCFR and the LMFBR follow. But, first some of the more salient observations which came to light during the analysis are worthy of note.

6.3 Salient Observations

Following the procedure just described not only provided

a self-consistent means for arriving at preferred core designs, but also developed a catalog of case study data which provided insight into a number of various important fast breeder reactor design issues. The subsections which follow summarize these findings.

6.3.1 Doubling Time Dependence on Fuel Volume Fraction

In optimizing the homogeneous core an optimum fuel volume fraction (and its corresponding fuel pin diameter) was determined. To show the key role played by the constraints, two key constraints were removed, one at a time. First, it was observed that larger assembly volumes were needed for higher fuel volume fractions. This would not be so if a larger pressure drop could be tolerated. Hence, the pressure drop constraint was removed and all fuel volume fractions accommodated in the same assembly volume as the smallest design studied (that having a 6 mm fuel pin diameter). Figure 6.2 shows the constrained design doubling times as a function of fuel volume fraction along with the doubling times if the pressure drop constraint were removed. As can be seen from this curve, the increase in doubling time with increasing volume fraction was totally removed. Second, it was observed that for small pin diameters, where the doubling time was decreasing with increasing volume fraction the cycle Δk was also decreasing. Where there was little dependence of the doubling time on the fuel volume fraction, the cycle Δk

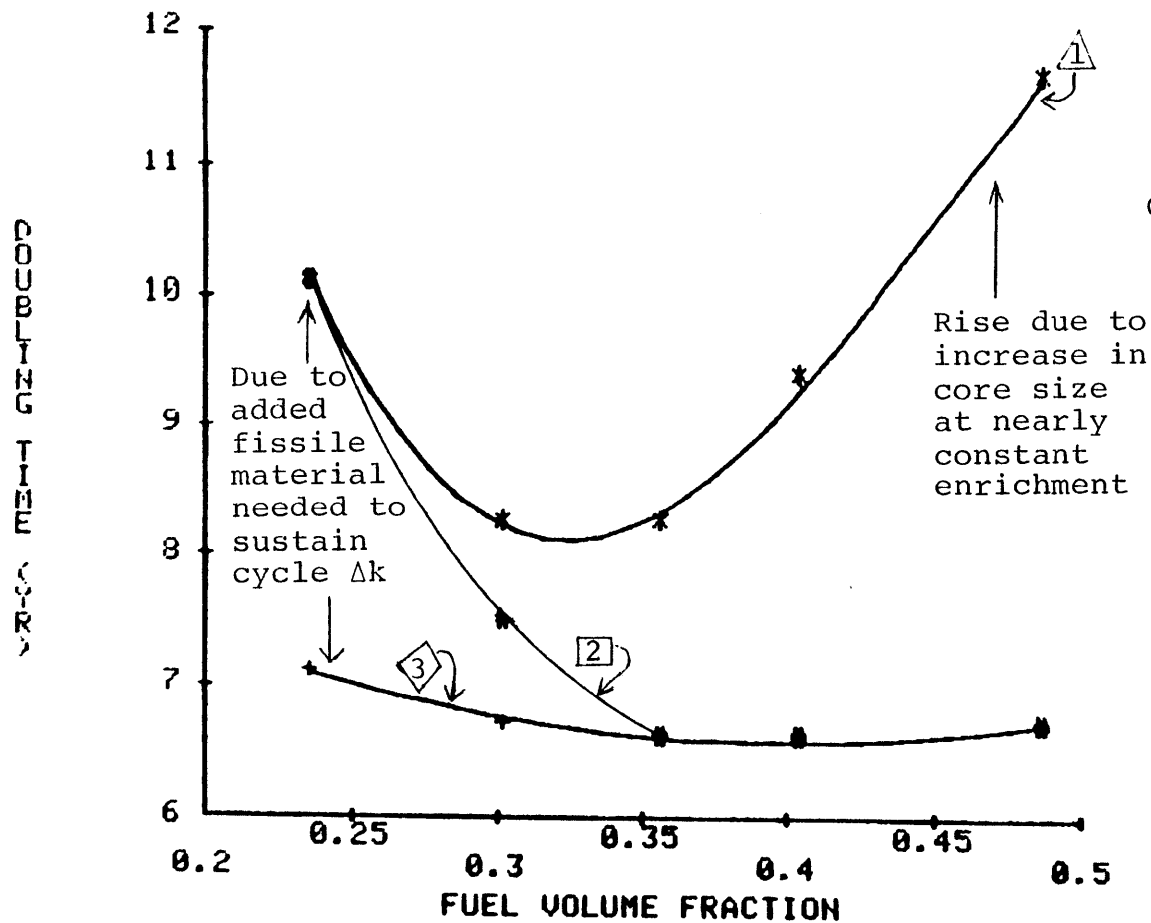


Fig. 6.2 Doubling Time as a Function of Fuel Volume Fraction Under Various Constraints

- Curve \triangle Thermal-hydraulic constraints (15 kw/ft, 750°C peak clad temperature, 63.2 psi pressure drop)
- \square Only constrained to be at least critical at the beginning and end of cycle
- \diamond Only constrained to be critical at the beginning of cycle

was zero or increasing. Thus it was decided to reanalyze the first two assembly designs, removing the criticality constraint at the end of cycle (actually replacing it by a beginning-of-cycle criticality requirement). The doubling times with this constraint removed (and for constant volume) are plotted as the third curve in Fig. 6.2. Figure 6.2 demonstrates that the existence of an optimum fuel volume fraction is due to the competing effects of decreasing excess reactivity, and increasing fissile inventory (due to the increase in assembly volume) as the fuel volume fraction increases.

Before discussing heterogeneous cores the effect of increasing the assembly volume should be addressed more carefully. For curve 3 of Fig. 6.2 the fissile inventory per unit of rated power is increasing, but so is the breeding gain. These two variables grow at compensating rates, making the doubling time independent of the fuel volume fraction (Recall that the doubling time is proportional to the specific inventory divided by the breeding gain.) The selection of a fuel volume fraction determines the critical enrichment and thereby the fissile inventory. As the fuel volume fraction increases the critical enrichment decreases, which improves the breeding gain. For the constant assembly (hence core) volume cases (curve 3) the increasing inventory and breeding gain compensate. When the volume of the assembly (hence core) is permitted to increase, the critical enrichment for a given fuel volume fraction does not change, therefore,

neither does the breeding gain; only the fissile inventory (enrichment times volume) increases. It is this effect that causes an increase in doubling time with increasing assembly volume. It is also this effect which guarantees that the performance of the homogeneous core will be superior to that of the heterogeneous core.

6.3.2 Method for Heterogeneous Core Optimization

ANL has pointed out that the dominant parameter in fast reactor optimization is the effective fuel volume fraction (C2). (The effective fuel volume fraction is defined as the volume weighted fuel volume fraction of the assemblies in the active core region; i.e., within the I.D. of the radial blanket). This is because the neutron mean free path in fast reactors is so long that average compositions rather than local fine structure determines the critical enrichment. This enrichment in turn defines the fissile inventory and breeding gain, and through them the doubling time. The work carried out by Sheaffer (S7) shows the strong linkage between composition and spectrum-averaged one-group cross sections which supports these assertions. A design procedure consistent with this observation is straightforward:

- 1) Establish a set of acceptable driver fuel assembly designs having a range of fuel volume fractions
- 2) Establish an acceptable blanket assembly design with an appropriately larger fuel volume fraction (0.5 for the present work, which represents a practical upper limit for the GCFR).

- 3) Neutronically analyze the homogeneous core arrangement for each assembly design. For the present work the homogeneous arrangement consisted of 384 fuel assemblies each with about 106 cm of active fuel. (The active fuel length is actually determined by the 15 kW/ft limit, the peak-to-average power, which varies, and the total number of fuel pins).
- 4) For each acceptable driver fuel assembly design progressively add internal blanket assemblies, thereby increasing the effective fuel volume fraction.
- 5) For each combination perform plutonium concentration searches to yield a critical configuration at the end of cycle. From these cycle one calculations determine the doubling time.
- 6) The optimum heterogeneous design is the design which has the minimum doubling time.

There are two major assumptions underlying this approach. The first is that the arrangement of the internal blankets does not effect the doubling time. To test this assertion six different arrangements of the optimum heterogeneous core were investigated. The doubling time difference among all six cases was less than 0.1 year. The second assumption is that the first cycle (i.e., a clean core analysis) would accurately forecast the best configuration under equilibrium conditions. For the present work both the optimum heterogenous and homogeneous cores were analyzed cycle-by-cycle through their approach to equilibrium. The doubling times of the equilibrium cores were longer, but by essentially the same increment. This increment was due to the buildup of fission

products and added inventory in the axial and radial blankets. The assumption that first cycle analysis is acceptable for optimization studies has only been shown valid for two designs of the same fuel volume fraction; further tests are expensive and are left for future work. However any variation in the equilibrium doubling time increment would only shift the optimum design point slightly and not alter the ranking between the heterogeneous and homogeneous cores being compared.

Although this optimization procedure may appear to be complex, the number of calculations required can be reduced once it is noticed that the optimum effective fuel volume fraction for the heterogeneous core is always less than that for the homogeneous core. With experience it should be possible to estimate the optimum effective fuel volume fraction of a heterogeneous core once the optimum homogeneous core value is known. This implies that the optimization procedure could require very few analyses in practice.

The optimization procedure described in this section may in fact never be used again for a GCFR, since the optimum design is a homogeneous core; however, it may prove useful in minimizing the doubling time loss associated with low sodium void worth LMFBRs. This application is left for future work.

6.3.3 Qualitative Explanation for Doubling Time Differences

Figure 6.3 shows that the best heterogeneous core always has a longer doubling time than the best homogeneous core.

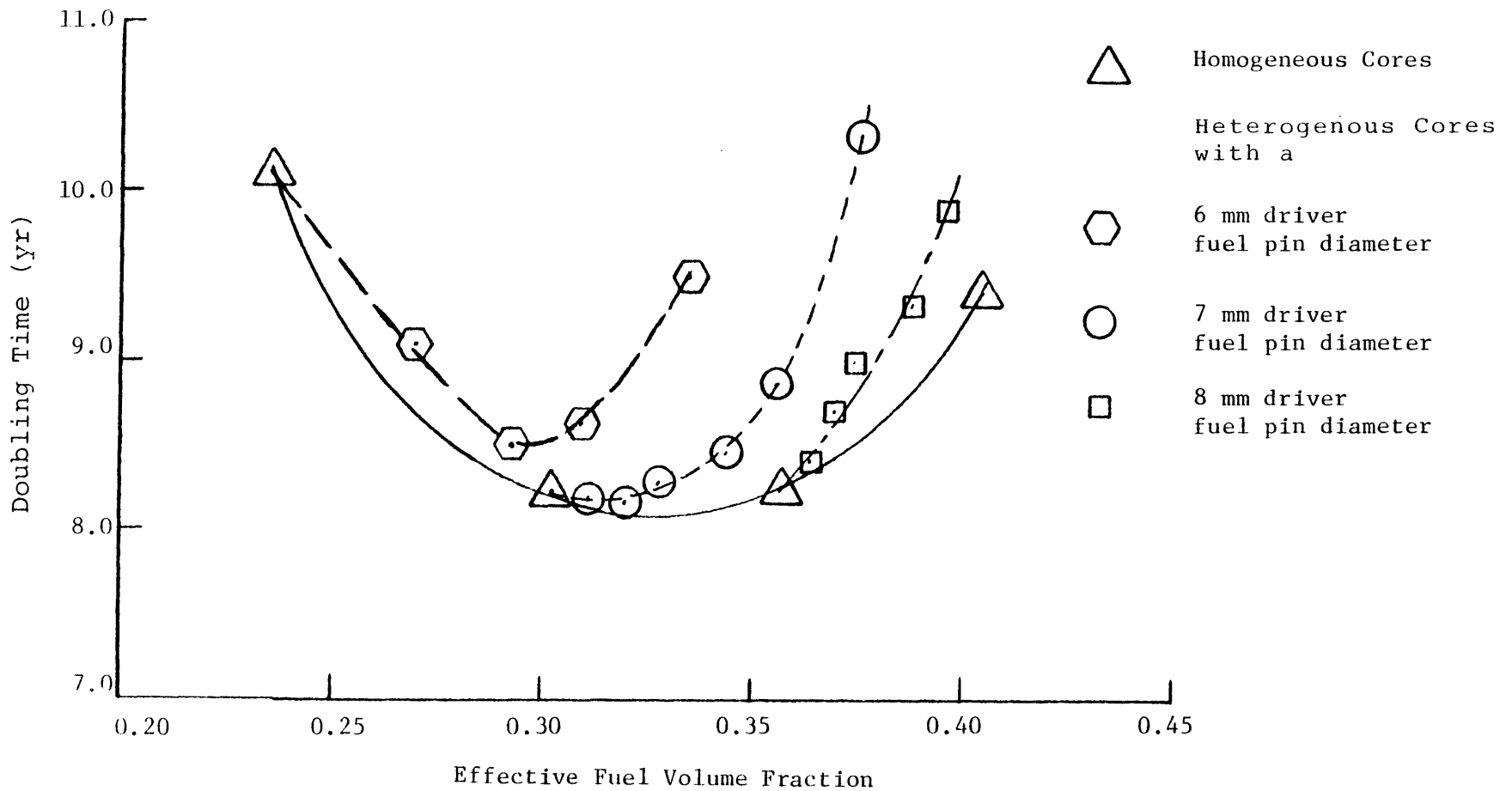


Fig. 6.3 Doubling Time as a Function of the Effective Fuel Volume Fraction for Various Homogeneous and Heterogeneous Designs

The evaluation of the equilibrium cores of the heterogeneous and homogeneous designs selected in the present research confirms this. The reason for this was foreshadowed by the analysis of the doubling time dependence on fuel volume fraction for the homogeneous core. The complete logic follows:

- 1) Specification of the core-average fuel volume fraction establishes an enrichment, which is essentially independent of local micro or macro heterogeneity.
- 2) The core-averaged enrichment determines the breeding ratio.
- 3) The core volume and core-averaged enrichment yield the fissile inventory.
- 4) Since the power density of an internal blanket is low, the core volume to produce the same power is higher for a heterogeneous core than for a homogeneous core.
- 5) Because the core volume of the heterogeneous core is larger and the core-averaged enrichment is essentially the same, the fissile inventory is larger than for the homogeneous core.
- 6) Thus, because the heterogeneous core has a higher fissile inventory and the same fissile gain (breeding ratio minus 1.0) as the homogeneous core, for each fuel volume fraction the heterogeneous core always must have a longer doubling time.

In this logical development several approximations were introduced in the interests of simplicity. For example, the enrichment and breeding ratio were approximated as functions only of the fuel volume fraction. In practice, core size and heterogeneity was found to have little impact on these values; however, a heterogeneous core will have a slightly higher enrichment and breeding ratio than the homogeneous core. The net effect, though, follows very closely the logic presented. In fact if it were possible to relax the peak linear heat generation rate in the heterogeneous core and allow it to have the same average power density (average of driver assemblies and internal blankets) as that in the homogeneous core the doubling time difference would almost be eliminated! Even-handed optimization, however, will always force the heterogeneous core to have a longer doubling time.

6.4 Conclusions

Now, thanks to consistent optimization analyses, it is possible to establish the real effects of heterogeneity and to make a recommendation for the GCFR design, and to offer comments relevant to LMFBR design.

6.4.1 Real Heterogeneous Effects

Over the recent past many advantages have been claimed for heterogeneous cores. Some are:

- 1) Higher breeding ratio,
- 2) Shorter doubling times,

- 3) Reduced fast fluence,
- 4) Improved power flattening,
- 5) Less fuel fabrication,
- 6) Enhanced safety,
- 7) Less reactivity swing over a cycle

Some of these assertions were found to be true but most of the claims appear to have come from comparing unequally-well-optimized cores. Table 6.2 compares most of the important parameters of the reference versions of the homogeneous and heterogeneous cores which were examined in depth in the final stages of the present work.

Examination of this list reveals the true effects of heterogeneity. The heterogeneous core has:

- 1) Higher fissile inventory, longer doubling time
(but a slightly higher breeding ratio)
- 2) Lower fast fluence. (The design procedure leading to the final results also showed that the greater the heterogeneity the lower the fast fluence).
- 3) Less driver fuel assembly fabrication but more blanket assembly fabrication. For every three to four internal blanket assemblies added, a fuel assembly can be removed.
- 4) Potentially poorer safety-related performance. The heterogeneous core's prompt Doppler (power-weighted Doppler) coefficient of reactivity is smaller and its fuel worth is greater.
- 5) A lower mixed-mean core outlet temperature: for the case studied up to a 14% reduction in the ΔT

Table 6.2
 Summary Comparison of the Reference Homogeneous
 and Heterogeneous Cores

	<u>Homogeneous</u>	<u>Heterogeneous</u>
Number of Driver Fuel Assemblies	384	348
Number of Radial Blanket Assemblies	234	258
Number of Internal Blanket Assemblies	--	132
Total Number of Blanket Assemblies	<u>234</u>	<u>390</u>
Total Number of Core Assemblies	618	738
Driver Fuel Pin Diameter (mm)	8	7
Assembly Flat to Flat Dimension (assembly pitch) (cm)	18.5	17.3
Average Number of Driver Fuel Assemblies Charged/Discharged Each Year	128	116
Average Number of Blanket Assemblies Charged/Discharged Each Year	39	111
Total Assemblies Charged/Discharged Each Year	<u>167</u>	<u>227</u>
Kg Heavy Metal Charged/Discharged Each Year ($\times 10^{-3}$)	39.6	48.0
Fissile Inventory (Kg) (BØEC)	5096	5617
Breeding Ratio (BØEC)	1.57	1.61
Mean Core Neutron Energy (KeV)	160	170
Core-Averaged (Driver plus Internal Blanket) Enrichment (%) (BØEC)	13.0	13.2
Doubling Time (yrs)	10.9	11.4
Peak Linear Heat Generation Rate (KW/ft)		
Driver Fuel	14.0	13.5
Internal Blanket Fuel	--	14.0
Radial Blanket Fuel	6.8	9.7

Table 6.2 (continued)

	<u>Homogeneous</u>	<u>Heterogeneous</u>
Axial Peak to Average Power Density	1.21	1.22
Radial Peak to Average Power Density	1.23	1.21
Mean Temperature Rise Across the Core (°C)		
Re-Orificed Every Cycle	260	240
Fixed Assembly Orifices	260	220
Peak Flux (neutrons/cm ² .sec x 10 ¹⁵)	6.4	5.6
Peak Fast Fluences (neutrons > 0.1 MeV/cm ² x 10 ²³)	2.4	2.1
Peak Burnup (MWD/MT)	99,000	123,000
Delayed Neutron Yield, β _{eff} (BOEC)	0.0039	0.0038
Doppler Coefficient ($-T \frac{dk}{dT} \times 10^{-4}$) (BOEC)		
Driver Fuel	63.2	32.8
Internal Blankets	--	33.7
Radial Blankets	2.9	6.9
Axial Blanket	7.3	4.3
Relative Power Weighted Prompt Doppler Feedback	1.41	1.0
Cycle Δk	0.00030	0.0078
Temperature Defect (Cold to HFP) (Δk/k)	-0.0132	-0.0131
Control Worth (Total Δk for 13 rods)	0.0517	0.0501
Clad Worth (Driver Fuel Averaged) (Δk/Kg)	3.7 x 10 ⁻⁶	2.8 x 10 ⁻⁶
Average Driver Fuel Worth (Δk/Kg)	7.8 x 10 ⁻⁶	16.0 x 10 ⁻⁶
Helium Depressurization Worth	\$1.78	\$1.83
Fast Flux at the Radial Blanket Periphery (BOEC) (neutrons > 0.1 MeV/cm ² .sec x 10 ¹³)	1.8	3.6
Fuel Cycle Cost (mills/KWhe)	6.55	7.56
Capital Cost Difference (\$ million)	0	60

across the core, leading to a capital cost penalty of up to \$60 million.

The only advantages in this list are the lower fast fluence and the reduction in driver fuel fabrication cost. However, the lower fluence is accompanied by a higher burnup. The reduction in the fuel fabrication costs is not enough to prevent a 13% higher fuel cycle cost for the heterogeneous core. All in all, the disadvantages heavily outweigh the advantages of heterogeneity for a GCFR. It should be pointed out that a lower sodium void worth is an inherent feature of heterogeneity, so the decision for an LMFBR is not as obvious.

6.4.2 Recommendations for the GCFR

The central objective of the present work was to decide whether or not to use internal blankets in a GCFR. It is recommended that radial internal blankets should not be used in the GCFR. The reasons supporting this recommendation are:

- 1) The heterogeneous core has a lower energy growth potential due to its longer doubling time and higher fissile inventory.
- 2) The heterogeneous core has higher fuel cycle costs and associated capital costs by 13 to 25 percent.
- 3) The heterogeneous core has a safety disadvantage due to the lower prompt Doppler feedback and no corresponding safety advantage of much note in a GCFR.

- 4) The heterogeneous core has a proliferation-related disadvantage due to the larger number of annual fuel shipments, and larger traffic in weapons grade blanket plutonium.

The disadvantages so greatly outweigh the advantages (lower fuel fabrication costs and lower fast fluence) that no further study of heterogeneous GCFRs is recommended.

6.4.3 Comments Relevant to the LMFBR

Since the LMFBR and GCFR are very similar neutronically much of the present work would be valid for LMFBRs. However, throughout the present work the doubling time has been the dominant figure of merit rather than coolant void worth. Although void worth is a major LMFBR concern at present, the degree of emphasis on this issue has varied in the past, and concern may diminish again in the future. As noted in the present work, the consequences of the smaller prompt Doppler coefficient (the power density weighted value) of the heterogeneous cores should be taken into account as part of an overall safety assessment.

Perhaps the most relevant part of the present work for the LMFBR community is that segment dealing with doubling time as a function of the fuel volume fraction. The line of reasoning supporting the conclusion that a heterogeneous core

will always have inferior doubling time performance is just as true for LMFBRs. Although the constrained design process for LMFBRs and GCFRs differs, the heterogeneous LMFBRs still have an inherently lower core-averaged power density, and therefore the heterogeneous core's doubling time is still expected to be longer than that of the comparable homogeneous design.

The present work cannot substitute for a similar study for LMFBRs since design constraints differ, however some observations can be made. The LMFBR does not have vented fuel as does the GCFR so the higher burnup attributed to the heterogeneous core represents a larger penalty for the LMFBR. While the components of the capital cost of an LMFBR are considerably different than those of the GCFR, it is believed that the capital cost increases due to heterogeneity would be less for an LMFBR than a GCFR due to less sensitivity in the LMFBR to the primary coolant pump size and the core diameter.

6.5 Recommendations for Future Work

The GCFR contributes to diversity among breeder reactor systems and provides the potential for faster energy growth at cheaper generating costs. The best GCFR design, however, is a homogeneous design and there seems to be little advantage in further studying a GCFR with "radial" internal blankets. The insertion of "axial" internal blankets in a GCFR had been previously studied by Ducat (D1). This study does not invalidate his work since it is of an entirely

different nature. A "radial" heterogeneous core yields no power flattening advantage, but an axial parfait may yield power flattening advantages. More work could be done to compare the advantages of an axial parfait to those attained through axial enrichment zoning.

The GCFR may change in many ways in future designs; however, none of the projected design changes in the GCFR would suggest the need to reconsider the use of a heterogeneous core. Most of the advanced fuels (carbides, nitrides and metal fuels as well as annular fuels) increase the driver fuel power density, thereby increasing the differences in the power density between the driver fuel assemblies and the internal blanket assemblies. This effectively further emphasizes the decrease in the core averaged power density associated with heterogeneity, making the heterogeneous core an even less desirable option for advanced fuels. For limited circulator power designs of the GCFR, the disparity between the performance of the heterogeneous and homogeneous cores is heightened by the heterogeneous core's need for greater circulator power. It is believed that changes in the design would favor the homogeneous core over the heterogeneous.

As a result of the present work three projects for future work are apparent:

- 1) The present work should be repeated for an LMFBR to quantify the cost penalty paid to achieve the sodium void worth benefits.

- 2) The LMFBR community would benefit from a design tool such as CALIØP. The current LMFBR analog closest to CALIØP, CØRØPT, depends heavily on empirical relationships. The one-group neutronic model of CALIØP, although still limited, should be preferable. Therefore a project is recommended to make a version of CALIØP which could be used for LMFBR design.
- 3) With a modest amount of additional work a simple version of 2DB could be produced which will do 30°, 60°, 90° and 120° symmetric problems, as well as maintain its R-Z capabilities. Also, the identification of isotopes by their atomic weight could be used to simplify the burnup cards and shuffling routines.

Appendix A
Changes to 2DB

2DB is a widely used two-dimensional diffusion theory neutronic code with burnup capability. Many of the industrial facilities, such as WARD and GA, and some of the national laboratories, such as HEDL and BNL, use the code. Over the years minor changes have been made in 2DB at these locations, but have never been published for proprietary reasons. Without knowledge of the actual coding of these proprietary versions, but with a general knowledge of the type of adaptations in effect elsewhere, the MIT version was comparably modified. This appendix will describe all of the changes made to the MIT version relative to the initially published version of 2DB (H3). The coding changes are displayed in a manner which will make implementation by others as easy as possible.

The changes made to 2DB are 1) a 30° symmetry option was added, 2) a change in the search parameters was made to allow a search-burn capability, along with a total inventory edit, and 3) temporary changes were introduced to permit fuel shuffling. These changes were effected in a manner which was more utilitarian than elegant. For example, the coding changes for the 30° symmetry option made that version of the code only applicable for 30° symmetric hexagonal problems. No time was spent

devising warning flags or pretty edits. With this as a qualification, the description of the changes commences.

A.1 30° Symmetry Changes

The changes for the 30° symmetry version of 2DB required modifying only three subroutines: S862, INNERT, and INNER2.

The changes follow:

1) A 30° sector can be modeled by making the first X direction mesh half the normal size, and then using every mesh point where the mesh number in the X direction is less than or equal to the mesh number in the Z direction (see Figure A.1). To do this S862 was modified to zero the flux everywhere else. The flux, when set equal to zero, will stay zero. This implies that the reaction rate outside the modeled regions of interest is zero, so only the inner iteration subroutines need to be changed. (Note that for any zone in the region not used in the calculation the zone averaged flux and kilogram edit will not be of any use. Further note that this approach makes this 2DB version only good for 30° symmetric problems.) The change needed in the S862 subroutine is only three cards. Remove card 0741 and place between cards 0740 and 0742 the following:

```
      NO(ITEMP) = 1.0
      IF(I.GT.J)  NO(ITEMP) = 0.0
59  CØNTINUE
```

For the card numbers see page E-16 of Ref. H3.

2) INERT establishes the coupling coefficients between mesh points for the finite difference scheme. On the right

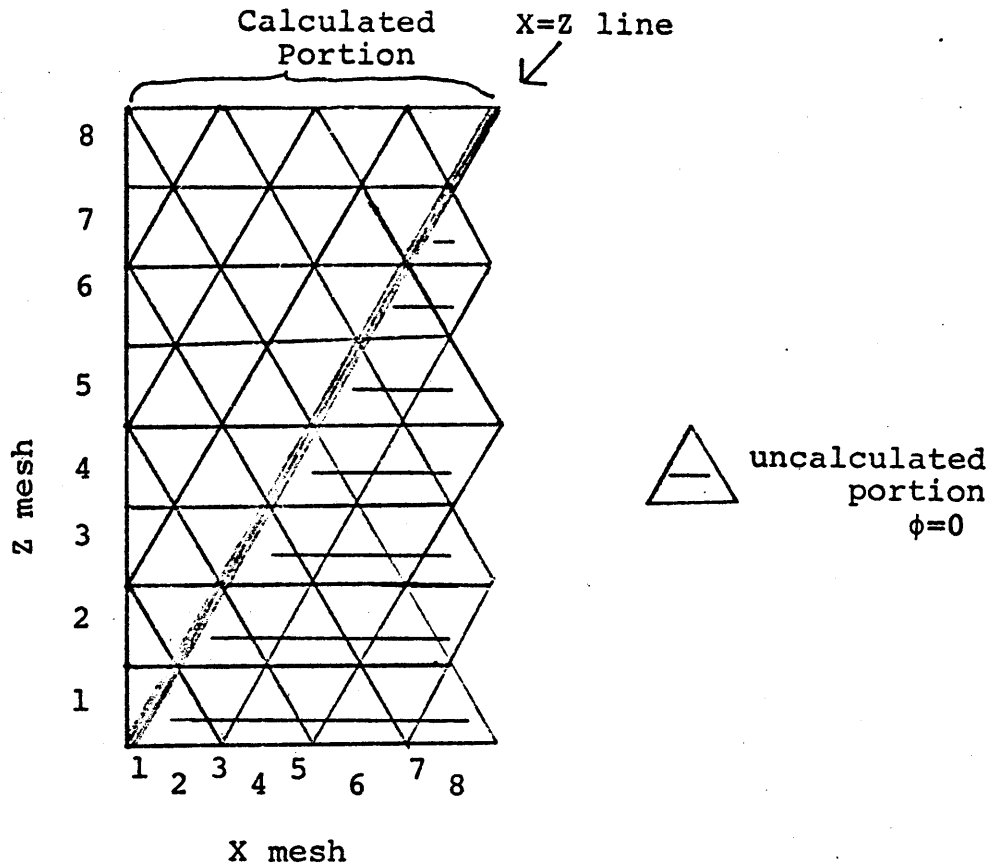


Fig. A.1 A 30° symmetry mesh map

Note: Zone data must be given for uncalculated mesh points (i.e. $X > Z$). Since the flux in the uncalculated zone is zero, at least one mesh point for every zone must be in the calculated portion. Therefore, a zone without burnable isotopes is required for the uncalculated portion (e.g. a shield zone).

hand border shown in Fig. A.1 a reflective boundary must be placed. The user is expected to properly use the normal input method for the desired left and top boundary conditions. This is also a very quick and easy change. Simply remove cards 1536 through 1541 and insert in their place one card:

```
145  IF(KI.LT.KJ) GØ TØ 165
```

3) The actual inner iterations are performed in INNER2. The iteration scheme requires three mesh points, so the finite difference equations for the bottom two rows (which have less than three mesh points) were solved to allow a separate approach for these mesh points. The sweeping was then modified to remain in the modeled region shown in Figure A.1. Since changes were made throughout the subroutine a full listing is included as Table A.1. Statements without card numbers on the right were those changed for this modification.

With the above changes it is possible to run any 30° symmetry problem whether it is a keff problem, or a concentration search, or a burnup analysis. In the burnup analysis, however, it is important that the zone that will be used in the uncalculated region (See Fig. A.1) not have any burnable isotopes, since the zone averaged flux is not real. If no burnup is being done it does not matter what the zones are in the uncalculated region, so whatever is convenient to the user can be employed.

These coding changes have been thoroughly tested, yielding identical results to a 90° test model.

Table A.1
The INNER2 Subroutine for 30° Symmetry

	SUBROUTINE INNER2(NC, N2, CXS, S2, MC, M2, VC, CC, JIM, JJM, JTL, CXR, CXT, HA, PA)	2DB 1649
1	INCLUDE ABC	2CB 1650
	DIMENSION N2(1), CXS(JIM, JJM, 3), S2(1), MC(1), M2(1), VC(1), CC(JTL, 1), CXR(1), CXT(1), HA(1), PA(1)	2DB 1652
1	CALL IFLXN (N2, CC, VC, CXS, MC, M2, JTL, IM, JM, CXR, CXT)	2DB 1653
2	DO 4 I=1, IMJM	2DB 1654
4	N2(I) = N2(I)	2DB 1655
C	BEGIN FLUX CALCULATION	2DB 1656
C	JKB = JM - 1	2DB 1657
C	FLUX CALCULATION USING SOR WITH LINE INVERSION	2DB 1659
C		2DB 1660
C		2DB 1661
C	CALCULATION OF BOTTOM BOUNDARY FLUX	2DB 1662
	N2(1)=(S2(1)+CXS(1,2,2)*N2(1+IM))/CXS(1,1,3)	
	N2(1)=NC(1)+CRF*(N2(1)-NC(1))	
	DET=CXS(1,2,3)*CXS(2,2,3)-CXS(2,2,1)*CXS(2,2,1)	
	RH1=S2(IM+1)+CXS(1,2,2)*N2(1)	
	RH2=S2(IM+2)+CXS(2,3,2)*N2(2*IM+2)	
	N2(IM+1)=(CXS(2,2,3)*RH1+CXS(2,2,1)*RH2)/DET	
	N2(IM+2)=(CXS(1,2,3)*RH2+CXS(2,2,1)*RH1)/DET	
	N2(IM+2)=NC(IM+2)+CRF*(N2(IM+2)-NC(IM+2))	
	N2(IM+1)=NC(IM+1)+CRF*(N2(IM+1)-NC(IM+1))	
C	PRINCIPAL FLUX LOOP	2DB 1684
	DO 40 KJ = 3, JKB	
	KI = 1	2DB 1686
	I = KI + (KJ - 1)*IM	2DB 1687
	HA(KI) = CXS(KI+1, KJ, 1)/CXS(KI, KJ, 3)	2DB 1688
	PA(KI) = (S2(I) + CXS(KI, KJ, 2)*N2(I-IM) + CXS(KI, KJ+1, 2)*N2(I+IM))/	2DB 1689
1	CXS(KI, KJ, 3)	2DB 1690
	IKB=KJ-1	
	DO 25 KI = 2, IKB	2DB 1691
	I = KI + (KJ - 1)*IM	2DB 1692
	HA(KI) = CXS(KI+1, KJ, 1)/(CXS(KI, KJ, 3) - CXS(KI, KJ, 1)*HA(KI-1))	2DB 1693
25	PA(KI) = (S2(I) + CXS(KI, KJ, 2)*N2(I-IM) + CXS(KI, KJ+1, 2)*N2(I+IM) +	2DB 1694
1	CXS(KI, KJ, 1)*PA(KI-1))/(CXS(KI, KJ, 3) - CXS(KI, KJ, 1)*HA(KI-1))	2DB 1695
	KI=KJ	
	I = KI + (KJ - 1)*IM	2DB 1697
	N2(I) = (S2(I) + CXS(KI, KJ, 2)*N2(I-IM) + CXS(KI, KJ+1, 2)*N2(I+IM) +	2DB 1698
1	CXS(KI, KJ, 1)*PA(KI-1))/(CXS(KI, KJ, 3) - CXS(KI, KJ, 1)*HA(KI-1))	2DB 1699
	DO 30 KII = 2, KJ	
	KI = KJ - KII + 1	
	I = KI + (KJ - 1)*IM	2DB 1702
30	N2(I) = PA(KI) + HA(KI) * N2(I+1)	2DB 1703
	CC 35 KI = 1, KJ	
	I = KI + (KJ - 1)*IM	2DB 1705
35	N2(I) = NJ(I) + CRF*(N2(I) - NC(I))	2DB 1706
40	CONTINUE	2DB 1707
C	CALCULATION OF TOP BOUNDARY FLUX	2DB 1708
	IKB=IM-1	
	KJ = JM	2DB 1709
	KI = 1	2DB 1710
	I = KI + (KJ - 1)*IM	2DB 1711
	HA(KI) = CXS(KI+1, KJ, 1)/CXS(KI, KJ, 3)	2DB 1712
	PA(KI) = (S2(I) + CXS(KI, KJ, 2)*N2(I-IM))/CXS(KI, KJ, 3)	2DB 1713
	CC 45 KI = 2, IKB	2DB 1714
	I = KI + (KJ - 1)*IM	2DB 1715
	HA(KI) = CXS(KI+1, KJ, 1)/(CXS(KI, KJ, 3) - CXS(KI, KJ, 1)*HA(KI-1))	2DB 1716
45	PA(KI) = (S2(I) + CXS(KI, KJ, 2)*N2(I-IM) + CXS(KI, KJ, 1)*PA(KI-1))/	2DB 1717

A.2 Search-Burn Capability and Added Edits

The original version of 2DB forced the user to employ a special form of the I0, I1, and I2 arrays to perform a concentration search calculation. This special form made it impossible to perform a burnup analysis after an enrichment search without redoing the input deck. This makes many analyses awkward and expensive. By simply adding an array of search parameters, I3, to the input requirements for a concentration search, not only is it possible to perform a burnup analysis after the search but it is accomplished via an easier input format which requires no added storage (the I3 array was already in 2DB for a similar purpose).

For a concentration search the effective number density, I2, is calculated by:

$$I2 = I2 + I3*EV \quad (A.1)$$

Notice that this is the same form as Eq. 4.4 of the 2DB input manual (H3). In this case, however, I3 is an added input array. In accordance with this change the input manual should be changed. On page B-11 (of reference H3), after the card 19 input description, the following should now be incorporated:

Card 19' (Optional, required if I04=3)

I3 (MOI)	1 - 12	E12(GI)	0
I3 (MOI)	13 - 24	E12(GI)	Search parameter of first material in Mix 1 (atoms/barn-cm)
I3 (MOI)	25 - 36	E12(GI)	Search parameter of second material in Mix 1.
...			

While putting this improvement into 2DB three other improvements were included: 1) an edit of the storage a problem requires and the storage available, 2) an improvement in the storage system by some overlaying of storage, and 3) an edit of the total kilograms of every isotope in the reactor.

The actual coding will now be described for each subroutine modified.

1) MAIN: following the statement specifying the size of the container A array a statement such as:

```
ISIZE = 35000
```

is included where the value, 35000, is the same as the dimension of the A array. This is then passed to INP by changing card 322 (see page E-6 of reference H3) to:

```
CALL INP(ISIZE)
```

Since INIT now needs the I3 array, A(LI3) must be added to the end of the argument list.

2) INP: the first statement must be changed to:

```
SUBROUTINE INP(ISIZE)
```

To overlay some arrays and to check the amount of storage and print it, cards 548 through 570 should be removed and the 25 cards listed in Table A.2 should be inserted. In order to read the I3 array and print it out, after card 617 add:

```
IF (I04.EQ.3) CALL REAG2(6H I3,A(LI3),M01)
```

Finally, in order to fully use ISIZE, card 631 should be:

```
IF (LAST-ISIZE) 470,470,450
```

3) INIT: INIT is the subroutine that changes the number

Table A.2
Changes in INP for Improved Storage

```
LMATN= LZ5 + JM
LNBP = LMATN + ML
LLC = LNBP + ML
LLCN = LLD + ML
LLFN = LLCN + ML*2
LGAM = LLFN + ML*7
LPHIB=LGAM+IZM
LAXS = LPHIB + IZM
LFXS = LAXS + ML*IZM
LMASSP=LFXS+ML*IZM
LVCL=LMASSP+ML*IZM
LMASS=LVCL+IZM
LAST=LMASS+ML*(IZM+1)
LCXS=LPHIB
LCXR=LCXS+IMJM+3
LCXT = LCXR + JM
LHA = LCXT + IM
LPA = LHA + MAX0(IM,JM)
LAST2= LPA + MAX0(IM,JM)
ITEMP = 1 + 3*ML + ICP*ITL*NT
IF(LAST - ITEMP) 216,218,218
316 LAST = ITEMP
318 IF (LAST2.GT.LAST) LAST=LAST2
WRITE(ACUT,327) LAST,ISIZE
320 FORMAT(9H STORAGE ,I7,3F CF,I7,11F WCRCS USED)
```

2CB 0552
2DB 0553
2CB 0554
2DB 0555
2CB 0557
2DB 0558
2CB 0561
2DB 0562
2CB 0563
2CB 0566
2DB 0567
2DB 0568

densities in a concentration search calculation, therefore, the changes with respect to using the new I3 array are made in this subroutine. The first change is to include I3 at the end of the argument list in the SUBROUTINE statement. Also, I3(1) must be included in the DIMENSION list. In order to make the I3 array more evident in the output, several changes can be made. Remove card 943 and insert:

```
60 IF (I04.EQ.3) GØ TØ 760
      WRITE (NØUT,65) (J,I0(J),I1(J),I2(J), J=1,M01)
```

Then, after card 945 insert:

```
      GØ TØ 70
760 WRITE(NØUT,761) (J,I0(J),I1(J),I2(J),I3(J), J=1,M01)
761 (then duplicate card 944)
      124H MATERIAL ATØMIC DENSITY, 3X,I3HSEARCH FACTØR,/,/,
      2(I5,I9,I16,E27.6,E20.6))
```

For the actual calculation of the new number densities remove cards 960 through 964 and insert there:

```
IF (I04.EQ.3) E01=I2(M)+ I3(M)*EV
```

4) GRAM: GRAM is the subroutine that calculates the material inventories. It also was the only subroutine that had employed I3 in the original coding. Therefore, changes to this subroutine are needed to change the use of I3 over to our current purposes, and to add a reactor total inventory edit. For ease in coding the total inventory edit will appear as an added zone in the zonewise material edit; therefore, the new effective number of zones is:

IZN = IZM+1

This statement should follow card 2216. Due to this change the IZMs found on cards 2222, 2258, 2260, 2261, and 2269 should all be changed to IZN. For concentration search calculations in the original version of 2DB, I3 was needed for temporary storage of the number densities. Now no temporary storage is needed, so the old use of I3 is served by I2; therefore, all I3s of card 2249 and 2254 should be changed to I2. In order to correctly use the new I3 array, remove cards 2228 through 2235 and insert:

IF (I04.NE.3) GØ TØ 38

DØ 39 M=1,M01

I2(M) = I2(M)+I3(M)*EV

39 CØNTINUE

38 CØNTINUE

Finally, to actually calculate total reactor inventories, insert the following after card 2257:

DØ 450 N=1,IZM

DØ 450 L=1,ML

450 MASS(L,IZN)=MASS(L,N)+MASS(L,IZN)

It should be pointed out that the "volume" printed for the pseudo zone (the "zone" corresponding to the total reactor) is really the mass of the first isotope in zone one, and not a volume at all.

5) INPB: INPB reads the burnup input cards. In order to allow a normal keff calculation after a burnup step, or in

order to allow a search calculation after a shuffle, the variables I04,EV and S03 must be allowed to change. To do this, remove cards 2279 and 2280 and insert there:

```
      READ(NINP,10) ITEMP,NPRT,NPUN,ITEMPI,DELT,ITEMT,ETEMP,STEMP
10  FØRMAT(4I6,E12.0,I6,2E12.0)
      IF (ITEMT,NE.0) I04=ITEMT
      IF (ETEMP,NE.0) EV=ETEMP
      IF (STEMP.NE.0) S03=STEMP
      WRITE(NØUT,11) ITEMP,NPRT,NPUN,ITEMP1,DELT,I04,EV,S03
11  FØRMAT(7H ITEMP=,I3,6H NPRT=,I2,6H NPUN=,I2,8H ITEMP1=,I2,
      16H DELT=,F12.4,5H I04=,I2,4H EV=,E12.5,4H S03=,F12.6)
```

Notice that the IF statements allow all problems which satisfy the original 2DB burnup card input instructions to run without error. This change should be accompanied by a change in the input manual on page B-12 (Ref. H3). Following the entry on DELT should be:

I04	37 - 42	I6	See page B-2
EV	43 - 54	E12	See page B-4
S03	55 - 66	E12	See page B-5

These changes are all that are required to allow search-burn in 2DB, while also decreasing the storage requirements and providing a reactor total inventory edit. Inserting these changes into 2DB will take very little time and effort yet greatly increase the ease of reactor analysis and design.

A.3 Temporary Changes for Shuffling

For the present work, changes were needed in the SHUF subroutine to allow number densities of one material to be shuffled into those of a different material. This was needed since the cross section set for the first row of the radial blanket was different than that for the second and third rows. Although the number densities were being transferred to the same isotope in another mix, since the isotope was no longer the same material number, 2DB would not allow the transfer. To allow such transfers the approach in SHUF was changed. These changes have not been put into the permanent MIT version, since they remove an important check 2DB does on the users input. It is possible through slightly more complex coding to use the approach in the original version of 2DB, but to test for equal atomic weights rather than equal material numbers. This would be the recommended approach for a permanent change.

The temporary changes in SHUF also allow shuffling of the search parameters by using a negative value for ITEMP. The new coding for SHUF requires the isotope order in the two shuffled mixtures to be the same. Since about half the coding in SHUF has been changed, the entire subroutine is listed in Table A.3. The call to SHUF in MAIN must be changed to:

```
190 CALL SHUF(A(LI0),A(LI1),A(LI2),A(LI3))
```

If this change were to be made permanent the description of ITEMP on page B-14 of the input manual should be changed to:

Table A.3
The SHUF Subroutine Allowing Shuffling of Number
Densities Between Cross Section Sets

```

SUBROUTINE SHUF(I0,I1,I2,I3)
  INCLUDE ABC
  DIMENSION IC(1), I1(1), I2(1), I3(1)
  THIS SUBROUTINE SHUFFLES MIXTURES.
  DELT = .0
  WRITE(NOUT,10) DAY
  10  FORMAT(1H1,1CX,51H M I X T U R E S S H U F F L E D A T T I M E
  1 =,F8.3,BH D ? Y S///)
  I = 0
  15  I = I + 1
  READ(NIMP,20) ITEMP,ITEMP1,ITEMP2
  20  FORMAT(3I6)
  IF (ITEMP) 25,100,05
  25  WRITE(NOUT,30) I,ITEMP1,ITEMP2
  30  FORMAT(I6, 6X, 4H MIX, I6, 19H IS REPLACED BY MIX, I6 )
  DO 90 II=1,M01
  IF (ITEMP2 - IC(II)) 90,40,90
  90  CONTINUE
  40  ITP2=II
  DO 70 JJ=1,M01
  IF (ITEMP1 - IC(JJ)) 70,50,70
  70  CONTINUE
  50  ITP1=JJ
  DO 60 JJ=1,M01
  II=ITP2+JJ
  IF (II.GT.M01) GO TO 15
  IF (ITEMP2.NE.IC(II)) GO TO 15
  J=ITP1+JJ
  IF (ITEMP.LT.0) GO TO 65
  I2(J)=I2(II)
  GO TO 60
  65  I3(J)=I3(II)
  60  CONTINUE
  100 RETURN
  END
  200 2458
  200 2459
  200 2460
  200 2461
  200 2462
  200 2463
  200 2464
  200 2465
  200 2466
  200 2467
  200 2468
  200 2469
  200 2470
  200 2471
  200 2478
  200 2473
  200 2477
  200 2480
  200 2481
```


ITEMP	1 - 6	I6	This card replaces the densities of mix ITEMP1 with those of mix ITEMP2. =0, end of shuffling data >0, the I2 array is shuffled <0, the I3 array is shuffled.
-------	-------	----	--

A.4 Summary

2DB is a widely used code which has often been changed to make it easier to use for reactor analysis. This appendix has described three sets of changes that can be made easily, but which increase the code's capability and speed of execution. Since the implementation of these changes is so simple, it is hoped that they get wider usage.

Appendix B
Changes in PERT-V

As with 2DB, PERT-V is a widely used code which has been changed by its users, but again few of the changes have been published because of proprietary concerns. For the present work PERT-V was changed for two purposes: 1) to yield zone dependent axial bucklings, and 2) to yield zone-wise reactivity worths. To do this only three subroutines were changed; MAIN, INP, and SLOPE; and one subroutine was added, CALZ. The changes in MAIN and INP were made to aid both purposes. The changes in SLOPE were for the bucklings, and the subroutine CALZ was added for the zone-wise reactivity edit. In this appendix first the buckling changes in SLOPE will be presented, then the zone-wise reactivity subroutine CALZ, and finally the changes needed in MAIN and INP.

B.1 Buckling and Current Edit

Using Fick's law:

$$J_z = -D \frac{d\phi}{dz}, \quad (B.1)$$

where J_z is the current in the z direction,

ϕ is the flux, and

D is the diffusion coefficient.

an axial buckling is used to account for the axial leakage through the following relationship:

$$(J_{\text{Bottom}} - J_{\text{Top}})A - DB^2\bar{\phi}AH \quad (\text{B.2})$$

where B^2 is the axial buckling,

$\bar{\phi}$ is the zone-averaged flux,

H is the zone height, and

A is the cross-sectional area.

By rearranging this equation:

$$B^2 = \frac{J_{\text{Bottom}} - J_{\text{Top}}}{D\bar{\phi}H} \quad (\text{B.3})$$

Since the subroutine SLOPE already was calculating $\frac{d\phi}{dz}$ for the perturbation calculations, making it calculate the currents and bucklings was not difficult. To make implementation of the changes by others easy, the entire subroutine SLOPE is included as Table B.1. Cards without information in columns 73-80 are the ones that were changed.

Table B.2 shows a sample output of the subroutine. As can be seen from the Table, a warning is included, "This edit is valid for RZ analysis with only 4 surfaces." This warning is a slight over-statement. More correctly, the edit is valid in the left-right dimension if there is only one left boundary and one right boundary, and it is valid in the axial dimension if there is only one top boundary and one bottom boundary. Clearly, if the zone is four-sided

Table B.1

The SLOPE Subroutine Modified to Provide
a Zone-wise Flux, Current, and Axial Buckling Edit

```

SUBROUTINE SLOPE(NJ,N1,JIM,R5,Z5,R4,CO,JTL,M0,M2,DEL,VO,A0,A1,      SLOPE001
1 ZED,Z1,ZT,ZB,VOL,ZBA)
DOUBLE PRECISION ID
DIMENSION      ZBA(1),          R5(1), Z5(1), R4(1),
1 ZED(IZM,IGM,7),Z1(1),ZT(1),M2(1),ZB(1),VOL(1),      AJ(1), A1(1)  SLOPE003
REAL N0(JIM,1),N1(JIM,1)
DIMENSION CO(JTL,1),
1M2(JIM,1),DEL(JIM,1),VO(JIM,1)
COMMON      NIMP,  ADUT,  ACR1,  NSCR1,  NSCR2,  NFLUX1,  NFLUX2,  ABC00002
1      DENOM,  ICARD,  IGEP,  IHA,  IHF,  IHG,  IHN,  ABC00003
2      IJI,  IJJ,  IJIG,  IJMAX,  IMJM,  IP,  ITEM,  ABC00004
3      ITEMPI,  ITL,  JP,  NDIM,  NFP,  NFXIN,  NNCR,  ABC00005
4      PI2,  TEMP,  TEMPI,  TSD,  NADIN
COMMON      ID(12),  NO,  ML,  NPRT,  IGM,  IST,  IHT,  ABC00007
1      NDELK,  NACT,  NIBC,  IPG,  IPS,  NPEL,  IGE,  ABC00008
2      IM,  JM,  IZM,  MT,  M21,  B01,  B02,  ABC00009
3      B03,  B04,  ZKEFF,  FLPO,  VF,  BUCK
INTEGER      B01,  B02,  B03,  B04
C THIS SUBROUTINE CALCULATES (GRAD FLUX*GRAD ADJOINT)/SIGTR**2  SLOPE008
D0 88 I=1,IZM
80 ZBA(I)=0.0
NW=IGM*IZM*7
CALL CLEAR(0,0,ZED,NW)
IF (IGE - 3) 10,2,10
2 D0 4 I = 1,IM
4 R5(I) = 2.*Z5(I)/3.
TEMP1 = Z5(1)
D0 6 J = 1,JM
6 Z5(J) = 1.0
10 D0 1400 IIG=1,IGM
READ(NCR1) ((CO(I,J), I=1,ITL), J=1,MT)
READ(NFLUX1) ((NO(I,J), I=1,IM), J=1,JM)
READ(NFLUX2) ((N1(I,J), I=1,IM), J=1,JM)
D0 1200 J=1,JM
D0 1200 I=1,IM
IZ=NO(I,J)
ITEMP=M2(IZ)
ZED(IZ,IIG,1)=ZED(IZ,IIG,1)+NO(I,J)*VO(I,J)
ZED(IZ,IIG,6)= 1.0/(3.0*CO(IHT,ITEMP))
IF (I-1) 14,14,12
12 IZL = NO(I-1,J)
ITEMPL = M2(IZL )
IF(I-IM) 14,15,15
14 IZR = NO(I+1,J)
ITEMPR = M2(IZR )
15 CONTINUE
IF(J - 1) 17,17,16
16 IZB = NO(I,J-1)
ITEMPB = M2(IZB )
17 IF(J - JM) 18,19,19
18 IZT = NO(I,J+1)
ITEMPT = M2(IZT )
19 CONTINUE
SL1 = 0.0
SL2 = 0.0
SR1 = 0.0
SR2 = 0.0
SBL = 0.0
SLOPE009
SLOPE010
SLOPE011
SLOPE012
SLOPE013
SLOPE014
SLOPE015
SLOPE016
SLOPE017
SLOPE018
SLOPE019
SLOPE020
SLOPE023
SLOPE026
SLOPE029
SLOPE030
SLOPE033
SLOPE036
SLOPE037
SLOPE038
SLOPE039
SLOPE040
SLOPE041

```

Table B.1 (contd.)

	SB2 = 0.0	SLOPE042
	ST1 = 0.0	SLOPE043
	ST2 = 0.0	SLOPE044
	IF(I-1) 30,30,100	SLOPE045
30	IF(BC1-1) 40,110,50	SLOPE046
C	VACUUM BOUNDARY	SLOPE047
40	SIGTR = C0(IHT,ITEMP)	SLOPE048
	SL1 = (N0(I,J)/(0.5*R5(I) + (.71/SIGTR)))/SIGTR	SLOPE049
	SL2 = (N1(I,J)/(0.5*R5(I) + (.71/SIGTR)))/SIGTR	SLOPE050
	ZED(IZ,IIG,2)=ZED(IZ,IIG,2)+SL1*Z5(J)/3.0	
	GO TO 110	SLOPE051
C	PERIODIC BOUNDARY	SLOPE052
50	ITEMPP = M0(IM,J)	SLOPE053
	ITEMPP = M2(ITEMPP)	SLOPE054
	SIGTR = (R5(I)*C0(IHT,ITEMP) + R5(IM)*C0(IHT,ITEMPP))/	SLOPE055
	(R5(I) + R5(IM))	SLOPE056
	SL1 = ((N0(I,J) - N0(IM,J))/(0.5*R5(I) + 0.5*R5(IM)))/SIGTR	SLOPE057
	SL2 = ((N1(I,J) - N1(IM,J))/(0.5*R5(I) + 0.5*R5(IM)))/SIGTR	SLOPE058
	ZED(IZ,IIG,2)=ZED(IZ,IIG,2)+SL1*Z5(J)/3.0	
	GO TO 110	SLOPE059
C	INTERIOR INTERVAL	SLOPE060
100	SIGTR = (R5(I)*C0(IHT,ITEMP) + R5(I-1)*C0(IHT,ITEMPL))/	SLOPE061
	(R5(I) + R5(I-1))	SLOPE062
	SL1 = ((N0(I,J) - N0(I-1,J))/(0.5*R5(I) + 0.5*R5(I-1)))/SIGTR	SLOPE063
	SL2 = ((N1(I,J) - N1(I-1,J))/(0.5*R5(I) + 0.5*R5(I-1)))/SIGTR	SLOPE064
	IF (IZL.EQ.IZ) GO TO 110	
	ZED(IZ,IIG,2)=ZED(IZ,IIG,2)+SL1*Z5(J)/3.0	
110	IF(I-IM) 200,130,130	SLOPE065
130	IF(BO2-1) 140,210,150	SLOPE066
C	VACUUM BOUNDARY	SLOPE067
140	SIGTR = C0(IHT,ITEMP)	SLOPE068
	SR1 = -(N0(I,J)/(0.5*R5(I) + (.71/SIGTR)))/SIGTR	SLOPE069
	SR2 = -(N1(I,J)/(0.5*R5(I) + (.71/SIGTR)))/SIGTR	SLOPE070
	ZED(IZ,IIG,3)=ZED(IZ,IIG,3)+SR1*Z5(J)/3.0	
	GO TO 210	SLOPE071
C	PERIODIC BOUNDARY	SLOPE072
150	ITEMPP = M0(I,J)	SLOPE073
	ITEMPP = M2(ITEMPP)	SLOPE074
	SIGTR = (R5(I)*C0(IHT,ITEMP) + R5(I)*C0(IHT,ITEMPP))/	SLOPE075
	(R5(I) + R5(I))	SLOPE076
	SR1 = ((N0(I,J) - N0(I,J))/(0.5*R5(I) + 0.5*R5(I)))/SIGTR	SLOPE077
	SR2 = ((N1(I,J) - N1(I,J))/(0.5*R5(I) + 0.5*R5(I)))/SIGTR	SLOPE078
	ZED(IZ,IIG,3)=ZED(IZ,IIG,3)+SR1*Z5(J)/3.0	
	GO TO 210	SLOPE079
C	INTERIOR INTERVAL	SLOPE080
200	SIGTR = (R5(I)*C0(IHT,ITEMP) + R5(I+1)*C0(IHT,ITEMPR))/	SLOPE081
	(R5(I) + R5(I+1))	SLOPE082
	SR1 = ((N0(I+1,J) - N0(I,J))/(0.5*R5(I+1) + 0.5*R5(I)))/SIGTR	SLOPE083
	SR2 = ((N1(I+1,J) - N1(I,J))/(0.5*R5(I+1) + 0.5*R5(I)))/SIGTR	SLOPE084
	IF (IZR.EQ.IZ) GO TO 210	
	ZED(IZ,IIG,3)=ZED(IZ,IIG,3)+SR1*Z5(J)/3.0	
210	IF(N0IM-1) 220,1000,220	SLOPE085
220	IF(J-1) 230,230,300	SLOPE086
230	IF(BO4-1) 240,301,280	
C	VACUUM BOUNDARY	SLOPE088
240	SIGTR = C0(IHT,ITEMP)	SLOPE089
	GO TO (250,250,260,255), IGEF	SLOPE090
250	TEMP = 0.5*Z5(J)	SLOPE091

Table B.1 (contd.)

	GO TO 270	
255	TEMP = .5*R5(I)	SLOPE092
	ITEMP1 = I - 2*(I/2) - J + 2*(J/2)	SLOPE093
	IF (ITEMP1) 270,310,270	SLOPE094
260	TEMP = .5*PI2*Z5(J)*R4(I)	SLOPE095
270	SB1 = (N(I,J))/(TEMP + (.71/SIGTR))/SIGTR	SLOPE096
	SB2 = (N1(I,J))/(TEMP + (.71/SIGTR))/SIGTR	SLOPE097
	ZED(IZ,IIG,4)=ZED(IZ,IIG,4)+SB1*A1(I)/3.0	SLOPE098
301	ZB(IZ)=0.0	
	ZBA(IZ)=ZBA(IZ)+A1(I)	
	GO TO 310	
C	PERIODIC BOUNDARY	SLOPE099
280	ITEMPP = N0(I,JM)	SLOPE100
	ITEMPP = N2(ITEMPP)	SLOPE101
	SIGTR = (Z5(J)*CO(IHT,ITEMP) + Z5(JM)*CO(IHT,ITEMPP))/	SLOPE102
1	(Z5(J) + Z5(JM))	SLOPE103
	GO TO (285,285,290,288), IGEP	SLOPE104
285	TEMP = .5*Z5(J) + .5*Z5(JM)	SLOPE105
	GO TO 295	SLOPE106
288	TEMP = R5(I)	SLOPE107
	ITEMP1 = I - 2*(I/2) - J + 2*(J/2)	SLOPE108
	IF (ITEMP1) 295,310,295	SLOPE109
290	TEMP = .5*PI2*R4(I)*(Z5(J) + Z5(JM))	SLOPE110
295	SB1 = ((N0(I,J) - N0(I,JM))/TEMP)/SIGTR	SLOPE111
	SB2 = ((N1(I,J) - N1(I,JM))/TEMP)/SIGTR	SLOPE112
	ZED(IZ,IIG,4)=ZED(IZ,IIG,4)+SB1*A1(I)/3.0	SLOPE113
	ZBA(IZ)=ZBA(IZ)+A1(I)	
	ZB(IZ)=0.0	
	GO TO 310	
C	INTERIOR INTERVAL	SLOPE114
300	SIGTR = (Z5(J)*CO(IHT,ITEMP) + Z5(J-1)*CO(IHT,ITEMP1))/	SLOPE115
1	(Z5(J) + Z5(J-1))	SLOPE116
	GO TO (302,302,304,303), IGEP	SLOPE117
302	TEMP = .5*Z5(J) + .5*Z5(J-1)	SLOPE118
	GO TO 306	SLOPE119
303	TEMP = R5(I)	SLOPE120
	ITEMP1 = I - 2*(I/2) - J + 2*(J/2)	SLOPE121
	IF (ITEMP1) 306,310,306	SLOPE122
304	TEMP = .5*PI2*R4(I)*(Z5(J) + Z5(J-1))	SLOPE123
306	SB1 = ((N0(I,J) - N0(I,J-1))/TEMP)/SIGTR	SLOPE124
	SB2 = ((N1(I,J) - N1(I,J-1))/TEMP)/SIGTR	SLOPE125
	IF (IZB.EQ.IZ) GO TO 310	SLOPE126
	ZED(IZ,IIG,4)=ZED(IZ,IIG,4)+SB1*A1(I)/3.0	
	ZBA(IZ)=ZBA(IZ)+A1(I)	
	ZB(IZ)=Z1(J)	
310	IF (J-JM) 400,330,330	SLOPE127
330	IF(B03-1) 340,1001,380	
C	VACUUM BOUNDARY	SLOPE129
340	SIGTR = CO(IHT,ITEMP)	SLOPE130
	GO TO (350,350,360,355), IGEP	SLOPE131
350	TEMP = .5*Z5(J)	SLOPE132
	GO TO 370	SLOPE133
355	TEMP = .5*R5(I)	SLOPE134
	ITEMP1 = I - 2*(I/2) - J + 2*(J/2)	SLOPE135
	IF (ITEMP1) 1000,370,1000	SLOPE136
360	TEMP = .5*PI2*Z5(J)*R4(I)	SLOPE137
370	ST1 = -(N0(I,J))/(TEMP + (.71/SIGTR))/SIGTR	SLOPE138
	ST2 = -(N1(I,J))/(TEMP + (.71/SIGTR))/SIGTR	SLOPE139

Table B.1 (contd.)

```

ZED(IZ,IIG,5)=ZED(IZ,IIG,5)*ST1*A1(I)/3.0
1001 ZT(IZ)=Z1(J+1)
      GO TO 1000
C PERIODIC BOUNDARY
380 ITEMPP = MC(I,I)
      ITEMPP = M2(ITEMPP)
      SIGTR = (Z5(J)*CO(IHT,ITEMP) + Z5(1)*CO(IHT,ITEMPP))/
              (Z5(J) + Z5(1))
1 GO TO (385,385,390,388), IGEP
385 TEMP = .5*Z5(J) + .5*Z5(1)
      GO TO 395
388 TEMP = R5(I)
      ITEMPI = I - 2*(I/2) - J + 2*(J/2)
      IF (ITEMPI) 1000,395,1000
390 TEMP = .5*PI2*R4(I)*(Z5(J) + Z5(1))
395 ST1 = ((NO(I,1) - NO(I,J))/TEMP)/SIGTR
      ST2 = ((N1(I,1) - N1(I,J))/TEMP)/SIGTR
      ZED(IZ,IIG,5)=ZED(IZ,IIG,5)*ST1*A1(I)/3.0
      ZT(IZ)=Z1(J+1)
      GO TO 1000
C INTERIOR INTERVAL
400 SIGTR = (Z5(J)*CO(IHT,ITEMP) + Z5(J+1)*CO(IHT,ITEMPT))/
              (Z5(J) + Z5(J+1))
1 GO TO (402,402,404,403), IGEP
402 TEMP = .5*Z5(J) + .5*Z5(J+1)
      GO TO 406
403 TEMP = R5(I)
      ITEMPI = I - 2*(I/2) - J + 2*(J/2)
      IF (ITEMPI) 1000,406,1000
404 TEMP = .5*PI2*R4(I)*(Z5(J) + Z5(J+1))
406 ST1 = ((NO(I,J+1) - NO(I,J))/TEMP)/SIGTR
      ST2 = ((N1(I,J+1) - N1(I,J))/TEMP)/SIGTR
      IF (IZT.EQ.IZ) GO TO 1000
      ZED(IZ,IIG,5)=ZED(IZ,IIG,5)*ST1*A1(I)/3.0
      ZT(IZ)=Z1(J+1)
100 GO TO (1010,1010,1020,1030), IGEP
1010 TEMP = Z5(J)
      GO TO 1050
1020 TEMP = Z5(J)*PI2*R4(I)
      GO TO 1050
1030 TEMP = R5(I)
1050 DEL(I,J) = .5*(SL1*SL2*Z5(J)*A0(I)*R5(I) + SR1*SR2*Z5(J)*A0(I+1)*
1 R5(I) + SB1*SB2*A1(I)*TEMP + ST1*ST2*A1(I)*TEMP)/VO(I,J)
1200 CONTINUE
DC 1447 IZ=1, IZM
ZED(IZ,IIG,1)=ZED(IZ,IIG,1)/(VCL(IZ)*1000.)
ZED(IZ,IIG,2)=ZED(IZ,IIG,2)/(ZT(IZ)-ZB(IZ))
ZED(IZ,IIG,3)=ZED(IZ,IIG,3)/(ZT(IZ)-ZB(IZ))
ZED(IZ,IIG,4)=ZED(IZ,IIG,4)/ZBA(IZ)
ZED(IZ,IIG,5)=ZED(IZ,IIG,5)/ZBA(IZ)
ZBA(IZ)=0.0
DNJ=ZED(IZ,IIG,4)-ZED(IZ,IIG,5)
IMIX=M2(IZ)
SIGTR=CO(IHT,IMIX)
DNJ=DNJ*SIGTR*3.0
1447 ZED(IZ,IIG,7)=DNJ/((ZT(IZ)-ZB(IZ))*ZED(IZ,IIG,1))
1400 WRITE(NSCR1) ((DEL(I,J), I=1,IM), J=1,JM)
      IF (IGF - 3) 1500,1410,1500

```

SLOPE 140
SLOPE 141
SLOPE 142
SLOPE 143
SLOPE 144
SLOPE 145
SLOPE 146
SLOPE 147
SLOPE 148
SLOPE 149
SLOPE 150
SLOPE 151
SLOPE 152
SLOPE 153
SLOPE 154

SLOPE 155
SLOPE 156
SLOPE 157
SLOPE 158
SLOPE 159
SLOPE 160
SLOPE 161
SLOPE 162
SLOPE 163
SLOPE 164
SLOPE 165
SLOPE 166
SLOPE 167

SLOPE 168
SLOPE 169
SLOPE 170
SLOPE 171
SLOPE 172
SLOPE 173
SLOPE 174
SLOPE 175
SLOPE 176

SLOPE 177
SLOPE 178

Table B.1 (contd.)

1410	DO 1420 I = 1,IM	SLOPE179
1420	R5(I) = TEMPI/1.73205	SLOPE180
	DO 1430 J = 1,JM	SLOPE181
1430	Z5(J) = TEMPI	SLOPE182
1500	CONTINUE	SLOPE183
	WRITE(6,79)	
79	FORMAT(42H1 ZONE FLUXES,CURRENTS,AND AXIAL BUCKLINGS,/,8H WARNING 1,6CH THIS EDIT ONLY VALID FOR RZ ANALYSIS WITH ZONES WITH ONLY 2,1CH4 SURFACES)	
	DO 1600 J=1,IZM	
	WRITE(6,80) J	
80	FORMAT(6H- ZONE, I,/,/, 10X,7H AVERAGE,7X,4H LEFT,9X,5H RIGHT,7X, J 6H BOTTOM,9X,3H TOP,7X,9H DIFFUSION,5X,5H AXIAL,/,6H GROUP,5X, 2 4H FLUX,2X,4(6X,7H CURRENT),4X,11H COEFFICIENT,3X,8H BUCKLING,/,/)	
	WRITE(6,81) (I,(ZED(J,I,K),K=1,7),I=1,IGM)	
81	FORMAT(15,1X,7E13.4)	
	DPHI=ZED(J,1,1)*ZED(J,1,6)	
	ZED(J,1,7)=ZED(J,1,7)*ZED(J,1,6)*ZED(J,1,1)	
	ZED(J,1,6)=ZED(J,1,1)/(ZED(J,1,6)*3.0)	
	DO 1631 I=2,IGM	
	DPHI=ZED(J,1,1)*ZED(J,1,6)+DPHI	
	DO 1632 K=1,5	
1632	ZED(J,1,K)=ZED(J,1,K)+ZED(J,1,K)	
	ZED(J,1,7)=ZED(J,1,7)+ZED(J,1,6)*ZED(J,1,1)+ZED(J,1,7)	
1631	ZED(J,1,6)=ZED(J,1,1)/(ZED(J,1,6)*3.0)+ZED(J,1,6)	
	ZED(J,1,6)=ZED(J,1,1)/(ZED(J,1,6)*3.0)	
	ZED(J,1,7)=ZED(J,1,7)/DPHI	
1600	WRITE(6,82) (ZED(J,1,K),K=1,7)	
82	FORMAT(3X,3H SUM,7E13.4)	
	REWIND NSCR1	SLOPE184
	REWIND NFLUX1	SLOPE185
	REWIND NFLUX2	SLOPE186
	REWIND NSCR1	SLOPE187
	RETURN	SLOPE188
	END	SLOPE189

Table B.2
 Sample Output From the Edit of the Zone-wise Fluxes, Currents, and Axial Bucklings

ZONE FLUXES, CURRENTS, AND AXIAL BUCKLINGS

WARNING THIS EDIT ONLY VALID FOR RZ ANALYSIS WITH ZONES WITH ONLY 4 SURFACES

ZONE	1							
GROUP	AVERAGE FLUX	LEFT CURRENT	RIGHT CURRENT	BOTTOM CURRENT	TOP CURRENT	DIFFUSION COEFFICIENT	AXIAL BUCKLING	
1	0.6534E 14	0.3013E 14	-0.1156E 14	0.0	-0.1112E 14	0.4564E 01	0.7031E-03	
2	0.2017E 15	0.9498E 14	-0.3754E 14	0.0	-0.3684E 14	0.3836E 01	0.5433E-03	
3	0.6310E 15	0.8857E 14	-0.3660E 14	0.0	-0.4893E 14	0.3049E 01	0.4795E-03	
4	0.7265E 15	0.3795E 14	-0.1877E 14	0.0	-0.3267E 14	0.2089E 01	0.4059E-03	
5	0.7744E 15	0.6975E 13	-0.4336E 13	0.0	-0.2449E 14	0.1894E 01	0.3149E-03	
6	0.5321E 15	-0.1141E 14	0.5736E 13	0.0	-0.1155E 14	0.1535E 01	0.2670E-03	
7	0.4039E 15	-0.9804E 13	0.2206E 13	0.0	-0.6960E 13	0.1848E 01	0.1759E-03	
8	0.1732E 15	-0.8026E 13	0.3316E 13	0.0	-0.5129E 12	0.1101E 01	0.5069E-04	
9	0.9699E 14	-0.8400E 13	0.3230E 13	0.0	0.1107E 13	0.1244E 01	-0.1737E-03	
10	0.4081E 13	-0.1865E 13	0.1782E 13	0.0	0.6768E 12	0.1073E 01	-0.2913E-02	
SJM	0.3683E 16	0.2191E 15	-0.9324E 14	0.0	-0.1713E 15	0.1988E 01	0.3956E-03	

the entire edit is correct. The zone-averaged flux and diffusion coefficient are always correct. As a final note, the diffusion coefficient in the sum row is reciprocal flux weighted.

B.2 Zone-wise Reactivity Edit

PERT-V in its original form calculates reactivity traverses for any material; however, it would require requesting traverses for every column or row in a zone and then summing them by hand to obtain the zone-wise reactivity worth. To avoid this the subroutine CALZ was added to PERT-V. It performs the same perturbation calculations as described in Section II of the PERT-V manual (H3), except rather than editing $\Delta k/Kg$ it edits out $\Delta k/cc$. This approach was needed to allow finding the worth of switching two macroscopic cross sections as would be required for the calculation of the Doppler reactivity worth. The subroutine multiplies all the $\Delta k/cc$ values by their respective volumes and sums them to yield a total reactivity edit.

To use this new subroutine the input required is different. Now on Card 2 of the input, where NPDEL used to be, substitute in the input manual (H3).

NZET	67-72	Number of zone-wise reactivity edits.
------	-------	---------------------------------------

The input Card 28 should be changed to:

CARD 28: FORMAT [7I6]
Optional--required if NZET>0

NZ	1-6	Zone number for the reactivity edit
MNW	7-12	Material number added to the zone.
MOL	13-18	Material number removed from the zone.
IB	19-24	Use all mesh points of zone NZ starting at IB of the first dimension and ending at IE
IE	25-30	
JB	31-36	Use all mesh points of zone NZ starting at JB of the second dimension and ending at JE.
JE	37-42	

Table B.3 shows a sample output of this subroutine.

Table B.4 lists the subroutine.

B.3 Changes in MAIN and INP

Due to the changes already described, MAIN and INP had to be changed in order to pass the variables needed for the changes and to store them efficiently in the container array, A. Also, the order of calculation was changed slightly to accommodate the new subroutine, CALZ. Since MAIN is short, the new version is listed as Table B.5. Due to INP's length and because comparatively few changes were made, a completed listing of INP is not included.

The first change to INP is in the last card of blank COMMON. It should be the same in INP as the corresponding card in MAIN (see Table B.5). In order to read in NZET, substitute NZET for NPDEL on card 267 (for card numbers see Ref. H3 page B-6). Card 279 must be changed to a

Table B.3
Sample Output of the Zone-wise Reactivity Worth Calculation

ZONE EDIT OF MATERIAL WORTHS FOR ZONE 21
NEW MATERIAL NO. 58 OLD MATERIAL NO. 72 IB= 14 IS= 17 JB= 15 JE= 19

I	J	DK/K PER CC TOTAL	FK/K PER CC FISSION	DK/K PER CC ABSORPTION	DK/K PER CC LEAKAGE	DK/K PER CC MODERATION	VOLUME (CC)	DK/K PER MESH
14	15	-0.1075E-07	0.1019E-07	-0.1772E-07	0.9797E-09	-0.1702E-07	0.5550E 04	-0.5963E-04
14	16	-0.7812E-08	0.7396E-08	-0.1305E-07	0.7901E-08	-0.1005E-07	0.5550E 04	-0.4335E-04
14	17	-0.5607E-08	0.5323E-08	-0.9455E-08	0.6141E-08	-0.7616E-08	0.5550E 04	-0.3112E-04
14	18	-0.3744E-08	0.3806E-08	-0.6752E-08	0.4666E-08	-0.5664E-08	0.5550E 04	-0.2189E-04
14	19	-0.2771E-08	0.2702E-08	-0.4752E-08	0.3495E-08	-0.4145E-08	0.5550E 04	-0.1497E-04
15	15	-0.1162E-07	0.9382E-08	-0.1537E-07	0.7919E-08	-0.1255E-07	0.5992E 04	-0.6762E-04
15	16	-0.8295E-08	0.6713E-08	-0.1217E-07	0.6634E-09	-0.9671E-08	0.5992E 04	-0.4971E-04
15	17	-0.5861E-08	0.5025E-08	-0.8872E-08	0.5273E-08	-0.7306E-08	0.5992E 04	-0.3512E-04
15	18	-0.4078E-08	0.3616E-08	-0.6361E-08	0.4089E-08	-0.5423E-08	0.5992E 04	-0.2444E-04
15	19	-0.2774E-08	0.2578E-08	-0.4487E-08	0.3096E-08	-0.3962E-08	0.5992E 04	-0.1662E-04
16	15	-0.1164E-07	0.9418E-08	-0.1544E-07	0.7879E-08	-0.1250E-07	0.6434E 04	-0.7486E-04
16	16	-0.8317E-08	0.6538E-08	-0.1223E-07	0.6620E-08	-0.9647E-08	0.6434E 04	-0.5352E-04
16	17	-0.5887E-08	0.5044E-08	-0.8922E-08	0.5293E-08	-0.7301E-08	0.6434E 04	-0.3788E-04
16	18	-0.4106E-08	0.3632E-08	-0.6405E-08	0.4098E-08	-0.5430E-08	0.6434E 04	-0.2642E-04
16	19	-0.2777E-08	0.2591E-08	-0.4526E-08	0.3111E-08	-0.3975E-08	0.6434E 04	-0.1801E-04
17	15	-0.1074E-07	0.1024E-07	-0.1779E-07	0.9411E-08	-0.1280E-07	0.6877E 04	-0.7523E-04
17	16	-0.7777E-08	0.7435E-08	-0.1315E-07	0.7671E-08	-0.9738E-08	0.6877E 04	-0.5487E-04
17	17	-0.5757E-08	0.5357E-08	-0.9561E-08	0.6212E-08	-0.7566E-08	0.6877E 04	-0.3959E-04
17	18	-0.4073E-08	0.3638E-08	-0.6858E-08	0.4607E-08	-0.5650E-08	0.6877E 04	-0.2801E-04
17	19	-0.2806E-08	0.2732E-08	-0.4651E-08	0.3482E-08	-0.4169E-08	0.6877E 04	-0.1929E-04
THE TOTAL DK/K FOR THIS ZONE IS		-0.7942E-03						

Table B.4
The CALZ Subroutine to Calculate
Zone-wise Reactivity Worths

```

SUBROUTINE CALZ(CQ,CO,JTL,NO,N1,JM,DEL,K6,CX,VO,DAJ,M)
DIMENSION CQ(5,JM,1),CO(JTL,1),NO(JM,1),N1(JM,1),DEL(JM,1),
1 K6(1),CX(JTL,1),VO(JM,1),DAJ(JM,1),NO(JM,1)
REAL NO,N1, K6
DOUBLE PRECISION ID
COMMON NINP, NOUT, NCR1, NSCR1, NSCR2, NFLUX1, NFLUX2, ABC0002
1 DENOM, ICARD, IGEP, IHA, IHF, IHG, IHM, ABC0003
2 III, IIJJ, IJIG, IJMA, IMJM, IP, ITEMP, ABC0004
3 ITEMP1, ITL, JP, NDIM, NFP, NFXIN, NNCR, ABC0005
4 PI2, TEMP, TEMP1, TSD, NADIN ABC0006
COMMON ID(12), NC, ML, NPRT, IGM, IST, IHT, ABC0007
1 NDELK, NACT, NIBC, IPG, IPS, NZET, IGE, ABC0008
2 IM, JM, IZM, MT, MCI, B71, B02, ABC0009
3 B03, B04, ZKEFF, FLPO, VF, BUCK ABC0010
C THIS SUBROUTINE CALCULATES ZONEWISE REACTIVITY WORTHS
DO 5 IG=1,IGM
READ(NFLUX2) ((N1(I,J),I=1,IM),J=1,JM)
DO 6 IIG=1,IST
J=IG+IIG
IF (J.GT.IGM) GO TO 9
READ(NFLUX2) ((DAJ(I,J),I=1,IM),J=1,JM)
DO 7 J=1,JM
DO 7 I=1,IM
7 CAJ(I,J)=N1(I,J)-DAJ(I,J)
6 WRITE(NSCR2) ((DAJ(I,J),I=1,IM),J=1,JM)
9 REWIND NFLUX2
DO 8 ISK=1,IG
8 READ(NFLUX2)
5 CONTINUE
REWIND NFLUX2
REWIND NSCR2
DO 11 IK=1,NZET
SUM=0.0
READ(5,12) NZ,MNW,MOL,IB,IE,JB,JE
12 FORMAT(7I6)
WRITE(6,13) NZ,MNW,MOL,IB,IE,JB,JE
13 FORMAT(1H1,' ZONE EDIT OF MATERIAL WORTHS FOR ZONE',I5,'/,
1 ' NEW MATERIAL NO.',I4,' OLD MATERIAL NO.',I4,5X,'IB=',I4,' IE='
2,I4,' JB=',I4,' JE=',I4,'/,/, ' I',3X,'J',5(' DK/K PER CC'),
3 ' VOLUME ',5X,'DK/K ',/,15X,' TOTAL ',8X,'FISSION',5X,'ABS
JORPTION',6X,'LEAKAGE',5X,'MODERATION',7X,'(CC)',7X,'PER MESH')
ITEMP=5*IM*JM
CALL CLEAR(0.0,CQ,ITEMP)
DO 601 IIG=1,IGM
REAC(NCR1) ((CO(II,JJ), II=1,ITL), JJ=1,MT)
IF (MOL.EQ.0) GO TO 30
DO 151 II=1,ITL
151 CX(II,IIG)=CO(II,MNW)-CO(II,MOL)
GO TO 601
30 DO 150 II=1,ITL
150 CX(II,IIG) = CO(II,MNW)
601 CONTINUE
DO 600 IIG=1,IGM
READ(NFLUX1) ((NO(II,JJ), II=1,IM), JJ=1,JM)
READ(NFLUX2) ((N1(II,JJ), II=1,IM), JJ=1,JM)
READ(NSCR1) ((DEL(II,JJ), II=1,IM), JJ=1,JM)
DO 640 I=IB,IE
DO 640 J=JB,JE

```

Table B.4 (contd.)

```
C      IF (MO(I,J).NE.NZ) GO TO 640
      FISSION SOURCE*ADJOINT
      CQ(1,I,J)=K6(IIG)*N1(I,J)+CQ(1,I,J)
      C      NU SIGF*FLUX
      CQ(2,I,J)=CX(IMN,IIG)*NO(I,J)+CQ(2,I,J)
      C      SIGA*FLUX*ADJOINT
      CQ(3,I,J)=CX(IMA,IIG)*NO(I,J)*N1(I,J)+CQ(3,I,J)
      C      LEAKAGE COMPONENT
      CQ(4,I,J)=CX(IMT,IIG)*DEL(I,J)/3.+CQ(4,I,J)
640    CONTINUE
      C      DOWNSCATTERING COMPONENT
      DO 880 NN=1,IST
      JYG = NN + IIG
      IF(JYG - IGM) 850,850,600
850    L = IHG + NN
      READ(NSCR2) ((DAJ(I,J),I=1,IM),J=1,JM)
      DO 920 I=IB,IE
      DO 920 J=JB,JE
      IF (MO(I,J).NE.NZ) GO TO 920
      CQ(5,I,J)=NO(I,J)*CX(L,JYG)*DAJ(I,J)+CQ(5,I,J)
920    CONTINUE
880    CONTINUE
600    CONTINUE
      DO 950 I=IB,IE
      DO 950 J=JB,JE
      IF (MO(I,J).NE.NZ) GO TO 950
      C      FISSIONS
      CQ(2,I,J)=(CQ(1,I,J)*CQ(2,I,J))/(ZKEFF*DENOM*VF)
      C      ABSORPTIONS
      CQ(3,I,J)=-CQ(3,I,J)/(DENOM*VF)
      C      LEAKAGE
      CQ(4,I,J)=CQ(4,I,J)/(DENOM*VF)
      C      SLOWING DOWN
      CQ(5,I,J)=-CQ(5,I,J)/(DENOM*VF)
      CQ(1,I,J)=CQ(2,I,J)+CQ(3,I,J)+CQ(4,I,J)+CQ(5,I,J)
      TOT=CQ(1,I,J)*V(I,J)
      SUM=SUM+TOT
      WRITE(6,113) I,J,(CQ(K,I,J),K=1,5),VO(I,J),TOT
113    FORMAT(I5,I4,7E14.4)
950    CONTINUE
      WRITE(6,114) SUM
114    FORMAT(' THE TOTAL CK/K FOR THIS ZONE IS',E14.4)
      REWIND NSCR1
      REWIND NFLUX1
      REWIND NFLUX2
      REWIND NSCR1
11    REWIND NSCR2
      RETURN
      END
```

Table B.5

The MAIN Subroutine Modified for
the PERT-V Improvements

```

DOUBLE PRECISION ID
COMMON      NINP,      NOUT,      NCR1,      NSCR1,      NSCR2,      NFLUX1,      NFLUX2,      ABC00002
1          DENOM,      ICARD,      IGEP,      IHA,      IHF,      IHG,      IHN,      ABC00003
2          III,      IIJJ,      IJGM,      IJMAX,      IMJM,      IP,      ITEM,      ABC00004
3          ITEPPI,      ITL,      JP,      NDIM,      NFP,      NFXIN,      NNCR,      ABC00005
4          PI2,      TEMP,      TEPP1,      TSD,      NADIN,      ABC00006
COMMON      ID(12),      ND,      ML,      NPRT,      IGM,      IST,      IHT,      ABT00007
1          NDELK,      NACT,      NIBC,      IPG,      IPS,      NZET,      IGE,      ABC00008
2          IM,      JM,      IZH,      MT,      M01,      B01,      B02,      ABC00009
3          B03,      B04,      ZKEFF,      FLPO,      VF,      BUCK,      ABC00010
COMMON      LATW,      LHOLN,      LCO,      LNO,      LN1,      LAO,      LA1,      ABC00011
1          LIO,      LI1,      LI2,      LI3,      LK6,      LMC,      LM2,      ABC00012
2          LRL,      LR4,      LR5,      LVO,      LV7,      LZ1,      LZ4,      ABC00013
3          LZ5,      LVOL,      LMASS,      LGAM,      LPW,      LSORC1,      LSORC2,      ABC00014
4          LNBET,      LBETA,      LD7,      LAB,      LAL,      LZPHI,      LZPOW,      ABC00015
5          LNA,      LNX,      LZACT,      LDEL,      LNCR,      LMATOK,      LCP,      ABC00016
6          LCX,      LFLUX,      LADJF,      LX,      LY,      LZED,      LZT,      LZB,      LZBA,      LCQ,      LDAJ
INTEGER      B01,      B02,      B03,      B04
COMMON A(3000)
LIMIT = 3000
INTEGER      B01,      B02,      B03,      B04
10 CALL INP(LIMIT)
GO TO (18,14), NDIM
14 CALL MAPR(A(LMC),A(LM2),IM,JM,A(LDEL))
18 CALL SETUP(A(LK6),A(LIO),A(LI1),A(LI2),A(LMO),A(LM2),A(LNO),
1      A(LR1),A(LR4),A(LR5),A(LZ1),A(LZ4),A(LZ5),A(LAO),
2      A(LA1),A(LC0),A(LVO),ITL,IM,JM,MT,A(LGAM),A(LHOLN))
CALL GRAM(A(LMASS),A(LVGL),A(LATW),A(LHOLN),IM,JM,A(LM0),A(LM2),
1      A(LVO),A(LIO),A(LI1),A(LI2),ML,A(LI3))
CALL NORM(A(LC0),ITL,A(LNO),A(LN1),IM,A(LSORC1),A(LSORC2),A(LM0),
1      A(LM2),A(LVO),A(LK6),A(LPOW),A(LZ5),A(LAO),A(LR5),
2      A(LR4),A(LA1),A(LZ4),A(LZPHI),A(LZPOW),A(LVOL))
IF(NIBC) 30,30,20
20 CALL ABETA(A(LPOW),IM,A(LSORC1),A(LNO),A(LN1),A(LC0),ITL,A(LMO),
1      A(LV7),A(LNBET),A(LBETA),A(LMASS),ML,A(LD7),A(LSORC2),
2      A(LATW),A(LVGL),A(LVO),IGM,IPG,A(LAB),A(LAL))
30 IF(NACT) 70,70,60
60 CALL ACT(A(LMA),A(LNX),A(LNO),IM,A(LC0),ITL,A(LSORC1),A(LZACT),
1      A(LM0),A(LVO),A(LVOL),A(LZ4))
70 IF(NDELK) 50,50,40
50 IF(NZET) 10,10,40
40 CALL SLOPE(A(LNO),A(LN1),IM,A(LR5),A(LZ5),A(LR4),A(LC0),ITL,
1      A(LMO),A(LM2),A(LDEL),A(LVO),A(LAO),A(LA1),A(LZED),
2      A(LZ1),A(LZT),A(LZB),A(LVOL),A(LZBA))
IF(NDELK.EQ.0) GO TO 80
CALL CALC(A(LNCR),A(LMATOK),A(LATW),A(LCP),A(LC0),ITL,A(LNO),
1      IM,A(LN1),A(LDEL),A(LK6),A(LCX),A(LFLUX),TGM,A(LADJF),
2      A(LHOLN),A(LVO),A(LR4),A(LZ4),A(LX),A(LY))
IF(NZET.EQ.0) GO TO 10
80 CALL CALZ(A(LC0),A(LC0),ITL,A(LNO),A(LN1),IM,A(LDEL),A(LK6),A(LCX),
1      A(LVO),A(LDAJ),A(LMO))
GO TO 10
END
MAIN0170
ABC00018
MAIN0171
MAIN0172
MAIN0173
MAIN0174
MAIN0175
MAIN0176
MAIN0177
MAIN0178
MAIN0179
MAIN0180
MAIN0181
MAIN0182
MAIN0183
MAIN0184
MAIN0185
MAIN0193
MAIN0194
MAIN0189
MAIN0190
MAIN0191
MAIN0195
MAIN0196

```

description of NZET, the number of zone-wise reactivity edits, rather than NPDEL. The only remaining changes are due to a re-ordering and overlay of arrays in the container array, A. To implement these, remove cards 342 through 401 and add the cards shown in Table B.6.

B.4 Summary

PERT-V has been modified to produce an edit of zone-wise fluxes, currents, and axial bucklings as well as to allow zone-wise reactivity worth calculations. These changes have proven very useful in aiding reactor design and analysis. The changes are presented in a form for easy implementation to promote widespread usage.

Table B.6
Changes to the Subroutine INP

```
SET UP DIMENSION POINTERS FOR SMALL CORE
NPDEL=0
LCX=1
LDEL=LCX+ITL*IGM
LV0=LDEL+IMJM
LM0=LV0+IMJM
LAW=LMO+IMJM
LHOLN = LATH + ML
LCO=LHOLN+2*ML
LV0 = LCO + ITL*MT
LNI = LNO + IMJM
LAI = LA0 + IP
LI0 = LA1 + IM
LI1 = LI0 + M01
LI2 = LI1 + M01
LI3 = LI2 + M01
LK6 = LI3 + M01
LM2 = LK6 + IGM
LR1 = LM2 + IZM
LR4 = LR1 + IP
LR5 = LR4 + IM
LV7 = LR5 + IM
LZ1 = LV7 + IGM
LZ4 = LZ1 + JP
LZ5 = LZ4 + JM
LV0L = LZ5 + JM
LMASS = LV0L + IZM
LGAM = LMASS + ML*IZM
LP0W = LGAM + IZM
LSORC1 = LP0W + IMJM
LSORC2 = LSORC1 + IMJM
LNBET = LSORC2 + IMJM
LBETA = LNBET + NIBC
LD7 = LBETA + NIBC
LAB = LD7 + IGM*IPG
LAL = LAB + NIBC*IPG
LZPHI = LAL + IPG
LZPGW = LZPHI + IZM
LMA = LZPGW + IZM
LNX = LMA + NACT
LZACT = LNX + NACT
LNCR = LZACT + IZM
LMAOK = LNCR + NDELK
LCP = LMAOK + NCELK
LFLUX=LCP + 5*IJMAX
LADJF = LFLUX + IGM*IJMAX
LX = LADJF + IGM*IJMAX
LY = LX + (IJMAX+2)*NPDEL
LZED =LY + (IJMAX+2)*NPDEL
LZT=LZED+7*IGM*IZM
LZB=LZT+IZM
LZBA=LZB+IZM
LAST=LZBA+IZM
LCQ=LM2
LDAJ=LCO+5*IMJM
LAST2=LDAJ+IMJM
IF (LAST2.GT.LAST) LAST=LAST2
```

INPO122
INPO124
INPO126
INPO127
INPO128
INPO129
INPO130
INPO131
INPO132
INPO133
INPO134
INPO137
INPO138
INPO139
INPO142
INPO143
INPO144
INPO145
INPO146
INPO147
INPO148
INPO149
INPO150
INPO151
INPO152
INPO153
INPO154
INPO155
INPO156
INPO157
INPO158
INPO159
INPO160
INPO163
INPO164
INPO167
INPO168
INPO169

Table B.6 (contd.)

```
ITEMP=LCO+ITL*IGM*MT
LAST = MAX0(LAST,ITEMP)
WRITE(NDOUT,190) LAST,LIMIT
190 FORMAT(7H LAST =,16,8H LIMIT =,16)
IF(LAST - LIMIT) 196,196,192
192 CALL ERRO2(6H INP,192,1)
196 DO 198 I=1,LAST
198 A(I) = 0.0
C READ CROSS SECTIONS, PERFORM ADJACENT REVERSALS, AND WRITE XS DATA
C TO DRUM (BY GROUP)
CALL XSINP(A(LCO),ITL,IGM,MT,A(LAT#),A(LHGLN))
DO 240 I=LCO,LAST
240 A(I) = 0.0
```

INP0172
INP0174
INP0175
INP0176
INP0177
INP0179
INP0180
INP0181
INP0182
INP0185

REFERENCES

- A1 L. S. Abbott, D. E. Bartine, T. J. Burns, "Interim Assessment of Denatured 233-U Fuel Cycle: Feasibility and Nonproliferation Characteristics, ORNL-5388, December 1978.
- A2 B. Atefi, M. J. Driscoll, and D. D. Lanning, "An Evaluation of the Breed/Burn Fast Reactor Concept," COO-2250-40, December, 1979.
- A3 D. C. Aldrich, "Parfait Blanket Systems Employing Mixed Progeny Fuels," M.S. Thesis, Massachusetts Institute of Technology, 1976.
- A4 A. T. Abbaspour, and M. J. Driscoll, "The Fuel Cycle Economics of Improved Uranium Utilization in Light Water Reactors," COO-4570-9, MITNE-224, MIT-EL-79001, Massachusetts Institute of Technology, January, 1979.
- B1 A. H. Barnes, L. J. Koch, H. O. Monson, and F. A. Smith, "The Engineering Design of EBR-11, A Prototype Fast Neutron Reactor Power Plant" in "Proceedings of the International Conference on the Peaceful Uses of Atomic Energy, Geneva, 1955," Vol. 3, pp. 330-344, United Nations, Geneva, 1955.
- B2 W. P. Barthold and J. Beitel, "Potential and Limitations of Heterogeneous LMFBR Reactor Concepts I. Survey Analysis of Radial Parfait Core in the 1200 MWe Class," FRA-TM-93, February 8, 1977.
- B3 H. S. Bailey, and Y. S. Lu, "Nuclear Performance of LMFBRs Designed to Preclude Energetic HCDAs," Trans. Am. Nucl. Soc., 26, 557-8 (1977). In more detail in Nuclear Technology, 44, pp. 76-82, June, 1979.
- B4 W. P. Barthold and C. P. Tzanos, "Performance Potential of Reference Fuel in 1200 MWe LMFBRs," FRA-TM-104, November 15, 1977.
- B5 W. P. Barthold and J. C. Beitel, "Physics Aspects in the Design of Heterogeneous Cores," Advances in

Reactor Physics, Proceedings of an American Nuclear Society Topical Meeting, Edited by E. G. Silver, pp. 423-435, Gatlinburg, Tennessee, April 10-12, 1978, CONF-780401. More detail in Nuclear Technology, 44, pp. 44-60, June, 1979.

- B6 K. W. Brindley, "Cores Proposed for the UK Commercial Demonstration Fast Breeder Reactor," Trans. Am. Nucl. Soc., 31, pp. 239-240, 1979.
- B7 I. I. Bondarenko, "Group Constants for Nuclear Reactor Calculations," Consultants Bureau, New York, 1964.
- B8 R. C. Borg and K. O. Ott, "A Stationary Definition of the Doubling Time for Breeder Reactor Fuel," Trans. Am. Nucl. Soc., 23, pp. 533-4, June, 1976.
- B9 W. P. Barthold and Y. I. Chang, "Breeding Ratio and Doubling Time Definitions Used for Advanced Fuels Performance Characterization," Trans. Am. Nucl. Soc. 26, pp. 588-90, June, 1977.
- B10 S. T. Brewer, E. A. Mason, and M. J. Driscoll, "The Economics of Fuel Depletion in Fast Breeder Reactor Blankets," COO-3060-4, MITNE-123, November, 1972.
- B11 W. P. Barthold, S. K. Lam, and Y. Orechwa, "Assumptions, Constraints, and Methodology of ANL Advanced Fuels System Studies," Advanced LMFBR Fuels, Editors J. Leary and H. Kittle, ANS Topical Meeting Proceedings, pp. 594-613, Tucson, Arizona, October 10-13, 1977.
- C1 Y. I. Chang, "Review of the French Concept of Heterogeneous Core to Improve the Doubling Time," FRA-TM-77, Aug. 18, 1975.
- C2 Y. I. Chang, W. P. Barthold, and C. E. Till, "An Evaluation of the Cylindrical Parfait Core Concept," FRA-TM-88, Aug. 19, 1976.
- C3 "1976 CRBRP Technical Progress Report," CRBRP-ATD-0171.
- C4 J. C. Chandler, D. R. Marr, D. C. McCurry, D. A. Cantley, and R. P. Omberg, "The Development of LMFBR Core Designs Using Reference and Advanced

- Oxide Fuel," Advanced LMFBR Fuels, Editors J. Leary and H. Kittle, pp. 583-913, ANS Topical Meetings Proceedings, Tucson, Arizona, October 10-13, 1977.
- C5 B. M. Carmichael, "Standard Interface Files and Procedures for Reactor Physics Codes, Version III," LA-5486-MS, February 1974.
- C6 "Clinch River Breeder Reactor Plant Project: 1977 Technical Progress Report, CRBRP-ARD-0211.
- C7 S. A. Cox, "Delayed Neutron Data: Review and Evaluation," ANL-NDM-5, April, 1974.
- C8 S. A. Caspersson, et al., "Optimum System Design Studies of Advanced Carbide Fuel," Advanced LMFBR Fuels, Editors J. Leary and H. Kittle, ANS Topical Meeting Proceedings, Tucson, Arizona, pp. 614-33, October 10-13, 1977.
- C9 "CRBR Preliminary Safety Analysis Report," Vol. 4, Project Management Corporation, December, 1975.
- C10 A. G. Croff, "MITCØST-II--A Computer Code for Nuclear Fuel Cycle Costs," Nucl. Engr. Thesis, Massachusetts Institute of Technology, Department of Nuclear Engineering, 1974.
- C11 "Clinch River Breeder Reactor Plant Project: 1978 Technical Progress Report," CRBRP-ARD-0230.
- D1 G. A. Ducat, M. J. Driscoll, and N. T. Todreas, "Evaluation of the Parfait Blanket Concept For Fast Breeder Reactors," C00-2250-5, MITNE-157, January, 1973.
- D2 W. J. Davis, M. B. Yarbrough, and A. B. Bartz, "SPHINX: A One Dimensional Diffusion and Transport Nuclear Cross Section Processing Code," WARD-XS-3045-17, August, 1977.
- D3 R. A. Doncals, J. A. Lake, and N. C. Park, "Use of Integral Data in the Development of Design Methods For Fast Reactors," Advances in Reactor Physics, Proceedings of an American Nuclear Society Topical Meeting, Edited by E. G. Silver, pp. 191-206,

Gatlinburg, Tennessee, April 10-12, 1978, CONF-750401.

- D4 W. Davison, "VFAC, A Self-contained, Non-energetic, Two-dimensional Diffusion Theory Subroutine," GAMD-9358, August 29, 1969.
- D5 "Preliminary Safety and Environmental Information Document, Volume 5: Gas Cooled Fast Reactors," Nonproliferation Alternative Systems Assessment Program, U.S. Department of Energy, Assistant Secretary for Nuclear Energy, January, 1980, DOE/NE-0003/5.
- D6 "Nuclear Proliferation and Civilian Nuclear Power: Report of the Nonproliferation Alternative Systems Assessment Program. Volume IX: Reactor and Fuel Cycle Descriptions," U.S. Department of Energy, Assistant Secretary for Nuclear Energy, December, 1979, DOE/NE-0001.
- E1 M. Estavoyer, et al., "Evolution of French Fast Neutron Reactor Core Design and Performance," Optimization of Sodium-Cooled Fast Reactors, Proceedings of the international conference organized by the British Nuclear Energy Society, pp. 189-196, London, 1977.
- F1 E. Fermi, "The Future of Atomic Energy," MDDC-1, May 27, 1946.
- F2 P. Fortescue, et al., "GAZALLACAURUS-REX, An Expansion of GAZELLE V," GAMD-8434, January 12, 1968.
- G1 General Atomic Company, "GCFR Information for NASAP Studies," June 14, 1978.
- G2 D. Garber, Ed., "Data Formats and Procedures for the ENDF Neutron Cross Section Library," BNL-50274 (1976).

- G3 "GCFR Upflow/Downflow Study Summary Report,"
GA-A15455, General Atomic Company, in publication.
- G4 "Gas-Cooled Fast Breeder Reactor Quarterly Progress
Report for the Period August 1, 1979 through
October 31, 1979," GA-A15628, November, 1979.
- H1 W. Hafele, "On the Development of Fast Breeders,"
Reactor Technology, 13, 18-35 (1969-70).
- H2 H. Henryson, "A Comparison of Fast-Reactor Neutron
Cross Section Processing Codes," FRA-TM-101,
April 26, 1977.
- H3 R. W. Hardie and W. W. Little, Jr., "PERT-V, A
Two-Dimensional Perturbation Code For Fast Reactor
Analysis," BNWL-1162, September 1969.
- H4 C. J. Hamilton, Personal Communication.
- H5 A. L. Hess, R. A. Moore, and D. R. Mathews, "Testing
of ENDF/B-4 with GCFR Design Codes Through Analysis
of Critical Experiments," GA-A-14084, September, 1977.
- K1 R. B. Kidman and R. E. MacFarlane, "LIB-IV, A Library
of Group Constants for Nuclear Reactor Calculations,"
LA-6260-MS, March, 1976.
- K2 Y. Kikuchi, A. Hasegawa, H. Nishimura, and K. Tasaka,
"Fission Product Fast Reactor Constants System of
JNDC," JAERI-1248, November, 1976.
- K3 E. Kujawski and J. W. Lewellen (editors), "The Large
Core Code Evaluation Working Group Benchmark Analysis
of a Homogeneous Fast Reactor, Part I," Report to
Department of Energy, September, 1978.

- L1 Y. S. Lu, C. L. Cowan, and H. S. Bailey, "Nuclear Characteristics of Large LMFBRs--Homogeneous and Heterogeneous Designs," Advances in Reactor Physics, Proceedings of an American Nuclear Society Topical Meeting, Edited by F. G. Silver, pp. 527-538, Gatlinburg, Tennessee, April 10-12, 1978, CONF-780401.
- L2 W. W. Little, Jr., and R. W. Hardie, "2DB User's Manual--Revision 1," BNWL-831 REVI, August, 1979.
- L3 D. Lancaster, "A Review of the Effects of Design Decisions on the Doubling Time of the Commercial GCFR (Oxide Fueled)," General Atomic Company, Internal Memo 790828101, August 28, 1979.
- L4 J. A. Lake, "CRBR Doubling Time," Westinghouse internal memo LRA-76-873, September 30, 1976.
- L5 S. M. Lee, "The Effect of Finite Plant Life on the Doubling Time of a Breeder Reactor Population," Nuclear Technology, 38, pp. 384-6, May, 1978.
- L6 J. A. Lake, et al., "Breeding Ratio and Doubling Time Characteristics of the Clinch River Breeder Reactor," Advanced Reactors: Physics, Design and Economics, Editors: Kallfelz and Karam, pages 665-676, Proceedings of the International Conference held at Atlanta, Georgia, September 8-11, 1974, Pergamon Press, 1975.
- M1 J. C. Mougnot, et al., "Gains de Regeneration des Reacteurs Rapides a Combustible Oxyde et a Refrigerant Sodium," Proceedings of the European Nuclear Conference, Vol. 4, p. 133 (April, 1975). Full text translated as ORNL-TR-2994.
- M2 J. M. Morelle, et al., "Physics and safety aspects of preliminary SNR2 core designs," Optimization of Sodium-Cooled Fast Reactors, Proceedings of the international conference organized by the British Nuclear Energy Society, pp. 31-36, London, 1977.
- M3 T. Moffette, et al., "GCFR Commercial Plant Parameter Interim Selection," GA-A15397, March 1979.
- M4 T. Macken, et al., "Preliminary Evaluation of the Effect of Varying Helium Circulator Pumping Power on

- the Design and Performance of a Large GCFR,"
GA-A15311, March, 1979.
- M5 G. J. Malik, Personal Communication, July 17, 1979.
- O1 Y. Orechwa, M. J. King, and R. B. Turski, "Potential
and Limitations of Heterogeneous Reactor Concepts V.
Pin Diameter Optimization in 1200 MW_e Heterogeneous vs.
Homogeneous LMFBRs," FRA-TM-112, April 20, 1978.
- P1 E. Paxson (editor), "Radial Parfait Core Design Study,"
WARD-353, June, 1977.
- R1 R. A. Rucker, Personal Communication, Summer, 1979.
- S1 B. R. Sehgal, C. Lin, J. Naser, and W. B. Lowenstein,
"Low Sodium Void Coefficient LMFBR Cores," Proceed-
ings of the International Meeting on Fast Reactor
Safety and Related Physics, Chicago, Illinois,
October 5-8, 1976, Vol. II, pp. 565-574, CONF-761001.
- S2 B. Sicard, J. C. Mougnot, H. Sztark, J. E. Cabrillat,
C. Giacometti, M. Carnoy, and P. Clauzon, "Prelimin-
ary Physics Studies of a Large Fast Core Based on
the Heterogeneous Concept," Trans. Am. Nucl. Soc., 26,
553 (1977).
- S3 M. S. Saidi and M. J. Driscoll, "Interfacial Effects
in Fast Reactors," COO-2250-37, May, 1976.
- S4 T. Schoene, R. Hansen, and H. Menzel, "Major GCFR
Design Changes," GA-A15936, May, 1980.

- S5 J. I. Shin and M. J. Driscoll, "Evaluation of Advanced Fast Reactor Blanket Designs," COO-2250-25, MITNE-199, March, 1977.
- S6 I. I. Saragossi, "Assigning a Value to Plutonium: Methodology and Policy Implications," PhD Thesis, expected December 1980, Massachusetts Institute of Technology.
- S7 M. K. Shaeffer, M. J. Driscoll, and I. Kaplan, "A One-Group Method for Fast Reactor Calculations," MIT-4105-1, MITNE-108, September, 1970.
- T1 "An Evaluation of Four Design Studies of a 1000 MW_e Ceramic-Fueled Fast Breeder Reactor," Reactor Engineering Division Chicago Operations Office, U.S.A.E.C., COO-279, December 1, 1964.
- T2 "1000-MW_e Fast Breeder Reactor Follow-On Study. Task 1 Final Report," Westinghouse Electric Corp., Madison, PA, Advanced Reactors Div., WARD-2000-33, June 1968, Revised Jan. 1969.
- T3 C. P. Tzanos, J. C. Beitel, and W. P. Barthold, "Potential and Limitations of the Heterogeneous LMFBR Concept III. Performance Evaluation of Large Heterogeneous LMFBRs," FRA-TM-105, July 5, 1977.
- T4 D. E. J. Thornton and K. W. Brindley, "Recent commercial fast reactor designs with improved safety features." Optimization of Sodium-Cooled Fast Reactors, Proceedings of the international conference organized by the British Nuclear Energy Society, pp. 77-84, London, 1977.
- T5 W. I. Thompson, "CALIØP: A Multichannel Design Code for Gas-Cooled Fast Reactors," General Atomic Company, Internal Memo 760728028 GCFR, July 28, 1976.
- T6 "Fuel Cycles and Advanced Core Designs for the GCFR," GA-A-15603, expected release, Summer, 1980.
- T7 "Final Report--GCFR Main Helium Circulator Electric Motor Drive Study," A.P. Report No. 78-001, Rev. A, Westinghouse Electric Corporation, submitted to General Atomic Company, February, 1979.
- T8 C. E. Till, et al., "ZPR-6 Assemblies 6A and 7: Benchmark Specifications for the Two Large Single-Core-Zone Critical Assemblies-²³⁵U-Fueled Assembly GA and Plutonium-Fueled Assembly 7-LMFBR Demonstration

- Reactor Benchmark Program," ANL-7910, January, 1972, p. 86.
- T9 R. F. Twiner, R. H. Brogli, D. M. Ligon, and C. J. Hamilton, "Analysis of Nuclear Systems Satisfying U.S. Energy Needs," GA-A14848, February 1978.
- T10 A. Torri and M. J. Driscoll, "Reactivity Insertion Mechanisms in the GCFR," GA-A12934, April 10, 1974.
- T11 I. Tang, Personal Communication, Spring, 1979.
-
- V1 J. A. Vitti, L. D. Felton, N. G. Galluzzo, and J. M. Otler, "Nuclear Design and Economic Comparison of a Conventional and Bullseye LMFBR Core," Trans. Am. Nucl. Soc., 26, 553-4 (1977). In longer form in Nuclear Technology, 44, pp. 10-20, June, 1979.
- V2 J. A. Vitti, N. G. Galluzzo, and J. C. Brittingham, "Recommended CRBRP Reload Core Designs Using (U-Pu)C Fuel," Trans. Am. Nucl. Soc., 28, 565-6, 1978. Also AI-DOE-13228.
-
- W1 J. R. White and T. J. Burns, "Alternate Heterogeneous GCFR Fuel Cycles," Trans. Am. Nucl. Soc., 32, pp. 403-4, 1979. Supplemented by notes from the convention.
- W2 C. R. Weisbin, et al., "MINX: A multigroup interpretation of nuclear X-sections from ENDF/B," LA-6486-MS, September, 1976.
- W3 W. A. Wittkopf, BAW-320, December, 1966.
- W4 H. L. Wyckoff and P. Greebler, "Definition of Breeding Ratio and Doubling Time," Nuclear Technology, 21, pp. 158-64, March, 1974.